Neutrino Reactions in Hot and Dense Matter

Neutrino Reaktionen in heißer und dichter Materie
Zur Erlangung des Grades eines Doktors der Naturwissenschaften (Dr. rer. nat.)
genehmigte Dissertation von M.Sc. Andreas Lohs aus Bad Homburg
Tag der Einreichung: 10. Februar 2015, Tag der Prüfung: 13. April 2015
Darmstadt — D 17

1. Gutachten: Prof. Dr. Gabriel Martínez-Pinedo
2. Gutachten: Prof. Dr. Bengt Friman

TECHNISCHE
UNIVERSITÄT
DARMSTADT

Neutrino Reactions in Hot and Dense Matter
Neutrino Reaktionen in heißer und dichter Materie

Genehmigte Dissertation von M.Sc. Andreas Lohs aus Bad Homburg

1. Gutachten: Prof. Dr. Gabriel Martínez-Pinedo
2. Gutachten: Prof. Dr. Bengt Friman

Tag der Einreichung: 10. Februar 2015
Tag der Prüfung: 13. April 2015

Darmstadt — D 17

Erklärung zur Dissertation

Hiermit versichere ich, die vorliegende Dissertation ohne Hilfe Dritter nur mit den angegebenen Quellen und Hilfsmitteln angefertigt zu haben. Alle Stellen, die aus Quellen entnommen wurden, sind als solche kenntlich gemacht. Diese Arbeit hat in gleicher oder ähnlicher Form noch keiner Prüfungsbehörde vorgelegen.

Darmstadt, den 22. Juni 2015

_____

(Andreas Lohs)

Andreas Lohs

alohs@gmx.de

Caroline-Herschel-Str. 12
64293 Darmstadt

Tel.::(+49) 06151/ 9505851
Mobil: (+49) 0173/ 32549367

Persönliche Daten

Geburtsdatum	10.04.1985
Geburtsort	Bad Homburg
Nationalität	Deutsch
Familienstand	verheiratet

Erfahrung

2011–2014	**Doktorand** Stipendium im Rahmen des GSI-TUD Kooperationsvertrages
2014–2015	**Doktorand** Stipendium im Rahmen des Nuclear-Astrophysics-Virtual-Institute (NAVI)
2011–	Doktorand im H-QM Graduiertenkolleg

Bildung

2008–2011	**MSc in Physik, Univ. Frankfurt, Frankfurt am Main, Deutschland** Externe Masterthesis an Univ. Heidelberg, Heidelberg, Deutschland "Neutrino interactions in hot strange quark matter"
2005–2008	**BSc in Physik, Univ. Frankfurt, Frankfurt am Main, Deutschland** "Thermische Strahlung beim stellaren Kollaps zu einem Schwarzen Loch"
2004–2005	**Zivildienst, Rind'sches Bürgerstift, Bad Homburg, Deutschland**
1995–2004	**Kaiserin-Friedrich-Gymnasium, Bad Homburg, Deutschland** Altsprachliches Gymnasium Erlangung der allgemeinen Hochschulreife
1991-1995	**Grundschule Obereschbach, Bad Homburg, Deutschland** Grundschule

Sprachkenntnisse

Deutsch	Muttersprache
Englisch	Fließend
Latein	Latinum
Französisch	Grundkenntnisse

Zusammenfassung

Die vorliegende Arbeit befasst sich mit den Wechselwirkungen von Neutrinos in heißer und dichter Materie. Dabei geht es insbesondere um die relevanten Neutrino-Wechselwirkungen im Kontext von Neutrino-Transport in *Kern-Kollaps-Supernovae* (CCSNe). Beim Kollaps eines massereichen Sterns und der sich anschließenden Explosion wird Gravitationsenergie in Höhe von ungefähr 10^{53} erg hauptsächlich in Form von Neutrinos freigesetzt. Die dementsprechend hohen Neutrinoflüsse haben Auswirkungen auf die verschiedensten Vorgänge im Rahmen einer Supernova.

Beim Zurückfedern des Sternenkerns nach Kontraktion über die Kerndichte hinaus entsteht eine auswärts gerichtete Stoßwelle. Simulationen von CCSNe finden, dass diese Stoßwelle beim Durchlaufen des Sterns durch das Aufheizen von akkretierten Masseströmen soviel Energie verliert, dass sie zum Halten kommt und keine prompte Explosion stattfindet. Die meisten Studien sagen voraus, dass die Supernova-Explosion letztendlich durch den Mechanismus des verzögerten Neutrino-Heizens ausgelöst wird. Demzufolge werden Neutrinos, die in tieferen Schichten emittiert wurden, im Bereich hinter der Schockfront wieder absorbiert. Dadurch wird genug Energie auf die Stoßwelle übertragen um sie wiederaufleben zu lassen. Hieraus wird ersichtlich, dass verlässliche Modelle für Explosionen durch Neutrino-Heizen auf eine präzise Beschreibung der Neutrino-Wechselwirkungen in der heißen und dichten Materie des *Protoneu-tronensterns* (PNS) angewiesen sind.

Eine Reihe weiterer Prozesse hängt ebenfalls von den Eigenschaften der Neutrinospektren ab. Man erwartet, dass die Absorption von Neutrinos an der Oberfläche des PNS zu einem beträchtlichen Massenausfluss führt, dem sogenannten *Neutrino getriebenen Wind* (NDW). Der NDW wird als möglicher Ort für die Synthese schwerer Elemente durch den sogenannten r-Prozess diskutiert. Der Verlauf der Elementsynthese hängt entscheidend von den thermody-namischen und chemischen Bedingungen im NDW ab, welche wiederum hauptsächlich durch die Neutrinospektren bestimmt werden.

Weiterhin wird erwartet, dass die direkte Messung der Neutrinospektren der nächsten na-hen Supernova mit modernen Detektoren einen detaillierten Einblick in die Vorgänge bei einer CCSN liefern wird. Zusätzlich könnte eine solche Messung Aufschluss über das Verhalten von Materie bei extrem hohen Dichten liefern. Solche Zustände sind im Labor selbst in modernen Schwerionen-Beschleunigern wenn überhaupt nur schwer zu reproduzieren. Diese Information kann jedoch nur dann gewonnen werden wenn die Theorie gleichzeitig verlässliche Modelle für die Emission von Neutrinos liefert. Ein weiterer interessanter Aspekt sind Neutrinooszillationen in der Nähe des PNS, deren Auftreten sowohl die Ausbeute der Elementsynthese als auch mess-bare Neutrinosignale auf der Erde modifizieren könnte. Die Modelle für Neutrinooszillationen hängen ebenfalls von den detaillierten Eigenschaften der Neutrinospektren ab.

Neutrino-Transport in PNS ist insofern ein besonders Konzept als das die Neutrinos aufgrund der hohen Dichten nicht einfach aus dem Stern entweichen können. Neutrinos spüren im Allgemeinen nur die schwache Wechselwirkung (und die Gravitation) weshalb sie kaum mit anderen Teilchen reagieren. Ihre mittlere freie Weglänge ist in den meisten Umgebungen größer als jedes relevante Objekt. Bei einer CCSN wird die Materie im Inneren eines PNS aber so heiß und dicht, dass die Neutrinos quasi gefangen sind. Sie befinden sich dann im thermischen und chemischen Gleichgewicht mit der Materie. Weiter draußen bei niedrigen Dichten wird die freie Weglänge wieder groß, so dass die Neutrinos einfach entweichen. Im Übergangsbereich zwischen diesen beiden Grenzfällen stellt Neutrino-Transport ein nicht-triviales Problem dar. Das Spektrum der Neutrinos wird hauptsächlich durch den Bereich bestimmt indem sie von der Materie entkoppeln, jedoch ist die Position dieser Zone im Allgemeinen unterschiedlich je nach Neutrinoenergie und -spezies. Neutrinos mit niedrigen Energien entkoppeln normalerweise bei höheren Dichten, da die meisten Reaktionsraten mit der Energie zunehmen. Weiter entkoppeln Elektron-Neutrinos bei niedrigeren Dichten als alle anderen weil sie die kürzeste freie Weglänge haben, gefolgt von Elektron-Antineutrinos. Für die Neutrinospezies der schweren μ- und τ-Leptonen werden die längsten freien Weglängen und entsprechend die höchsten Entkopplungsdichten vorausgesagt.

Die Modellierung von Neutrino-Transport muss sich nun unter anderem mit den folgenden zwei Fragen beschäftigen. Die erste Frage ist die nach den relevanten Neutrinoreaktionen. Es müssen alle Reaktionen berücksichtigt werden die für wenigsten eine Neutrinospezies bei einer beliebigen aber relevanten Energie eine bedeutenden Rate aufweisen.

Die zweite Frage beschäftigt sich mit dem Ansatz nachdem die Raten berechnet werden. Die Simulation von Neutrino-Transport in heutigen CCSNe-Simulationen kann rechnerisch extrem aufwendig sein. Da Rechenzeit in dieser Größenordnung eine begrenzte Ressource darstellt, gilt es bei der Bestimmung der Reaktionsraten eine Balance zu finden zwischen Präzision und Aufwand. Deshalb werden nach Möglichkeit passende Näherungen verwendet, welche die Wechselwirkungen numerisch vereinfachen. Dies beinhaltet z.B. vereinfachte Beschreibungen der starken Wechselwirkung oder die Annahme nicht-relativistischer Kinematik für Nukleonen. Solche Näherungen müssen mit Bedacht gewählt werden, da sie nicht in jeder Situation gleichermaßen berechtigt sind. Da aber die Eigenschaften der Neutrinospektren z.B. stark von der Beschreibung der starken Wechselwirkung bei hohen Dichten abhängen können, kann eine ungenaue Beschreibung zu signifikanten Abweichungen bei den Vorhersagen für Neutrinoemissionen führen.

Die vorliegende Arbeit beschäftigt sich im Detail mit genau diesen Fragestellungen. Zum einen wird die Bedeutung schwacher Wechselwirkungen mit geladenen Strömen (CC) zwischen Neutrinos und Myonen sowie die Bedeutung des inversen Neutronzerfalls für Elektron-Antineutrinos in CCSN bestimmt. Myonische CC-Reaktionen sind in heutigen Simulationen nicht implementiert. Dabei wird argumentiert, dass die Teilchenenergien im Inneren eines PNS noch zu klein seien um die schweren Myonen mit einer Masse von 105.7 MeV mit Reaktionsraten zu produzieren, die relevant sind im Vergleich zu anderen Reaktionen dieser Neutrinos. Dieses Argument wird in dieser Arbeit auf die Probe gestellt, da die Teilchenenergien bei Dichten oberhalb von 10^{12} g/cm^3 im Prinzip hoch genug sein können. Der inverse Neutronenzerfall wird in

bisherigen Simulationen vernachlässigt, da man die entsprechende Rate für $\bar{\nu}_e$ im Vergleich zur Absorption an Protonen oder Streuung an Nukleonen für nachrangig hält. Bei hohen Dichten in neutronenreicher Materie sorgt aber die starke Wechselwirkung für eine Vergrößerung der Energiedifferenz zwischen Neutronen und Protonen, wodurch die Absorptionsrate an Protonen gerade für niederenergetische $\bar{\nu}_e$ stark unterdrückt wird. Der inverse Neutronenzerfall leidet hingegen nicht an diesem Problem und stellt somit eine interessante Alternative dar.

Das zweite Ziel dieser Arbeit ist eine verbesserte Beschreibung der Neutrino-Nukleon Wechselwirkung bei hohen Dichten. Dazu wird versucht neue semianalytische Ausdrücke zur Beschreibung der Reaktionen herzuleiten ohne gängige Näherungen für die Kinematik der Nukleonen zu verwenden. Weiter sollen die Ausdrücke eine genauere Beschreibung der schwachen hadronischen Ströme inklusive des sogenannten schwachen Magnetismus enthalten, ohne dass dies zu einem Anstieg des numerischen Aufwands führt.

Im ersten Abschnitt dieser Arbeit werden entsprechende Ausdrücke, insbesondere für die *inverse mittlere freie Weglänge* (IMFP), für mehrere Neutrinoreaktion hergeleitet. Dabei handelt es sich im Einzelnen um die folgenden Reaktionen: Absorption von ν_e an Neutronen; Absorption von $\bar{\nu}_e$ an Protonen; inverser Neutronenzerfall; inverser Myonenzerfall; Umwandlung von $\bar{\nu}_e$ und Elektronen in $\bar{\nu}_\mu$ und Myonen; Absorption von ν_μ an Neutronen; Umwandlung von ν_μ und Elektronen in ν_e und Myonen. Dafür werden zuerst die entsprechenden Matrixelemente hergeleitet, wobei die Abhängigkeit der schwachen Kopplung und der hadronischen Kopplungskonstanten vom Impulsübertrag aufgrund der vergleichbar kleinen Energieskalen im PNS vernachlässigt wird. Die starke Wechselwirkung bei hohen Dichten wird im Rahmen der *relativistischen mittleren Feldtheorie* (RMF) durch starke Wechselwirkungs-Potentiale berücksichtigt. Diese Herleitungen reproduzieren frühere Ergebnisse aus der Literatur und erweitern diese, so dass sie zusätzliche Korrekturen für endliche Massen und die starken Wechselwirkungs-Potentiale enthalten. Basierend auf diesen Matrixelementen werden dann Ausdrücke wie der IMFP für Absorptionsreaktionen oder Streu-Kerne für Streureaktionen ermittelt. Diese Berechnungen berücksichtigen die exakte Kinematik aller Teilchen. Beiträge des schwachen Magnetismus sind ebenfalls in allen Ordnungen enthalten. Die resultierenden Ausdrücke werden entweder zum ersten mal explizit hergeleitet oder sind präziser als die meisten vergleichbaren Ausdrücke in gegenwärtigen CCSN-Simulationen, ohne größeren numerischen Aufwand zu erfordern. Dieser Teil der Arbeit ist in zwei Abschnitte gegliedert, einen für rein leptonische Reaktionen und einen für Wechselwirkungen zwischen Neutrinos und Nukleonen.

Im Anschluss an diese rein analytischen Herleitungen werden im zweiten Teil der Arbeit die Transportgrößen für die Bedingungen in einem PNS numerisch berechnet. Zu diesem Zweck werden Materieprofile und Neutrinospektren aus einer 1-dimensionalen, allgemein relativistischen, hydrodynamisch CCSN-Simulation mit Boltzmann-Neutrino-Transport herangezogen. Die Bedeutung der neuen Reaktionen wird verglichen mit einem Standard-Set von Neutrinoreaktionen, welches für gegenwärtige Supernova-Simulationen repräsentativ ist.

Für $\bar{\nu}_e$ stellt sich der inverse Myonenzerfall als eine wichtige Reaktion bei Neutrinoenergien unterhalb $5 - 10\,\mathrm{MeV}$ während der ersten Sekunde nach Bildung der Stoßwelle heraus. Ähnlich ist der inverse Neutronenzerfall eine wichtige Reaktionen bei den gleichen Energien für die Zeit nach mehr als einer Sekunde. Dies liegt daran, dass die Entkopplungsregion in Folge der

Kühlung und Deleptonisierung des PNS zu Dichten oberhalb von $10^{13}\,\mathrm{g/cm^3}$ wandert. Dort ist die Energiedifferenz zwischen Neutronen und Protonen durch die starke Wechselwirkung deutlich vergrößert, was zu einer starken Unterdrückung der Absorption von $\bar{\nu}_e$ an Protonen im Vergleich zum inversen Neutronenzerfall führt. Für die Entkopplung von Myonneutrinos findet man, dass die Absorption an Neutronen nur bei sehr hohen Energien oberhalb $95\,\mathrm{MeV}$ entscheidend ist. Im Bereich darunter bis zu Energien zwischen $30-50\,\mathrm{MeV}$ ist die Umwandlung von ν_μ und Elektronen in ν_e und Myonen eine wichtige inelastische Reaktion, vergleichbar in der Rate mit Neutrinostreuung an Elektronen. Für niedrige Neutrinoenergien unterhalb $5-10\,\mathrm{MeV}$ findet man schließlich das der inverse Myonenzerfall in der ersten Sekunde für ν_μ ähnlich wichtig ist wie für $\bar{\nu}_e$.

Dementsprechend kommt man zu dem Schluss, dass schwache myonische CC-Reaktionen und der inverse Neutronenzerfall in dynamische CCSN-Simulationen implementiert werden sollten. Es wird erwartet, dass dies zu einer Änderung der Spektren von $\bar{\nu}_e$ und ν_μ führt. Weiterhin koppeln diese Reaktionen unterschiedliche Neutrinospezies auf eher asymmetrische Weise. So kann z.B. ein hochenergetisches $\bar{\nu}_e$ tief im Kern in ein niederenergetisches $\bar{\nu}_\mu$ umgewandelt werden. Letzteres kann aufgrund seiner vielfach größeren freien Weglänge ungehindert entweichen und beeinflusst damit die Deleptonisierungsrate. Ein analoges Argument gilt für die Umwandlung hochenergetischer ν_μ in niederenergetische ν_e. Aufgrund der vielen Feedback-Mechanismen die in einer Supernova aktiv sind ist es jedoch nahezu unmöglich das Ausmaß der Änderungen in den Spektren mit einer an die Simulation nachgelagerten Berechnung wie im Rahmen dieser Arbeit zu bestimmen.

Die Relevanz myonischer Reaktionen führt auch dazu, dass Myonen schon zu einem sehr frühen Zeitpunkt während der Supernova auftreten. Die genau Häufigkeit der Myonen und mögliche Konsequenzen für die Neutrinoemissionen sind jedoch auch hier ohne eine dynamische Simulation schwer vorherzusagen.

Weiter wird die Implementierung des schwachen Magnetismus in dieser Arbeit mit genäherten analytischen Korrekturfaktoren verglichen, die gegenwärtig in CCSN-Simulationen Verwendung finden. Dabei stellt sich heraus, dass für Neutrino-Transport bei hohen Dichten in PNS der Effekt des schwachen Magnetismus durch solche Korrekturfaktoren nur unzureichend beschrieben wird.

Zusammenfassend lässt sich festhalten, dass die Implementierung der neuen Reaktionen und der verbesserten Transportausdrücke in dynamische CCSN-Simulation empfohlen wird. Nur so kann der mögliche Einfluss auf die Explosions-Dynamik, auf die Deleptonisierung und Kühlung eines PNS und auf die Neutrinospektren verlässlich und aussagekräftig bestimmt werden.

Danksagung

Mein Dank geht zuallererst an meinen Betreuer Gabriel Martínez-Pinedo. Ich danke ihm für die Möglichkeit in seiner Gruppe in einem so exzellenten Rahmen meinen persönlichen Forschungsinteressen nachgehen zu können. Seine Tür stand mir zu jedem Zeitpunkt offen und für jede meiner Fragen wusste er eine hilfreiche Antwort. Auch im universitären Umfeld stellt das keine Selbstverständlichkeit dar und ich weiß diesen Umstand äußerst zu schätzen. Darüber hinaus war seine tiefe Faszination für die Fragen der Physik mir Antrieb und Vorbild. In meinem Arbeiten hat er mich angeleitet und motiviert wo es angebracht war und mir darüber hinaus die Freiheit gelassen meinen eigenen Weg zu finden.

Gleicher Dank geht an meinen weiteren Betreuer Bengt Friman. Auch er stand mir zu jeder Zeit mir Rat zu meinen Fragen, gleich welcher Art, zu Seite. Für meine Probleme hatte er stets Verständnis und er hat mir einige wertvolle Anreize geliefert, die in den Ergebnissen dieser Arbeit gefruchtet sind. Die Betreuung durch ihn habe ich zu jeder Zeit als äußerst angenehm und respektvoll empfunden.

Ein besonders großer Dank geht dann an Tobias Fischer. Ohne ihn wäre ich nicht nach Darmstadt gekommen, ohne ihn hätte ich mein Thema vielleicht nie gefunden, und ich hätte sicher nicht all die wertvollen Kontakte in der akademischen Familie geknüpft, die mir heute so teuer sind. Gerade in der ersten Zeit meiner Promotion hat er mir geholfen mein Gebiet besser zu verstehen und mir ein echtes Arbeitsfeld herauszuarbeiten. Außerdem wäre meine Zeit in Darmstadt ohne ihn um die Hälfte aller guten Anekdoten ärmer. Danke dafür.

Von meinen Kollegen möchte ich besonders Lutz Huther, Joel Mendoza-Temis und Heiko Möller danken. Sie waren meine Begleiter und manchmal auch Leidensgenossen über die längste Zeit dieses Weges. Sie haben mir als Neu-Darmstädter geholfen mich im neuen Umfeld zurechtzufinden. Der Austausch mit Ihnen, gleich ob wissenschaftlich oder alltäglich war mir sehr wertvoll. Wir haben uns über die Jahre gemeinsam weiterentwickelt und ich bin froh bei so guten Menschen Freundschaft gefunden zu haben. Danke auch an Meng-Ru Wu, besonders für seine fachliche Expertise, mit der er mir gerade in der Endphase der Arbeit immer wieder zur Seite stand. Aber natürlich gilt der Dank auch allen anderen meiner Kollegen, die mich über die Jahre begleitet haben. Danke für die gemeinsame Zeit; für die Kart-Rennen bei denen sie mich vorgelassen haben; für heitere Abende; und für all die Gespräche über Physik, über Fußball, über Politik, über gutes Essen und Deutsches Essen, über die Leiden der Prokrastination und über alles alltägliche. Danke für die gemeinsame Zeit.

Danke unseren DSA-Freunden, die in all den Jahren an unserer Seite waren. Danke für all die Stunden in anderen Welten oder bei guten Gesprächen und für alles gemeinsam erlebte. Danke auch allen anderen Begleitern der letzten Jahre, wie z.B. den kickenden Physikern und allen die ich vergessen habe.

Ich danke meinen Eltern für Ihre Liebe und dafür, dass Sie mir immer das Gefühl geben den richtigen Weg zu gehen. Meinen Schwiegereltern danke ich für unschätzbar wertvollen Rat in nahezu unbegrenztem Umfang und für vielfache tatkräftige Unterstützung.

Meiner ganzen Familie gilt der Dank dafür, dass sie immer wieder einen wichtige Hilfe waren auf dem Weg dies alles zu erreichen.

Der allergrößte Dank aber gilt meiner Frau, meiner besten Freundin und Seelengefährtin, meiner Nina. Ich bin was ich bin und wo ich bin wegen Ihr. Sie liebt mich unbedingt. Sie hat immer Verständnis, egal ob ich es verdiene oder nicht. Sie unterstützt mich bei allem was ich tue so gut es nur jemand kann. Wann immer der Druck besonders groß war hat sie sich hintenangestellt und die Last mit mir geteilt. Ich habe ihr all das sicher nicht immer einfach gemacht und ich bin ihr unendlich dankbar für alles. Wir sind diesen Weg bis hierhin gemeinsam gegangen und so werden wir ihn weitergehen.

Loves you soo much, und mehr als alles andere.

Contents

1. Introduction

Neutrinos interact by one of the basic forces of nature, the weak interaction. Understanding and observing the behaviour of neutrinos can thus tell us about this basic force. However, the weak interaction has its name for a reason. One finds neutrinos as particles of most elusive kind. Of all particles that are known to us they are the ones that are the least likely to react with anything else. Every second tens of billions of neutrinos pass through each square centimeter of the Earth's surface (and our skin's) and cross the whole Earth (and our body). Yet we are completely unaware of this as almost none of them will interact with us. It is this property which makes them as interesting as a probe as they are a nuisance. For instance, in particle physics most experiments measure neutrinos by observing the fact that they are not there. If some energy is missing that is not found in any of the detectors then it was probably carried away by a neutrino. Likewise, the active observation and measurement of a neutrino requires major efforts, patience, and huge detectors. But this is also the origin of their relevance in astrophysics. In general, neutrinos can be messengers from the deepest regions of stars where nuclear burning takes place. In this way they helped us to understand the nuclear burning processes that power our Sun. Even though most life on Earth thrives in some way on the energy of solar light, for a long time it was not known what made the Sun shining. The Sun's light itself consists of photons from the photosphere, a layer at the surface of the Sun. After nuclear forces were discovered a century ago, it was speculated that nuclear fusion reactions in the core of the Sun are the source of thermal energy. Later it was understood that these reactions would also result in the production of neutrinos. Once emitted, most of these neutrinos would leave the Sun and could later be detected on earth. And so it happened eventually in the famous Homestake neutrino experiment. Not only could it qualitatively confirm the theory of neutrino production by nuclear fusion in the Sun, but one could actually quantify the neutrino flux and compare it against theoretical models of stellar burning to great success. On top of that, the very same measurement gave the first hint at the phenomena of neutrino oscillations. These neutrino oscillations are among the prime examples of physics that cannot be explained within the famous Standard Model. This serves to underline the important role that research on astrophysical neutrino signals has today and will have in the future. The corresponding questions gave rise to the field of neutrino astronomy, where one uses huge underground tanks, the polar ice, or the water of the ocean as detectors.

Understanding supernova explosions is another big field of astrophysics that is very much concerned with the measurement of neutrinos. Just like for the Sun, a part of this connection stems from the fact that only neutrinos (besides possibly gravitational waves) can probe the dynamics of the collapse and explosion in the cores of supernovae. Thereby neutrinos could also be microscopes into some of the most extreme states of elementary matter that can be
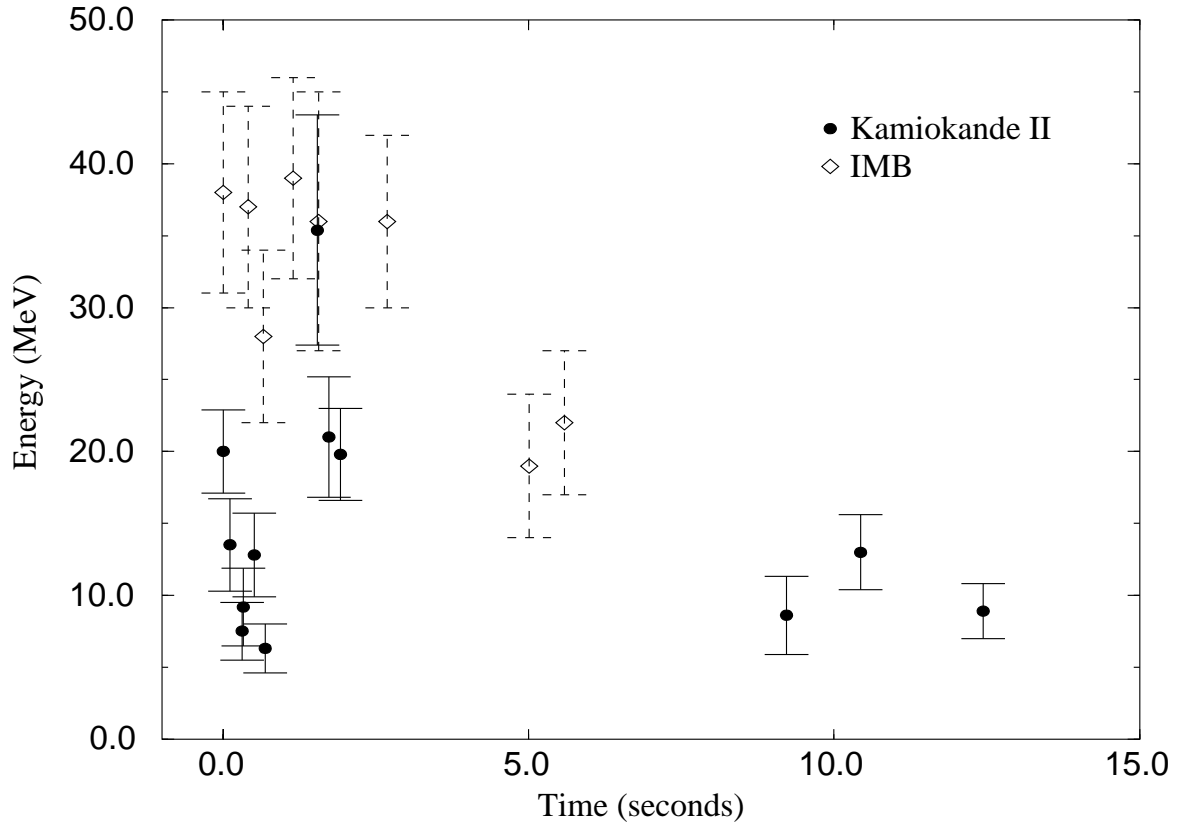
Figure 1.1.: Neutrino signal from SN1987A. Measured neutrino energies are plotted vs. arrival time after beginning of signal.

encountered in the universe. However, the role of supernova neutrinos goes beyond this. It was predicted that most of the energy of a core collapse supernova will be released in neutrinos. In the young protoneutron star that forms by the collapse of a massive star, the temperature and density are so extremely high that neutrino emission is by far the most efficient cooling process. The core will actually be so dense that not even the neutrinos can leave it immediately all at once. Instead, theory predicts a particular neutrino light curve that would be observed from a core collapse supernova. It took until the event of the famous supernova 1987A to measure the first (and up to now only) supernova neutrino signal by several experiments all over the world. Even though only a few dozen neutrinos were measured, the signal was showing a striking quantitative agreement with models. It encouraged scientists that their principle understanding of these most violent events in the universe was correct. At that time it was already clear that the actual understanding of core collapse supernova explosions would be a fine-tuning problem of neutrino transport in the protoneutron star. This problem has not been fully solved today, although in recent years the answer looks to become clear.

There are further fundamental questions coupled to supernova neutrinos. Researchers discuss the possibility of heavy element nucleosynthesis in supernovae. The corresponding scenario depends crucially on the spectra of several neutrino flavours. Also, supernova neutrinos could undergo oscillations similar to the ones in our Sun, observations of which would enlarge our view on new physics. Eventually, neutrino signals from supernovae would probably carry information about the state of matter at nuclear density and about the nuclear interaction itself.

1.1. Core-Collapse Supernovae

This section will focus on the scenario of an Iron *core-collapse supernova* (CCSN). At the end of their lifetime many massive stars have lost much of their material through stellar winds and expulsion of their extended envelope. What is left is a star that contains all the products of different stages of stellar burning i.e. nuclear fusion in stars. The material is almost sorted in different layers, each of them dominated by different nuclei. On the surface is a small layer of Hydrogen, followed by Helium and then subsequently the heavier metals Carbon, Oxygen and Neon. In the center one finds Silicon and inside the Silicon layer there is eventually the Iron core. This picture is often coined as the onion shell structure of massive stars. It is illustrated in Figure 1.2
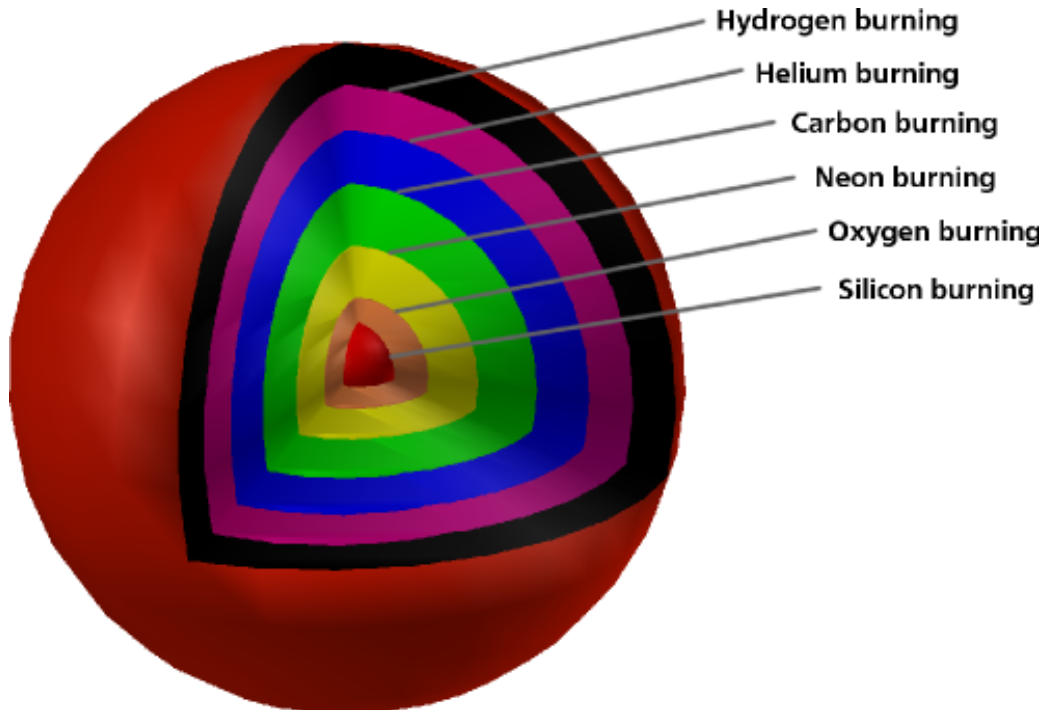
Figure 1.2.: Onion shell structure of massive star at the end of its lifetime. Elements are sorted, with the lightest outside and the heaviest in the center. In the Silicon layer eventually the Iron core forms. At the inner boundary of each layer shell burning frequently takes place and contributes more mass to the subsequent layer.

The Iron core itself cannot undergo further fusion. The reason for this is that the nuclear binding energy reaches a maximum for nuclei in the Iron group. In particular, ^{62}Ni is the chemical element with the largest binding energy per nucleon. The behaviour of the binding energy curve is very well approximated by the semi-empirical Bethe-Weizsäcker mass formula which describes nuclei as drops of incompressible nuclear fluid. The resulting binding energy curve is shown in Figure 1.3. The pressure in the Iron core is very high and so is the temperature, it exceeds 5 billion Kelvin (or $0.5\,\mathrm{MeV}$). Under this conditions nuclear matter is in *nuclear statistical equilibrium* (NSE), an equilibrium between photodisintegration and strong interactions. All nuclei heavier than Iron are strongly suppressed because of their smaller binding energy and no nuclear fusion occurs that would release new energy. Without sufficient radia-

tion pressure from fusion, the Iron core contracts under gravity until it is stabilized by electron degeneracy pressure due to Pauli blocking. At the bottom of the other layers contraction will frequently trigger shell burning. The shell burning will increase the amount of more massive metals inside. This will lead to a growth of the Iron core. However there exists a maximum mass of the Iron core that can be stabilized by the degeneracy pressure of electrons. It is called the Chandrasekhar mass M_{Ch}. This limit lies close to $1.44\,M_\odot$, the exact value depends on the electron fraction Y_e in the core. Once the Iron core becomes heavier than this limit, the degeneracy pressure of the electron gas can no longer withstand the gravitational pull. Consequently the core starts to contract beyond a stable configuration, causing the temperature to rise further. Eventually it will heat up to $\sim 1\,\mathrm{MeV}$. At this point NSE favours a partial photodissociation of some of the Iron into alpha particles. This is an endogenous process, taking away further energy from the core. Also, when contraction starts, the electron chemical potential rises. Electrons are then absorbed onto heavy nuclei. The neutrinos created in these electron captures leave the star since their cross section with matter is still very small for the present densities. Hence the core deleptonizes and the electron abundance decreases. As a consequence the pressure against gravity decreases, too, and the contraction accelerates. This feedback evolves into a runaway situation and the contraction becomes a collapse. The core falls inward almost freely. The velocity is supersonic at nearly a quarter of the speed of light [1]. If the core is not too massive, the collapse comes to a halt when matter reaches densities
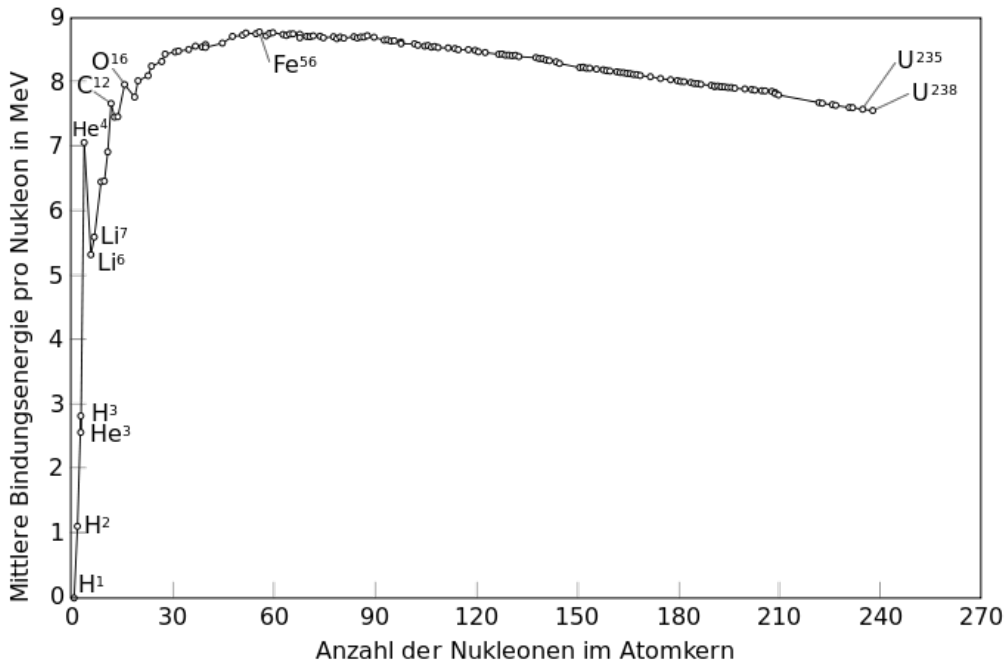
Figure 1.3.: Average binding energy per nucleon

above the nuclear saturation density. At this point the nuclear interaction becomes strongly repulsive and the nuclear *equation of state* (EOS) stiffens. The idea that the core collapse of a degenerate star is the birth of a neutron star was first brought up already in 1934 [2]. Initial works in the early sixties realized that the gravitational collapse releases a huge amount of gravitational binding energy $E_G > 10^{53}\,\mathrm{erg}$. It was expected that part of this energy should

be able to trigger the explosions which astronomers observed as supernovae [3]. At the same time first simulations of the gravitational collapse found that the forming neutron star will bounce back at nuclear densities. Since the outer core will still fall inwards, this will launch a shock that will propagate outwards into the outer layers. This could reverse the in fall of the outer layers and make them gravitationally unbound [4, 5]. But it was also understood that most of the gravitational binding energy would be emitted in the form of neutrinos. It was further found that without additional help the initial shock would eventually stall. The shock must overcome the large mass inflow that gets accreted on the *protoneutron star* (PNS) from the outer shells. Upon shock passage all heavy nuclei in the accretion flow are dissociated into nucleons due to the large temperatures in the shocked region. Yet, these reactions are endogenous and drain too much of the shock's energy to allow for an explosion. It will be stuck at a radius $R \sim 100\,\mathrm{km}$ after a few $100\,\mathrm{ms}$. However, if only a small fraction of the neutrinos (on the order of 1%) can be captured above the surface of the PNS, this will deposit enough energy to revive the shock and trigger an explosion [6]. Since then the study of CCSNe was, among many other things, always also a question of fine-tuning neutrino transport.

1.1.1. Explosion Mechanism

Today still the favoured mechanism to explode a CCSN is the delayed neutrino-heating mechanism, discussed by Bethe & Wilson [7]. During the collapse phase the density increases so high that even neutrinos become trapped in the matter. This is mainly due to elastic neutral-current scattering on nucleons [8, 9, 10] and charged-current absorption on neutrons. The neutral-current reaction channels affect all neutrino flavours, including those that are thermally created. However, after the PNS has formed there is a certain density region where the mean free path of neutrinos grows large enough for them to become gradually untrapped again and diffuse out of the star [11]. This region is called the neutrinosphere. At even lower density neutrinos become eventually free streaming. When the shock passes through the PNS, the matter is heated up into NSE. Under these conditions a large neutron fraction is energetically favoured. Thus many electrons will be captured on protons, producing a large amount of electron neutrinos. However, these neutrinos are trapped, too, as long as the shock progresses through the high density region inside the neutrinosphere. Once the shock crosses the neutrinosphere (before it stalls), the neutrinos from transition to NSE at lower densities can immediately escape. Consequently a large initial pulse of neutrinos is emitted. Afterwards there emerges a region where the cooling of matter due to neutrino emission and the heating due to absorption of neutrinos from further inside are in equilibrium. This region is called the *gain radius* R_g [7] and it lies below the stalled accretion shock. Outside R_g up to the *shock radius* R_s the matter is heated by neutrinos. In the delayed explosion mechanism this heating transports enough energy to the shock to revive it. However, for Iron core progenitors the problem is that the dynamics are so complicated that sophisticated multidimensional simulations are required. As a consequence 1D simulations of CCSNe fail to explode. In multidimensional simulations, non spherical hydrodynamic instabilities develop. They cause matter to be heated more efficiently. Of special relevance is convective overturn through Raleigh-Taylor instabilities

that form in the convectively unstable heating region [12, 13, 14, 15]. Another important mode is the *standing accretion shock instability* (SASI) with its sloshing motion [16]. The underlying instability is thought to be an advective-acoustic cycle [17, 18]. Modeling of these mechanisms is essential for the success of the neutrino-heating mechanism [19, 20]. In recent years several groups were finally able to achieve exploding CCSNe in 2D [21, 20, 22, 23, 24, 25, 26]. However their exact results differ, as do the details of their numerical simulations. Different approaches were undertaken with respect to neutrino transport, gravity treatment and the set of weak interactions. This led to calls for code comparisons to identify sensible ingredients of the simulation [27].

Alternative models to explode a CCSN are the *magnetohydrodynamic* (MHD) approach (e.g. [28]), an acoustic mechanism [21, 29], and a nuclear phase transition in the PNS to quark matter [30, 31].

1D models, even though they cannot achieve exploding CCSNe without parametric adjustments such as artificial heating, can be powerful tools to investigate certain properties of supernovae. This holds especially for the time after shock release when the region above the PNS is very well approximated by spherical symmetry again. For the special case of an *electron-capture supernova* (ECSN) the situation with respect to shock revival appears to be less critical. The progenitor stars of ECSNe are probably massive AGB stars. They are eventually not massive enough to trigger fusion stages beyond Carbon burning. ECSNe represent thus the low mass limit of collapsing stars. Their core consists of O-Ne-Mg [32, 33, 34]. Just as the Iron core in a CCSN progenitor or matter in a white dwarf, it is stabilized by electron degeneracy pressure. The Neon and the Magnesium have a low threshold towards electron capture, thereby decreasing the pressure. Hence, once these reactions start to happen, a gravitational runaway evolves, very similar to the collapse of an Iron core, including bounce and shock formation. A special feature of the O-Ne-Mg core is the very steep drop of density in the C-O shell. As a consequence the mass accretion on the shock fades sufficiently fast to allow for a continuous shock expansion. This presents ideal conditions for neutrino heating and therefore ECSNe are found to explode even in 1D simulations, without need for hydrodynamical instabilities [35, 36, 37]. Such simulations predict rather low explosion energies $\sim 10^{50}$ erg and Nickel ejecta of only several $10^{-3} M_\odot$. These results compare nicely with observations of the famous historical Crab SN [38, 39]. It is estimated that 20%-30% of all SNe could be ECSNe [40, 39].

1.2. Nuclear Equation of State

The previous section made clear that a precise understanding of the hydrodynamics of hot and dense matter and of its interactions with neutrinos is required to achieve a successful supernova explosion. The study of high density nucleonic matter is non trivial, as the densities that are present in a PNS cannot be easily obtained in the laboratory, if at all. The next generation of heavy ion colliders such as the FAIR facility might be able to investigate matter under such extreme conditions. Until then there are only certain boundaries on the behaviour of dense matter in limiting cases, such as the binding energy at nuclear saturation density.

Theory suggests that a large variety of phases can be encountered, depending on how dense

exactly the matter is. For example, one expects that close to the surface of neutron stars, protons form a regular crystal lattice and the electrons move as clouds between them, similar to the situation in metals. Also, meson condensates could emerge at higher densities, e.g. pion or kaon condensates, or the matter could contain a significant amount of hyperons. Eventually, the constitution of the matter that gets advected onto the shock depends sensitively on the structure of the progenitor star and therefore its precise evolution up to the collapse. However, it turns out that nearly all these differences vanish in a hot PNS. They key here is the large matter temperature after shock passage. As noted repeatedly before, above $T = 0.5\,\mathrm{MeV}$ matter is in NSE. The interior of a PNS is well above this threshold with temperatures reaching up as high as several tens of MeV. Under this condition, almost all theories predict that nuclei disappear. The only thing that remains are nucleons, i.e. neutrons and protons, as well as electrons, all mixed homogeneously to build a uniform matter. An exception is the possibility of the so called pasta phase [41], which could survive at somewhat higher temperatures. In it the nucleons are not homogeneously distributed, instead the different species clump together to build macroscopic structures. While in principle the pasta phase could significantly affect neutrino transport, it is strongly discussed whether it really would survive the large temperatures in the first seconds after core bounce. It is also questioned whether the pasta phase would extend large enough in space to be actually felt by the neutrinos. If the size of the pasta phase is small compared to the neutrino mean free path, the neutrinos will not see the substructure. Another alternative to nucleonic matter is a phase transition to quark matter at high densities. Yet, this is such a distinct scenario that it will not be covered in this work. Also, quark matter is expected to emerge only above saturation density, while the most relevant regions for neutrino transport are initially below saturation density. In general it has to be noted that for the regime above nuclear saturation density the uncertainties are larger, yet this region is mostly irrelevant for the studies in this work.

Coming back to the established picture of nucleons and electrons, the state of matter is still not sufficiently constrained. The main culprit here is the uncertain nature of the strong interaction between the nucleons. There are a variety of differing models to describe this force. Also, once a model is chosen one still has to compute the actual thermodynamical and chemical properties of matter. That means one has to derive the corresponding equations of state. The EOS contains all the relations between the main thermodynamical properties. It tells us e.g. how large the pressure is for a given density and temperature; how many protons are present in a state of chemical equilibrium; what is the speed of sound and how viscous is the nucleonic fluid? For neutrino transport, one is particularly interested in the dispersion relations and distribution functions of the particles. This corresponds especially to quantities such as the chemical potentials or interaction potentials.

Historically, there were mainly two nuclear EOS that are implemented in CCSN simulations, namely those of Lattimer & Swesty (LS) [42] and of Shen and collaborators [43]. Since then the number of nuclear EOS that are tabulated or formatted in a suitable way for CCSN has grown [44, 45, 46, 47]. They cover a wide set of parameters and phenomenological properties.

The question for the correct EOS for CCSNe is one with different aspects. The first question is what is actually the most precise description of dense nuclear matter? Practically all of

the available EOS reproduce certain experimental observations. In particular they achieve the correct binding energy and the correct saturation density for nuclear matter. But beyond that many further constraints have meanwhile arisen from theory, experiment and astronomical observation. For example, a nuclear EOS that describes the matter in a hot PNS should be able to support the maximum neutron stars masses that are observed. This limit lies currently at $\sim 2 M_\odot$ [48, 49]. Also, recently constraints emerged on the radius of neutron stars from a wide range of observations and statistical analysis [50]. The EOS should then be able to agree with these findings, too. Relevant and precise theoretical constraints at low density arise e.g. from recent calculations of the neutron matter EOS in *chiral effective field theory* (CEFT) [51, 52].
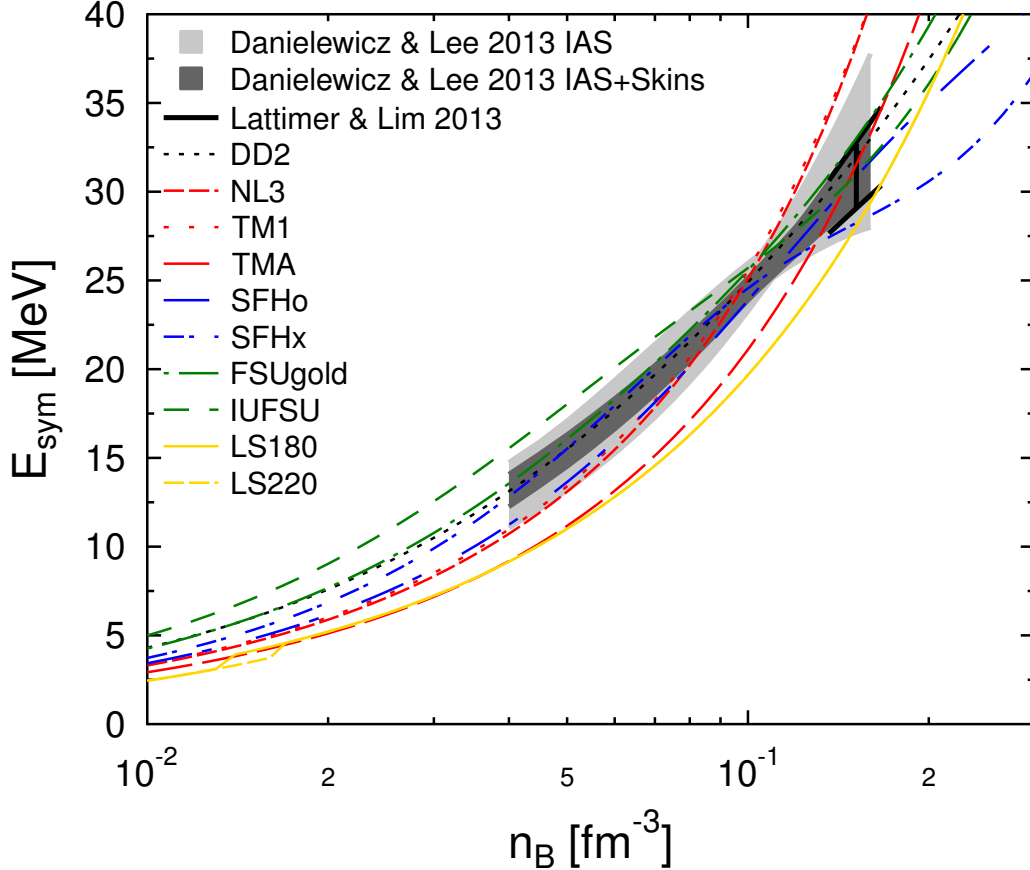
Figure 1.4.: Constraints on nuclear symmetry energy from isobaric analog states (IAS) and neutron skin thickness (NS) [53, 54]. The constraints are depicted as gray boxes, compared against a set of RMF-EOS. Figure courtesy of M. Hempel.

Eventually, all of these observations and many other independent experiments and calculations also put boundaries on the nuclear symmetry energy $S(n_B)$ (for a review and summarizing analysis see [54]). As one example out of many, Figure 1.4 shows constraints on the symmetry energy from isobaric analog states and neutron skin thickness [53, 54], compared to predictions from various EOS [44]. The symmetry energy is the difference between the bulk energy per nucleon in pure neutron matter ($Y_p = 0$) and in isospin symmetric matter ($Y_p = Y_n = 0.5$). One can write down an expansion of the bulk energy per baryon $e(n_B, Y_p)$ for a given baryon density n_B and a proton fraction Y_p, around the symmetric configuration $Y_p = 1/2$

$$e(n_B, Y_p) = e(n_B, 1/2) + S_2(n_B) \left(1 - 2Y_p\right)^2 + \text{higher order terms.}$$

Note that there is no linear expansion coefficient as the expressions has to be symmetric in neutron-to-proton excess. In a common approximation the terms in higher order of neutron excess are dropped. The symmetry energy is then equivalent to the lowest order expansion coefficient $S(n_B) = S_2(n_B)$ (for densities above nuclear saturation density this approximation has to be used with care [55]). The two parameters of the symmetry energy that are constrained the most are the lowest order parameter S_ν and its slope L_ν at nuclear saturation density n_0, which are defined by

$$S_\nu = S_2(n_0) \qquad \text{and} \qquad L_\nu = 3n_0 \left. \frac{dS}{dn} \right|_{n_0}.$$

Of the EOS that are available for CCSNe most are adjusted to agree nicely with certain constraints but might not agree as well with others. It is no surprise that especially the traditional LS and Shen EOS fail to reproduce several experimental results that were found after these EOS were calculated. At this point one has to note that most EOS which are considered for core collapse supernovae are based on *relativistic mean field theory* (RMF). The idea of RMF is to describe the nuclear interaction by an effective coupling of nucleons to meson fields. These meson fields are incorporated into the Lagrangian of the system so the interaction is intrinsically Lorentz invariant (*Relativistic*). One approximates then the meson fields by their mean values (*mean field*). An RMF-EOS builds on this basis to derive the thermodynamical and chemical properties of the matter.

The next important question for choosing an EOS is, which properties of the EOS are crucial for the evolution of a CCSN? First comparisons of the impact of different EOS were made in 1D simulations between the rather soft LS180 EOS and the stiffer Shen EOS. Quantitative differences in properties characterizing collapse, bounce, and early post bounce evolution were found not to exceed a range of 5% to 25% [56, 57, 58]. This behaviour was coined as Mazurek's law. It states that changes in the microphysics of collapsing stellar cores are moderated by strong feedback mechanisms between the different ingredients of CCSNe simulations [59]. This seeming insensitivity of the early shock phase to the properties of the EOS near saturation density also holds for the new set of EOS [58]. As long as the EOS does not disagree too strongly with the current constraints, there seems to be no impact in the early stage. However, the situation changes at later times. Especially for neutrino diffusion out of the dense matter, the particular choice of an EOS can matter a lot. As will be discussed in the next section, the spectral properties of neutrinos are determined in the region where they decouple. After the shock revival, at the timescale of several $100\,\mathrm{ms}$ up to seconds, the decoupling region moves towards large densities above $10^{12}\,\mathrm{g/cm^3}$. There, the strong interaction starts to be important for the description of weak interactions. Hence, different nuclear EOS could in principle result in different neutrino spectra. It can be easily understood (and will be discussed in detail later) that especially the important charged-current reactions for ν_e and $\bar{\nu}_e$ are particularly sensitive to the energy difference between neutrons and protons. This energy difference has a very close relationship to the symmetry energy. As an example, the chemical difference between neutrons and protons in nuclear matter can be expressed in terms of $S(n_B)$ [60]

$$\mu_n - \mu_p = 4S(n_B)\left(1 - 2Y_p\right).$$

With this relation one can further connect the symmetry energy to the chosen microscopic description of nuclear matter that the determines the chemical potentials μ_n and μ_p. The interaction potentials and the chemical potentials from an EOS are among the most relevant parameters for the calculation of neutrino transport. Figure 1.5 illustrates this issue by comparing the inverse mean free path for absorption of electron neutrinos on neutrons for different EOS. In all cases the temperature, density, and composition agree. Yet the inverse mean free path can differ by a factor of 3-5 or even more.
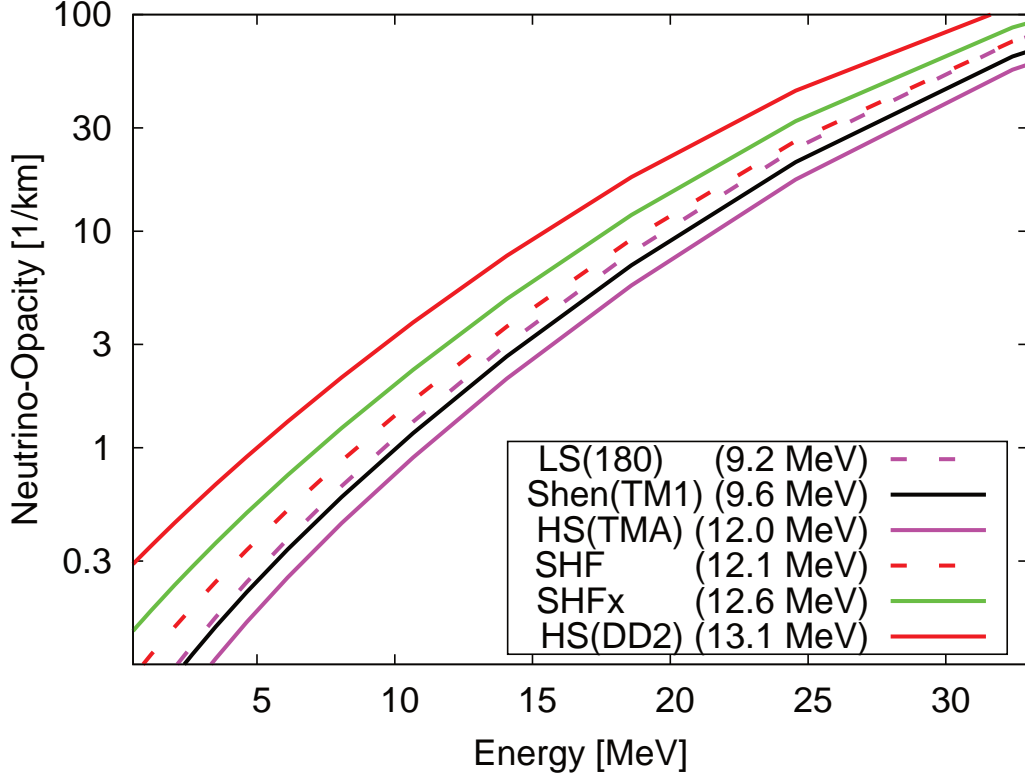
Figure 1.5.: Inverse mean free path for absorption of ν_e on neutrons for various RMF-EOS. Evaluated at $T = 7.4\,\text{MeV}$, $\rho = 2.1 \times 10^{13}\,\text{g/cm}^3$, $Y_e = 0.035$. EOS are from Shen [43], Lattimer&Swesty (LS)[42], and various parameter sets from Hempel [44]. The number in brackets indicates the value of the nuclear symmetry energy at the given conditions.

It was recently emphasized that it is important to correctly implement the EOS-dependence of this energy difference into the neutrino transport [61, 62, 63]. For reliable predictions of neutrino spectra one should then choose an EOS that shows good agreement with the constraints on the nuclear symmetry energy. Such an EOS is e.g. the DD2-EOS [64]. It compares nicely against many of the aforementioned constraints. It is an RMF-EOS with the correct limiting behaviour at high and at low densities. For low density it reproduces the model-independent virial EOS [65]. Furthermore it contains light clusters as explicit degrees of freedom.

1.3. Neutrino Transport and Neutrino Signals

It was stated already that neutrino transport is such a crucial aspect of CCSNe because neutrinos become trapped in the high density matter. Deep in the PNS, the mean free path of

neutrinos is so short that they are in thermal and chemical equilibrium with the matter. Moving outwards, the density decreases and the mean free path increases until neutrinos can leave the system. This process is very sensitive to the particular energy and one expects that neutrinos of different energies decouple at different densities. Right after shock break out, when temperatures are the highest, the decoupling region of electron neutrinos extends down to 10^{11} g/cm^3 and lower. When the PNS gradually cools down, the mean free paths become larger for a given density as average energy decreases and the decoupling region moves inwards. The phenomena of neutrino decoupling can be approximately described by the concept of the neutrinosphere. It states that neutrino spectra almost behave as thermal radiation emitted from the neutrinosphere. The position of this decoupling region is in general different for all neutrino flavours, and it varies with the neutrino energy. This is because the neutrinosphere is determined by the interactions of neutrinos with matter, which also differ for varying flavours and energy.

Discussing now the different neutrino reactions, one first has to know that the matter in the PNS is very neutron rich. Consequently, protons are more bound than neutrons, similar to the situation in a neutron rich nucleus. For ν_e, one knows then that absorption on neutrons is the dominant reaction in the hot PNS. Neutrons are very abundant target particles and the conversion into a proton always releases energy. For $\bar{\nu}_e$ this picture is more complicated. The absorption on protons is an important reaction as well, yet there are less protons than neutrons. Also this reaction requires energy to convert the proton into a neutron. The latter is a problem especially for low energy $\bar{\nu}_e$, as they decouple from higher densities where the difference in strong interaction potentials adds up on the mass difference. Consequently the neutral current scattering off of neutrons is similar as important as the charged current absorption on protons. Eventually, for μ- and τ-flavour neutrinos charged current reactions are considered negligible. Their main interaction proceeds via scattering on neutrons and protons, and scattering on electrons. Already from this simple picture it becomes clear that the ν_e, having the highest interaction rates with matter, decouples further outside than the $\bar{\nu}_e$. The heavy flavour leptons will then for the same reason decouple even further inside. As the spectral properties are determined by the decoupling region, and the temperature is higher at larger densities, one will expect the average neutrino energies to follow the order $\langle \epsilon_{\nu_e} \rangle < \langle \epsilon_{\bar{\nu}_e} \rangle \lesssim \langle \epsilon_{\nu_x} \rangle$. It is predicted that this spectral behaviour should be observable for a next SN comparable to the famous SN1987A. At the current level of understanding many processes in a SN are sensitive to the detailed value of average energies and their differences. It is then necessary to describe the neutrino interactions at the required precision. This means to include subleading terms in the main reactions, such as weak magnetism [66]. It also means to make sure, that all relevant reactions are considered. These are precisely the two questions that are addressed in this work and they will be discussed in more detail in the main body. In particular it will be assessed, whether certain reactions that are negligible at the initial neutrinosphere position, might become relevant once the sphere moves to high densities where differences in energy for neutrons and protons become larger. For example, it is expected that, due to temperatures and chemical potentials of several tens of MeV, neutrinos will be able to overcome the threshold of muon production. Yet it is unclear up to now whether these reactions are relevant for neutrino decoupling. This question will be investigated by deriving and computing the corresponding

inverse mean free paths. Also it will be studied whether improved descriptions of interactions with nucleons will lead to significant changes for neutrino transport.

Once a sufficiently precise description of neutrino interactions is achieved, one can look at the neutrino signals that will be predicted. The measurement of a neutrino signal from a galactic SN comparable to the famous SN1987A but with modern observation technology would give many insights into the explosion mechanism. Current simulations expect that the propagation of the shock through the neutrinospheres will lead to an initial burst, especially in ν_e and all heavy flavour neutrinos ν_x. Directly afterwards all luminosities will decrease. The luminosities of ν_e and $\bar{\nu}_e$ will become similar but larger than for ν_x. For the mean neutrino energies one expects indeed the following hierarchy $\langle \epsilon_{\nu_e} \rangle < \langle \epsilon_{\bar{\nu}_e} \rangle \lesssim \langle \epsilon_{\nu_x} \rangle$ with $\langle \epsilon_{\nu_x} \rangle \lesssim 13 - 16\,\mathrm{MeV}$ [67]. At late times when accretion has ceased, the mean energies become practically equal. This is attributed to the flat temperature profile in the PNS and the close proximity of all neutrino spheres [68, 69]. Given the high densities of neutrino decoupling at later times it could also be possible to learn about the nuclear physics at these conditions, in particular about the nuclear EOS. Furthermore, from the differences in mean energies one could conclude better upon the possible path for heavy element nucleosynthesis, which will be reviewed in the next section. Eventually, while neutrino oscillations play probably no role in the decoupling region, the emitted neutrinos can become subject to oscillations once they are mostly free streaming. The observation of neutrino flavour oscillations in the form of unexpected swaps in the spectra could significantly improve their understanding [70, 71]. For even later times neutrino emission becomes an indirect probe of the high density matter. While the neutrino flux might be too low to be observed, it is still the main cooling process of the *neutron star* (NS) (for a review see e.g. [72]). The occurrence of a pasta phase close to the neutron star crust could affect this cooling process [41]. Also, as the NS becomes completely transparent to neutrinos, they emerge from the inner core, where densities could reach a multiple of nuclear saturation densities. The state of matter under these conditions is unclear, and many models differ in the predictions for neutrino interactions. The standard charged current reactions for electron flavour neutrinos might become forbidden by energy-momentum conservation in degenerate matter [73]. The most relevant reaction in nuclear matter should then be the so called modified URCA process [74, 75]. Other relevant neutrino sources might be interactions between nucleons and hyperons [76] or meson condensates [77, 78, 79]. Also, nucleon pairs could form Bose condensates below a critical temperature. This would suppress many standard emission channels but also offer additional reactions in form of pair breaking and formation processes. All of these models differ in their prediction for the cooling curve of the NS. Hence, the observation of such a cooling curve would significantly restrict the possible models for baryonic matter at supranuclear densities.

1.4. Nucleosynthesis of Heavy Elements

The exothermic nuclear burning process in stars can only explain nuclear fusion up to the Iron group. The critical problem here is the maximum in the binding energy for the Iron group and the high temperatures that result in NSE. Elements heavier than Iron must then be created in other environments.

One can study the shape of the element abundance pattern that is observed in the Sun. Since the Sun is expected to be a star of a later generation, the matter from which it formed already contained metals that were created by previous generations of stars. Also, all the metals that are observed in the Sun must be created before its formation, as no metals were produced in the Sun itself yet.
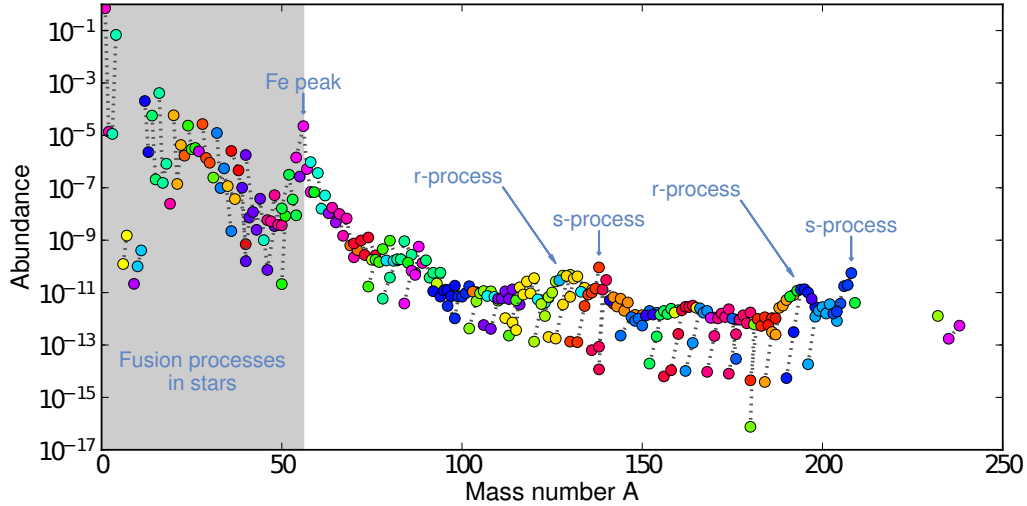
Figure 1.6.: Solar photospheric and meteoritic isotopic abundances given as described in [80]. Elements up to the iron peak that are produced in stellar burning show much larger abundance then heavy metals above A=56. For the heavy metals two peaks can be identified. Both of them are related to nuclear shell closures in the neutron shell, pointing to the dominant role of neutron captures for the production of heavy elements. For each peak region two peaks can be identified, one related to the slow neutron capture or s-process and one related to the rapid neutron capture or r-process. Figure courtesy of L.Huther

In the solar elemental abundance pattern (Figure 1.6) several important features can be observed that hint at how nucleosynthesis proceeds in the universe [81]. One recognizes immediately that the lighter metals up to Iron are produced in a much higher amount than the heavy metals above A=56. The lighter elements are produced in exothermic stellar burning phases which convert matter in every massive star. A peak at Iron is formed because here the fusion products gather, as Iron cannot be processed any further in regular fusion processes. Also one can find relatively large abundances of so called α-nuclei. These are isotopes with equal number of neutrons and protons that can be formed through repeated alpha capture on lighter seed nuclei.

Beyond the Iron peak, abundances decrease significantly and the pattern becomes rather flat. However, two regions with relatively increased abundances can be seen. It is found that the corresponding peak nuclei can be identified as isotopes with a closed neutron shell. The neutrons in such a configuration are relative strongly bound but the nucleus is very reluctant to capture an additional neutron. One can naturally explain these peaks by neutron capture on heavy nuclei. It is intuitive that neutron captures play a significant role for heavy element nucleosynthesis. Neutrons cannot feel the electric Coulomb barrier, so they can approach a heavy nucleus much easier than protons could. Also the capture of free nucleons will increase

the total binding energy even for many nuclei beyond Iron. So since neutron captures should be important for heavy element nucleosynthesis, it will proceed until nuclei are formed that are very reluctant to capture additional neutrons. Therefore one observes a peak at closed neutron shell nuclei.

Further study of the heavy peak regions reveals that in each of them there are actually two peaks present. The right one (larger A for similar N) is connected to isotopes in the valley of stability while the left one consists of more neutron rich isotopes. It can be infered that there should be two distinct scenarios that are responsible for this substructure. The difference between them is expected to be the exposure of the heavy nuclei to free neutrons. The right peaks are then connected to the so called s-process and the left peaks to the r-process. In the context of core collapse supernova, the r-process is of special interest. It requires a scenario with large neutron abundances. In such an environment of high neutron density, neutron capture rates on heavy nuclei are larger than beta-decay rates. Nuclei repeatedly capture neutrons until a configuration is reached where an additional neutron would not be bound any more. For high temperatures it can alternatively happen that an equilibrium between a further neutron capture and photodissociation back to the original nucleus are in equilibrium. Either way the nucleus waits in this configuration for a β^--decay to take place. Once it occurs, the next sequence of neutron captures follows.

However, astrophysical sites have to feature very extreme conditions to obtain the required neutron flux. The favorite candidates for r-process sites are neutrino-driven winds in CCSNe or in *neutron star mergers* (NSMs). For CCSNe this will be discussed in detail. Current studies indicate that core-collapse supernovae might actually not be able to produce a full r-process but can only create the lighter of the heavy elements. Simulations of NSMs on the other hand are able to produce neutrino driven winds that allow for a full r-process [82, 83, 84]. A NSM is the coalescence of two neutron stars in a binary system. Due to gravitational wave emission the system loses energy and angular momentum and the neutron stars approach each other. The eventual merger results in the release of large amounts of gravitational energy. The matter becomes very hot and an accretion disk of neutron rich material is formed. However a problem with NSMs is that they require two neutron stars to be formed and to spiral in on each other, which takes a lot of time. Yet observations of some metal poor stars already show the presence of light r-process nuclei but a lack of heavy r-process nuclei [85]. This might be a problem to r-process from NSMs only, as metal poor stars are discussed to be among the oldest in the universe, from the first generations of star formation. One argument for this says that they would contain more metals from previous stars and thus not be metal poor, if they were not created very early in the universe. Under this assumption, one can further argue that as these stars were formed so early in the universe, there was no time for previous NSMs and distribution of the corresponding matter outflow into star formation regions. Also, some studies suggest that NSMs cannot reproduce the particular r-process pattern in those metal poor stars [86]. In contrast, core-collapse supernovae represent the formation of neutron stars at the end of the lifetime of a massive star. This process takes much less time and could therefore explain the r-process abundance in metal poor stars. In addition, parametric simulations of supernovae explosions were able to reproduce the corresponding abundance pattern [87].

An important aspect of the r-process is that it mostly operates through isotopes which are so extreme and unstable that many of them are not accessible in laboratory experiments, yet. Therefore many features of the r-process are attached with significant uncertainties e.g. because masses of the nuclei are not measured. On the other hand, astrophysical observations and simulations put constraints on these uncertainties. This is an important manifestation of the connection between nuclear physics and astrophysics, building the essence of nuclear astrophysics. Any improvement on either field affects the predictions of the other. Nuclear physics is fundamental to model and understand astrophysical processes while simulations and observations of these processes probe the nuclear physics at extreme conditions.

1.5. Nucleosynthesis in CCSN

In the case of a successful SN explosion, the shock will move outwards and on its way it will compress and heat matter. After passing a certain distance, the conditions in the shock will not be violent enough anymore to dissociate nuclei into free nucleons. Instead it will allow for explosive nuclear burning, e.g. in the form of Si- or O/Ne-burning [88]. Beyond that there are several scenarios of nucleosynthesis that are enabled or determined by the large flux of neutrinos of all flavours from the hot PNS. The most interesting one in the context of this work is the neutrino driven wind.

As it was noted before the newly formed PNS consists of dense hot matter with temperatures of several $10\,\mathrm{MeV}$ that emits a large flux of neutrinos. An initial neutrino burst comes from the transition of the shock-heated matter to a new, neutron rich chemical equilibrium in NSE. Later the PNS cools by producing neutrinos thermally in pairs from e^+-e^- conversion and nucleon-nucleon bremsstrahlung [89]. After the stalled shock has been launched/revived, neutrino luminosities are still very high for several seconds. At the surface of the PNS these neutrinos are free streaming, i.e. most of them will leave the envelope without further interaction. Yet there will be a small fraction that is scattered or absorbed by the surrounding matter. The basic idea for any scenario of neutrino related nucleosynthesis is that through the large neutrino luminosities, even a small fraction of reacting neutrinos translates into a relative large number of reactions from the perspective of the nucleons. For example, the gravitational binding energy of a nucleon at the surface of the PNS is $\simeq 100\,\mathrm{MeV}$. Assuming an average neutrino energy of $\langle \epsilon_\nu \rangle \simeq 10\,\mathrm{MeV}$, ten neutrinos must be captured to make one nucleon unbound.

Yet, it is found that neutrinos indeed deposit enough energy on the surface of the PNS to eject a gravitationally unbound matter outflow, the *neutrino driven wind* (NDW) [90, 91]. Consequently the properties of this outflow are determined by the emitted neutrino spectrum. Total ejected masses are expected in the order of $10^{-3} M_\odot$ [92, 93]. Due to its unique properties, the NDW is considered as a possible site for heavy element nucleosynthesis, in particular for the r-process [94, 95]. It is found that the path for nucleosynthesis in the NDW depends crucially on the electron fraction Y_e, the entropy per baryon s, and the expansion timescale τ [96, 97, 98, 87]. The electron fraction and its evolution over time can be related rather directly to the luminosities and mean energies of electron type neutrinos [99]. One finds the following

approximation for Y_e in the NDW [91]

$$Y_e \sim \left[1 + \frac{L_{\bar{\nu}_e}\left(\langle\epsilon_{\bar{\nu}_e}\rangle - 2\Delta\right)}{L_{\nu_e}\left(\langle\epsilon_{\nu_e}\rangle + 2\Delta\right)}\right]^{-1}, \qquad (1.1)$$

where the $\langle\epsilon_\nu\rangle$ are the respective average neutrino energies, $L_{\bar{\nu}}$ are the neutrino luminosities and Δ is the mass difference between neutrons and protons. Under the assumption of equal luminosities, a neutron rich NDW with $Y_e < 0.5$ requires that the average electron neutrino energies fulfill the relation $\langle\epsilon_{\bar{\nu}_e}\rangle - \langle\epsilon_{\nu_e}\rangle > 4\Delta$.

When the neutrino driven wind expands, the first nuclei to form are α-particles. For $Y_e < 0.5$ basically all protons will then become bound in α while some free neutrons remain. In a next step nuclei like ^{12}C are formed by three-body reactions involving α-particles. Further α-captures can lead to heavier elements up to ^{56}Ni. However, in the case of a fast expansion less ^{12}C and subsequent nuclei can form, since the triple-α-process is very sensitive towards density changes. Also some of the ^{12}C can be destroyed by photodissociation if the entropy is large enough. This scenario is then called an α-rich freeze-out. The remaining free nucleons can be captured on these seeds to form heavy elements. It was found that a full r-process would require a short expansion timescale τ on the order of milliseconds, entropy $s > 150 \, k_B$, and $Y_e < 0.5$ [91, 100, 96]. Hydrodynamic simulations found that the short timescale can be achieved but they fail to come up with enough entropy [101, 98, 102, 103]. Furthermore the difference in the average neutrino energies turned out too small so that instead of a neutron-rich wind a proton-rich wind was predicted [68, 37]. Especially at late times after several seconds the NDW will always obey $Y_e > 0.5$ as luminosities and average energies of ν_e and $\bar{\nu}_e$ become equal. However, recent improvements in the calculation of neutrino opacities at high densities have put parts of this picture in question [61, 62, 63]. They found that initially the wind can indeed be neutron rich, although they agree that it will become proton rich within seconds. It was subsequently found that a light or weak r-process might be allowed by these conditions. Such a scenario could produce elements up to Molybdenum (Z=42) [104]. For the elements that are produced a nice agreement is found with the observations of metal poor stars [85]. Beyond these developments one must note that it proves difficult to reach Y_e significantly different from 0.5 at all, because of the so called α-effect [105], which tends to suppress asymmetries in Y_e.

All the above findings regarding the sensitivity to neutrino spectra highlight the importance of a sophisticated neutrino transport in CCSN simulations to achieve reliable predictions of nucleosynthesis yields. A recent investigation of a possible r-process in NDW from CCSNe that considers updated results on most relevant aspect was performed in [106].

One can look now also to the possible behaviour of a proton-rich NDW. For this conditions the NDW is thought to produce mainly N=Z nuclei up to ^{64}Ge through a series of (p,γ), (α,γ) and (α,p) reactions. Even in proton rich ejecta there might be the possibility to produce some elements heavier than ^{64}Ge via the νp-process [107, 93]. If Y_e is very large i.e. very proton-rich, many free protons will be left after the formation of nuclei. The more protons are left, the more of them will be converted into neutrons by $\bar{\nu}_e$-capture. These neutrons can then be captured on the seed nuclei. Subsequent (p,γ) reactions will eventually form proton-rich nuclei with higher mass number A.

Recently additional scenarios for the evolution of the NDW opened through physics beyond the standard model. It was found for an ECSN that active-sterile neutrino flavour conversions (ASFC), as they are suggested by the reactor neutrino anomaly [108], can lead to a significantly lower Y_e. This would allow for nucleosynthesis beyond $Z = 42$ up to Cd [109]. Without ASFC only elements with $Z \lesssim 30$ were produced in the same simulation.

Another important path for nucleosynthesis in CCSN is the so called neutrino nucleosynthesis, or ν-process. I takes place in the outer shells above the PNS [110]. The large neutrino flux results in neutral-current scatterings on already existing nuclei, but also in charged current absorptions if the neutrino energies are large enough [111]. Thereby the neutrinos deposit energy which leads to evaporation of light particles such as protons, neutrons, and α. These reactions are thus also described as neutrino-spallation reactions. Since the neutral-current cross sections are the same for all neutrino lepton flavours, also μ- and τ-flavour neutrinos can contribute, in contrast to the NDW. To be precise, these neutrino flavours might dominate the ν-process as they have the highest energies and the cross sections are energy-dependent. For neutrino nucleosynthesis as well as for the NDW, an accurate knowledge of the neutrino spectra is important as the nucleosynthesis yields might vary strongly.

For most regions further outside, the temperature will be too small to reach NSE even after shock passage so the result of the ν-process will be depending on the progenitor composition, especially on its metallicity. The main outcome will be the nuclei ^{7}Li, ^{11}B, ^{19}F, ^{138}La, and ^{180}Ta, plus possibly odd Z nuclei up to Copper [88]. Many of these elements are difficult to produce in any other scenario.

1.6. Outline

For the next supernova event similar to SN1987A, neutrino observations are expected to measure the spectra in great detail. One must then produce predictions from theory that are equally precise to make the best use out of these measurements. To achieve such predictions for many of the processes that were mentioned before, a sufficiently accurate and consistent description of the interactions and the transport of supernova neutrinos at high temperatures and densities is required. This is the context of the present work. In particular, this thesis presents a comprehensive formalism for the calculation of neutrino interactions and investigates the significance of various neutrino reactions. For this purpose, Chapter 2 will review the textbook basics of the quantum field theory of weak interactions, which describes the interactions of neutrinos. This work will then deliver the derivations to compute the corresponding interaction rates. Chapter 3 will derive the matrix elements for leptonic and semileptonic neutrino interactions. Here, well known results from the literature will be reproduced, discussed, and adjusted for the particular reactions of interest. In Chapters 4 and 5, mean free paths and scattering kernels for all these reactions will be derived. To be precise, Chapters 4 and 5 deal with leptonic and semileptonic neutrino reactions, respectively. Also, in Chapter 5 an alternative approach will be derived to calculate reactions between neutrinos and nucleons. This approach attempts to achieve higher accuracy of rate calculations without the cost of additional computational demand, which is a crucial resource in computational physics. Eventually, Chapter 6 will then assess under which

conditions and to which degree the inclusion of the new reactions might modify the outcome of state of the art supernova simulations. Also, the results for the new calculation approach will be compared to other current standard implementations of neutrino interactions, and the significance of the difference will be discussed. In this way this work attempts on adding another small puzzle piece to the large picture of neutrino physics and explosive astrophysics.

2. Fundamentals of Neutrinos and their Interactions

2.1. Notation

For all derivations in this work natural units are employed. This means

$$\hbar = c = k_{\mathrm{B}} = 1.$$

Four-vectors are denoted by

$$p = (E, \vec{p})\,. \tag{2.1}$$

3-dimensional vectors are consequently denoted by

$$\vec{p} \qquad \text{with} \qquad \sqrt{\vec{p}^2} = |\vec{p}| = \bar{p}. \tag{2.2}$$

Greek indices always denote components of four-vectors, while roman letters denote components of 3-dimensional vectors. Exceptions are stated explicitly.

2.2. Electroweak Interaction in the Standard Model of Physics

2.2.1. Symmetry and Interaction

Today many features of neutrinos are properly described in the *Standard Model* (SM) of physics [112, 113, 114]. In the SM, the strong, electromagnetic, and weak interactions of elementary particles are described within a quantum field theory. In particular, the SM is a so called gauge theory. It makes a certain use of a special class of symmetries that we believe are present in our world to describe the interactions between all elementary particles.

If a symmetry exists in nature, this means the laws of physics will not change under a transformation corresponding to this symmetry. As an example, if a system does not change under a global rotation, it is said to have rotational symmetry or to be invariant under rotation. Rotation symmetry is an example of a continuous symmetry, as it means a rotation can be performed by an angle of arbitrary size.

There are also discrete symmetries, where the transformation parameter can have only discrete values. An example of such a symmetry is the parity symmetry, i.e. the invariance of

a system to spatial inversion. Obviously, only integer multiples of spatial inversions can be performed and there is no such thing as an infinitesimal "mirroring".

A very important finding regarding symmetries is Noether's theorem. It says that for every continuous symmetry in a sytem there is also a conservation law. Rotational invariance of a system is connected to conservation of angular momentum. For discrete symmetries there are also conservation laws. Parity invariance implies that the parity of a system, its behaviour under parity transformations, must be conserved through all the evolution of the system.

A very basic symmetry of nature which we believe to be ever present is Lorentz symmetry. Lorentz symmetry means symmetry under (specific) translations and rotations in the 4-dimensional spacetime. In special relativity, space and time are described on an equal footing. Hence, Lorentz symmetry extends and unifies the classical picture of invariance under rotation, translation in space, and translation in time. It is connected to conservation of angular momentum, momentum, and energy. Lorentz invariance demands that the Lagrangian, which contains all information on the dynamics of a system, must be written in terms of Lorentz scalars, i.e. quantities that do not change under Lorentz transformations. This strongly constraints the general structure that the dynamic equations describing our universe can have.

Gauge theories are based on internal symmetries. Internal symmetries do not refer to transformations in spacetime but to the internal space of particle fields only. A very important example is the symmetry of a system's wave function Ψ under transformation of the charge phase

$$\Psi \rightarrow \Psi' = U_C(\alpha)\Psi,$$
$$U_C(\alpha) = \exp{(i\alpha Q)},$$

where Q is the electrical charge operator. This symmetry is a $U(1)$ symmetry i.e. the transformations form a unitary group of 1×1 matrices. The operator Q is called the generator of this particular group and the group is named $U(1)_Q$. Symmetry under transformations of this group results in conservation of the total charge Q. It is then a general finding that the generator of a symmetry group is conserved in the symmetric system. A $U(n)$ group has n^2 generators. Another class of groups that are important for field theories are the special unitary groups $SU(n)$. They differ from $U(n)$ by the additional requirement that the determinant of the transformations must be one. A $SU(n)$ group has $n^2 - 1$ generators.

All transformations on internal spaces are called gauge transformations, since one can "gauge" a symmetric system by an arbitrary phase. The phase can be chosen favorable to study a certain question without affecting any physical observable.

The important step in the derivation of a gauge theory is to demand that the global gauge symmetries of a system become local. For the group $U(1)_Q$ this means that the parameter α is not the same everywhere but depends on spacetime.

$$U(\alpha) \rightarrow U(\alpha(x)) = \exp{(i\alpha(x)Q)}.$$

However, no Lagrangian that contains only free particle fields is invariant under such transformations. To preserve the symmetry, additional terms have then to be introduced in the Lagrangian. These terms couple the free particles to massless vector fields. Yet, such vector

fields represent bosonic particles with spin 1. To complete the Lagrangian eventually, one has to include further terms to describe the dynamics of these new vector fields. In case of the $U(1)_Q$ symmetry, local gauge invariance gives rise to the photon field and the electromagnetic interaction of charged particles by coupling them to the photons. It can be summarized then: In a gauge theory all interactions between particles arise from the demand that all the global gauge symmetries of the Lagrangian become local. This gives rise to a number of massless vector fields equal to the number of generators of the respective symmetry groups. The vector fields couple to all particles with a finite charge of the corresponding generator.

These fundamental considerations on symmetries almost suffice to build a basis for electroweak interactions, if it wasn't for the finding that some of the electroweak vector bosons are actually massive. To explain this observation, the concept of spontaneous symmetry breaking is required.

The idea of spontaneous symmetry breaking is to introduce special scalar fields Φ into the Lagrangian. In particular, this is done in such a fashion that the Lagrangian retains all its gauge symmetries. In vacuum however, these scalars Φ have minima in their potentials for non-vanishing fields, which do not obey the gauge symmetries. An example and analogy of such spontaneous symmetry breaking is the finite magnetization of ferromagnets below their critical temperature T_C. Even though the underlying theory of electromagnetism is invariant under rotation, the spins of particles in a ferromagnet will all align in one common direction for $T < T_C$. One can not predict which orientation this spontaneous magnetization will have. Each orientation is equally possible and each has the same total energy. Yet all of them break the rotational symmetry of the system. It is then said that the symmetry of the Lagrangian is spontaneously broken, or hidden, in the system. For a local gauge symmetry to be spontaneously broken, the scalar field must couple to the vector bosons of the symmetry. From this coupling arise new terms that are equivalent to mass terms for the vector fields. Furthermore, all other elementary particles can acquire mass by coupling to the scalar field, too. In the SM, this scalar particle is the Higgs-boson and the corresponding mechanism of spontaneous symmetry breaking is called the Higgs mechanism.

To summarize now the construction of a gauge theory (in a highly simplified manner) the following steps have to be performed:

- Identify all symmetries of the dynamics of a system.

- Construct a Lagrangian that conserves all these symmetries and contains free fields of all elementary particles.

- Make all global gauge symmetries local by including massless vector fields, introducing thereby interactions to the Lagrangian.

- Include scalar fields that have a non-vanishing vacuum value. This leads to spontaneous symmetry breaking of local gauge symmetries of those gauge fields that couple to the scalars. Thereby the respective vector bosons acquire mass.

- Couple elementary particles to the scalar fields to attribute mass to the former.

2.2.2. The Standard Model

Following the recipe from the previous section, the Standard Model is constructed as a Lorentz-invariant gauge theory. It's Lagrangian is based on the local gauge symmetry group $SU(3)_C \times SU(2)_L \times U(1)_Y$.

The group $SU(3)_C$ corresponds to the conservation of color charge and gives rise to 8 massless gluon fields. The gluons mediate the strong interaction.

The group $SU(2)_L$ corresponds to the conservation of weak isospin. The L denotes that the transformation of this symmetry affects only states of left-handed chirality (this will be explained later in more detail). The group $U(1)_Y$ corresponds to conservation of the weak hypercharge Y. It is connected to the third generator of weak isospin T_3 and the electrical charge operator Q by the Gell-Mann-Nishijima relation:

$$Q = T_3 + \frac{Y}{2}.$$

The $SU(2)_L \times U(1)_Y$ local gauge symmetry is partly broken in the universe. The scalar Higgs boson has a non-vanishing vacuum field. Through the Higgs mechanism three of the four vector bosons of the group $SU(2)_L \times U(1)_Y$ become massive by coupling to the Higgs. However, a $U(1)_Q$ symmetry related to charge conservation is contained in the original $SU(2)_L \times U(1)_Y$. This symmetry is conserved in the system even after spontaneous symmetry breaking. Thus, the corresponding vector boson, the photon, remains massless. The three massive vector bosons are the W^-, the W^+ and the Z. They mediate the weak interaction, while the photons mediate the electromagnetic interaction.

The gauge theory of the SM describes almost all interactions of elementary particles in very good agreement with experimental observations. However, the SM itself does not explain the actual number of different elementary particles. The scalar boson i.e. the Higgs particle is chosen to implement the Higgs mechanism in a minimal way. The fermions, which are all other elementary particles other than the Higgs and the Vector bosons, are chosen as they are observed in experiments. Since it is the aim of this work to discuss weak interactions of neutrinos, and since all elementary fermions couple to the weak interaction, a short review on their most important properties will be given.

The SM contains 12 elementary fermions and their 12 antiparticles. All of them have a spin of 1/2. The antiparticles have the exact same properties as the particles except that all their generalized charges (electrical charge, lepton or baryon number,...) are inverted. For example, the positron has the same spin and mass as the electron but a positive unit of electrical charge.

The 12 particles can be separated into two families, the leptons and the quarks. The main difference between them is that quarks carry color charge and are subject to the strong interaction while leptons are not. Both quarks and leptons couple to the electroweak interaction. The net number of quarks $N_q - N_{\bar{q}}$ and the net number of leptons $N_l - N_{\bar{l}}$ are conserved quantities in all interactions of the SM (outside of the SM however lepton number might not be conserved, e.g. if neutrinos are Majorana particles). Further, all the fermions can be grouped in three generations. Within each generation, there are two quarks and two leptons. Each of the pairs forms a doublet of the weak isospin. The lepton doublet consist of a massive lepton with one

negative unit of electrical charge and a massless lepton with no electrical charge, the neutrino (massive neutrinos are physics beyond the SM). The quark doublet consist of a quark with electrical charge 2/3 and one with the negative charge $-1/3$. The difference between the three generations is the mass of the quarks and the charged lepton. They all become significantly heavier going from one family to the next.

		Generations		
		1st	2nd	3rd
Family	Quarks	u	c	t
		d	s	b
	Leptons	e^-	μ^-	τ^-
		ν_e	ν_μ	ν_τ

Table 2.1.: Elementary fermions of the Standard Model

Beyond the conservation of the total net lepton number, one finds that the net number of leptons in a particular family $N_{l,i} - N_{\bar{l},i}$, with i $= e, \mu, \tau$, is conserved in all interactions of the SM, too. However, this is not the same for the quarks. Weak interactions with the charged bosons $W^\pm$ can transform quarks of one family into quarks of another family. The reason for this is that the mass eigenstates and the weak eigenstates are not the same for a given quark flavour. The coupling between different quark families by the charged weak current is described by the Cabibbo-Kobayashi-Maskawa (CKM) matrix [115, 116] (more on that later on).

2.2.3. Dirac Spinors and Dirac Equation

As mentioned before, all elementary particles in the SM are spin 1/2 fermions. In a Lorentz-invariant field theory, spin 1/2 particles are described by Dirac spinors Ψ. Dirac spinors are four dimensional spinor field operators that follow the Dirac equation. The Dirac equation reads

$$(i\gamma^\mu \partial_\mu - m)\Psi(x) = 0.$$

Here m is the mass of the fermion. The γ_μ are the Dirac gamma matrices. They are 4x4 matrices that obey the anticommutation relation

$$\{\gamma^\mu, \gamma^\nu\} = 2\eta^{\mu\nu}\mathbf{1},$$

where $\eta^{\mu\nu}$ is the Minkowski metric. The γ^μ are related to the generators $\sigma^{\mu\nu}$ of Lorentz-transformations by the commutation relation

$$\sigma^{\mu\nu} = \frac{i}{2}[\gamma^\mu, \gamma^\nu].$$

The Dirac equation is obtained via the Euler-Lagrange procedure from the Dirac Lagrangian for a free fermion field

$$\mathcal{L}(x) = \bar{\Psi}(x)(i\gamma^\mu \partial_\mu - m)\Psi(x).$$

For any four-vector A^μ, the Feynman-slashed expression $A\!\!\!/$ is defined by

$$A\!\!\!/ = \gamma^\mu A_\mu.$$

In the Feynman-slashed notation the Dirac equation reads

$$\left(i\partial\!\!\!/ - m\right)\Psi(x) = 0.$$

The solutions to the Dirac equation are the wave functions for particles and antiparticles. The dispersion relation is the one that is expected from special relativity

$$p_\mu p^\mu = m^2 \rightarrow E^2 = \vec{p}^2 + m^2.$$

The Dirac equation has the eigenspinors $\Psi^{(+)}_{\vec{p},s}(x)$ and $\Psi^{(-)}_{-\vec{p},-s}(x)$ which are defined according to

$$\Psi^{(+)}_{\vec{p},s}(x) = u(\vec{p},s)e^{-ip\cdot x} \qquad \text{and} \qquad \Psi^{(-)}_{-\vec{p},-s}(x) = v(\vec{p},s)e^{ip\cdot x} \qquad , s = 1, 2. \qquad (2.3)$$

The stationary eigenspinors $u(\vec{p},s)$ and $v(\vec{p},s)$ are given by

$$u(\vec{p},s) = \frac{1}{\sqrt{E+m}}\begin{pmatrix} \chi_s \\ \frac{\vec{\sigma}\cdot\vec{p}}{E+m}\chi_s \end{pmatrix} \quad \text{and} \quad v(\vec{p},s) = \frac{1}{\sqrt{E+m}}\begin{pmatrix} \frac{\vec{\sigma}\cdot\vec{p}}{E+m}\eta_s \\ \eta_s \end{pmatrix}, \qquad (2.4)$$

where χ_s and η_s each are any two linear independent, normalized Pauli spinors with $\chi_s^\dagger\chi_{s'} = \eta_s^\dagger\eta_{s'} = \delta_{ss'}$. The $\vec{\sigma}$ is the vector of the 2×2 Pauli-matrices. For the calculation of transitions the following property of the spinors will be very useful

$$\sum_s u(\vec{p},s)\bar{u}(\vec{p},s) = p\!\!\!/ + m, \qquad (2.5)$$

$$\sum_s v(\vec{p},s)\bar{v}(\vec{p},s) = p\!\!\!/ - m.$$

Here $\bar{u}$ and $\bar{v}$ are the adjoint spinors of u and v, respectively.

$$\bar{u} = u^\dagger\gamma^0 \qquad \text{and} \qquad \bar{v} = v^\dagger\gamma^0.$$

It is then understood that $\Psi^+_{\vec{p},s}(x)$ is the wave function for a particle with momentum $\vec{p}$ and polarization s, while $\Psi^-_{-\vec{p},-s}(x)$ describes an antiparticle with momentum $\vec{p}$ and polarization s.

In second quantization, the field operator $\Psi(x)$ can be expressed in the following Fourier-series

$$\Psi(x) = \sum_{\vec{p},s}\left[\Psi^+_{\vec{p},s}(x)\,b(\vec{p},s) + \Psi^-_{-\vec{p},-s}(x)\,d^\dagger(\vec{p},s)\right],$$

$$\bar{\Psi}(x) = \sum_{\vec{p},s}\left[\bar{\Psi}^+_{\vec{p},s}(x)\,b^\dagger(\vec{p},s) + \Psi^-_{-\vec{p},-s}(x)\,d(\vec{p},s)\right],$$

where the expansion coefficients are creation and destruction operators

- $b(\vec{p},s)$ destroys a particle with momentum $\vec{p}$ and polarization s.

- $b^\dagger(\vec{p},s)$ creates a particle with momentum $\vec{p}$ and polarization s.

- $d(\vec{p},s)$ destroys an antiparticle with momentum $\vec{p}$ and polarization s.

- $d^\dagger(\vec{p},s)$ creates an antiparticle with momentum $\vec{p}$ and polarization s.

2.2.4. Helicity, Chirality, and Parity Violation

An important representation of the Pauli spinors χ_s and η_s are the eigenspinors of the hermitian helicity operator $\vec{\Sigma} \cdot \hat{p}$, where $\vec{\Sigma}$ is the spin operator

$$\Sigma^k = \epsilon^{ijk}\sigma_{ij} = \begin{pmatrix} \sigma^k & 0 \\ 0 & \sigma^k \end{pmatrix}.$$

The eigenvalues of the helicity operator are ± 1 and allow for the notation $u(\vec{p}, h)$ and $v(-\vec{p}, h)$ with

$$\begin{aligned} \vec{\Sigma} \cdot \hat{p}\, u(\vec{p}, h) &= h\, u(\vec{p}, h) \\ \vec{\Sigma} \cdot \hat{p}\, v(-\vec{p}, h) &= h\, v(-\vec{p}, h) \end{aligned} \qquad , h = \pm 1.$$

In weak interactions, besides helicity also chirality or "handedness" plays a crucial role. The chirality matrix γ^5 is a product of all the γ^μ

$$\gamma^5 = i\gamma^0\gamma^1\gamma^2\gamma^3 \qquad \text{with} \qquad \left\{\gamma^5, \gamma^\mu\right\} = 0.$$

Every spinor can be decomposed into a so called left-handed chirality part Ψ_L and a right-handed chirality part Ψ_R (now as the Weyl spinors)

$$\Psi = \Psi_L + \Psi_R,$$

where Ψ_L and Ψ_R are eigenfunctions of γ^5 with

$$\gamma^5\Psi_R = +\Psi_R,$$
$$\gamma^5\Psi_L = -\Psi_L.$$

Therefore one can define projection operators $\Pi_{R/L}$ that project on the right- and left-handed component of a state, respectively.

$$\Pi_R = \frac{1 + \gamma^5}{2} \rightarrow \Pi_R\Psi = \Psi_R,$$
$$\Pi_L = \frac{1 - \gamma^5}{2} \rightarrow \Pi_L\Psi = \Psi_L.$$

The Lagrangian for a free Dirac particle can also be written in terms of the Weyl spinors

$$\mathcal{L} = \bar{\Psi}_R i\gamma^\mu\partial_\mu\Psi_R + \bar{\Psi}_L i\gamma^\mu\partial_\mu\Psi_L - m\left(\bar{\Psi}_R\Psi_L + \bar{\Psi}_L\Psi_R\right).$$

In general it is not obvious what the meaning of chirality is. However, for massless fermions such as the neutrinos in the SM, it can be shown that γ_5 commutates with the Hamiltonian $\hat{H}$. The helicity eigenspinors of the Dirac equation are then also eigenspinors of the chirality matrix with

$$\begin{aligned} \gamma_5 u(\vec{p}, h) &= h\, u(\vec{p}, h) \\ \gamma_5 v(-\vec{p}, h) &= -h\, v(-\vec{p}, h) \end{aligned} \qquad , h = \pm 1.$$

Also, the dynamic equations of the two Weyl spinors decouple in the Lagrangian since the mixed term vanishes.

It is an important observational finding that only chiral left-handed neutrinos (left-handed or negative helicity) and chiral left-handed antineutrinos (right-handed or positive helicity) exist in nature. More precisely, only chiral left-handed neutrinos are observed to participate in weak interactions. Therefore (charged-current) weak interactions are maximally violating parity. This observation is the reason for postulating the $SU(2)_L$ symmetry group in the SM. It dictates the structure of the coupling between the elementary fermions and the vector bosons of the weak interaction.

2.2.5. Bilinear Covariants

The structure of interaction terms in the Lagrangian of the SM can be constrained significantly by some basic considerations. First, it can be shown that all physical observables of Dirac fields must be build from even powers of spinors $\Psi(x)$. The most interesting one turns out to be the simplest, being of order two. Also, the term must transform covariant under Lorentz-transformations. Such an expression is called a covariant bilinear and can be written in the general form

$$\bar{\Psi}\Gamma\Psi.$$

Since Γ is a 4×4 matrix there exist 16 different, linearly independent covariant bilinears. They all can be constructed from products of the γ^μ. They are named according to their behaviour under Lorentz-transformations:

- Lorentz scalar: $\Gamma_S = 1$,

- Lorentz pseudoscalar: $\Gamma_P = i\gamma_5$,

- Lorentz vector: $\Gamma_V^\mu = \gamma^\mu$,

- Lorentz axial vector: $\Gamma_A^\mu = \gamma_5\gamma^\mu$,

- Lorentz tensor: $\Gamma_T^{\mu\nu} = \sigma^{\mu\nu}$.

2.2.6. Weak Interactions of Elementary Particles

To understand the coupling of elementary fermions to the vector bosons of the electroweak interaction one must take a look at the quantum numbers of the fermions in the group $SU(2)_L \times U(1)_Y$. Chiral left-handed leptons form a doublet of the weak isospin. For right-handed chirality there are no neutrinos, and the charged leptons form a weak isospin singlet. A possible notation for this is

$$\Psi_{l,L} = \begin{pmatrix} \nu_{l,L} \\ l_L \end{pmatrix}, \qquad \Psi_{l,R} = l_R.$$

Here ν_l and l are the Dirac spinors of neutrinos and leptons, respectively.

Taking into account the observational constraints on the parity violating behaviour of weak interactions and the chirality of neutrinos, the SM finds that the isospin changing, or charged-current, weak interaction acts generally only on left-handed chirality states. Also, the quarks

can likewise be grouped into left-handed weak isospin doublets and right-handed weak isospin singlets. In the example of the 1st generation quarks this is described by

$$\Psi_{q,L} = \begin{pmatrix} u_L \\ d_L \end{pmatrix}, \qquad \Psi_{q,R} = u_R, d_R.$$

Here u and d are the Dirac spinors of up quark and down quark, respectively. The two components of the doublet have the same total weak isospin $T = 1/2$ but different polarizations $T_3 = \pm 1/2$. The singlet has the trivial quantum numbers $T = T_3 = 0$. The quantum numbers of the weak hypercharge Y can be expressed through T_3 and Q and will therefore not be needed explicitly in what follows.

	T	T_3	Q	$Z_{L/R}$	Z_V	Z_A
$\nu_{e,L}, \nu_{\mu,L}, \nu_{\tau,L}$	$\frac{1}{2}$	$+\frac{1}{2}$	0	$+\frac{1}{2}$	$+\frac{1}{2}$	$+\frac{1}{2}$
e_L, μ_L, τ_L	$\frac{1}{2}$	$-\frac{1}{2}$	-1	$-\frac{1}{2} + s_W^2$	$-\frac{1}{2} + 2s_W^2$	$-\frac{1}{2}$
e_R, μ_R, τ_R	0	0	-1	s_W^2		
u_L, c_L, t_L	$\frac{1}{2}$	$+\frac{1}{2}$	$+\frac{2}{3}$	$+\frac{1}{2} - \frac{2}{3}s_W^2$	$+\frac{1}{2} - \frac{4}{3}s_W^2$	$+\frac{1}{2}$
u_R, c_R, t_R	0	0	$+\frac{2}{3}$	$-\frac{2}{3}s_W^2$		
d_L, s_L, b_L	$\frac{1}{2}$	$-\frac{1}{2}$	$-\frac{1}{3}$	$-\frac{1}{2} + \frac{1}{3}s_W^2$	$-\frac{1}{2} + \frac{2}{3}s_W^2$	$-\frac{1}{2}$
d_R, s_R, b_R	0	0	$-\frac{1}{3}$	$+\frac{1}{3}s_W^2$		

Table 2.2.: Electroweak quantum numbers of elementary fermions

The Standard model delivers the following expression for the coupling term of electron type leptons to the charged vector bosons

$$\mathcal{L}_{cc}^{l_e} = -\frac{g}{\sqrt{2}} \left[\bar{\nu}_{e,L} \gamma^\mu e_L W_\mu + \bar{e}_L \gamma^\mu \nu_{e,L} W_\mu^\dagger \right]$$
$$= -\frac{g}{2\sqrt{2}} \left[\bar{\nu}_e \gamma^\mu \left(1 - \gamma_5 \right) e \, W_\mu + \bar{e} \gamma^\mu \left(1 - \gamma_5 \right) \nu_e W_\mu^\dagger \right].$$

W^μ denotes the charged vector bosons and g is the corresponding coupling constant. The coupling has a "vector minus axial vector" or V-A coupling. The coupling of both bilinears has exactly the same strength and therefore the total expression is maximally parity violating. One can rewrite the Lagrangian in terms of the weak charged current $J_{l_e}^\mu$:

$$\mathcal{L}_{cc}^{l_e} = -\frac{g}{2\sqrt{2}} \left[J_{l_e}^{\mu\dagger} W_\mu + J_{l_e}^\mu W_\mu^\dagger \right] \qquad \text{with} \qquad J_{l_e}^\mu = \bar{e} \gamma^\mu \left(1 - \gamma_5 \right) \nu_e.$$

The other two lepton families couple in the exact same way to W^μ. Hence, the total leptonic Lagrangian for charged-current weak interaction reads

$$\mathcal{L}_{cc}^l = \sum_{l=e,\mu,\tau} -\frac{g}{2\sqrt{2}} \left[J_l^{\mu\dagger} W_\mu + J_l^\mu W_\mu^\dagger \right] \qquad \text{with} \qquad J_l^\mu = \bar{l}\gamma^\mu \left(1 - \gamma_5\right) \nu_l.$$

For the charged-current coupling of the quarks, it has to be considered that the quark eigenspinors of the weak interaction are a linear combination of the mass eigenspinors of the three generations. In terms of the weak eigenspinors, which we denote by q_w with $q = u, d, c, s, t, b$, the quark current reads exactly the same as the one for leptons

$$\mathcal{L}_{cc}^{ud} = -\frac{g}{2\sqrt{2}} \left[J_{ud}^{\mu\dagger} W_\mu + J_{ud}^\mu W_\mu^\dagger \right] \qquad \text{with} \qquad J_{ud}^\mu = \bar{u}_w \gamma^\mu \left(1 - \gamma_5\right) d_w.$$

The q_w are related to the mass eigenstates q by the CKM matrix V

$$\begin{pmatrix} d_w \\ s_w \\ b_w \end{pmatrix} = \begin{pmatrix} V_{ud} & V_{us} & V_{ub} \\ V_{cd} & V_{cs} & V_{cb} \\ V_{td} & V_{ts} & V_{tb} \end{pmatrix} \begin{pmatrix} d \\ s \\ b \end{pmatrix}.$$

The weak charged current for u-quarks reads then

$$J_u^\mu = J_{ud}^\mu = V_{ud}\bar{u}\gamma^\mu \left(1 - \gamma_5\right) d + V_{us}\bar{u}\gamma^\mu \left(1 - \gamma_5\right) s + V_{ub}\bar{u}\gamma^\mu \left(1 - \gamma_5\right) b.$$

The total quark current is then given by

$$J_Q^\mu = \sum_q J_q^\mu = \sum_{q=u,c,t} \sum_{q'=d,s,b} V_{qq'}\bar{q}\gamma^\mu \left(1 - \gamma_5\right) q'.$$

The elements V_{ud} and V_{us} are historically given by

$$V_{ud} = \cos\theta_C = 0.97427 \qquad \text{and} \qquad V_{us} = \sin\theta_C = 0.22534,$$

where θ_C is called the Cabibbo angle with $\theta_C = 13.02°$.

The neutral-current coupling to the Z-boson is different from the charged current as it couples to both chiral spinor components. This is because the Z-boson couples partly to the electromagnetic current of the fermions which does not vanish for right-handed chirality. The general Lagrangian for neutral weak interaction can then be derived as

$$\mathcal{L}_{nc} = -\frac{g}{c_W} \left[\bar{\Psi}_L \gamma_\mu \left(T_3 - s_W^2 Q\right) \Psi_L + \bar{\Psi}_R \gamma_\mu \left(-s_W^2 Q\right) \Psi_R \right] Z^\mu$$
$$= -\frac{g}{c_W} \left[\bar{\Psi}_L \gamma_\mu Z_L \Psi_L + \bar{\Psi}_R \gamma_\mu Z_R \Psi_R \right] Z^\mu.$$

with

$$Z_L = T_{3,L} - Q s_W^2 \qquad \text{and} \qquad Z_R = -Q s_W^2.$$

The expressions $c_W = \cos\theta_W$ and $s_W = \sin\theta_W$ refer to the Weinberg angle θ_W. They are defined through the weak coupling g and the electromagnetic coupling e by

$$s_W = \frac{e}{g} \qquad \text{with} \qquad s_W^2 \simeq 0.231.$$

In Table 2.2 the respective left- and right-handed neutral couplings for elementary fermions are listed. Defining the neutral current j_μ^Z by

$$\mathcal{L}_{nc} = -\frac{g}{2c_W} j_\mu^Z Z^\mu \qquad \frac{1}{2} j_\mu^Z = \bar{\Psi}_L \gamma_\mu Z_L \Psi_L + \bar{\Psi}_R \gamma_\mu Z_R \Psi_R.$$

The leptonic neutral current becomes

$$j_\mu^{Z,l} = \bar{\nu}_{l,L} \gamma_\mu \nu_{l,L} + \bar{l}_L \gamma_\mu \left(-1 + 2s_W^2\right) l_L + \bar{l}_R \gamma_\mu \left(2s_W^2\right) l_R,$$

and for the quarks of the first generation one finds for example

$$j_\mu^{Z,q} = \bar{u}_L \gamma_\mu \left(1 - \frac{4}{3}s_W^2\right) u_L + \bar{d}_L \gamma_\mu \left(-1 + \frac{2}{3}s_W^2\right) d_L + \bar{u}_R \gamma_\mu \left(-\frac{4}{3}s_W^2\right) u_R + \bar{d}_R \gamma_\mu \left(\frac{2}{3}s_W^2\right) d_R.$$

It has to be noted that there is no neutral-current mixing between quarks of different generations, unlike for the charged current. The neutral current weak spinors are the same as the mass spinors.

With hindsight to the calculation of rates it is more convenient to express the neutral coupling in terms of the full spinors instead of the chiral components. Using the projection operator one finds

$$\bar{\Psi}_L \gamma_\mu \Psi_L = \bar{\Psi} \gamma_\mu \frac{1 - \gamma_5}{2} \Psi \qquad \text{and} \qquad \bar{\Psi}_R \gamma_\mu \Psi_R = \bar{\Psi} \gamma_\mu \frac{1 + \gamma_5}{2} \Psi.$$

The neutral weak current can then by written as

$$j_\mu^Z = \bar{\Psi} \gamma_\mu \left(Z_V - Z_A \gamma_5\right) \Psi,$$

with the couplings Z_V and Z_A given by

$$Z_V = Z_L + Z_R \qquad \text{and} \qquad Z_A = Z_L - Z_R.$$

Hence the leptonic neutral current becomes

$$j_\mu^{Z,l} = \frac{1}{2} \left[\bar{\nu}_l \gamma_\mu \left(1 - \gamma_5\right) \nu_l + \bar{l} \gamma_\mu \left(-1 + 4s_W^2 + \gamma_5\right) l\right],$$

while for the quarks one finds

$$j_\mu^{Z,q} = \frac{1}{2} \left[\bar{u} \gamma_\mu \left(1 - \frac{8}{3}s_W^2 - \gamma_5\right) u + \bar{d} \gamma_\mu \left(-1 + \frac{4}{3}s_W^2 + \gamma_5\right) d\right].$$

2.2.7. Weak Currents of Nucleons

Due to the confining character of the strong interaction, free quarks do not exist in nature. Instead they are always contained in color-free objects. The two known classes of these objects are baryons and mesons. Baryons consist of three quarks with antibaryons made off three antiquarks. Mesons are build from quark-antiquark pairs. In the context of nuclear astrophysics and neutrino interactions the most abundant and important baryons are neutrons and protons. Neutrons consist of two down quarks and one up quark, protons consist of one down quark and

two up quarks. For some scenarios at high densities, it is also relevant to study interactions with Λ, which is constructed from one of each down quarks, up quarks, and strange quarks.

When neutrinos interact with nucleons i.e. baryons this cannot be described by interaction with free quarks. Converting a neutron into a proton by neutrino absorption is not the same as converting a free down quark into a free up quark. Instead it means to convert one bound state of strong interaction into another. Hence one has to replace the quark current by the appropriate hadronic transition matrix element. In the example of neutrino absorption on neutrons this is described by

$$\bar{u}\gamma^\mu \left(1 - \gamma_5\right) d \to \langle p(p_p)|h_W^\mu(0)|n(p_n)\rangle \,,$$

with $h_W^\mu(x)$ being the hadronic current

$$\begin{aligned} h_W^\mu(x) &= v_W^\mu(x) - a_W^\mu(x) \\ &= \bar{u}(x)\gamma^\mu d(x) - \bar{u}(x)\gamma^\mu\gamma_5 d(x). \end{aligned}$$

The transition matrix element can differ in two ways from the quark current. First the coupling terms can have a different structure within the restriction of being of the V-A-type. Secondly the coupling constants will be dependent on momentum transfer. This is because the wavelength of the neutrino relates to the resolution of the baryon that is felt upon reacting. Hence high energy neutrinos (or particles in general) see more of the substructure of the baryons.

The transition matrix element must keep the $V - A$-structure. Also it must satisfy the invariance of strong interactions under weak isospin transformations. Under these constraints, the most general matrix elements can be written as

$$\langle p(p_p)|v_W^\mu(0)|n(p_n)\rangle = V_{ud}\bar{u}_p(p_p)\left[\gamma^\mu G_V\left(q^2\right) + \sigma^{\mu\nu}q_\nu\frac{iF_2(q^2)}{2m_N}\right] u_n(p_n)$$

and

$$\langle p(p_p)|a_W^\mu(0)|n(p_n)\rangle = V_{ud}\bar{u}_p(p_p)\left[\gamma^\mu\gamma_5 G_A\left(q^2\right) + \gamma_5 q^\mu\frac{G_P(q^2)}{m_N}\right] u_n(p_n).$$

Here q^μ is the momentum transfer, which is defined by

$$q^\mu = p_{N,f}^\mu - p_{N,i}^\mu. \tag{2.6}$$

From QCD it is known that the QCD Lagrangian of strong interaction obeys isospin invariance i.e. fulfills isospin symmetry. Noether's theorem implies then that the isovector currents are conserved. This is known as the the conserved vector current (CVC) hypothesis. From there one can derive a connection between the weak charged-current vector matrix element and the electromagnetic matrix elements of nucleons.

$$\langle p(p_p)|v_W^\mu(0)|n(p_n)\rangle = \langle p(p_p)|j_{\gamma,Q}^\mu(0)|p(p_p)\rangle + \langle n(p_n)|j_{\gamma,Q}^\mu(0)|n(p_n)\rangle \,.$$

Now one can relate the respective weak form factors $G_V(q^2)$ and $F_2(q^2)$, which would be difficult to measure directly, to the well known electromagnetic form factors $F_1^N(q^2)$ and $F_2^N(q^2)$

$$\begin{aligned} G_V\left(q^2\right) &= F_1^p\left(q^2\right) - F_1^n\left(q^2\right), \\ F_2\left(q^2\right) &= F_2^p\left(q^2\right) - F_2^n\left(q^2\right). \end{aligned}$$

Assuming the same q^2 dependence for all electromagnetic form factors of the nucleons, fitted to electron scattering data, one finds eventually (see e.g. [117])

$$G_V(q^2) = \left(1 - \frac{q^2}{4m_N^2}\right)^{-1} \left(1 - \frac{q^2}{M_V^2}\right)^{-2} \left[1 - \frac{q^2}{4m_N^2}(\mu_p - \mu_n)\right],$$

$$F_2(q^2) = \left(1 - \frac{q^2}{4m_N^2}\right)^{-1} \left(1 - \frac{q^2}{M_V^2}\right)^{-2} [\mu_p - \mu_n - 1].$$

The vectorial mass is fitted to $M_V \simeq 0.84\,\text{GeV}$, the anomalous proton magnetic moment is $\mu_p = 2.793$ and the neutron magnetic moment $\mu_n = -1.913$.

Throughout this work the low momentum exchange approximation will be used, where all form factors will be evaluated at $q^2 = 0$. They become then

$$G_V = G_V(0) = g_v = 1 \qquad \text{and} \qquad F_2 = F_2(0) = (\mu_p - \mu_n - 1) \simeq 3.706.$$

Since F_2 depends on the large anomalous magnetic moments of the nucleons, the corresponding contributions to the weak matrix element are called "weak magnetism".

In contrast to the CVC hypothesis, the axial current is not conserved. Instead, it can be shown that the pion decay requires non conservation of the axial current The partially conserved axial current (PCAC) hypothesis is then connecting the axial current to the pion field π

$$\partial_\mu a_W^\mu(x) = f_\pi m_\pi^2 \pi^-(x).$$

From there one can derive a relation connecting the axial and the pseudoscalar form factors $G_A(q^2)$ and $G_P(q^2)$ to the pion-nucleon form factor $g_{\pi N}(q^2)$

$$\left(-q^2 + m_\pi^2\right) \left[2m_N G_A(q^2) + \frac{q^2}{m_N} G_P(q^2)\right] = \sqrt{2} g_{\pi N}(q^2) f_\pi m_\pi^2.$$

For vanishing momentum exchange $q^2 \to 0$ this results in the Goldberg-Treiman relation

$$g_A = G_A(0) = \frac{f_\pi g_{\pi N}}{\sqrt{2} m_N} \simeq 1.3,$$

with $g_{\pi N} = g_{\pi N}(m_\pi^2)$ and the assumption $g_{\pi N}(0) \simeq g_{\pi N}$. The result of the Goldberg-Treiman relation is in rather good agreement with precise measurements of g_A from neutron decay

$$\frac{g_A}{g_V} \simeq 1.27.$$

Furthermore, measurements of neutrino scattering reactions have been used to fit the q^2-dependence of G_A to be

$$G_A(q^2) = \frac{g_A}{\left(1 - \frac{q^2}{m_A^2}\right)^2},$$

with the axial mass $m_A \simeq 1.206\,\text{GeV}$.

The pseudoscalar form factor $G_P(0)$ for vanishing momentum transfer can then be derived to

$$G_P(0) \simeq \frac{2m_N^2}{m_\pi^2} g_A.$$

Dropping the pseudoscalar term and using the low q^2 approximation, the charged current nuclear matrix element becomes eventually

$$\langle p(p_p)|h_W^\mu(0)|n(p_n)\rangle = V_{ud}\bar{u}_p(p_p)\left[\gamma^\mu + \sigma^{\mu\nu}q_\nu\frac{iF_2}{2m_N} - \gamma^\mu\gamma_5 g_A\right]u_n(p_n). \qquad (2.7)$$

The neutral current transition matrix is initially subject to the same arguments regarding the general structure of the vector and axial currents. First, the quark neutral current $j_{Z,q}^\mu$ is replaced by $\langle p(p_p)|j_{Z,Q}^\mu(0)|n(p_n)\rangle$. The neutral hadronic current $j_{Z,Q}^\mu(x)$ can be decomposed into a vector and an axial vector part

$$j_{Z,Q}^\mu(x) = v_Z^\mu(x) - a_Z^\mu(x).$$

Both the vector current and the axial current can then be split (somewhat analogous to the quark case) into

$$v_Z^\mu(x) = v_3^\mu(x) - 2\sin^2\theta_W j_{\gamma,Q}^\mu(x) - \frac{1}{2}v_s^\mu(x),$$
$$a_Z^\mu(x) = a_3^\mu(x) - \frac{1}{2}a_s^\mu(x).$$

where $v_3^\mu(x)$ and $a_3^\mu(x)$ are the vector and axial currents of the isospin operator I_3, respectively. $v_s^\mu(x)$ and $a_s^\mu(x)$ are the vector and axial contributions of strange and heavier quarks and $j_{\gamma,Q}^\mu$ is the electromagnetic current.

The general structure of the neutral currents is analogous to the charged currents

$$\langle N(p_f)|v_Z^\mu(0)|N(p_i)\rangle = \bar{u}_N(p_f)\left[\gamma^\mu F_1^{ZN}(q^2) + \sigma^{\mu\nu}q_\nu\frac{iF_2^{ZN}(q^2)}{2m_N}\right]u_N(p_i)$$

and

$$\langle N(p_f)|a_Z^\mu(0)|N(p_i)\rangle = \bar{u}_N(p_f)\left[\gamma^\mu\gamma_5 G_A^{ZN}(q^2) + \gamma_5 q^\mu\frac{G_P^{ZN}(q^2)}{m_N}\right]u_N(p_i).$$

The form factors of the vectorial part can be connected again to the electromagnetic form factors by

$$F_1^{Zp}(q^2) = \frac{1}{2}(F_1^p - F_1^n) - 2\sin^2\theta_W F_1^p - \frac{1}{2}F_1^{sp},$$
$$F_1^{Zn}(q^2) = \frac{1}{2}(F_1^n - F_1^p) - 2\sin^2\theta_W F_1^n - \frac{1}{2}F_1^{sn},$$
$$F_2^{Zp}(q^2) = \frac{1}{2}(F_2^p - F_2^n) - 2\sin^2\theta_W F_2^p - \frac{1}{2}F_2^{sp},$$
$$F_2^{Zn}(q^2) = \frac{1}{2}(F_2^n - F_2^p) - 2\sin^2\theta_W F_2^n - \frac{1}{2}F_2^{sn}.$$

The strange form factors are not well constrained by experiment, yet. Hence, they are neglected in many studies of neutrino interactions which is done in this work, too. Using the already known electromagnetic form factors with the same assumptions as for the charged current one

arrives then at

$$F_1^{Zp}(q^2) = \frac{1}{2} \frac{\left[1 - \frac{q^2}{4m_N^2}(\mu_p - \mu_n) - 4\sin^2\theta_W\left(1 - \frac{q^2}{4m_N^2}\mu_p\right)\right]}{\left(1 - \frac{q^2}{4m_N^2}\right)\left(1 - \frac{q^2}{M_V^2}\right)^2},$$

$$F_1^{Zn}(q^2) = \frac{1}{2} \frac{\left[-1 + \frac{q^2}{4m_N^2}(\mu_p - \mu_n) + 4\sin^2\theta_W\frac{q^2}{4m_N^2}\mu_n\right]}{\left(1 - \frac{q^2}{4m_N^2}\right)\left(1 - \frac{q^2}{M_V^2}\right)^2},$$

$$F_2^{Zp}(q^2) = \frac{1}{2} \frac{\left[\mu_p - \mu_n - 1 - 4\sin^2\theta_W(\mu_p - 1)\right]}{\left(1 - \frac{q^2}{4m_N^2}\right)\left(1 - \frac{q^2}{M_V^2}\right)^2},$$

$$F_2^{Zp}(q^2) = \frac{1}{2} \frac{\left[\mu_n - \mu_p + 1 - 4\sin^2\theta_W\mu_n\right]}{\left(1 - \frac{q^2}{4m_N^2}\right)\left(1 - \frac{q^2}{M_V^2}\right)^2}.$$

In the low momentum exchange approximation the form factors simplify to

$$F_1^{Zp} = F_1^{Zp}(0) = \frac{1}{2}\left(1 - 4\sin^2\theta_W\right) \simeq \frac{1}{2} \times 0.076,$$

$$F_1^{Zn} = F_1^{Zn}(0) = -\frac{1}{2},$$

$$F_2^{Zp} = F_2^{Zp}(0) \simeq \frac{1}{2}\left(3.706 - 4\sin^2\theta_W \cdot 1.793\right) \simeq \frac{1}{2} \times 2.049,$$

$$F_2^{Zn} = F_2^{Zn}(0) \simeq \frac{1}{2}\left(-3.706 + 4\sin^2\theta_W \cdot 1.913\right) \simeq -\frac{1}{2} \times 1.938.$$

For the neutral current axial form factors one finds a relation with the charged current axial form factors that is given by

$$G_A^{Zp}(q^2) = \frac{1}{2}G_A(q^2) - \frac{1}{2}G_A^{sp}(q^2),$$

$$G_A^{Zn}(q^2) = -\frac{1}{2}G_A(q^2) - \frac{1}{2}G_A^{sn}(q^2),$$

$$G_P^{Zp}(q^2) = \frac{1}{2}G_P(q^2) - \frac{1}{2}G_P^{sp}(q^2),$$

$$G_P^{Zn}(q^2) = -\frac{1}{2}G_P(q^2) - \frac{1}{2}G_P^{sn}(q^2).$$

Neglecting again the strange quark form factors a simple equivalence is found

$$G_A^{Zp}(q^2) = -G_A^{Zn}(q^2) = \frac{1}{2}G_A(q^2),$$

$$G_P^{Zp}(q^2) = -G_P^{Zn}(q^2) = \frac{1}{2}G_P(q^2).$$

2.3. Matrix Elements

The study of neutrino transport in compact astrophysical objects requires the calculation of certain transport properties. Such are e.g. the rates with which neutrinos interact with the particles in their environment by certain reactions. In this respect, a very fundamental transport property is the cross section per unit volume $\frac{\sigma}{V}$ or inverse mean free path λ^{-1}. The mean free

path describes how far a neutrino will travel on average before it experiences a reaction. The inverse mean free path is in general a quantity that depends on the energy of a neutrino. According to the distribution of its reaction partners it can also be angle dependent. In the interior of compact stellar objects the distribution of all baryons and charged leptons is basically isotropic and given by conditions of thermal and chemical equilibrium. However, this is not the case for neutrinos (which is why one needs to study neutrino transport). Hence, reactions that absorb or emit a single neutrino and do not involve additional neutrinos are sufficiently described by $\lambda^{-1}(E_\nu)$. For neutrino scattering or neutrino flavour converting reactions one needs a quantity that depends on the energies of all participating neutrinos and the angles between them. This quantity can then be folded with the discrete neutrino distributions. Such a quantity is often called a scattering kernel R. For a reaction involving 2 neutrinos one would need then $R(E_{\nu 1}, E_{\nu 2}, \theta_{1,2})$. Actually, transport calculations need a scattering kernel that depends on the angles of both neutrinos with respect to a predefined axis (mostly the radial direction) $R(E_{\nu 1}, E_{\nu 2}, \theta_1, \theta_2)$. How two derive these quantities from each other will be discussed in more detail later when the respective reactions are studied.

For any neutrino reaction (in the picture of free quasi particles), the inverse mean free path $\lambda^{-1}(E_\nu)$ can be calculated in the following way (see e.g. [118])

$$\frac{1}{\lambda(E_\nu)} = \int \left(\prod_i \frac{d^3 p_i}{2E_i (2\pi)^3} \right) \left(\prod_f \frac{d^3 p_f}{2E_f (2\pi)^3} \right) \frac{1}{2E_\nu} g \left\langle |M(p_\nu, \{p_i\} \to \{p_f\})|^2 \right\rangle \qquad (2.8)$$

$$\times (2\pi)^4 \delta^4 \left(p_\nu + \sum_i p_i - \sum_f p_f \right) \left(\prod_i f_i(E_i) \right) \left(\prod_f (1 - f_f(E_f)) \right).$$

Here, f_i and f_f denote the (isotropic) distribution functions of all participating particles except for the neutrino. Since the particles are fermions, final state Pauli blocking must be taken into account. The degeneracy factor g sums essentially over different possibilities of spins (and colors) of initial particles (it is not to be mistaken with the weak coupling constant g with the same notation). Eventually, $\left\langle |M(p_\nu, \{p_i\} \to \{p_f\})|^2 \right\rangle$ is the square of the Lorentz invariant matrix element M of the reaction, summed over final state spins and averaged over initial state spins. The invariant matrix element can be derived from quantum field theory by its definition through the T-matrix

$$\langle \{p_f\} |T| p_\nu \{p_i\} \rangle = (2\pi)^4 \delta^4 \left(p_\nu + \sum_i p_i - \sum_f p_f \right) \cdot iM(p_\nu, \{p_i\} \to \{p_f\}).$$

For the electroweak interaction, the expression on the left-hand side can be evaluated using perturbation theory i.e. Feynman diagrams and Feynman rules. The derivation of these concepts will not be discussed here. It suffices to note that one has to choose all possible connected, amputated diagrams up to a certain order of perturbation and sum them with the correct respective sign. The calculation of the matrix element of a single diagram follows then the corresponding Feynman rules.

In the scope of this work only lowest oder perturbation theory will be studied. Hence, only so called tree level diagrams are considered. They contain only a single weak vector boson

propagator, either charged or neutral, which connects the incoming and outgoing fermions. It can be shown that the corresponding matrix elements basically consist of the respective charged or neutral particle currents coupled to each other by the corresponding charged or neutral boson propagator

$$|M_{cc}| = \frac{g^2}{8} J_{W,1}^\mu \left(\frac{g_{\mu\nu} - \frac{q_\mu q_\nu}{m_W^2}}{q^2 - m_W^2} \right) J_{W,2}^\nu \qquad |M_{nc}| = \frac{g^2}{4c_W^2} J_{Z,1}^\mu \left(\frac{g_{\mu\nu} - \frac{q_\mu q_\nu}{m_Z^2}}{q^2 - m_Z^2} \right) J_{Z,2}^\nu,$$

in agreement with the definition of charged and neutral currents in previous sections. Here, $g_{\mu\nu}$ is the metric tensor. As an example one can consider absorption of electron neutrinos on down quarks for charged interactions, and scattering of muon neutrinos on electrons for neutral interactions. The absorption will have the matrix element

$$\left| M\left(\nu_e + d \to u + e^- \right) \right| = \frac{g^2}{8} V_{ud} \left[\bar{u}_u^{(s')}(p_u) \gamma^\mu \left(1 - \gamma_5 \right) u_d^{(s)}(p_d) \right] \left(\frac{g_{\mu\nu} - \frac{q_\mu q_\nu}{m_W^2}}{q^2 - m_W^2} \right)$$
$$\times \left[\bar{u}_e^{(t')}(p_e) \gamma^\nu \left(1 - \gamma_5 \right) u_{\nu_e}^{(t)}(p_\nu) \right].$$

while for the scattering one has

$$\left| M\left(\nu_\mu + e^- \to \nu_\mu + e^- \right) \right| = \frac{g^2}{16c_W^2} \left[\bar{u}_{\nu_\mu}^{(s')}(p_\nu') \gamma^\mu \left(1 - \gamma_5 \right) u_{\nu_\mu}^{(s)}(p_\nu) \right] \left(\frac{g_{\mu\nu} - \frac{q_\mu q_\nu}{m_Z^2}}{q^2 - m_Z^2} \right)$$
$$\times \left[\bar{u}_e^{(t')}(p_e') \gamma^\nu \left(-1 + 4s_W^2 + \gamma_5 \right) u_e^{(t)}(p_e) \right].$$

2.3.1. Four-point interaction

For low momentum transfer $|q^2| \ll m_W^2, m_Z^2$ the weak boson propagators simplify to

$$\lim_{|q^2/m_{W,Z}^2| \to 0} \left(\frac{g_{\mu\nu} - \frac{q_\mu q_\nu}{m_{W,Z}^2}}{q^2 - m_{W,Z}^2} \right) = -\frac{g_{\mu\nu}}{m_{W,Z}^2}.$$

The weak interaction Lagrangian can then be approximated by a so called current-current Lagrangian.

$$\mathcal{L}_{\text{eff}}^{CC} = -\frac{G_F}{\sqrt{2}} j_{W\mu}^\dagger j_W^\mu \qquad \text{and} \qquad \mathcal{L}_{\text{eff}}^{NC} = -\frac{G_F}{\sqrt{2}} j_{Z\mu}^\dagger j_Z^\mu.$$

The effective Fermi coupling constant G_F is defined by

$$\frac{G_F}{\sqrt{2}} = \frac{g^2}{8m_W^2}.$$

Furthermore the matrix elements for tree level diagrams simplify to

$$|M_{cc}| = \frac{G_F}{\sqrt{2}} J_{W,1}^\mu J_{W,2,\mu} \qquad \text{and} \qquad |M_{nc}| = \frac{2G_F}{\sqrt{2}} J_{Z,1}^\mu J_{Z,2,\mu}. \qquad (2.9)$$

Hence, all terms that contribute to the effective interaction Lagrangian represent a possible matrix element. For the absorption of electron neutrinos on down quarks this equates into

$$\left| M\left(\nu_e + d \to u + e^- \right) \right| = \frac{G_F}{\sqrt{2}} V_{ud} \left[\bar{u}_u^{(s')}(p_u) \gamma^\mu \left(1 - \gamma_5 \right) u_d^{(s)}(p_d) \right]$$
$$\times \left[\bar{u}_e^{(t')}(p_e) \gamma_\mu \left(1 - \gamma_5 \right) u_{\nu_e}^{(t)}(p_\nu) \right].$$

while for the scattering of muon neutrinos on electrons the matrix element becomes

$$\left| M\left(\nu_\mu + e^- \to \nu_\mu + e^-\right) \right| = \frac{G_F}{2\sqrt{2}} \left[\bar{u}_{\nu_\mu}^{(s')}(p_\nu') \gamma^\mu \left(1 - \gamma_5\right) u_{\nu_\mu}^{(s)}(p_\nu) \right]$$
$$\times \left[\bar{u}_e^{(t')}(p_e') \gamma_\mu \left(-1 + 4s_W^2 + \gamma_5\right) u_e^{(t)}(p_e) \right].$$

In general the matrix element is now of the form

$$|M| = Q^\mu(s, s') E_\mu(t, t').$$

The squared matrix element $\left\langle |M|^2 \right\rangle$, summed over final spins and averaged over initial spins can then by written

$$\left\langle |M|^2 \right\rangle = g_S^{-1} \sum_{s,s',t,t'} \left(Q^\mu(s,s') E_\mu(t,t')\right) \left(Q^\nu(s,s') E_\nu(t,t')\right)^\dagger \qquad (2.10)$$
$$= g_S^{-1} \sum_{s,s',t,t'} \left[Q^\mu(s,s') Q^{\nu\dagger}(s,s')\right] \left[E_\mu(t,t') E_\nu^\dagger(t,t')\right].$$

where g_S is averaging over initial spins with $g_S = \sum_s 1 \times \sum_t 1$. The right-hand side expression for $\left\langle |M|^2 \right\rangle$ is then solved by transforming it into traces of γ-matrices. It will be discussed in detail for the various reactions later on.

2.4. Nuclear Matter Effects

The previous sections laid out the formalism to compute weak interactions as singular events with certain probabilities. The reacting particles were free elementary fermions and free nucleons. Distribution functions and especially Pauli blocking of these particles were included in the calculation of cross sections in Eq.(2.8). Thereby it was taken into account that neutrinos move in a multi-particle environment which is subject to the laws of quantum statistics. At the high densities as encountered in PNSs the effects of final state blocking are highly relevant for any reaction process. Furthermore, the description of nuclear transitions was paying tribute to the observation that quarks do not appear as free particles in nature. Due to the self-coupling behaviour of strong interactions, quarks are confined in color-neutral objects, especially nucleons in the region of interest. Hence the picture of free nucleons is indeed a phenomenological description of interacting quarks. It is appropriate to leading orders for the energy scales that are relevant for neutrino decoupling in young PNSs. However, even in this effective picture, particles are not free. Except for the neutrinos, they all continuously experience strong and/or electromagnetic interaction. This is actually the reason why matter can be assumed to be in thermal equilibrium on the timescale of weak interactions. But these forces will also cause deviations of the actual particle distributions from ideal Fermi gases. For low densities these deviations are so small that they can be neglected to leading order. Yet, at large densities they might significantly modify the dispersion relations of particles and give rise to collective phenomena like pair excitations, resulting in modified amplitudes for certain reactions. Predicting reliable neutrino rates at large densities above 10^{12} g/cm^3 can only be achieved by considering

these effects. Depending on the exact situation (density and composition), different approaches can be used and are used in nuclear astrophysics. Neutrino opacities in supernova simulations mostly account for mean field effects. In some cases they go beyond and consider collective effects in the form of correlations from linear response theory, also called random phase approximation (RPA), mainly by pion exchange. Both methods have the advantage that they merge easily with RMF-EOS, which are very popular for the description of high density matter in nuclear astrophysics. A nice review of these approaches can be found in [119]. They will be briefly illustrated in the following since they are also implemented in the scope of this work. Recent studies consider more realistic nucleon-nucleon (NN) interactions e.g. from chiral effective field theory (EFT) [120]. Yet, their treatment is beyond the calculations presented here and cannot be covered in detail.

2.4.1. Relativistic mean field theory

The basic idea of a mean field theory in general is to describe an interaction by a potential. Furthermore, the potential should not be explicitly dependent on the position of particle i with respect to all other particles j, but it should be an average potential, depending on the density of particles j at the position $\vec{r}_i$.

$$U(\vec{r}_i) = \sum_j V(\vec{r}_i, \vec{r}_j) \mapsto U(\rho(\vec{r}_i)).$$

In RMF theory such an averaged potential arises from nucleon-meson interaction terms in the Lagrangian. From experiment it is known that nucleon-nucleon (NN) interactions can be described by meson exchange. The idea of RMF is to begin with a Lorentz invariant Lagrangian that contains terms to describe the meson fields and terms which couple these mesons to the nucleons. This way, the strong interaction between nucleons is mediated by the meson fields of the theory. The most important mesons for RMF are the pions π, the σ-meson, the ω-meson, and the ρ-meson. However, the single π-meson does not contribute initially at mean field level but becomes important beyond mean field e.g. for pairing. Also, the charged ρ-meson fields have zero expectation value. Only a neutral ρ-meson is included then. Hence the respective NN Lagrangian would have the structure (see e.g. [121])

$$
\begin{aligned}
\mathcal{L}_{NN} &= \mathcal{L}_N + \mathcal{L}_m + \mathcal{L}_{int}, \\
\mathcal{L}_N &= \bar{\Psi}(x) \left(i\slashed{\partial} - m \right) \Psi(x), \\
\mathcal{L}_m &= \frac{1}{2}\left(\partial_\mu \sigma \partial^\mu \sigma - m_\sigma^2 \sigma^2\right) - \frac{1}{2}\left(\frac{1}{2}\Omega_{\mu\nu}\Omega^{\mu\nu} - m_\omega^2 \omega_\mu \omega^\mu\right) - \frac{1}{2}\left(\frac{1}{2}\vec{R}_{\mu\nu}\vec{R}^{\mu\nu} - m_\rho^2 \rho_\mu \rho^\mu\right), \\
\mathcal{L}_{int} &= g_\sigma \bar{\Psi}\sigma\Psi - g_\omega \bar{\Psi}\slashed{\omega}\Psi - g_\rho \bar{\Psi}\gamma_\mu \vec{\tau}\rho^\mu \Psi.
\end{aligned}
$$

Here m_σ, m_ω, and m_ρ are the respective meson masses, g_σ, g_ω, g_ρ are the nucleon-meson couplings. The field tensors $\Omega^{\mu\nu}$ and $\vec{R}^{\mu\nu}$ are given by

$$
\begin{aligned}
\Omega^{\mu\nu} &= \partial^\mu \omega^\nu - \partial^\nu \omega^\mu, \\
\vec{R}^{\mu\nu} &= \partial^\mu \vec{\rho}^\nu - \partial^\nu \vec{\rho}^\mu.
\end{aligned}
$$

Right from the start, this representation is an effective picture. The parameters like the meson masses are thus not expected to agree with the actual physical values of these properties, as are the meson fields not to be identified with the actual meson fields. Instead, the parameters are fitted to agree with measurements of nuclear matter properties, like the saturation density.

From the above Lagrangian $\mathcal{L}_{NN}$ one derives the Dirac equation in medium for nucleons

$$\left[\left(i\slashed{\partial} - g_\omega\slashed{\omega} - \gamma_\mu\vec{\tau}\rho^\mu\right) - (m - g_\sigma\sigma)\right]\Psi = 0.$$

In the rest frame of nuclear matter the spatial components of the vector fields vanish. The Dirac equation simplifies then to

$$\left[\left(i\slashed{\partial} - g_\omega\gamma_0\omega^0 - \gamma_0\tau_3\rho^0\right) - (m - g_\sigma\sigma)\right]\Psi = 0.$$

In the mean field approximation the meson fields are treated as classical fields

$$\sigma \mapsto \langle\sigma\rangle = S \qquad \text{and} \qquad \omega^0 \mapsto \langle\omega^0\rangle = U \qquad \text{and} \qquad \rho^0 \mapsto \langle\rho^0\rangle = V.$$

The (particle-)solution to the Dirac equation in medium can be derived in analogy to equations (2.3)-(2.5). For the positive energy eigenspinor of nucleons one finds

$$\Psi^+_{\vec{p},s}(x) = u(\vec{p},s)e^{-ip\cdot x} \qquad , s = 1, 2,$$

where the stationary eigenspinor $u(\vec{p}, s)$ is given by

$$u(\vec{p}, s) = \frac{1}{\sqrt{E^* + m^*}}\begin{pmatrix} \chi_s \\ \frac{\vec{\sigma}\cdot\vec{p}}{E^*+m^*}\chi_s \end{pmatrix} \qquad \text{with} \qquad \sum_s u(\vec{p}, s)\bar{u}(\vec{p}, s) = \slashed{p}^* + m^*. \tag{2.11}$$

The effective mass m^* and the effective four momentum p^* are defined by

$$m^* = m - g_\sigma S \qquad \text{and} \qquad p^* = (E^*, \vec{p}) = \left(\sqrt{\vec{p}^2 + m^{*2}}, \vec{p}\right). \tag{2.12}$$

and the positive single particle energies for protons and neutrons are

$$E_p = E^* + g_\omega U + \frac{1}{2}g_\rho V = \sqrt{\vec{p}^2 + m^{*2}} + g_\omega U + \frac{1}{2}g_\rho V, \tag{2.13}$$

$$E_n = E^* + g_\omega U - \frac{1}{2}g_\rho V = \sqrt{\vec{p}^2 + m^{*2}} + g_\omega U - \frac{1}{2}g_\rho V. \tag{2.14}$$

Now one can define the mean field potentials for neutrons and protons

$$U_n = g_\omega U - \frac{1}{2}g_\rho V \qquad \text{and} \qquad U_p = g_\omega U + \frac{1}{2}g_\rho V. \tag{2.15}$$

In this picture, the distribution of fermions is described by a free Fermi-gas distribution of nucleons with an effective mass. The chemical potential is then replaced by a so called effective Fermi potential $\mu_{F,n/p}$ with

$$\mu_{F,n/p} = \mu_{n/p} - U_{n/p} \quad \rightarrow \quad f_{n,p} = \left[1 + \exp\left(\frac{\sqrt{\vec{p}^2 + m^{*2}} - \mu_{F,n/p}}{T}\right)\right]^{-1}. \tag{2.16}$$

(a)

(b)

(c)
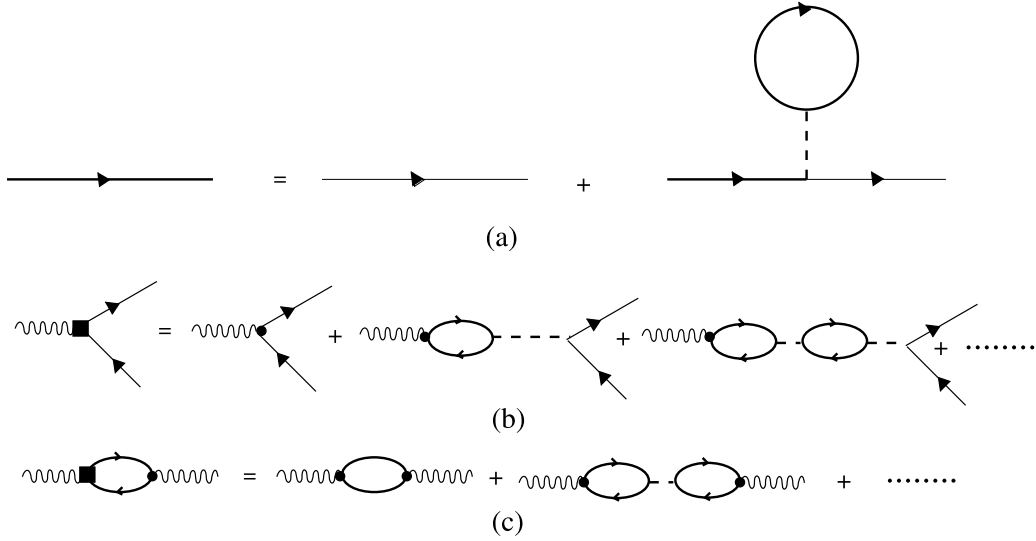
Figure 2.1.: Feynman diagrams of Dyson-Schwinger equation for NN-interaction in mean field approximation[119]: a) nucleon propagator in mean field; b) dressed vertex for coupling to external current; c) current-current correlation function or polarization tensor, also called bubble series; Thick and thin solid lines are medium and free propagators, respectively. Dashed lines represent strong/electromagnetic interaction while weak lines represent weak interactions. The squares and circles are medium and free weak vertices, respectively.

Eventually another replacement has to be made. In the normalization factor $\left(\prod_i 2E_i\right)$ the nucleon energy E_N has to be replaced by E_N^*. This comes from the normalization of the phase space integral which is actually a spacetime integral over the mass shell condition. Since the latter is modified for the quasiparticles in the medium one finds

$$d^4 p_N \delta\big((E_N - U_N)^2 - \vec{p}_N^2 - m_N^{*2}\big) = d^3 p_N dE_N \frac{\delta\left(E_N - U_N - \sqrt{\vec{p}_N^2 - m_N^{*2}}\right)}{2(E_N - U_N)} = \frac{d^3 p_N}{2E_N^*}. \quad (2.17)$$

Applying all these modifications into (2.8) one can calculate the transport properties in RMF-theory analogous to free fermions.

2.4.2. Random Phase Approximation RPA

In RMF-theory, nuclear interactions are implemented in a non-perturbative and self-consistent way. The nucleon propagator, which describes the motion of a nucleon, is modified with respect to a free nucleon by its coupling to the medium. In the mean field approximation this modification is due to a particular series of diagrams/couplings ([122, 121]). These diagrams are shown in Figure 2.1a) [119]. The nucleon propagator in medium can be described by the effective free propagator plus the so called tadpole diagram. Note that the tadpole contains again the modified propagator. Therefore all orders of couplings are contained in these diagrams. In order to consistently describe reactions on the basis of this approach, one has to consider the possibility that external currents can couple not only to the bare nucleon but also to the tadpole. Coupling to the tadpole describes a particle-hole or nucleon-antinucleon excitation. This is an initial-state or final-state interaction (and hence not incorporated in the S-matrix

approach [119]). These excitations are not covered in the intuitive treatment of section 2.4.1. Fully consistent computation of transport properties based on an RMF-EOS requires then the use of RPA, also called ring-approximation or linear response theory. Figure 2.1c) depicts the diagrams corresponding to RPA, the so-called bubble series. However, RPA demands an approach to compute transport properties that is different to the S-matrix approach previously employed. It focuses on the calculation of correlation functions or medium polarization tensors.

2.4.3. Cross Sections in RPA

For a two-particle charged-current interaction between leptons and nucleons, in the absence of a medium, the squared matrix element $\langle |M|^2 \rangle$ can be written (see Eq.(2.10))

$$\langle |M|^2 \rangle = g_S^{-1} \frac{G_F^2}{2} L_{\mu\nu} T^{\mu\nu},$$

where $L_{\mu\nu}$ and $T^{\mu\nu}$ are the spin sums over the lepton and the nucleon currents, respectively. It will be shown later that the nucleon current can be written in the form

$$T^{\mu\nu} = Tr\left[(\not{p} + m)\, \bar{J}_N^\mu\, (\not{p} + \not{q} + m)\, \bar{J}_N^\nu \right],$$

where $\bar{J}_N^\mu$ is the coupling part of the nucleon current. For charged-current reactions one finds (see Eq.(2.7))

$$\bar{J}_N^\mu = V_{ud} \left[\gamma^\mu + \sigma^{\mu\nu} q_\nu \frac{iF_2}{2m_N} - \gamma^\mu \gamma_5 g_A \right]$$

From Eq.(2.8) one finds then for the inverse mean free path (with $g_S = g$)

$$\frac{1}{\lambda(E_l)} = \int \frac{d^3 p_N}{2E_N\,(2\pi)^3} \frac{d^3 p_N'}{2E_N'\,(2\pi)^3} \frac{d^3 p_l'}{2E_l'\,(2\pi)^3} \frac{1}{2E_l} \frac{G_F^2 V_{ud}^2}{2} L_{\mu\nu} T^{\mu\nu} \tag{2.18}$$
$$\times (2\pi)^4\, \delta^4(p_l + p_N - p_l' - p_N') f_N(E_N)\,(1 - f_l'(E_l'))\,(1 - f_N'(E_N'))$$
$$= \frac{G_F^2 V_{ud}^2}{32\pi^2} \int \frac{d^3 p_l'}{E_l E_l'} (1 - f_l'(E_l'))\, L_{\mu\nu} \int \frac{d^3 p_N d^3 p_N'}{4E_N E_N'\,(2\pi)^3} T^{\mu\nu} \delta^4(\ldots) f_N(E_N)\,(1 - f_N'(E_N'))$$

One can show that Equation 2.18 is only a special version of a more general expression. One can write

$$\frac{1}{\lambda(E_l)} = \frac{G_F^2 V_{ud}^2}{32\pi^2} \int \frac{d^3 p_l'}{E_l E_l'} (1 - f_l'(E_l'))\, L_{\mu\nu} S^{\mu\nu} \tag{2.19}$$

Here, $S^{\mu\nu}$ is the so called medium response function. In this most general notation $S^{\mu\nu}$ contains all the information on the interaction among the nucleons. Therefore $S^{\mu\nu}$ can also be computed in a more sophisticated approach. In order to calculate the $S^{\mu\nu}$ that corresponds to RPA, one needs to start by evaluating $S^{\mu\nu}$ in terms of the retarded/medium polarization $\Pi_R^{\mu\nu}$ [122, 123, 124]

$$\frac{1}{\lambda(E_l)} = \frac{G_F^2}{32\pi^2} \int \frac{d^3 p_l'}{E_l E_l'} (1 - f_l'(E_l'))\, L_{\mu\nu} \Im(\Pi_R^{\mu\nu}) \left[1 - \exp\left(-\frac{q_0 + \mu_N - \mu_N'}{T} \right) \right]. \tag{2.20}$$

The retarded polarization tensor is connected to the time-ordered/causal polarization tensor $\Pi^{\mu\nu}$ by

$$\Pi_R^{\mu\nu} = \tanh\left(\frac{q_0 + \mu_N - \mu'_N}{2T}\right)\Pi^{\mu\nu}.$$

The time-ordered polarization is given by

$$\Pi^{\mu\nu} = -i \int \frac{d^4p}{(2\pi)^4} Tr\left[T\left(G_N(p)\bar{J}_N^\mu G_{N'}(p+q)\bar{J}_N^\nu\right)\right],$$

where $G_i(p)$ is the respective nucleon propagator for a non-interacting nucleon in a Fermi gas, and T stands for time ordering. The subsequent steps to compute the respective polarizations will not be discussed here. However, it has to be noted that up to now, the approach via the T-matrix in Equation 2.18 and the approach via the polarization in Equation 2.20 are completely analogous and none of them has anything to do with RPA.

When considering mean field interactions in the T-matrix, Eq.(2.18) is modified in the following way

$$\frac{1}{\lambda(E_l)} = \frac{G_F^2}{32\pi^2} \int \frac{d^3p'_l}{E_l E'_l}\left(1 - f'_l(E'_l)\right) L_{\mu\nu} \int \frac{d^3p_N d^3p'_N}{4E_N^* E_N^{*'}(2\pi)^3}$$
$$T^{*\mu\nu}\delta^4(p_l + p_N - p'_l - p'_N)f_N(E_N)\left(1 - f'_N(E'_N)\right)$$

The effective nucleon tensor $T^{*\mu\nu}$ becomes

$$T^{*\mu\nu} = Tr\left[\left(\slashed{p}^* + m^*\right)\bar{J}_N^\mu\left(\left(\slashed{p} + \slashed{q}\right)^* + m^*\right)\bar{J}_N^\nu\right]$$

To account for the same level of interaction in the polarization tensor one has to replace the free nucleon propagator $G_i(p)$ with the effective nucleon propagator $G_i^*(p)$

$$G_i^*(p) = G_i(p^*)$$

Even after these replacements, again both approaches via the T-matrix and the polarization are equivalent and none gives the RPA-response.

The consistent approach of linear response theory goes beyond this intuitive modification. It replaces the free polarization tensor $\Pi^{\mu\nu}$ by the dressed polarization $\Pi^{*\mu\nu}$ according to the bubble series in 2.1c). For a detailed derivation of the standard vector and axial-vector contributions to the polarization the reader is referred to [125, 123, 126]. Additional contributions from weak magnetism are derived in [127].

2.4.4. Neutrino Transport in Core Collapse Supernova

As mentioned before, the surface of a PNS posses a region of transition in terms of neutrino transport. At high densities above $10^{13}\,\mathrm{g/cm^3}$ neutrino spectra are in thermal and chemical equilibrium with matter. They are effectively trapped due to the short mean free path or conversely the large opacities that they experience. At densities below $10^{10}\,\mathrm{g/cm^3}$ they will be decoupled from the matter. The neutrino mean free path will become so large that neutrinos

are free streaming and will most likely leave the PNS without further interaction. In between these two extremes there is a region where neutrinos decouple from the matter. Understanding and modeling this transition is necessary to predict the spectra of neutrinos. For numerical simulations of core collapse supernovae there are various approaches to treat neutrino transport. In particular, one has to decide for a trade off between accuracy and computational effort. On the basis of most approaches lies the evolution of the neutrino radiation field within kinetic theory. To be precise, the time evolution of the neutrino distribution is determined by the solution to the Boltzmann equation. In a very simplified notation this equation can be written in the form

$$\frac{\partial f}{\partial t} + T(f) + G(f) = C(f) \tag{2.21}$$

For a more thorough discussion of the Boltzmann equation see e.g. [128]. The term T describes the evolution due to spatial transport through a volume. The term G accounts for effects that arise from a particular choice of a coordinate system, from special relativity, and from general relativity. Eventually, the term C is the so called *collision term* that describes the interaction of neutrinos with particles. The consistent and simultaneous solution of both terms G and C proves to be a difficult task that can up to now only be solved by making significant approximations to the general case. A most famous example is probably the assumption of certain spatial symmetries to reduce the problem of simulating a supernova to 2D or even 1D in space. Also various simplifications to the collision term are in use such as neglecting certain types of reactions e.g. inelastic scatterings that couple different neutrino energies to each other.

One of the aims of this work is basically to improve the description of the collision term by studying neutrino reactions which are not present in current neutrino transport codes but might contribute significantly. Hence, a connection has to be made between the collision term and the transport properties that are derived here. A common assumption of basically all neutrino transport schemes is that the neutrino distribution f is symmetric for polar rotations around the radial axis. Thus f depends on time t, position $\vec{x}$, energy E and azimuthal angle θ with respect to the radial outward direction. The collision term can then be written out in the following form

$$
\begin{aligned}
C(f(E,\theta)) = & j(E)\left(1 - f(E,\theta)\right) - \chi(E)f(E,\theta) \\
& + (1 - f(E,\theta)) \int d\cos\theta' \, dE' \, E'^2 R_S^{in}(\theta,\theta',E,E') f'(E',\theta') \\
& - f(E,\theta) \int d\cos\theta' \, dE' \, E'^2 R_S^{out}(\theta,\theta',E,E') \left(1 - f'(E',\theta')\right) \\
& + (1 - f(E,\theta)) \int d\cos\theta' \, dE' \, E'^2 R_{PR}^{in}(\theta,\theta',E,E') \left(1 - \bar{f}'(E',\theta')\right) \\
& - f(E,\theta) \int d\cos\theta' \, dE' \, E'^2 R_{PR}^{out}(\theta,\theta',E,E') \bar{f}'(E',\theta')
\end{aligned} \tag{2.22}
$$

The term j describes the emission of neutrinos while χ represents the absorption. Treating neutrino transport in a comoving frame, both j and χ become equal to the inverse mean free path or cross section per unit volume for neutrino absorbing or emitting reactions.

$$j(E) = \left.\frac{1}{\lambda(E)}\right|_{\nu_{out}} \qquad \chi(E) = \left.\frac{1}{\lambda(E)}\right|_{\nu_{in}} \tag{2.23}$$

For example, the inverse mean free path for electron neutrino absorption on neutrons is a contribution to χ_{ν_e}, while the same expression for electron capture is a contribution to j_{ν_e}. Next, the expression R_S represents all the scattering reactions which have a neutrino among the initial and the final state particles. In particular R_S^{in} describes reactions where a neutrino of the distribution f with a particular energy E is an outgoing particle. One can also say that it scatters *into* the distribution. Likewise R_S^{out} describes reactions where such a neutrino is an initial state particle and goes *out* of the distribution. To achieve the rate of these reactions one has to integrate over the phase space of the other neutrino distribution f'. This has to be done numerically as the neutrino distributions are discrete and not necessarily an equilibrium distribution (otherwise there would be no need to solve the Boltzmann Equation in the first place). It should be noted that f' is not necessarily equal to f. The present work deals in particular with reactions where f and f' refer to different neutrino flavours. However, f and f' describe both either neutrinos or antineutrinos. Eventually R_{PR} describes neutrino pair processes such as production of a neutrino-antineutrino pair in electron-positron annihilation or nucleon bremsstrahlung. The indices *in* and *out* denote again whether the neutrino pair is in the final or initial state of the reaction i.e. whether they are created or destroyed, respectively. The distribution of the other neutrino $\bar{f}'$ describes antineutrinos of f represents neutrinos, and vice versa. A notable omission in the above collision term are reactions where neutrino pairs are incoming and outgoing, such as a neutrino flavour conversion $\nu_e + \bar{\nu}_e \rightarrow \nu_\mu + \bar{\nu}_\mu$. These reactions were found to be relevant for neutrino transport in PNS [129], however they are not included in the scope of this work.

There exists a useful relation that connects the cross section for emission of a neutrino by a certain reaction to the one for absorption by the inverse of the reaction, called *detailed balance*. The idea behind detailed balance builds on the fact that the matrix element is the same for any reaction and its inverse. Thus the cross sections for both reactions differ only by the exchange of initial and final state statistical factors for all particles other than the neutrino. It can be shown that the integrand differs then only by a factor which depends on the neutrino energy, the chemical potentials of all other particles, and the temperature. Hence this factor can be taken out of the phase space integral. In particular one finds

$$j(E) = \chi(E) \cdot \exp\left[\left(\mu_f - \mu_i - E\right)/T\right] \tag{2.24}$$

where μ_f is the sum of chemical potentials of final state particles in the absorption reaction. Likewise μ_i is the chemical potential of the initial state reaction partner. Similar relations can be found for scattering and pair reactions kernels.

$$R_S^{in}(\theta, \theta', E, E') = R_S^{out}(\theta, \theta', E, E') \cdot \exp\left[\left(\mu_f - \mu_i + E' - E\right)/T\right] \tag{2.25}$$

$$R_{PR}^{in}(\theta, \theta', E, E') = R_{PR}^{out}(\theta, \theta', E, E') \cdot \exp\left[\left(-E' - E\right)/T\right] \tag{2.26}$$

With the detailed balance equations one needs to calculate only the absorption or emission process explicitly and can then derive the inverse process immediately by an analytic transformation. Alternatively one can calculate both expressions explicitly and use the detailed balance condition as a crosscheck for the results.

3. Matrix Elements for Weak Interactions

This work wants to study the relevance of weak interactions that were not included in CCSN simulations, yet. It further tries to improve the expressions for some reactions that are already routinely included. These new expressions are supposed to be less approximative with respect to the treatment of relativity and mean field effects. Also a more complete treatment of the weak current is implemented. At the same time they are meant to be no more demanding in computation than the previously used expressions. Hence, they could be implemented in current neutrino transport schemes without significant modifications.

The first step to derive these expressions is the computation of the corresponding matrix elements according to equations (2.9) and (2.10). Nuclear interactions will be accounted for according to equations (2.11)-(2.15).

Some of the results in this section are well known textbook examples on the derivation of matrix elements. Relevant modifications beyond known expressions will arise due to the nuclear interaction potentials.

leptonic reactions	semileptonic reactions
$\nu_\mu/\bar{\nu}_\mu + e^- \rightarrow \nu_\mu/\bar{\nu}_\mu + e^-$	$\nu_e + n \rightarrow p + e^-$
$\nu_\mu + e^- \rightarrow \nu_e + \mu^-$	$\bar{\nu}_e + p \rightarrow n + e^+$
$\nu_\mu + \bar{\nu}_e + e^- \rightarrow \mu^-$	$\bar{\nu}_e + e^- + p \rightarrow n$
$\bar{\nu}_e + e^- \rightarrow \bar{\nu}_\mu + \mu^-$	$\nu_\mu + n \rightarrow p + \mu^-$

Table 3.1.: Table of reactions that are studied in the present work

3.1. Matrix Elements for Leptonic Reactions

$\boxed{\nu_\mu + e^- \to \nu_\mu + e^-}$

The scattering of muon neutrinos and antineutrinos on electrons is a purely neutral current reaction. The matrix element for these reactions and the subsequent scattering kernels are well known expressions in the literature. Nevertheless the derivation will be repeated in this work because it serves as the starting point for the derivation of the new leptonic reactions. It has then to be noted that the expression for the scattering of tau neutrinos is exactly the same as for muon neutrinos. First the expression for neutrinos will be considered. The weak neutral current for the muon neutrino reads

$$J^\alpha_{Z,\nu_\mu} = \frac{1}{2} \bar{u}^{s'}_{\nu_\mu} \gamma^\alpha \left(1 - \gamma_5\right) u^s_{\nu_\mu}.$$

For the electron one finds

$$J^\alpha_{Z,e^-} = \frac{1}{2} \bar{u}^{t'}_{e^-} \gamma^\alpha \left(-1 + 4s^2_W + \gamma_5\right) u^t_{e^-}.$$

Please note at this point the notation $u^s_{\nu_\mu}$ instead of $\nu_{\mu,s}$ and $\bar{u}^s_{\nu_\mu}$ instead of $\bar{\nu}_{\mu,s}$ for the eigenspinors of the muon neutrino (and equivalently for all other particles). This is done to avoid confusion with the eigenspinors of antiparticles which will be denoted by v instead of u. Those must not be mixed since they result in different spin sums, see Eq.(2.5). Further the explicit momentum dependence of the spinors is dropped in the notation although it is understood that it still applies.

The neutral current matrix element takes the form

$$\left| M\left(\nu_\mu + e^- \to \nu_\mu + e^-\right) \right| = \frac{G_F}{2\sqrt{2}} \left[\bar{u}^{s'}_{\nu_\mu} \gamma_\alpha \left(1 - \gamma_5\right) u^s_{\nu_\mu} \right] \left[\bar{u}^{t'}_{e^-} \gamma^\alpha \left(-1 + 4s^2_W + \gamma_5\right) u^t_{e^-} \right].$$

For the squared matrix element one has to average over initial spins. The respective spin degeneracy factor is $g_S = 2 \times 1 = 1$. The are two possible spins for the incoming electron but only one for the neutrino. The squared matrix element can then be written in the form

$$\left\langle |M|^2 \right\rangle = \frac{G_F^2}{16} \left(\sum_{s,s'} Q^{\alpha\beta}(s,s') \right) \left(\sum_{t,t'} E_{\alpha\beta}(t,t') \right).$$

The neutrino tensor $Q^{\alpha\beta}(s,s')$ and the electron tensor $E_{\alpha\beta}(t,t')$ are defined by

$$Q^{\alpha\beta}(s,s') = \left[\bar{u}^{s'}_{\nu_\mu} \gamma^\alpha \left(1 - \gamma_5\right) u^s_{\nu_\mu} \right] \left[\bar{u}^{s'}_{\nu_\mu} \gamma^\beta \left(1 - \gamma_5\right) u^s_{\nu_\mu} \right]^\dagger,$$

$$E_{\alpha\beta}(t,t') = \left[\bar{u}^{t'}_{e^-} \gamma_\alpha \left(-1 + 4s^2_W + \gamma_5\right) u^t_{e^-} \right] \left[\bar{u}^{t'}_{e^-} \gamma_\beta \left(-1 + 4s^2_W + \gamma_5\right) u^t_{e^-} \right]^\dagger.$$

First the neutrino tensor will be computed

$$\begin{aligned}
Q^{\alpha\beta}(s,s') &= \left[\bar{u}^{s'}_{\nu_\mu} \gamma^\alpha \left(1 - \gamma_5\right) u^s_{\nu_\mu} \right] \left[\bar{u}^{s'}_{\nu_\mu} \gamma^\beta \left(1 - \gamma_5\right) u^s_{\nu_\mu} \right]^\dagger \\
&= \left[\bar{u}^{s'}_{\nu_\mu} \gamma^\alpha \left(1 - \gamma_5\right) u^s_{\nu_\mu} \right] \left[\bar{u}^s_{\nu_\mu} \gamma^\beta \left(1 - \gamma_5\right) u^{s'}_{\nu_\mu} \right].
\end{aligned}$$

Performing the spin sum over s according to Eq.(2.5) one finds

$$\sum_s u^s_{\nu_\mu} \bar{u}^s_{\nu_\mu} = \slashed{p}_{\nu_\mu} + m_{\nu_\mu} = \gamma^\delta p_{\nu_\mu,\delta}.$$

The result can be plugged into the neutrino tensor

$$\sum_{s,s'} Q^{\alpha\beta}(s,s') = p_{\nu_\mu,\delta} \sum_{s'} \bar{u}^{s'}_{\nu_\mu} \gamma^\alpha \left(1 - \gamma_5\right) \gamma^\delta \gamma^\beta \left(1 - \gamma_5\right) u^{s'}_{\nu_\mu}.$$

Considering now that the spinors are vectors and the product of γ-matrices is a matrix itself. he spin sum over the neutrino tensor can then be transformed into a trace over γ-matrices by using simple matrix algebra

$$\sum_{s,s'} Q^{\alpha\beta}(s,s') = p_{\nu_\mu,\delta} \sum_{s'} \left(\bar{u}^{s'}_{\nu_\mu}\right)_i \left[\gamma^\alpha \left(1 - \gamma_5\right) \gamma^\delta \gamma^\beta \left(1 - \gamma_5\right)\right]_{ij} \left(u^{s'}_{\nu_\mu}\right)_j$$

$$= p_{\nu_\mu,\delta} \sum_{s'} \left[\gamma^\alpha \left(1 - \gamma_5\right) \gamma^\delta \gamma^\beta \left(1 - \gamma_5\right)\right]_{ij} \left(u^{s'}_{\nu_\mu} \bar{u}^{s'}_{\nu_\mu}\right)_{ji}$$

$$= p_{\nu_\mu,\delta} p'_{\nu_\mu,\epsilon} \left[\gamma^\alpha \left(1 - \gamma_5\right) \gamma^\delta \gamma^\beta \left(1 - \gamma_5\right)\right]_{ij} \left(\gamma^\epsilon\right)_{ji}$$

$$= p_{\nu_\mu,\delta} p'_{\nu_\mu,\epsilon} \mathrm{Tr}\left[\gamma^\alpha \left(1 - \gamma_5\right) \gamma^\delta \gamma^\beta \left(1 - \gamma_5\right) \gamma^\epsilon\right]$$

$$= p_{\nu_\mu,\delta} p'_{\nu_\mu,\epsilon} \mathrm{Tr}\left[2 \left(1 + \gamma_5\right) \gamma^\alpha \gamma^\delta \gamma^\beta \gamma^\epsilon\right]. \tag{3.1}$$

At this point one has to consider the traces of γ-matrices in general. The first rule is that any trace over an odd number of γ-matrices must vanish. The relevant nonvanishing traces are derived in the appendix in section A. Using these rules and the anticommutation $\gamma_5 \gamma^\alpha = -\gamma^\alpha \gamma_5$ one finds

$$\sum_{s,s'} Q^{\alpha\beta}(s,s') = p_{\nu_\mu,\delta} p'_{\nu_\mu,\epsilon} \left(2\mathrm{Tr}\left[\gamma^\alpha \gamma^\delta \gamma^\beta \gamma^\epsilon\right] + 2\mathrm{Tr}\left[\gamma_5 \gamma^\alpha \gamma^\delta \gamma^\beta \gamma^\epsilon\right]\right)$$

$$= 8 p_{\nu_\mu,\delta} p'_{\nu_\mu,\epsilon} \left(g_{\alpha\delta} g_{\beta\epsilon} - g_{\alpha\beta} g_{\delta\epsilon} + g_{\alpha\epsilon} g_{\beta\delta} + i\epsilon^{\alpha\delta\beta\epsilon}\right)$$

$$= 8 \left(p^\alpha_{\nu_\mu} p'^\beta_{\nu_\mu} + p^\beta_{\nu_\mu} p'^\alpha_{\nu_\mu} - g^{\alpha\beta} \left(p_{\nu_\mu} \cdot p'_{\nu_\mu}\right) - i\epsilon^{\alpha\beta\delta\epsilon} p_{\nu_\mu,\delta} p'_{\nu_\mu,\epsilon}\right).$$

Proceeding in analogous steps for the electron tensor one finds

$$\sum_{t,t'} E_{\alpha\beta}(t,t') = \sum_{t,t'} \left[\bar{u}^{t'}_{e^-} \gamma_\alpha \left(-1 + 4s^2_W + \gamma_5\right) u^t_{e^-}\right] \left[\bar{u}^t_{e^-} \gamma_\beta \left(-1 + 4s^2_W + \gamma_5\right) u^{t'}_{e^-}\right]$$

$$= 8 \left\{\left(1 - 4s^2_W + 8s^4_W\right) \left[p_{e^-,\alpha} p'_{e^-,\beta} + p_{e^-,\beta} p'_{e^-,\alpha} - g_{\alpha\beta} \left(p_{e^-} \cdot p'_{e^-}\right)\right]\right.$$

$$\left. - i \left(1 - 4s^2_W\right) \epsilon_{\alpha\beta\kappa\rho} p^\kappa_{e^-} p'^\rho_{e^-} - m^2_e \left(4s^2_W - 8s^4_W\right) g_{\alpha\beta}\right\}.$$

The contraction of both tensors is straightforward (see app. B). It yields

$$\sum_{s,s',t,t'} Q^{\alpha\beta}(s,s') \sum_{t,t'} E_{\alpha\beta}(t,t') = 64 \left(p_{\nu_\mu} \cdot p_{e^-}\right) \left(p'_{\nu_\mu} \cdot p'_{e^-}\right) \left(4 - 16s^2_W + 16s^4_W\right)$$

$$+ 64 \left(p_{\nu_\mu} \cdot p'_{e^-}\right) \left(p'_{\nu_\mu} \cdot p_{e^-}\right) \left(16s^4_W\right) + 64m^2_e \left[\left(p_{\nu_\mu} \cdot p'_{\nu_\mu}\right)\right] \left(8s^2_W - 16s^4_W\right).$$

Hence the squared matrix element for this reaction equates to

$$\left\langle \left|M \left(\nu_\mu + e^- \to \nu_\mu + e^-\right)\right|^2\right\rangle = 16G^2_F \left[\left(p_{\nu_\mu} \cdot p_{e^-}\right) \left(p'_{\nu_\mu} \cdot p'_{e^-}\right) \left(1 - 4s^2_W + 4s^4_W\right)\right. \tag{3.2}$$

$$\left. + \left(p_{\nu_\mu} \cdot p'_{e^-}\right) \left(p'_{\nu_\mu} \cdot p_{e^-}\right) \left(4s^4_W\right) + m^2_e \left(p_{\nu_\mu} \cdot p'_{\nu_\mu}\right) \left(2s^2_W - 4s^4_W\right)\right].$$

$$\boxed{\bar{\nu}_\mu + e^- \to \bar{\nu}_\mu + e^-}$$

For the scattering of antineutrinos on electrons, only the antineutrino tensor has to be calculated new. The difference here is that the incoming antineutrinos are described by outgoing spinors v, and vice versa. The neutrino current is given by

$$J^\alpha_{Z,\bar{\nu}_\mu} = \frac{1}{4} \bar{v}^{s'}_{\bar{\nu}_\mu} \gamma^\alpha \left(1 - \gamma_5\right) v^s_{\bar{\nu}_\mu}.$$

One then defines the Matrix element again by

$$\left\langle \left| M\left(\bar{\nu}_\mu + e^- \to \bar{\nu}_\mu + e^-\right)\right|^2 \right\rangle = \frac{G_F^2}{16} \left(\sum_{s,s'} \bar{Q}^{\alpha\beta}(s,s')\right) \left(\sum_{t,t'} E_{\alpha\beta}(t,t')\right).$$

The antineutrino tensor equates then to

$$\begin{aligned}
\bar{Q}^{\alpha\beta}(s,s') &= \left[\bar{v}^s_{\bar{\nu}_\mu} \gamma^\alpha \left(1 - \gamma_5\right) v^{s'}_{\bar{\nu}_\mu}\right]\left[\bar{v}^s_{\bar{\nu}_\mu} \gamma^\beta \left(1 - \gamma_5\right) v^{s'}_{\bar{\nu}_\mu}\right]^\dagger \\
&= \left[\bar{v}^s_{\bar{\nu}_\mu} \gamma^\alpha \left(1 - \gamma_5\right) v^{s'}_{\bar{\nu}_\mu}\right]\left[\bar{v}^{s'}_{\bar{\nu}_\mu} \gamma^\beta \left(1 - \gamma_5\right) v^s_{\bar{\nu}_\mu}\right].
\end{aligned}$$

The spin sum over the antispinors v gives the same result as the one over the spinors u since the neutrinos are massless

$$\sum_s v^s_{\bar{\nu}_\mu} \bar{v}^s_{\bar{\nu}_\mu} = \slashed{p}_{\bar{\nu}_\mu} - m_{\bar{\nu}_\mu} = \gamma^\delta p_{\bar{\nu}_\mu,\delta}.$$

The spin sum over the antineutrino tensor $\bar{Q}^{\alpha\beta}(s,s')$ can then again be transformed into a trace over γ-matrices, analogous to the sum for $Q^{\alpha\beta}(s,s')$

$$\sum_{s,s'} \bar{Q}^{\alpha\beta}(s,s') = p'_{\bar{\nu}_\mu,\delta} p_{\bar{\nu}_\mu,\epsilon} \text{Tr}\left[2\left(1 + \gamma_5\right) \gamma^\alpha \gamma^\delta \gamma^\beta \gamma^\epsilon\right].$$

The only difference between neutrinos and antineutrinos is the exchange of the initial and final neutrino four-momentum. Hence, the squared matrix element results into

$$\begin{aligned}
\left\langle \left| M\left(\bar{\nu}_\mu + e^- \to \bar{\nu}_\mu + e^-\right)\right|^2 \right\rangle &= 16 G_F^2 \left[\left(p'_{\bar{\nu}_\mu} \cdot p_{e^-}\right)\left(p_{\bar{\nu}_\mu} \cdot p'_{e^-}\right)\left(1 - 4s_W^2 + 4s_W^4\right)\right. & (3.3) \\
&\quad + \left.\left(p'_{\bar{\nu}_\mu} \cdot p'_{e^-}\right)\left(p_{\bar{\nu}_\mu} \cdot p_{e^-}\right)\left(4s_W^4\right) + m_e^2 \left(p_{\bar{\nu}_\mu} \cdot p'_{\bar{\nu}_\mu}\right)\left(2s_W^2 - 4s_W^4\right)\right]. \\
& & (3.4)
\end{aligned}$$

$$\boxed{\nu_\mu + e^- \to \nu_e + \mu^-}$$

This reaction, which exchanges the lepton flavour of the neutrino and the charged lepton, is purely charged current. It is described by an e^- that emits a W^- boson to become a ν_e while the ν_μ absorbs the W^- to become a μ^-. The weak charged current of the μ-type leptons is given by

$$J^\alpha_{W,\mu} = \bar{u}^{s'}_{\mu^-} \gamma^\alpha \left(1 - \gamma_5\right) u^s_{\nu_\mu}.$$

For the electron type leptons it is similarly

$$J_{W,e}^\alpha = \bar{u}_{\nu_e}^{t'} \gamma^\alpha \left(1 - \gamma_5\right) u_{e^-}^t.$$

The squared matrix element can then be defined by

$$\left\langle \left| M \left(\nu_\mu + e^- \to \nu_e + \mu^-\right)\right|^2 \right\rangle = \frac{G_F^2}{4} \left(\sum_{s,s'} M^{\alpha\beta}(s,s')\right) \left(\sum_{t,t'} E_{\alpha\beta}(t,t')\right).$$

The neutrino tensor $M^{\alpha\beta}(s,s')$ and the electron tensor $E_{\alpha\beta}(t,t')$ are defined by

$$M^{\alpha\beta}(s,s') = \left[\bar{u}_{\mu^-}^{s'} \gamma^\alpha \left(1 - \gamma_5\right) u_{\nu_\mu}^s\right] \left[\bar{u}_{\mu^-}^{s'} \gamma^\beta \left(1 - \gamma_5\right) u_{\nu_\mu}^s\right]^\dagger,$$

$$E_{\alpha\beta}(t,t') = \left[\bar{u}_{\nu_e}^{t'} \gamma_\alpha \left(1 - \gamma_5\right) u_{e^-}^t\right] \left[\bar{u}_{\nu_e}^{t'} \gamma_\beta \left(1 - \gamma_5\right) u_{e^-}^t\right]^\dagger.$$

Performing the spin sum over $M^{\alpha\beta}(s,s')$ it can be transformed into the following trace

$$\sum_{s,s'} M^{\alpha\beta}(s,s') = \sum_{s,s'} \left[\bar{u}_{\mu^-}^{s'} \gamma^\alpha \left(1 - \gamma_5\right) u_{\nu_\mu}^s\right] \left[\bar{u}_{\nu_\mu}^s \gamma^\beta \left(1 - \gamma_5\right) u_{\mu^-}^s\right]$$

$$= \mathrm{Tr}\left[\gamma^\alpha \left(1 - \gamma_5\right) \left(\gamma^\delta p_{\nu_\mu,\delta}\right) \gamma^\beta \left(1 - \gamma_5\right) \left(\gamma^\epsilon p_{\mu^-,\epsilon}' + m_\mu\right)\right]$$

$$= p_{\nu_\mu,\delta} p_{\mu^-,\epsilon}' \mathrm{Tr}\left[2\left(1 + \gamma_5\right) \gamma^\alpha \gamma^\delta \gamma^\beta \gamma^\epsilon\right] + p_{\nu_\mu,\delta} m_\mu \mathrm{Tr}\left[2\left(1 + \gamma_5\right) \gamma^\alpha \gamma^\delta \gamma^\beta\right].$$

The second trace vanishes as it sums over an odd number of γ-matrices. The remaining expression is equivalent to Eq.(3.1). The muon tensor consequently becomes

$$\sum_{s,s'} M^{\alpha\beta}(s,s') = 8 \left[p_{\nu_\mu}^\alpha p_{\mu^-}'^\beta + p_{\nu_\mu}^\beta p_{\mu^-}'^\alpha - g^{\alpha\beta}\left(p_{\nu_\mu} \cdot p_{\mu^-}'\right) - i\epsilon^{\alpha\beta\delta\epsilon} p_{\nu_\mu,\delta} p_{\mu^-,\epsilon}'\right].$$

It is further clear, that $E_{\alpha\beta}(t,t')$ can be derived completely analogous to $M^{\alpha\beta}(s,s')$. The only difference is that there the charged lepton is incoming and the neutrino outgoing.

$$\sum_{t,t'} E_{\alpha\beta}(t,t') = 8 \left[p_{e^-,\alpha} p_{\nu_e,\beta}' + p_{e^-,\beta} p_{\nu_e,\alpha}' - g_{\alpha\beta}\left(p_{e^-} \cdot p_{\nu_e}'\right) - i\epsilon_{\alpha\beta\kappa\rho} p_{e^-}^\kappa p_{\nu_e}'^\rho\right].$$

The contraction of muon and electron tensor is straightforward again (see app. B). It yields

$$\sum_{s,s',t,t'} M^{\alpha\beta}(s,s') \sum_{t,t'} E_{\alpha\beta}(t,t') = 256 \left(p_{\nu_\mu} \cdot p_{e^-}\right) \left(p_{\mu^-}' \cdot p_{\nu_e}'\right).$$

Therefore, the matrix element is found to be

$$\left\langle \left| M \left(\nu_\mu + e^- \to \nu_e + \mu^-\right)\right|^2 \right\rangle = 64 G_F^2 \left(p_{\nu_\mu} \cdot p_{e^-}\right) \left(p_{\mu^-}' \cdot p_{\nu_e}'\right). \tag{3.5}$$

$$\boxed{\nu_\mu + \bar{\nu}_e + e^- \to \mu^-}$$

Based on the previous reaction, the calculation of inverse muon decay proceeds almost the same. It is again a purely charged current interaction. The muon current and subsequently the

muon tensor do not change. The only minor difference is in the electron current. The incoming antineutrino replaces the outgoing neutrino.

$$J_{W,e}^\alpha = \bar{v}_{\bar{\nu}_e}^{t'} \gamma^\alpha \left(1 - \gamma_5\right) u_{e^-}^t.$$

However, this does not cause a change in the electron tensor. One only replaces

$$\sum_t{}' u_{\nu_e}^{t'} \bar{u}_{\nu_e}^{t'} = \not{p}_{\nu_e} + m_{\nu_e} = \gamma^\epsilon p_{\nu_e,\delta} \qquad \text{by} \qquad \sum_t{}' v_{\bar{\nu}_e}^{t'} \bar{v}_{\bar{\nu}_e}^{t'} = \not{p}_{\bar{\nu}_e} - m_{\bar{\nu}_e} = \gamma^\epsilon p_{\bar{\nu}_e,\delta}.$$

Therefore the derivation yields the same result for the squared matrix element as for the flavour exchanging scattering. The electron antineutrino simply replaces the neutrino in the momentum index.

$$\left\langle \left| M \left(\nu_\mu + e^- + \bar{\nu}_e \to \mu^-\right) \right|^2 \right\rangle = 64 G_F^2 \left(p_{\nu_\mu} \cdot p_{e^-}\right) \left(p_{\mu^-}' \cdot p_{\bar{\nu}_e}\right). \tag{3.6}$$

$$\boxed{\bar{\nu}_e + e^- \to \bar{\nu}_\mu + \mu^-}$$

This reaction converts the lepton flavour of a pair of electron leptons into a pair of muon leptons. The electron current and consequently the electron tensor are the same as for inverse muon decay. The muon current takes the following form

$$J_{W,\mu}^\alpha = \bar{u}_{\mu^-}^{s'} \gamma^\alpha \left(1 - \gamma_5\right) v_{\bar{\nu}_\mu}^s.$$

It is equivalent to the muon current for the flavour converting scattering reaction except for the replacement of the spinor $u_{\nu_\mu}^s$ by $v_{\bar{\nu}_\mu}^s$. Analogous to the argumentation for the electron tensor in the inverse muon decay, this does not result in a modification of the muon tensor. Hence, the matrix element is again the same as e.g. for the inverse muon decay. One only has to replace the incoming momentum p_{ν_μ} by the outgoing momentum $p_{\bar{\nu}_\mu}'$.

$$\left\langle \left| M \left(\bar{\nu}_e + e^- \to \bar{\nu}_\mu + \mu^-\right) \right|^2 \right\rangle = 64 G_F^2 \left(p_{\bar{\nu}_\mu}' \cdot p_{e^-}\right) \left(p_{\mu^-}' \cdot p_{\bar{\nu}_e}\right). \tag{3.7}$$

3.2. Matrix Elements for Semileptonic Reactions

$$\boxed{\nu_e + n \to p + e^-}$$

The absorption of electron neutrinos on neutrons is a pure charged current reaction. For the calculation of the lepton tensor one can use the results that were already derived for the leptonic reactions. The lepton current for this reaction is

$$J_{W,e}^\alpha = \bar{u}_{e^-}^{t'} \gamma^\alpha \left(1 - \gamma_5\right) u_{\nu_e}^t.$$

Subsequently the electron tensor becomes

$$\sum_{t,t'} E_{\alpha\beta}(t,t') = 8 \left[p_{\nu_e,\alpha} p_{e^-,\beta} + p_{\nu_e,\beta} p_{e^-,\alpha} - g_{\alpha\beta} \left(p_{\nu_e} \cdot p_{e^-}\right) - i\epsilon_{\alpha\beta\kappa\rho} p_{\nu_e}^\kappa p_{e^-}^\rho \right].$$

The effective charged nuclear current equals the respective nuclear transition element. It is given by

$$J_{W,N}^\alpha = \bar{u}_p^{s'} \left[\gamma^\alpha G_V(q^2) + \sigma^{\alpha\eta} q_\eta \frac{iF_2(q^2)}{2m_N} - \gamma^\alpha \gamma_5 G_A(q^2) - \gamma_5 q^\alpha \frac{G_P(q^2)}{m_N} \right] u_n^s.$$

From now on the pseudoscalar coupling term will be dropped. For absorption of electron type neutrinos this is justified by the smallness of the contribution. It can be shown that the pseudoscalar contribution to the nucleon trace are of the order $m_e^2/m_\pi^2 \ll 1$. However, for absorptions of muon neutrinos these terms would be of the order $m_\mu^2/m_\pi^2 \sim 1$. Therefore the respective terms should be considered for a more complete treatment of absorption of muon neutrinos. This study should then be undertaken in a future work.

Further, the momentum dependence of all the coupling constants will not be noted any more. The effective nucleon current becomes then

$$J_{W,N}^\alpha = \bar{u}_p^{s'} \left[\gamma^\alpha G_V - \gamma^\alpha \gamma_5 G_A + \sigma^{\alpha\eta} q_\eta \frac{iF_2}{2m_N} \right] u_n^s.$$

In analogy with the electron tensor $E_{\alpha\beta}(t, t')$, a hadron tensor $H^{\alpha\beta}(s, s')$ can be defined

$$H^{\alpha\beta}(s, s') = \bar{u}_p^{s'} \left[\gamma^\alpha G_V - \gamma^\alpha \gamma_5 G_A + \sigma^{\alpha\eta} q_\eta \frac{iF_2}{2m_N} \right] u_n^s \bar{u}_n^s \left[\gamma^\beta G_V - \gamma^\beta \gamma_5 G_A - \sigma^{\beta\lambda} q_\lambda \frac{iF_2}{2m_N} \right] u_p^{s'}.$$

The spin sum over the effective spinors results into (see Eq.2.11)

$$\sum_s u_n^s \bar{u}_n^s = \gamma^\delta p_{n,\delta}^* + m_n^* \qquad \text{and} \qquad \sum_{s'} u_p^{s'} \bar{u}_p^{s'} = \gamma^\epsilon p_{p,\epsilon}^* + m_p^*,$$

where p^* was previously defined by (see Eq.2.12)

$$p^* = \left(\sqrt{\vec{p}^2 + m^{*2}}, \vec{p} \right).$$

The spin sum over the hadron tensor equates to

$$\begin{aligned}
\sum_{s,s'} H^{\alpha\beta}(s, s') = \text{Tr} \Bigg[&\left(\gamma^\alpha G_V - \gamma^\alpha \gamma_5 G_A + \sigma^{\alpha\eta} q_\eta \frac{iF_2}{2m_N} \right) \left(\gamma^\delta p_{n,\delta}^* + m_n^* \right) \\
&\left(\gamma^\beta G_V - \gamma^\beta \gamma_5 G_A - \sigma^{\beta\lambda} q_\lambda \frac{iF_2}{2m_N} \right) \left(\gamma^\epsilon p_{p,\epsilon}^* + m_p^* \right) \Bigg].
\end{aligned}$$

For clarity the hadron tensor will be separated into several terms, each corresponding to a certain coupling

$$H^{\alpha\beta} = H_{VV}^{\alpha\beta} + H_{AA}^{\alpha\beta} + H_{VA}^{\alpha\beta} + H_{VF}^{\alpha\beta} + H_{AF}^{\alpha\beta} + H_{FF}^{\alpha\beta}.$$

The spin sum over the vector element becomes

$$\begin{aligned}
\sum_{s,s'} H_{VV}^{\alpha\beta} &= G_V^2 \text{Tr} \left[\gamma^\alpha \left(\gamma^\delta p_{n,\delta}^* + m_n^* \right) \gamma^\beta \left(\gamma^\epsilon p_{p,\epsilon}^* + m_p^* \right) \right] \\
&= 4G_V^2 \left[p_n^{*\alpha} p_p^{*\beta} + p_n^{*\beta} p_p^{*\alpha} - g^{\alpha\beta} \left(p_n^* \cdot p_p^* \right) + g^{\alpha\beta} m_n^* m_p^* \right].
\end{aligned}$$

The spin sum over the axialvector element becomes

$$\sum_{s,s'} H_{AA}^{\alpha\beta} = G_A^2 \mathrm{Tr}\big[\gamma^\alpha \gamma_5 \left(\gamma^\delta p_{n,\delta}^* + m_n^*\right) \gamma^\beta \gamma_5 \left(\gamma^\epsilon p_{p,\epsilon}^* + m_p^*\right)\big]$$

$$= 4G_A^2 \big[p_n^{*\alpha} p_p^{*\beta} + p_n^{*\beta} p_p^{*\alpha} - g^{\alpha\beta}\left(p_n^* \cdot p_p^*\right) - g^{\alpha\beta} m_n^* m_p^*\big].$$

The spin sum over the vector-axialvector element becomes

$$\sum_{s,s'} H_{VA}^{\alpha\beta} = - G_V G_A \mathrm{Tr}\big[\gamma^\alpha \left(\gamma^\delta p_{n,\delta}^* + m_n^*\right) \gamma^\beta \gamma_5 \left(\gamma^\epsilon p_{p,\epsilon}^* + m_p^*\right)\big]$$

$$- G_V G_A \mathrm{Tr}\big[\gamma^\alpha \gamma_5 \left(\gamma^\delta p_{n,\delta}^* + m_n^*\right) \gamma^\beta \left(\gamma^\epsilon p_{p,\epsilon}^* + m_p^*\right)\big]$$

$$= - 8i G_V G_A p_{n,\delta}^* p_{p,\epsilon}^* \epsilon^{\alpha\beta\delta\epsilon}.$$

The spin sum over the vector-tensor element becomes

$$\sum_{s,s'} H_{VF}^{\alpha\beta} = \frac{iG_V F_2}{2m_N} \big\{ -\mathrm{Tr}\big[\gamma^\alpha \left(\gamma^\delta p_{n,\delta}^* + m_n^*\right) \sigma^{\beta\lambda} q_\lambda \left(\gamma^\epsilon p_{p,\epsilon}^* + m_p^*\right)\big]$$

$$+ \mathrm{Tr}\big[\sigma^{\alpha\eta} q_\eta \left(\gamma^\delta p_{n,\delta}^* + m_n^*\right) \gamma^\beta \left(\gamma^\epsilon p_{p,\epsilon}^* + m_p^*\right)\big]\big\}$$

$$= \frac{2G_V F_2}{m_N} \big\{ 2g^{\alpha\beta} \big[m_n^*\ \left(q \cdot p_p^*\right) - m_p^* \left(q \cdot p_n^*\right)\big] + q^\beta \left(p_n^{*\alpha} m_p^* - p_p^{*\alpha} m_n^*\right) + q^\alpha \left(p_n^{*\beta} m_p^* - p_p^{*\beta} m_n^*\right)\big\}.$$

The spin sum over the axialvector-tensor element becomes

$$\sum_{s,s'} H_{AF}^{\alpha\beta} = \frac{iG_A F_2}{2m_N} \big\{ \mathrm{Tr}\big[\gamma^\alpha \gamma_5 \left(\gamma^\delta p_{n,\delta}^* + m_n^*\right) \sigma^{\beta\lambda} q_\lambda \left(\gamma^\epsilon p_{p,\epsilon}^* + m_p^*\right)\big]$$

$$- \mathrm{Tr}\big[\sigma^{\alpha\eta} q_\eta \left(\gamma^\delta p_{n,\delta}^* + m_n^*\right) \gamma^\beta \gamma_5 \left(\gamma^\epsilon p_{p,\epsilon}^* + m_p^*\right)\big]\big\}$$

$$= -\frac{4iG_A F_2}{m_N} \left(p_{n,\delta}^* q_\lambda m_p^* + p_{p,\delta}^* q_\lambda m_n^*\right) \epsilon^{\alpha\beta\delta\lambda}.$$

The spin sum over the tensor element becomes

$$\sum_{s,s'} H_{FF}^{\alpha\beta} = \frac{F_2^2}{4m_N^2} q_\eta q_\lambda \mathrm{Tr}\big[\sigma^{\alpha\eta} \left(\gamma^\delta p_{n,\delta}^* + m_n^*\right) \sigma^{\beta\lambda} \left(\gamma^\epsilon p_{p,\epsilon}^* + m_p^*\right)\big]$$

$$= \frac{F_2^2}{m_N^2} \big\{ m_n^* m_p^* \left(g^{\alpha\beta} q^2 - q^\alpha q^\beta\right) + \left(g^{\alpha\beta} \big[\left(p_n^* \cdot p_p^*\right) q^2 - 2 \left(p_n^* \cdot q\right) \left(p_p^* \cdot q\right)\big]\right.$$

$$+ p_n^{*\alpha} \big[q^\beta \left(p_p^* \cdot q\right) - p_p^{*\beta} q^2\big] + p_p^{*\alpha} \big[q^\beta \left(p_n^* \cdot q\right) - p_n^{*\beta} q^2\big]$$

$$+ q^\alpha \big[p_n^{*\beta} \left(p_p^* \cdot q\right) + p_p^{*\beta} \left(p_n^* \cdot q\right) - q^\beta \left(p_n^* \cdot p_p^*\right)\big]\big)\big\}.$$

To derive the squared matrix element one has to calculate the contraction of electron tensor and hadron tensor. For this purpose the squared matrix element will be separated into terms with different coupling, analogous to the hadron tensor

$$\left\langle |M\left(\nu_e + n \to p + e^-\right)|^2 \right\rangle = \frac{G_F^2 V_{ud}^2}{4} \left(\sum_{s,s'} H^{\alpha\beta}(s,s')\right) \left(\sum_{t,t'} E_{\alpha\beta}(t,t')\right) \tag{3.8}$$

$$= \left\langle |M|^2 \right\rangle_{VV} + \left\langle |M|^2 \right\rangle_{AA} + \left\langle |M|^2 \right\rangle_{VA} + \left\langle |M|^2 \right\rangle_{VF} + \left\langle |M|^2 \right\rangle_{AF} + \left\langle |M|^2 \right\rangle_{FF}.$$

The vector matrix element becomes

$$\left\langle |M|^2 \right\rangle_{VV} = 16 G_F^2 V_{ud}^2 G_V^2 \left[\left(p_n^* \cdot p_{\nu_e} \right) \left(p_p^* \cdot p_{e^-} \right) + \left(p_n^* \cdot p_{e^-} \right) \left(p_p^* \cdot p_{\nu_e} \right) - m_n^* m_p^* \left(p_{\nu_e} \cdot p_{e^-} \right) \right]. \quad (3.9)$$

The axialvector matrix element becomes

$$\left\langle |M|^2 \right\rangle_{AA} = 16 G_F^2 V_{ud}^2 G_A^2 \left[\left(p_n^* \cdot p_{\nu_e} \right) \left(p_p^* \cdot p_{e^-} \right) + \left(p_n^* \cdot p_{e^-} \right) \left(p_p^* \cdot p_{\nu_e} \right) + m_n^* m_p^* \left(p_{\nu_e} \cdot p_{e^-} \right) \right]. \quad (3.10)$$

The vector-axialvector matrix element becomes

$$\left\langle |M|^2 \right\rangle_{VA} = 32 G_F^2 V_{ud}^2 G_V G_A \left[\left(p_n^* \cdot p_{\nu_e} \right) \left(p_p^* \cdot p_{e^-} \right) - \left(p_n^* \cdot p_{e^-} \right) \left(p_p^* \cdot p_{\nu_e} \right) \right]. \quad (3.11)$$

Note that these three elements form the standard expression for the matrix element in the nonrelativisitic limit with $E_{\nu_e}, E_{e^-} << M_N$

$$\begin{aligned}
\left\langle |M|^2 \right\rangle_{NR} = {} & 16 G_F^2 V_{ud}^2 \left[\left(G_A + G_V \right)^2 \left(p_n^* \cdot p_{\nu_e} \right) \left(p_p^* \cdot p_{e^-} \right) + \left(G_A - G_V \right)^2 \left(p_n^* \cdot p_{e^-} \right) \left(p_p^* \cdot p_{\nu_e} \right) \right. \\
& \left. + \left(G_A^2 - G_V^2 \right) m_n^* m_p^* \left(p_{\nu_e} \cdot p_{e^-} \right) \right] \\
\simeq {} & 16 G_F^2 V_{ud}^2 \left[G_A^2 \left(3 - \cos \theta_{\nu_e, e^-} \right) + G_V^2 \left(1 + \cos \theta_{\nu_e, e^-} \right) \right] E_n^* E_p^* E_{\nu_e} E_{e^-}.
\end{aligned}$$

The vector-tensor matrix element becomes

$$\begin{aligned}
\left\langle |M|^2 \right\rangle_{VF} = {} & \frac{8 G_F^2 V_{ud}^2 G_V F_2}{m_N} \left\{ \left[\left(p_n^* \cdot p_{\nu_e} \right) m_p^* - \left(p_p^* \cdot p_{\nu_e} \right) m_n^* \right] \left(p_{e^-} \cdot q \right) \right. \quad (3.12) \\
& \left. + \left[\left(p_n^* \cdot p_{e^-} \right) m_p^* - \left(p_p^* \cdot p_{e^-} \right) m_n^* \right] \left(p_{\nu_e} \cdot q \right) + \left[\left(p_n^* \cdot q \right) m_p^* - \left(p_p^* \cdot q \right) m_n^* \right] \left(p_{\nu_e} \cdot p_{e^-} \right) \right\}.
\end{aligned}$$

The axialvector-tensor matrix element becomes

$$\begin{aligned}
\left\langle |M|^2 \right\rangle_{AF} = {} & \frac{16 G_F^2 V_{ud}^2 G_A F_2}{m_N} \left\{ \left[\left(p_n^* \cdot p_{\nu_e} \right) m_p^* + \left(p_p^* \cdot p_{\nu_e} \right) m_n^* \right] \left(p_{e^-} \cdot q \right) \right. \quad (3.13) \\
& \left. - \left[\left(p_n^* \cdot p_{e^-} \right) m_p^* + \left(p_p^* \cdot p_{e^-} \right) m_n^* \right] \left(p_{\nu_e} \cdot q \right) \right\}.
\end{aligned}$$

The tensor matrix element becomes

$$\begin{aligned}
\left\langle |M|^2 \right\rangle_{FF} = {} & \frac{2 G_F^2 V_{ud}^2 F_2^2}{m_N^2} \left[\left(p_n^* \cdot p_p^* \right) \left(p_{\nu_e} \cdot p_{e^-} \right) q^2 + 2 \left(p_n^* \cdot p_{\nu_e} \right) \left(p_p^* \cdot q \right) \left(p_{e^-} \cdot q \right) \right. \quad (3.14) \\
& - 2 \left(p_n^* \cdot p_p^* \right) \left(p_{\nu_e} \cdot q \right) \left(p_{e^-} \cdot q \right) - 2 \left(p_n^* \cdot p_{\nu_e} \right) \left(p_p^* \cdot p_{e^-} \right) q^2 + 2 \left(p_n^* \cdot p_{e^-} \right) \left(p_p^* \cdot q \right) \left(p_{\nu_e} \cdot q \right) \\
& - 2 \left(p_n^* \cdot p_{e^-} \right) \left(p_p^* \cdot p_{\nu_e} \right) q^2 + 2 \left(p_n^* \cdot q \right) \left(p_p^* \cdot p_{\nu_e} \right) \left(p_{e^-} \cdot q \right) + 2 \left(p_n^* \cdot q \right) \left(p_p^* \cdot p_{e^-} \right) \left(p_{\nu_e} \cdot q \right) \\
& \left. - m_n^* m_p^* \left[\left(p_{\nu_e} \cdot p_{e^-}' \right) q^2 + 2 \left(p_{\nu_e} \cdot q \right) \left(p_{e^-} \cdot q \right) \right] \right].
\end{aligned}$$

The above notation is not the most compact and convenient for further calculation, especially for the parts corresponding to weak magnetism. However, it is a very general notation of the matrix element that proves very useful for the remaining semileptonic interactions.

$$\boxed{\bar{\nu}_e + p \rightarrow n + e^+}$$

The charged lepton current for the absorption of antineutrinos on protons reads

$$J_{W,e}^\alpha = \bar{v}_{\bar{\nu}_e}^{t'} \gamma^\alpha \left(1 - \gamma_5 \right) v_{e^+}^t.$$

As it was noted before, there is no difference in the resulting lepton tensor whether it is constructed from spinors u or antispinors v. However, for antineutrino capture the positron is treated like an incoming particle in the notation, while the antineutrino is outgoing. The lepton tensor can then be constructed from the one for neutrino capture by replacing $\nu_e \to e^+$ and $e^- \to \bar{\nu}_e$

$$\sum_{t,t'} E_{\alpha\beta}(t,t') = 8 \left[p_{e^+,\alpha} p_{\bar{\nu}_e,\beta} + p_{e^+,\beta} p_{\bar{\nu}_e,\alpha} - g_{\alpha\beta} \left(p_{e^+} \cdot p_{\bar{\nu}_e} \right) - i\epsilon_{\alpha\beta\kappa\rho} p_{e^+}^\kappa p_{\bar{\nu}_e}^\rho \right].$$

The effective charged nucleon current reads

$$J_{W,N}^\alpha = \bar{u}_n^{s'} \left[\gamma^\alpha G_V - \gamma^\alpha \gamma_5 G_A + \sigma^{\alpha\eta} q_\eta \frac{iF_2}{2m_N} \right] u_p^s.$$

It differs from the charged nucleon current of neutrino absorption on neutron by the replacement $n \to p$ and $p \to n$. It is then immediately clear that also the resulting nucleon tensor for $\bar{\nu}_e$-absorption equals the one of ν_e-absorption with the same replacements. The matrix element is the contraction of nucleon and lepton tensor. Hence, it can be obtained by the combination of replacements for nucleons and leptons

$$\left\langle \left| M \left(\bar{\nu}_e + p \to n + e^+ \right) \right|^2 \right\rangle = \left\langle \left| M \left(\nu_e + n \to p + e^- \right) \right|^2 \right\rangle \bigg|_{\nu_e \to e^+, e^- \to \bar{\nu}_e, n \to p, p \to n}.$$

However, all parts of the matrix element are either symmetric (3.9, 3.10, 3.11, 3.14) or antisymmetric (3.12, 3.13) to the replacement $\{\nu_e \to e^-, e^- \to \nu_e, n \to p, p \to n\}$. Therefore, all that needs to be done is changing $\nu_e \to \bar{\nu}_e$ and $e^- \to e^+$ in the indices of the matrix element, and to invert the overall sign for the vector-tensor and the axialvector-tensor part.

$$\left\langle \left| M \left(\bar{\nu}_e + p \to n + e^+ \right) \right|^2 \right\rangle_{VV,AA,VA,FF} = \left\langle \left| M \left(\nu_e + n \to p + e^- \right) \right|^2 \right\rangle_{VV,AA,VA,FF} \bigg|_{\nu_e \to \bar{\nu}_e, e^- \to e^+},$$

$$\left\langle \left| M \left(\bar{\nu}_e + p \to n + e^+ \right) \right|^2 \right\rangle_{VF,AF} = - \left\langle \left| M \left(\nu_e + n \to p + e^- \right) \right|^2 \right\rangle_{VF,AF} \bigg|_{\nu_e \to \bar{\nu}_e, e^- \to e^+}.$$

$$\boxed{\bar{\nu}_e + e^- + p \to n}$$

For inverse neutron decay the charged lepton current is

$$J_{W,e}^\alpha = \bar{v}_{\bar{\nu}_e}^{t'} \gamma^\alpha \left(1 - \gamma_5 \right) u_{e^-}^t.$$

Hence the lepton tensor is the same as for antineutrino absorption with the replacement $e^+ \to e^-$. Further, the charged nucleon current and the corresponding tensor are exactly the same as for antineutrino absorption. Therefore, the matrix element has the same structure as for the previous reactions. It differs however by a factor $1/2$ from the average over incoming spins of electron and proton. It can be written

$$\left\langle \left| M \left(\bar{\nu}_e + e^- + p \to n \right) \right|^2 \right\rangle_{VV,AA,VA,FF} = \frac{1}{2} \left\langle \left| M \left(\nu_e + n \to p + e^- \right) \right|^2 \right\rangle_{VV,AA,VA,FF} \bigg|_{\nu_e \to \bar{\nu}_e},$$

$$\left\langle \left| M \left(\bar{\nu}_e + e^- + p \to n \right) \right|^2 \right\rangle_{VF,AF} = - \frac{1}{2} \left\langle \left| M \left(\nu_e + n \to p + e^- \right) \right|^2 \right\rangle_{VF,AF} \bigg|_{\nu_e \to \bar{\nu}_e}.$$

$$\boxed{\nu_\mu + n \to p + \mu^-}$$

The charged lepton current for muon neutrino absorption reads

$$J_{W,e}^\alpha = \bar{u}_{\mu^-}^{t'} \gamma^\alpha \left(1 - \gamma_5\right) u_{\nu_\mu}^t.$$

It is equivalent the one for electron neutrino absorption with the replacement $e \to \mu$. Hence the same applies for the subsequent lepton tensor. Also, the nucleon current and nucleon tensor are exactly the same as for electron neutrino absorption. No assumption was previously made concerning the mass of the charged lepton. Hence, the matrix element has the same structure for absorption of both electron and muon neutrinos

$$\left\langle \left| M \left(\nu_\mu + n \to p + \mu^- \right) \right|^2 \right\rangle = \left\langle \left| M \left(\nu_e + n \to p + e^- \right) \right|^2 \right\rangle \Big|_{e \to \mu}.$$

3.2.1. Compact Notation of Semileptonic Matrix Elements

$$\boxed{\nu_e + n \to p + e^-}$$

A more compact notation can be found for the tensor related parts of the matrix element. The momentum transfer q is the difference between outgoing and incoming nucleon four-momentum (2.6). Due to momentum conservation it can also be related to the lepton four-momenta instead. For neutrino absorption on neutrons this reads

$$q = p_p - p_n = p_{\nu_e} - p_{e^-} \qquad \text{and} \qquad q^2 = m_e^2 - 2 \left(p_{\nu_e} \cdot p_{e^-} \right).$$

The second relation accounts for the vanishing neutrino mass. Using the above notation the vector-tensor matrix element (Eq. 3.12) transforms into

$$
\begin{aligned}
\left\langle |M|^2 \right\rangle_{VF} = \frac{8 G_F^2 V_{ud}^2 G_V F_2}{m_N} \Big\{ 2 &\left[\left(p_n^* \cdot p_{\nu_e} \right) m_p^* - \left(p_p^* \cdot p_{\nu_e} \right) m_n^* - \left(p_n^* \cdot p_{e^-} \right) m_p^* + \left(p_p^* \cdot p_{e^-} \right) m_n^* \right] \\
&\times \left(p_{\nu_e} \cdot p_{e^-} \right) - \left[\left(p_n^* \cdot p_{\nu_e} \right) m_p^* - \left(p_p^* \cdot p_{\nu_e} \right) m_n^* \right] m_e^2 \Big\}.
\end{aligned}
\tag{3.15}
$$

The axialvector-tensor matrix element (Eq. 3.13) transforms into

$$
\begin{aligned}
\left\langle |M|^2 \right\rangle_{AF} = \frac{16 G_F^2 V_{ud}^2 G_A F_2}{m_N} \Big\{ &\left[\left(p_n^* \cdot p_{\nu_e} \right) m_p^* + \left(p_p^* \cdot p_{\nu_e} \right) m_n^* + \left(p_n^* \cdot p_{e^-} \right) m_p^* + \left(p_p^* \cdot p_{e^-} \right) m_n^* \right] \\
&\times \left(p_{\nu_e} \cdot p_{e^-} \right) - \left[\left(p_n^* \cdot p_{\nu_e} \right) m_p^* + \left(p_p^* \cdot p_{\nu_e} \right) m_n^* \right] m_e^2 \Big\}.
\end{aligned}
\tag{3.16}
$$

The tensor matrix element (Eq. 3.14) transforms into

$$
\left\langle |M|^2 \right\rangle_{FF} = \frac{2 G_F^2 V_{ud}^2 F_2^2}{m_N^2} \Big\{ 4 \left(p_{\nu_e} \cdot p_{e^-} \right) \left[\left(p_n^* \cdot p_{\nu_e} \right) \left(p_p^* \cdot p_{\nu_e} \right) + \left(p_n^* \cdot p_{e^-} \right) \left(p_p^* \cdot p_{e^-} \right) \right]
\tag{3.17}
$$

$$
- m_e^2 \left[4 \ \left(p_n^* \cdot p_{\nu_e} \right) \left(p_p^* \cdot p_{\nu_e} \right) + \left(p_n^* \cdot p_p^* \right) \left(p_{\nu_e} \cdot p_{e^-} \right) \right] + m_n^* m_p^* \left[4 \left(p_{\nu_e} \cdot p_{e^-} \right)^2 - 3 \left(p_{\nu_e} \cdot p_{e^-} \right) m_e^2 \right] \Big\}.
$$

$$\boxed{\bar{\nu}_e + p \rightarrow n + e^+}$$

For antineutrino absorption on proton the momentum transfer q is given by

$$q = p_n - p_p = p_{\bar{\nu}_e} - p_{e^+} \qquad \text{and} \qquad q^2 = m_e^2 - 2\left(p_{\bar{\nu}_e} \cdot p_{e^+}\right).$$

This is related to the momentum transfer of neutrino absorption by the replacement $\{\nu_e \rightarrow \bar{\nu}_e,\ e^- \rightarrow e^+\}$. Since this is the same relation that connects the matrix elements of the two reactions, also the compact notation can be obtained by the same replacement.

$$\boxed{\bar{\nu}_e + e^- + p \rightarrow n}$$

For inverse neutron decay the momentum transfer q is given by

$$q = p_n - p_p = p_{\nu_e} + p_{e^-} \qquad \text{and} \qquad q^2 = m_e^2 + 2\left(p_{\nu_e} \cdot p_{e^-}\right).$$

This is different from the relation for neutrino and antineutrino absorption. Using this notation the vector-tensor element transforms into

$$\left\langle |M|^2 \right\rangle_{VF} = \frac{4 G_F^2 V_{ud}^2 G_V F_2}{m_N} \left\{ 2 \left[\left(p_p^* \cdot p_{\bar{\nu}_e}\right) m_n^* - \left(p_n^* \cdot p_{\bar{\nu}_e}\right) m_p^* + \left(p_p^* \cdot p_{e^-}\right) m_n^* - \left(p_n^* \cdot p_{e^-}\right) m_p^* \right] \right.$$
$$\left. \times \left(p_{\bar{\nu}_e} \cdot p_{e^-}\right) + \left[\left(p_p^* \cdot p_{\bar{\nu}_e}\right) m_n^* - \left(p_n^* \cdot p_{\bar{\nu}_e}\right) m_p^* \right] m_e^2 \right\}. \tag{3.18}$$

The axialvector-tensor matrix element transforms into

$$\left\langle |M|^2 \right\rangle_{AF} = \frac{8 G_F^2 V_{ud}^2 G_A F_2}{m_N} \left\{ \left[\left(p_n^* \cdot p_{e^-}\right) m_p^* + \left(p_p^* \cdot p_{e^-}\right) m_n^* - \left(p_n^* \cdot p_{\bar{\nu}_e}\right) m_p^* - \left(p_p^* \cdot p_{\bar{\nu}_e}\right) m_n^* \right] \right.$$
$$\left. \times \left(p_{\bar{\nu}_e} \cdot p_{e^-}\right) - \left[\left(p_n^* \cdot p_{\bar{\nu}_e}\right) m_p^* + \left(p_p^* \cdot p_{\bar{\nu}_e}\right) m_n^* \right] m_e^2 \right\}. \tag{3.19}$$

The tensor matrix element transforms into

$$\left\langle |M|^2 \right\rangle_{FF} = \frac{G_F^2 V_{ud}^2 F_2^2}{m_N^2} \left\{ 4 \left(p_{e^-} \cdot p_{\bar{\nu}_e}\right) \left[\left(p_n^* \cdot p_{\bar{\nu}_e}\right) \left(p_p^* \cdot p_{\bar{\nu}_e}\right) + \left(p_n^* \cdot p_{e^-}\right) \left(p_p^* \cdot p_{e^-}\right) \right] \right. \tag{3.20}$$
$$\left. + m_e^2 \left[4 \ \left(p_n^* \cdot p_{\bar{\nu}_e}\right) \left(p_p^* \cdot p_{\bar{\nu}_e}\right) - \left(p_n^* \cdot p_p^*\right) \left(p_{\bar{\nu}_e} \cdot p_{e^-}\right) \right] - m_n^* m_p^* \left[4 \left(p_{\bar{\nu}_e} \cdot p_{e^-}\right)^2 + 3 \left(p_{\bar{\nu}_e} \cdot p_{e^-}\right) m_e^2 \right] \right\}.$$

$$\boxed{\nu_\mu + n \rightarrow p + \mu^-}$$

Analogous to the comparison between neutrino and antineutrino capture it can be shown that the compact notation for muon neutrino absorption can be derived from electron neutrino absorption by the known replacement $\{e \rightarrow \mu\}$.

3.2.2. Approximation for Single Nucleon Mass

In an EOS with a single effective nucleon mass the previous results can be further simplified. The corresponding matrix element can also be used as an approximation for the case of very similar effective nucleon masses $\left|m_n^* - m_p^*\right| \ll m_{n,p}^*$. However, it has to be noted that the corresponding error of this approximation is of the order $\Delta m^*/m_N^*$. This is actually larger than some of the other terms that are retained in the approximation. One should keep this in mind when discussing small effects.

$\boxed{\nu_e + n \rightarrow p + e^-}$

The vector-tensor matrix element simplifies to

$$\left\langle |M|^2 \right\rangle_{VF} = 8 G_F^2 V_{ud}^2 G_V F_2 \frac{m_N^*}{m_N} \left\{ 2 \left[\left(p_n^* - p_p^*\right) \cdot \left(p_{\nu_e} - p_{e^-}\right) \right] \left(p_{\nu_e} \cdot p_{e^-}\right) - \left[\left(p_n^* - p_p^*\right) \cdot p_{\nu_e} \right] m_e^2 \right\}. \tag{3.21}$$

The axialvector-tensor matrix element simplifies to

$$\left\langle |M|^2 \right\rangle_{AF} = 16 G_F^2 V_{ud}^2 G_A F_2 \frac{m_N^*}{m_N} \left\{ \left[\left(p_n^* + p_p^*\right) \cdot \left(p_{\nu_e} + p_{e^-}\right) \right] \left(p_{\nu_e} \cdot p_{e^-}\right) - \left[\left(p_n^* + p_p^*\right) \cdot p_{\nu_e} \right] m_e^2 \right\}. \tag{3.22}$$

The matrix elements for electron antineutrino and muon neutrino capture follow accordingly.

$\boxed{\bar{\nu}_e + e^- + p \rightarrow n}$

The vector-tensor matrix element simplifies to

$$\left\langle |M|^2 \right\rangle_{VF} = 4 G_F^2 V_{ud}^2 G_V F_2 \frac{m_N^*}{m_N} \left\{ 2 \left[\left(p_p^* - p_n^*\right) \cdot \left(p_{\bar{\nu}_e} + p_{e^-}\right) \right] \left(p_{\bar{\nu}_e} \cdot p_{e^-}\right) + \left[\left(p_p^* - p_n^*\right) \cdot p_{\bar{\nu}_e} \right] m_e^2 \right\}. \tag{3.23}$$

The axialvector-tensor element transforms into

$$\left\langle |M|^2 \right\rangle_{AF} = 8 G_F^2 V_{ud}^2 G_A F_2 \frac{m_N^*}{m_N} \left\{ \left[\left(p_n^* + p_p^*\right) \cdot \left(p_{e^-} - p_{\bar{\nu}_e}\right) \right] \left(p_{\bar{\nu}_e} \cdot p_{e^-}\right) - \left[\left(p_n^* + p_p^*\right) \cdot p_{\bar{\nu}_e} \right] m_e^2 \right\}. \tag{3.24}$$

Noninteracting Nonrelativistic Nucleons

In the case of noninteracting, nonrelativistic nucleons it can easily be shown that the above matrix elements agree with derivations and results in previous works, especially for the neutrino absorption reactions [66, 130]. For ν_e-absorption, four-momentum conservation demands

$$p_p = p_n + p_{\nu_e} - p_{e^-}.$$

For noninteracting nucleons the effective nucleon momenta become the regular nucleon momenta $p_{n,p}^* = p_{n,p}$ and the effective mass equals the rest mass $m_N^* = m_N$. Hence the vector-tensor matrix element becomes

$$\left\langle |M|^2 \right\rangle_{VF} = 8 G_F^2 V_{ud}^2 G_V F_2 \left\{ 4 \left(p_{\nu_e} \cdot p_{e^-}\right)^2 - 3 \left(p_{\nu_e} \cdot p_{e^-}\right) m_e^2 \right\}. \tag{3.25}$$

The axialvector-tensor matrix element becomes

$$\left\langle |M|^2 \right\rangle_{AF} = 32 G_F^2 V_{ud}^2 G_A F_2 \left\{ \left[p_n \cdot (p_{\nu_e} + p_{e^-}) \right] (p_{\nu_e} \cdot p_{e^-}) - (p_n \cdot p_{\nu_e}) \, m_e^2 \right\}. \tag{3.26}$$

Neglecting the lower order terms $\sim m_e^2$, both of these expressions agree with equation (12) of [66]. Further it can be shown that from 3.25, 3.26, 3.17 one can derive the exact cross section for noninteracting nucleons at rest which was given in equation (12) in [130].

4. Scattering Kernels for Leptonic Reactions

In this chapter scattering kernels for purely leptonic neutrino reactions will be derived. Starting point are the well known matrix elements from the literature, that have been discussed in chapter 3. In a first step a scattering kernel $R(\theta_{12}, E_{\nu 1}, E_{\nu 2})$ that depends on the relative angle θ_{12} between the neutrinos will be obtained. The procedure will be based on the work of [131, 132] for neutrino electron scattering. This expression will then be transformed into a scattering kernel $R(\theta_1, \theta_2, E_{\nu 1}, E_{\nu 2})$ that depends on the angle of each neutrino with respect to the radial outward direction. Such an expression is required for numerical neutrino transport where the discrete distribution function of neutrinos $f(E_\nu, \theta)$ is dependent on both the energy and the azimuthal angle with respect to the radial direction. The approach to develop this transport scattering kernel will follow the studies of [133, 134, 135].

4.1. Scattering Kernel with Relative Angle Dependence

4.1.1. General Expression

Let us assume we have a generalized reaction of an incoming neutrino (particle "1"), reacting with an incoming charged lepton (particle "2") into an outgoing neutrino (particle "3") and an outgoing charged lepton (particle "4").

$$\nu_1 + l_2 \rightarrow \nu_3 + l_4.$$

One can show that for such a reaction the matrix element can be expressed in a general form

$$\left\langle |M|^2 \right\rangle = C_1 \left(p_1 \cdot p_2 \right) \left(p_3 \cdot p_4 \right) + C_2 \left(p_1 \cdot p_4 \right) \left(p_2 \cdot p_3 \right) + C_3 \left(p_1 \cdot p_3 \right). \tag{4.1}$$

Here the C_i are constant prefactors that are different for each reaction. The scattering kernel for this general reaction be defined

$$R(\theta_{13}, E_1, E_3) = 2 \int \frac{d^3 p_2}{(2\pi)^3} \frac{d^3 p_4}{(2\pi)^3} \frac{\left\langle |M|^2 \right\rangle}{16 E_1 E_2 E_3 E_4} (2\pi)^4 \, \delta^4(p_1 + p_2 - p_3 - p_4) f_2(E_2) \left[1 - f_4(E_4) \right]$$

$$= C_1^* R_1 + C_2^* R_2 + C_3^* R_3. \tag{4.2}$$

The C_i^* are constant prefactors again, while the R_i are defined by

$$R_1(\theta_{13}, E_1, E_3) = \int d^3p_2 d^3p_4 \frac{(p_1 \cdot p_2)(p_3 \cdot p_4)}{E_1 E_2 E_3 E_4} \delta^4(p_1 + p_2 - p_3 - p_4) f_2(E_2)[1 - f_4(E_4)]. \quad (4.3)$$

$$R_2(\theta_{13}, E_1, E_3) = \int d^3p_2 d^3p_4 \frac{(p_1 \cdot p_4)(p_2 \cdot p_3)}{E_1 E_2 E_3 E_4} \delta^4(p_1 + p_2 - p_3 - p_4) f_2(E_2)[1 - f_4(E_4)]. \quad (4.4)$$

$$R_3(\theta_{13}, E_1, E_3) = \int d^3p_2 d^3p_4 \frac{(p_1 \cdot p_3)}{E_1 E_2 E_3 E_4} \delta^4(p_1 + p_2 - p_3 - p_4) f_2(E_2)[1 - f_4(E_4)]. \quad (4.5)$$

The R_i can be solved analytically up to a remaining integration over E_2, for the derivation see appendix C.1. For R_1 the result is given by

$$R_1 = \frac{2\pi}{\Delta^5} \int_{E_-}^{\infty} dE_2 f_2(E_2)[1 - f_4(E_4)] \left(\widetilde{A}_1 E_2^2 + \widetilde{B}_1 E_2 + \widetilde{C}_1 \right). \quad (4.6)$$

The integration limit E_- equals

$$E_- = \frac{1}{2} \left[(E_3 - E_1)(1 + k) + \sqrt{(E_1^2 + E_3^2 - 2E_1 E_3 \cos\theta) \left[(1 + k)^2 + \frac{2m_2^2}{E_1 E_3 (1 - \cos\theta)} \right]} \right], \quad (4.7)$$

with

$$k \equiv \frac{Q}{E_1 E_3 (1 - \cos\theta)} \qquad \text{and} \qquad Q \equiv \frac{1}{2} \left(m_4^2 - m_2^2 \right). \quad (4.8)$$

The coefficients $\widetilde{A}_1$, $\widetilde{B}_1$, $\widetilde{C}_1$, and Δ are defined as

$$\widetilde{A}_1 = E_1 E_3 (1 - \cos\theta)^2 \left[E_1^2 + E_1 E_3 (3 + \cos\theta) + E_3^2 \right], \quad (4.9)$$

$$\widetilde{B}_1 = E_1^2 E_3 (1 - \cos\theta)^2 \left[2E_1^2 + E_1 E_3 (3 - \cos\theta) - E_3^2 (1 + 3\cos\theta) \right] \quad (4.10)$$
$$+ Q(1 - \cos\theta) \left[E_1^3 + E_1^2 E_3 (2 + \cos\theta) - E_1 E_3^2 (2 + \cos\theta) - E_3^3 \right],$$

$$\widetilde{C}_1 = E_1^3 E_3 (1 - \cos\theta)^2 \left[E_1^2 - 2E_1 E_3 \cos\theta + E_3^2 \left(-\frac{1}{2} + \frac{3}{2} \cos^2\theta \right) \right] \quad (4.11)$$
$$+ QE_1 (1 - \cos\theta) \left[E_1^3 - E_1^2 E_3 \cos\theta + E_1 E_3^2 (-2 + \cos^2\theta) + E_3^3 \cos\theta \right]$$
$$+ Q^2 \left[E_1^2 \cos\theta - E_1 E_3 \left(\frac{3}{2} + \frac{1}{2} \cos^2\theta \right) + E_3^2 \cos\theta \right] + \frac{1}{2} E_1 E_3 (1 - \cos^2\theta) \Delta^2 m_2^2,$$

$$\Delta = \sqrt{E_1^2 - 2E_1 E_3 \cos\theta + E_3^2}. \quad (4.12)$$

For R_2 one finds similarly

$$R_2 = \frac{2\pi}{\Delta^5} \int_{E_-}^{\infty} dE_2 f_2(E_2)[1 - f_4(E_4)] \left(\widetilde{A}_2 E_2^2 + \widetilde{B}_2 E_2 + \widetilde{C}_2 \right). \quad (4.13)$$

The coefficients $\widetilde{A}_2$, $\widetilde{B}_2$, and $\widetilde{C}_2$ are given by

$$\widetilde{A}_2 = E_1 E_3 \left(1 - \cos\theta\right)^2 \left[E_1^2 + E_1 E_3 \left(3 + \cos\theta\right) + E_3^2\right], \tag{4.14}$$

$$\widetilde{B}_2 = E_1 E_3^2 \left(1 - \cos\theta\right)^2 \left[E_1^2 \left(1 + 3\cos\theta\right) + E_1 E_3 \left(-3 + \cos\theta\right) - 2E_3^2\right] \tag{4.15}$$
$$+ Q\left(1 - \cos\theta\right) \left[E_1^3 + E_1^2 E_3 \left(2 + \cos\theta\right) - E_1 E_3^2 \left(2 + \cos\theta\right) - E_3^3\right],$$

$$\widetilde{C}_2 = E_1 E_3^3 \left(1 - \cos\theta\right)^2 \left[E_1^2 \left(-\frac{1}{2} + \frac{3}{2}\cos^2\theta\right) - 2E_1 E_3 \cos\theta + E_3^2\right] \tag{4.16}$$
$$+ QE_3 \left(1 - \cos\theta\right) \left[E_1^3 \cos\theta + E_1^2 E_3 \left(-2 + \cos^2\theta\right) - E_1 E_3^2 \cos\theta + E_3^3\right]$$
$$+ Q^2 \left[E_1^2 \cos\theta - E_1 E_3 \left(\frac{3}{2} + \frac{1}{2}\cos^2\theta\right) + E_3^2 \cos\theta\right] + \frac{1}{2} E_1 E_3 \left(1 - \cos^2\theta\right) \Delta^2 m_2^2.$$

The expression R_3 becomes eventually

$$R_3 = \frac{2\pi}{\Delta^5} \int dE_2 f_2(E_2) \left[1 - f_4(E_4)\right] \widetilde{C}_3. \tag{4.17}$$

The coefficient $\widetilde{C}_3$ is given by

$$\widetilde{C}_3 = \left(1 - \cos\theta\right) \Delta^4 m_2 m_4. \tag{4.18}$$

Now the remaining energy integrals can be transformed into Fermi-Dirac integrals which are more convenient for numerical integration. One can show (see appendix C.1)

$$I_0 = \int_{E_-}^{\infty} dE_2 f_2(E_2) \left[1 - f_4(E_4)\right]$$
$$= T f_\gamma(\eta' - \eta) \left[F_0(\eta' - y) - F_0(\eta - y)\right], \tag{4.19}$$

$$I_1 = \int_{E_-}^{\infty} dE_2 E_2 f_2(E_2) \left[1 - f_4(E_2 + E_1 - E_3)\right]$$
$$= T^2 f_\gamma(\eta' - \eta) \left\{\left[F_1(\eta' - y) - F_1(\eta - y)\right] + y \left[F_0(\eta' - y) - F_0(\eta - y)\right]\right\}, \tag{4.20}$$

$$I_2 = \int_{E_-}^{\infty} dE_2 E_2^2 f_2(E_2) \left[1 - f_4(E_2 + E_1 - E_3)\right]$$
$$= T^3 f_\gamma(\eta' - \eta) \left\{\left[F_2(\eta' - y) - F_2(\eta - y)\right] + 2y \left[F_1(\eta' - y) - F_1(\eta - y)\right] \tag{4.21}$$
$$+ y^2 \left[F_0(\eta' - y) - F_0(\eta - y)\right]\right\}.$$

Here the Fermi-Dirac integrals $F_n(z)$ and the functions $f_\gamma(z)$ are given by

$$F_n(z) = \int_0^{\infty} dx \frac{x^n}{\exp\left(x - z\right) + 1} \qquad \text{and} \qquad f_\gamma(z) = \frac{1}{\exp\left(z\right) - 1}, \tag{4.22}$$

and the coefficients η, η', and y are determined by

$$y \equiv \frac{E_-}{T}, \qquad \eta = \frac{\mu_2}{T}, \qquad \eta' = \eta - \frac{E_1 - E_3 + \mu_2 - \mu_4}{T}. \tag{4.23}$$

The integrals R_i can then be expressed by

$$R_1 = \frac{2\pi}{\Delta^5} \left(\widetilde{A}_1 I_2 + \widetilde{B}_1 I_1 + \widetilde{C}_1 I_0\right), \quad R_2 = \frac{2\pi}{\Delta^5} \left(\widetilde{A}_2 I_2 + \widetilde{B}_2 I_1 + \widetilde{C}_2 I_0\right), \quad R_3 = \frac{2\pi}{\Delta^5} \widetilde{C}_3 I_0. \tag{4.24}$$

The Fermi-Dirac integrals can be numerically expressed e.g. by Chebychev expansions of polylogarithms [136, 135].

4.1.2. Muon Neutrino Scattering on Electrons

The special case of scattering of muon neutrinos on electrons can be derived from the general expression Eq.(4.2) by subsequently replacing

$$p_1 = p_{\nu_\mu}, \qquad p_2 = p_{e^-}, \qquad p_3 = p'_{\nu_\mu}, \qquad p_4 = p'_{e^-}, \qquad m_2 = m_4 = m_e. \tag{4.25}$$

The matrix element for scattering of muon neutrinos on electrons is given in Eq.(3.2). By inserting this into Eq.(4.2), the constants C_i^* equate to

$$C_1^* = \frac{G_F^2}{2\pi^2}\left(1 - 4s_W^2 + 4s_W^4\right), \qquad C_2^* = \frac{G_F^2}{2\pi^2}4s_W^4, \qquad C_3^* = \frac{G_F^2}{2\pi^2}m_e^2\left(2s_W^2 - 4s_W^4\right). \tag{4.26}$$

Thus one finds for the scattering kernel

$$\begin{aligned}
R\left(\theta, E_{\nu_\mu}, E'_{\nu_\mu}\right) = \frac{G_F^2}{\pi}\frac{1}{\Delta^5}\bigg[&\left(1 - 4s_W^2 + 4s_W^4\right)\left(\widetilde{A}_1 I_2 + \widetilde{B}_1 I_1 + \widetilde{C}_1 I_0\right) \\
&+ 4s_W^4\left(\widetilde{A}_2 I_2 + \widetilde{B}_2 I_1 + \widetilde{C}_2 I_0\right) + m_e^2\left(2s_W^2 - 4s_W^4\right)\widetilde{C}_3 I_0\bigg],
\end{aligned} \tag{4.27}$$

with

$$\begin{aligned}
\Delta =& \sqrt{E_{\nu_\mu}^2 - 2E_{\nu_\mu}E'_{\nu_\mu}\cos\theta + E'^{\,2}_{\nu_\mu}}, \\
\widetilde{A}_1 =& E_{\nu_\mu}E'_{\nu_\mu}(1 - \cos\theta)^2\left[E_{\nu_\mu}^2 + E_{\nu_\mu}E'_{\nu_\mu}(3 + \cos\theta) + E'^{\,2}_{\nu_\mu}\right], \\
\widetilde{B}_1 =& E_{\nu_\mu}^2 E'_{\nu_\mu}(1 - \cos\theta)^2\left[2E_{\nu_\mu}^2 + E_{\nu_\mu}E'_{\nu_\mu}(3 - \cos\theta) - E'^{\,2}_{\nu_\mu}(1 + 3\cos\theta)\right], \\
\widetilde{C}_1 =& E_{\nu_\mu}^3 E'_{\nu_\mu}(1 - \cos\theta)^2\left[E_{\nu_\mu}^2 - 2E_{\nu_\mu}E'_{\nu_\mu}\cos\theta + E'^{\,2}_{\nu_\mu}\left(-\frac{1}{2} + \frac{3}{2}\cos^2\theta\right)\right] \\
&+ \frac{1}{2}E_{\nu_\mu}E'_{\nu_\mu}(1 - \cos^2\theta)\Delta^2 m_e^2, \\
\widetilde{A}_2 =& E_{\nu_\mu}E'_{\nu_\mu}(1 - \cos\theta)^2\left[E_{\nu_\mu}^2 + E_{\nu_\mu}E'_{\nu_\mu}(3 + \cos\theta) + E'^{\,2}_{\nu_\mu}\right], \\
\widetilde{B}_2 =& E_{\nu_\mu}E'^{\,2}_{\nu_\mu}\left[E_{\nu_\mu}^2(1 + 3\cos\theta) + E_{\nu_\mu}E'_{\nu_\mu}(-3 + \cos\theta) - 2E'^{\,2}_{\nu_\mu}\right], \\
\widetilde{C}_2 =& E_{\nu_\mu}E'^{\,3}_{\nu_\mu}(1 - \cos\theta)^2\left[E_{\nu_\mu}^2\left(-\frac{1}{2} + \frac{3}{2}\cos^2\theta\right) - 2E_{\nu_\mu}E'_{\nu_\mu}\cos\theta + E'^{\,2}_{\nu_\mu}\right] \\
&+ \frac{1}{2}E_{\nu_\mu}E'_{\nu_\mu}(1 - \cos^2\theta)\Delta^2 m_e^2, \\
\widetilde{C}_3 =& (1 - \cos\theta)\Delta^4 m_e^2.
\end{aligned}$$

The functions I_0, I_1, and I_2 are given in equations (4.19)-(4.21). The coefficients therein take the form

$$y \equiv \frac{E_-}{T}, \qquad \eta = \frac{\mu_e}{T}, \qquad \eta' = \frac{\mu_e - E_{\nu_\mu} + E'_{\nu_\mu}}{T}, \tag{4.28}$$

with

$$E_- = \frac{1}{2}\left(E'_{\nu_\mu} - E_{\nu_\mu} + \sqrt{\left(E_{\nu_\mu}^2 + E'^{\,2}_{\nu_\mu} - 2E_{\nu_\mu}E'_{\nu_\mu}\cos\theta\right)\left[1 + \frac{2m_e^2}{E_{\nu_\mu}E'_{\nu_\mu}(1 - \cos\theta)}\right]}\right). \tag{4.29}$$

This result agrees perfectly with expressions from the literature, as in [134, 135].

4.1.3. Muon Antineutrino Scattering on Electrons

The only difference to muon neutrino scattering on electrons is the change in the notation $\nu_\mu \to \bar\nu_\mu$ and the coefficients C_i^*, which can be derived from Eq.(3.3).

$$C_1^* = \frac{G_F^2}{2\pi^2} 4s_W^4, \qquad C_2^* = \frac{G_F^2}{2\pi^2}\left(1 - 4s_W^2 + 4s_W^4\right), \qquad C_3^* = \frac{G_F^2}{2\pi^2}m_e^2\left(2s_W^2 - 4s_W^4\right). \qquad (4.30)$$

4.1.4. Absorption of Muon Neutrino on Electron

The scattering kernel for the reaction $\nu_\mu + e^- \to \nu_e + \mu^-$ can be obtained from the general expression Eq.(4.2) by subsequently replacing

$$p_1 = p_{\nu_\mu}, \qquad p_2 = p_{e^-}, \qquad p_3 = p'_{\nu_e}, \qquad p_4 = p'_{\mu^-}, \qquad m_2 = m_e, \qquad m_4 = m_\mu. \qquad (4.31)$$

The matrix element for absorption of muon neutrinos on electrons is given in Eq.(3.5). By inserting this into Eq.(4.2) the constants C_i^* equate to

$$C_1^* = \frac{2G_F^2}{\pi^2}, \qquad C_2^* = 0, \qquad C_3^* = 0. \qquad (4.32)$$

Thus one finds for the scattering kernel

$$R\big(\theta, E_{\nu_\mu}, E_{\nu_e}\big) = \frac{4G_F^2}{\pi}\frac{\widetilde A_1 I_2 + \widetilde B_1 I_1 + \widetilde C_1 I_0}{\Delta^5}, \qquad (4.33)$$

with

$$\Delta = \sqrt{E_{\nu_\mu}^2 - 2E_{\nu_\mu}E_{\nu_e}\cos\theta + E_{\nu_e}^2},$$

$$\widetilde A_1 = E_{\nu_\mu}E_{\nu_e}\left(1 - \cos\theta\right)^2\left[E_{\nu_\mu}^2 + E_{\nu_\mu}E_{\nu_e}\left(3 + \cos\theta\right) + E_{\nu_e}^2\right],$$

$$\widetilde B_1 = E_{\nu_\mu}^2 E_{\nu_e}\left(1 - \cos\theta\right)^2\left[2E_{\nu_\mu}^2 + E_{\nu_\mu}E_{\nu_e}\left(3 - \cos\theta\right) - E_{\nu_e}^2\left(1 + 3\cos\theta\right)\right]$$
$$\qquad + Q\left(1 - \cos\theta\right)\left[E_{\nu_\mu}^3 + E_{\nu_\mu}^2 E_{\nu_e}\left(2 + \cos\theta\right) - E_{\nu_\mu}E_{\nu_e}^2\left(2 + \cos\theta\right) - E_{\nu_e}^3\right],$$

$$\widetilde C_1 = E_{\nu_\mu}^3 E_{\nu_e}\left(1 - \cos\theta\right)^2\left[E_{\nu_\mu}^2 - 2E_{\nu_\mu}E_{\nu_e}\cos\theta + E_{\nu_e}^2\left(-\frac{1}{2} + \frac{3}{2}\cos^2\theta\right)\right]$$
$$\qquad + QE_{\nu_\mu}\left(1 - \cos\theta\right)\left[E_{\nu_\mu}^3 - E_{\nu_\mu}^2 E_{\nu_e}\cos\theta + E_{\nu_\mu}E_{\nu_e}^2\left(-2 + \cos^2\theta\right) + E_{\nu_e}^3\cos\theta\right]$$
$$\qquad + Q^2\left[E_{\nu_\mu}^2\cos\theta - E_{\nu_\mu}E_{\nu_e}\left(\frac{3}{2} + \frac{1}{2}\cos^2\theta\right) + E_{\nu_e}^2\cos\theta\right] + \frac{1}{2}E_{\nu_\mu}E_{\nu_e}\left(1 - \cos^2\theta\right)\Delta^2 m_e^2,$$

$$Q = \frac{m_\mu^2 - m_e^2}{2}.$$

The functions I_0, I_1, and I_2 are given in equations (4.19)-(4.21). The coefficients therein take the form

$$y \equiv \frac{E_-}{T}, \qquad \eta = \frac{\mu_e}{T}, \qquad \eta' = \frac{\mu_\mu - E_{\nu_\mu} + E_{\nu_e}}{T}, \qquad k = \frac{Q}{E_{\nu_\mu}E_{\nu_e}\left(1 - \cos\theta\right)}. \qquad (4.34)$$

with

$$E_- = \frac{1}{2}\left[\left(E_{\nu_e} - E_{\nu_\mu}\right)(1 + k) + \sqrt{\left(E_{\nu_\mu}^2 + E_{\nu_e}^2 - 2E_{\nu_\mu}E_{\nu_e}\cos\theta\right)\left[(1 + k)^2 + \frac{2m_e^2}{E_{\nu_\mu}E_{\nu_e}\left(1 - \cos\theta\right)}\right]}\right]. \qquad (4.35)$$

4.1.5. Flavour Conversion of Electron Antineutrino and Electron

The scattering kernel for the reaction $\bar{\nu}_e + e^- \to \bar{\nu}_\mu + \mu^-$ can be obtained from the general expression Eq.(4.2) by subsequently replacing

$$p_1 = p_{\bar{\nu}_e}, \qquad p_2 = p_{e^-}, \qquad p_3 = p'_{\bar{\nu}_\mu}, \qquad p_4 = p'_{\mu^-}, \qquad m_2 = m_e, \qquad m_4 = m_\mu. \qquad (4.36)$$

The matrix element for this flavour conversion is given in Eq.(3.7). By inserting this into Eq.(4.2) the constants C_i^* equate to

$$C_1^* = 0, \qquad C_2^* = \frac{2G_F^2}{\pi^2}, \qquad C_3^* = 0. \qquad (4.37)$$

Thus one finds for the scattering kernel

$$R\big(\theta, E_{\bar{\nu}_e}, E_{\bar{\nu}_\mu},\big) = \frac{4G_F^2}{\pi} \frac{\widetilde{A}_2 I_2 + \widetilde{B}_2 I_1 + \widetilde{C}_2 I_0}{\Delta^5}, \qquad (4.38)$$

with

$$\Delta = \sqrt{E_{\bar{\nu}_e}^2 - 2E_{\bar{\nu}_e}E_{\bar{\nu}_\mu}\cos\theta + E_{\bar{\nu}_\mu}^2},$$

$$\widetilde{A}_2 = E_{\bar{\nu}_e}E_{\bar{\nu}_\mu}(1-\cos\theta)^2\left[E_{\bar{\nu}_e}^2 + E_{\bar{\nu}_e}E_{\bar{\nu}_\mu}(3+\cos\theta) + E_{\bar{\nu}_\mu}^2\right],$$

$$\widetilde{B}_2 = E_{\bar{\nu}_e}E_{\bar{\nu}_\mu}^2(1-\cos\theta)^2\left[E_{\bar{\nu}_e}^2(1+3\cos\theta) + E_{\bar{\nu}_e}E_{\bar{\nu}_\mu}(-3+\cos\theta) - 2E_{\bar{\nu}_\mu}^2\right]$$
$$+ Q(1-\cos\theta)\left[E_{\bar{\nu}_e}^3 + E_{\bar{\nu}_e}^2 E_{\bar{\nu}_\mu}(2+\cos\theta) - E_{\bar{\nu}_e}E_{\bar{\nu}_\mu}^2(2+\cos\theta) - E_{\bar{\nu}_\mu}^3\right],$$

$$\widetilde{C}_2 = E_{\bar{\nu}_e}E_{\bar{\nu}_\mu}^3(1-\cos\theta)^2\left[E_{\bar{\nu}_e}^2\left(-\frac{1}{2}+\frac{3}{2}\cos^2\theta\right) - 2E_{\bar{\nu}_e}E_{\bar{\nu}_\mu}\cos\theta + E_{\bar{\nu}_\mu}^2\right]$$
$$+ QE_{\bar{\nu}_\mu}(1-\cos\theta)\left[E_{\bar{\nu}_e}^3\cos\theta + E_{\bar{\nu}_e}^2 E_{\bar{\nu}_\mu}(-2+\cos^2\theta) - E_{\bar{\nu}_e}E_{\bar{\nu}_\mu}^2\cos\theta + E_{\bar{\nu}_\mu}^3\right]$$
$$+ Q^2\left[E_{\bar{\nu}_e}^2\cos\theta - E_{\bar{\nu}_e}E_{\bar{\nu}_\mu}\left(\frac{3}{2}+\frac{1}{2}\cos^2\theta\right) + E_{\bar{\nu}_\mu}^2\cos\theta\right] + \frac{1}{2}E_{\bar{\nu}_e}E_{\bar{\nu}_\mu}(1-\cos^2\theta)\Delta^2 m_e^2,$$

$$Q = \frac{m_\mu^2 - m_e^2}{2}.$$

The functions I_0, I_1, and I_2 are given in equations (4.19)-(4.21). The coefficients therein take the form

$$y \equiv \frac{E_-}{T}, \qquad \eta = \frac{\mu_e}{T}, \qquad \eta' = \frac{\mu_\mu - E_{\bar{\nu}_e} + E_{\bar{\nu}_\mu}}{T}, \qquad k = \frac{Q}{E_{\bar{\nu}_e}E_{\bar{\nu}_\mu}(1-\cos\theta)}. \qquad (4.39)$$

with

$$E_- = \frac{1}{2}\left[(E_{\bar{\nu}_\mu} - E_{\bar{\nu}_e})(1+k) + \sqrt{\left(E_{\bar{\nu}_e}^2 + E_{\bar{\nu}_\mu}^2 - 2E_{\bar{\nu}_e}E_{\bar{\nu}_\mu}\cos\theta\right)\left[(1+k)^2 + \frac{2m_e^2}{E_{\bar{\nu}_e}E_{\bar{\nu}_\mu}(1-\cos\theta)}\right]}\right].$$
$$(4.40)$$

4.1.6. General Expression for Inverse Decay

Let us assume we have a generalized reaction of an incoming neutrino (particle "1"), reacting with an incoming charged lepton (particle "2") and another incoming neutrino (particle "3")

into an outgoing charged lepton (particle "4"). Again the matrix element can be expressed in a general form

$$\left\langle |M|^2 \right\rangle = C_1\,(p_1 \cdot p_2)\,(p_3 \cdot p_4) + C_2\,(p_1 \cdot p_4)\,(p_2 \cdot p_3) + C_3\,(p_1 \cdot p_3)\,. \tag{4.41}$$

The scattering kernel for this general reaction can then be defined

$$
\begin{aligned}
R(\theta_{13}, E_1, E_3) &= 2\int \frac{d^3p_2}{(2\pi)^3}\frac{d^3p_4}{(2\pi)^3}\frac{\left\langle |M|^2 \right\rangle}{16E_1E_2E_3E_4}\,(2\pi)^4\,\delta^4(p_1 + p_2 + p_3 - p_4)f_2(E_2)\left[1 - f_4(E_4)\right]\\
&= C_{D1}^*R_{D1} + C_{D2}^*R_{D2} + C_{D3}^*R_{D3}.
\end{aligned}
\tag{4.42}
$$

The C_{Di}^* are constant prefactors again, while the R_{Di} are defined by

$$R_{D1}(\theta_{13}, E_1, E_3) = \int d^3p_2 d^3p_4\frac{(p_1 \cdot p_2)\,(p_3 \cdot p_4)}{E_1E_2E_3E_4}\delta^4(p_1 + p_2 + p_3 - p_4)f_2(E_2)[1 - f_4(E_4)]\,, \tag{4.43}$$

$$R_{D2}(\theta_{13}, E_1, E_3) = \int d^3p_2 d^3p_4\frac{(p_1 \cdot p_4)\,(p_2 \cdot p_3)}{E_1E_2E_3E_4}\delta^4(p_1 + p_2 + p_3 - p_4)f_2(E_2)[1 - f_4(E_4)]\,, \tag{4.44}$$

$$R_{D3}(\theta_{13}, E_1, E_3) = \int d^3p_2 d^3p_4\frac{(p_1 \cdot p_3)}{E_1E_2E_3E_4}\delta^4(p_1 + p_2 + p_3 - p_4)f_2(E_2)\left[1 - f_4(E_4)\right]\,. \tag{4.45}$$

The R_{Di} can be solved up to a remaining integration over E_2, for the derivation see appendix C.2. For R_{D1} the result is given by

$$R_{D1} = \frac{2\pi}{\Delta_D^5}\int\limits_{E_{D-}}^{E_{D+}} dE_2 f_2(E_2)\left[1 - f_4(E_4)\right]\left(\widetilde{A}_{D1}E_2^2 + \widetilde{B}_{D1}E_2 + \widetilde{C}_{D1}\right)\Theta(k - 1). \tag{4.46}$$

The integration limits $E_{D\pm}$ equals

$$E_{D\pm} = \frac{1}{2}\left[(E_3 + E_1)(k - 1) \pm \sqrt{(E_1^2 + E_3^2 + 2E_1E_3\cos\theta)\left[(1 - k)^2 - \frac{2m_2^2}{E_1E_3\,(1 - \cos\theta)}\right]}\right]. \tag{4.47}$$

with k and Q given in Eq.(4.8). The coefficients $\widetilde{A}_{D1}$, $\widetilde{B}_{D1}$, $\widetilde{C}_{D1}$, and Δ are defined as

$$\Delta = \sqrt{E_1^2 + 2E_1E_3\cos\theta + E_3^2}, \tag{4.48}$$

$$\widetilde{A}_{D1} = E_1E_3\,(1 - \cos\theta)^2\left[-E_1^2 + E_1E_3\,(3 + \cos\theta) - E_3^2\right], \tag{4.49}$$

$$
\begin{aligned}
\widetilde{B}_{D1} = {}&E_1^2E_3\,(1 - \cos\theta)^2\left[-2E_1^2 + E_1E_3\,(3 - \cos\theta) + E_3^2\,(1 + 3\cos\theta)\right]\\
&+ Q\,(1 - \cos\theta)\left[E_1^3 - E_1^2E_3\,(2 + \cos\theta) - E_1E_3^2\,(2 + \cos\theta) + E_3^3\right],
\end{aligned}
\tag{4.50}
$$

$$
\begin{aligned}
\widetilde{C}_{D1} = {}&-E_1^3E_3\,(1 - \cos\theta)^2\left[E_1^2 + 2E_1E_3\cos\theta + E_3^2\left(-\frac{1}{2} + \frac{3}{2}\cos^2\theta\right)\right]\\
&+ QE_1\,(1 - \cos\theta)\left[E_1^3 + E_1^2E_3\cos\theta + E_1E_3^2\,(-2 + \cos^2\theta) - E_3^3\cos\theta\right]\\
&+ Q^2\left[E_1^2\cos\theta + E_1E_3\left(\frac{3}{2} + \frac{1}{2}\cos^2\theta\right) + E_3^2\cos\theta\right] - \frac{1}{2}E_1E_3\,(1 - \cos^2\theta)\,\Delta^2 m_2^2.
\end{aligned}
\tag{4.51}
$$

Similar expressions can be derived for R_{D2} and R_{D3}. They are given in appendix C.2. As for the scattering kernel, the remaining energy integrals can be transformed into Fermi-Dirac

integrals. One can show (see appendix C.2)

$$
\begin{aligned}
I_{D0} &= \int\limits_{E_{D-}}^{E_{D+}} dE_2 f_2(E_2) \left[1 - f_4(E_2 + E_1 + E_3) \right] \\
&= T f_\gamma(\eta_D' - \eta) \left[F_0(\eta_D' - y_-) - F_0(\eta - y_-) - F_0(\eta_D' - y_+) + F_0(\eta - y_+) \right],
\end{aligned}
\tag{4.52}
$$

$$
\begin{aligned}
I_{D1} &= \int\limits_{E_{D-}}^{E_{D+}} dE_2 E_2 f_2(E_2) \left[1 - f_4(E_2 + E_1 + E_3) \right] \\
&= T^2 f_\gamma(\eta_D' - \eta) \left\{ \left[F_1(\eta_D' - y_-) - F_1(\eta - y_-) - F_1(\eta_D' - y_+) + F_1(\eta - y_+) \right] \right. \\
&\qquad \left. + y_- \left[F_0(\eta_D' - y_-) - F_0(\eta - y_-) \right] - y_+ \left[F_0(\eta_D' - y_+) - F_0(\eta - y_+) \right] \right\},
\end{aligned}
\tag{4.53}
$$

$$
\begin{aligned}
I_{D2} &= \int\limits_{E_{D-}}^{E_{D+}} dE_2 E_2^2 f_2(E_2) \left[1 - f_4(E_2 + E_1 + E_3) \right] \\
&= T^3 f_\gamma(\eta_D' - \eta) \left\{ \left[F_2(\eta_D' - y_-) - F_2(\eta - y_-) - F_2(\eta_D' - y_+) + F_2(\eta - y_+) \right] \right. \\
&\qquad + 2 y_- \left[F_1(\eta_D' - y_-) - F_1(\eta - y_-) \right] - 2 y_+ \left[F_1(\eta_D' - y_+) - F_1(\eta - y_+) \right] \\
&\qquad \left. + y_-^2 \left[F_0(\eta_D' - y_-) - F_0(\eta - y_-) \right] - y_+^2 \left[F_0(\eta_D' - y_+) - F_0(\eta - y_+) \right] \right\}.
\end{aligned}
\tag{4.54}
$$

Here the Fermi-Dirac integrals $F_n(z)$ and the functions $f_\gamma(z)$ are given in Eq. (4.22), the coefficient η is given in Eq.(4.23), and η_D' and $y_\pm$ are determined by

$$
y_\pm \equiv \frac{E_{D\pm}}{T}, \qquad \eta_D' = \eta - \frac{E_1 + E_3 + \mu_2 - \mu_4}{T}.
\tag{4.55}
$$

The integrals R_{Di} can then be expressed by

$$
R_{D1} = \frac{2\pi}{\Delta^5} \left(\widetilde{A}_{D1} I_{D2} + \widetilde{B}_{D1} I_{D1} + \widetilde{C}_{D1} I_{D0} \right), \quad R_{D2} = \frac{2\pi}{\Delta^5} \left(\widetilde{A}_{D2} I_{D2} + \widetilde{B}_{D2} I_{D1} + \widetilde{C}_{D2} I_{D0} \right),
\tag{4.56}
$$
$$
R_{D3} = \frac{2\pi}{\Delta^5} \widetilde{C}_{D3} I_{D0}.
$$

4.1.7. Inverse Muon Decay

The scattering kernel for inverse muon decay $\nu_\mu + e^- + \bar{\nu}_e \rightarrow \mu_-$ can be obtained from the general expression Eq.(4.42) by subsequently replacing

$$
p_1 = p_{\nu_\mu}, \qquad p_2 = p_{e^-}, \qquad p_3 = p_{\bar{\nu}_e}', \qquad p_4 = p_{\mu^-}', \qquad m_2 = m_e, \qquad m_4 = m_\mu.
\tag{4.57}
$$

The matrix element for inverse muon decay is given in Eq.(3.6). By inserting this into Eq.(4.42) the constants C_{Di}^* equate to

$$
C_{D1}^* = \frac{2G_F^2}{\pi^2}, \qquad C_{D2}^* = 0, \qquad C_{D3}^* = 0.
\tag{4.58}
$$

Thus one finds for the scattering kernel

$$
R\big(\theta, E_{\nu_\mu}, E_{\bar{\nu}_e}\big) = \frac{4G_F^2}{\pi} \frac{\widetilde{A}_{D1} I_{D2} + \widetilde{B}_{D1} I_{D1} + \widetilde{C}_{D1} I_{D0}}{\Delta^5},
\tag{4.59}
$$

with

$$\Delta = \sqrt{E_{\nu_\mu}^2 + 2E_{\nu_\mu} E_{\bar{\nu}_e} \cos\theta + E_{\bar{\nu}_e}^2},$$

$$\widetilde{A}_{D1} = E_{\nu_\mu} E_{\bar{\nu}_e} \left(1 - \cos\theta\right)^2 \left[-E_{\nu_\mu}^2 + E_{\nu_\mu} E_{\bar{\nu}_e} \left(3 + \cos\theta\right) - E_{\bar{\nu}_e}^2\right],$$

$$\widetilde{B}_{D1} = E_{\nu_\mu}^2 E_{\bar{\nu}_e} \left(1 - \cos\theta\right)^2 \left[-2E_{\nu_\mu}^2 + E_{\nu_\mu} E_{\bar{\nu}_e} \left(3 - \cos\theta\right) + E_{\bar{\nu}_e}^2 \left(1 + 3\cos\theta\right)\right]$$
$$+ Q \left(1 - \cos\theta\right) \left[E_{\nu_\mu}^3 - E_{\nu_\mu}^2 E_{\bar{\nu}_e} \left(2 + \cos\theta\right) - E_{\nu_\mu} E_{\bar{\nu}_e}^2 \left(2 + \cos\theta\right) + E_{\bar{\nu}_e}^3\right],$$

$$\widetilde{C}_{D1} = - E_{\nu_\mu}^3 E_{\bar{\nu}_e} \left(1 - \cos\theta\right)^2 \left[E_{\nu_\mu}^2 + 2E_{\nu_\mu} E_{\bar{\nu}_e} \cos\theta + E_{\bar{\nu}_e}^2 \left(-\frac{1}{2} + \frac{3}{2}\cos^2\theta\right)\right]$$
$$+ Q E_1 \left(1 - \cos\theta\right) \left[E_{\nu_\mu}^3 + E_{\nu_\mu}^2 E_{\bar{\nu}_e} \cos\theta + E_{\nu_\mu} E_{\bar{\nu}_e}^2 \left(-2 + \cos^2\theta\right) - E_{\bar{\nu}_e}^3 \cos\theta\right]$$
$$+ Q^2 \left[E_{\nu_\mu}^2 \cos\theta + E_{\nu_\mu} E_{\bar{\nu}_e} \left(\frac{3}{2} + \frac{1}{2}\cos^2\theta\right) + E_{\bar{\nu}_e}^2 \cos\theta\right] - \frac{1}{2} E_{\nu_\mu} E_{\bar{\nu}_e} \left(1 - \cos^2\theta\right) \Delta^2 m_e^2,$$

$$Q = \frac{m_\mu^2 - m_e^2}{2}.$$

The functions I_{D0}, I_{D1}, and I_{D2} are given in equations (4.52)-(4.54). The coefficients therein take the form

$$y_\pm \equiv \frac{E_{D\pm}}{T}, \qquad \eta = \frac{\mu_e}{T}, \qquad \eta_D' = \frac{\mu_\mu - E_{\nu_\mu} - E_{\bar{\nu}_e}}{T}, \qquad k = \frac{Q}{E_{\nu_\mu} E_{\bar{\nu}_e} \left(1 - \cos\theta\right)}. \qquad (4.60)$$

with

$$E_{D\pm} = \frac{1}{2}\left[\left(E_{\bar{\nu}_e} + E_{\nu_\mu}\right)(k - 1) \pm \sqrt{\left(E_{\nu_\mu}^2 + E_{\bar{\nu}_e}^2 + 2E_{\nu_\mu} E_{\bar{\nu}_e} \cos\theta\right)\left[(1 - k)^2 - \frac{2m_e^2}{E_{\nu_\mu} E_{\bar{\nu}_e} \left(1 - \cos\theta\right)}\right]}\right]. \qquad (4.61)$$

4.2. Scattering Kernel with Radial Angle Dependence

In Section 2.4.4 it was shown that the solution of the transport problem via the Boltzmann equation of the neutrino radiation field considers local neutrino distributions which depend on energy and azimuthal angle with respect to the radial direction, $f = f(\theta, E)$. In this approach scattering reactions need to be described by expressions that depend on the separate energies and angles of both participating neutrinos.

$$\left(\frac{\partial f}{\partial t}\right)_{\text{scatt}} = (1 - f(E, \theta)) \int d\cos\theta' \, dE' \, E'^2 R_S^{in}(\theta, \theta', E, E') f'(E', \theta') \qquad (4.62)$$
$$- f(E, \theta) \int d\cos\theta' \, dE' \, E'^2 R_S^{out}(\theta, \theta', E, E') \left(1 - f'(E', \theta')\right).$$

At the same time one can define an inverse mean free path for a neutrino that participates in such reactions, analogous to Eq.(2.8). With the definition of the scattering kernels in this chapter one finds

$$\left(\frac{\partial f}{\partial t}\right)_{\text{scatt}} = (1 - f(E, \theta))\left(\frac{1}{\lambda(E)}\right)_{scatt,in} - f(E, \theta)\left(\frac{1}{\lambda(E)}\right)_{scatt,out} \qquad (4.63)$$

$$= (1 - f(E, \theta))\int \frac{d^3 p'}{(2\pi)^3}R^{in}(\theta_{\nu\nu'}, E, E')f'(E', \theta')$$

$$- f(E, \theta)\int \frac{d^3 p'}{(2\pi)^3}R^{out}(\theta_{\nu\nu'}, E, E')\left(1 - f'(E', \theta')\right).$$

Now one has to transform the kernel $R(\theta_{\nu\nu'}, E, E')$ into $R_S(\theta, \theta', E, E')$. The relation between the angles $\theta_{\nu\nu'}$, θ', and θ' is given by the well known expression

$$\cos\left(\theta_{\nu\nu'}\right) = \cos\left(\theta\right)\cos\left(\theta'\right)\sqrt{\left(1 - \cos^2\left(\theta\right)\right)\left(1 - \cos^2\left(\theta'\right)\right)}\cos\left(\phi'\right). \qquad (4.64)$$

Consequently one finds

$$R(\theta_{\nu\nu'}, E, E') = R(\theta, \theta', \phi', E, E'). \qquad (4.65)$$

One way to get rid of the ϕ'-dependence is to simply integrate it out. Comparing equations (4.62) and (4.63), there is already an additional $d\phi'$ integral in (4.63). So the scattering kernel for neutrino transport can be obtained by

$$R_S(\theta, \theta', E, E') = \int \frac{d\phi'}{(2\pi)^3}R(\theta_{\nu\nu'}, E, E'). \qquad (4.66)$$

This approach was proposed e.g. in [134, 135]. The ϕ' integral must be solved numerically. However, for "true" scattering reactions such as neutrino scattering on electrons, where the interacting particles only exchange four-momentum but not any of their generalized charges, this alone is not sufficient. In the special case of forward scattering, where $E = E'$ and $\theta = \theta'$, the kernel $R(\theta_{\nu\nu'}, E, E')$ has a pole. Yet the integral over it can be shown to be finite. Nevertheless, a numerical integration over ϕ' cannot be performed. Instead one can calculate $R_S(\theta, \theta', E, E')$ exactly in terms of Legendre expansions of $R(\theta_{\nu\nu'}, E, E')$, see [135]. However, for all the new leptonic reactions that are studied in this work, this problem of forward scattering is intrinsically absent. Equation (4.66) is then always sufficient to obtain the scattering kernel for Boltzmann transport.

5. Cross Sections for Semileptonic Reactions

5.1. Relativistic Interacting Nucleons

This section will derive semianalytic expressions for opacities with full consideration of the dispersion relation of relativistic and interacting nucleons. This dispersion relation is given in the relativistic mean field approach by

$$E_N = \sqrt{p_N^2 + m_N^{*2}} + U_N.$$

The opacities will be derived from the matrix elements in Section 3.2. In particular the vector, axialvector and vector-axialvector matrix elements are given by equations (3.9), (3.10), and (3.11) respectively. For the tensor related i.e. weak magnetism matrix elements, which are sub leading order contributions, the single effective nucleon mass approximation will be employed. For absorption of electron neutrinos, electron antineutrinos, and muon neutrinos the matrix elements are given in equations (3.21), (3.22), and (3.17). For inverse neutron decay they are given in equations (3.23), (3.24), and (3.20).

The derivations in this section are an improvement of the integration method in [137]. There nucleons were treated noninteracting and nonrelativistic, but the calculation can be extended to incorporate the above dispersion relation.

In a first step the weak magnetism matrix elements have to be transformed into expressions that are suitable for the procedure in [137]. Then the analytic integration will be performed up to the point were the cross section can be expressed as a two-dimensional integral. The two remaining integration steps have to be performed numerically. The advantage of the new expressions for the cross sections is that they are more exact than those expressions which consider nucelons as nonrelativistic, see e.g. [124]. Furthermore weak magnetism will be included explicitely, allowing for a comparison with the analytic correction factor of [130]. Despite these improvements, the new expressions are numerically equally demanding as comparable approximations which result in two-dimensional numerical integrals as well [124]. In contrast, relativistic RPA cross sections would lead to rates that are fully consistent with the underlying EOS but require three-dimensional numerical integrals [126]. This is true even for nonrelativistic RPA [138].

5.1.1. Absorption of Electron Neutrinos

Matrix Element

The matrix elements in equations (3.21), (3.22), and (3.17) that correspond to weak magnetism have to be transformed into a more convenient form. For this purpose the effective four momentum of the proton can be expressed by

$$p_p^* = p_p - (U_p, 0) = p_n^* + p_{\nu_e} - p_{e^-} + (\Delta U, 0) \qquad \text{with} \qquad \Delta U = U_n - U_p. \tag{5.1}$$

Putting this relation into the vector-tensor matrix element from Eq.(3.21) one obtains

$$\left\langle |M|^2 \right\rangle_{VF} = 8 G_F^2 V_{ud}^2 G_V F_2 \frac{m_N^*}{m_N} \left\{ 4 \left(p_{\nu_e} \cdot p_{e^-} \right)^2 - 3 \left(p_{\nu_e} \cdot p_{e^-} \right) m_e^2 \right. \tag{5.2}$$
$$\left. + \Delta U \left[2 \left(p_{\nu_e} \cdot p_{e^-} \right) \left(E_{e^-} - E_{\nu_e} \right) + m_e^2 E_{\nu_e} \right] \right\}.$$

Using the same relation for the axialvector-tensor matrix element one finds

$$\left\langle |M|^2 \right\rangle_{AF} = 16 G_F^2 V_{ud}^2 G_A F_2 \frac{m_N^*}{m_N} \left\{ 2 \left[p_n^* \cdot \left(p_{\nu_e} + p_{e^-} \right) \right] \left(p_{\nu_e} \cdot p_{e^-} \right) - 2 \left(p_n^* \cdot p_{\nu_e} \right) m_e^2 \right. \tag{5.3}$$
$$\left. + \Delta U \left[\left(p_{\nu_e} \cdot p_{e^-} \right) \left(E_{\nu_e} + E_{e^-} \right) - m_e^2 E_{\nu_e} \right] \right\}.$$

However, this form is still not suitable for integration. It can be further transformed (appendix B.3.1) into

$$\left\langle |M|^2 \right\rangle_{AF} = 16 G_F^2 V_{ud}^2 G_A F_2 \frac{m_N^*}{m_N} \left\{ 2 \left(p_n^* \cdot p_{\nu_e} \right) \left(p_p^* \cdot p_{e^-} \right) - 2 \left(p_n^* \cdot p_{e^-} \right) \left(p_p^* \cdot p_{\nu_e} \right) \right. \tag{5.4}$$
$$\left. + 2 \left(p_n^* \cdot p_{\nu_e} \right) \left(E_{\nu_e} - E_{e^-} \right) \Delta U + \left(p_{\nu_e} \cdot p_{e^-} \right) \left(E_{e^-} - E_{\nu_e} \right) \Delta U + \Delta U E_{\nu_e} \left(2Q + 2\Delta U E_p^* + \Delta U^2 \right) \right\}.$$

Likewise, the tensor matrix element can be transformed (see app. B.3.1) into

$$\left\langle |M|^2 \right\rangle_{FF} = \frac{8 G_F^2 V_{ud}^2 F_2^2}{m_N^2} \left[2 \left(p_n^* \cdot p_{\nu_e} \right)^2 \left(p_{\nu_e} \cdot p_{e^-} \right) - 2 \left(p_n^* \cdot p_{\nu_e} \right) \left(p_{\nu_e} \cdot p_{e^-} \right)^2 \right. \tag{5.5}$$
$$+ \left(p_n^* \cdot p_{\nu_e} \right) \left(p_{\nu_e} \cdot p_{e^-} \right) \left[2Q + m_e^2 + \Delta U \left(2 E_p^* + E_{\nu_e} + E_{e^-} \right) - \Delta U^2 \right] - \left(p_n^* \cdot p_{\nu_e} \right)^2 m_e^2$$
$$+ \left(p_{\nu_e} \cdot p_{e^-} \right)^2 \left[m_n^* m_p^* - Q + \frac{m_e^2}{4} - \Delta U \left(E_p^* + E_{e^-} \right) + \frac{\Delta U^2}{2} \right] - \left(p_n^* \cdot p_{\nu_e} \right) m_e^2 \Delta U E_{\nu_e}$$
$$+ \left(p_{\nu_e} \cdot p_{e^-} \right) \left\{ - \left(3 m_p^* + m_n^* \right) m_n^* \frac{m_e^2}{4} + Q^2 + Q \frac{m_e^2}{4} - \frac{m_e^4}{8} \right.$$
$$+ \Delta U \left[E_p^* \left(2Q + \frac{m_e^2}{4} \right) + E_{e^-} \left(Q + \frac{m_e^2}{2} \right) - E_n^* \frac{m_e^2}{4} \right]$$
$$\left. \left. + \Delta U^2 \left(E_p^{*2} + E_p^* E_{e^-} - Q - \frac{m_e^2}{8} \right) - \Delta U^3 \left(E_p^* + \frac{E_{e^-}}{2} \right) + \frac{\Delta U^4}{4} \right\} \right].$$

Summing up equations (3.9)-(3.11), (5.2), (5.4), and (5.5) the total matrix element for neutrino absorption on neutrons becomes

$$\left\langle |M|^2 \right\rangle = 16 G_F^2 V_{ud}^2 \left[\left(p_n^* \cdot p_{\nu_e} \right) \left(p_p^* \cdot p_{e^-} \right) A_1 + \left(p_n^* \cdot p_{e^-} \right) \left(p_p^* \cdot p_{\nu_e} \right) B_1 + \left(p_n^* \cdot p_{\nu_e} \right)^2 \left(p_{\nu_e} \cdot p_{e^-} \right) C_1 \right.$$
$$+ \left(p_n^* \cdot p_{\nu_e} \right) \left(p_{\nu_e} \cdot p_{e^-} \right)^2 D_1 + \left(p_n^* \cdot p_{\nu_e} \right)^2 E_1 + \left(p_{\nu_e} \cdot p_{e^-} \right)^2 G_1$$
$$\left. + \left(p_n^* \cdot p_{\nu_e} \right) \left(p_{\nu_e} \cdot p_{e^-} \right) H_1 + \left(p_n^* \cdot p_{\nu_e} \right) J_1 + \left(p_{\nu_e} \cdot p_{e^-} \right) K_1 + L_1 \right]. \tag{5.6}$$

where the coefficients A_1-L_1 are given in app. B.3.3.

Phase Space Integration

Combining the general formula for cross sections Eq.(2.8) with the medium modifications Eq.(2.17) and the matrix element in medium Eq.(5.6), the cross section per unit volume or inverse mean free path for absorption of electron neutrinos on neutrons is given by

$$\frac{1}{\lambda(E_{\nu_e})} = \int \frac{d^3 p_n}{(2\pi)^3} \frac{d^3 p_{e-}}{(2\pi)^3} \frac{d^3 p_p}{(2\pi)^3} 2G_F^2 V_{ud}^2 \frac{(A_1 M_A + ... + L_1 M_L)}{E_{\nu_e} E_n^* E_{e-} E_p^*} (2\pi)^4 \delta^4(p_{\nu_e} + p_n - p_{e-} - p_p)$$

$$\times f_n(E_n) \left[1 - f_{e-}(E_{e-})\right] \left[1 - f_p(E_p)\right]. \tag{5.7}$$

where $(M_A, ..., M_L)$ are the four-momenta products from Eq.(5.6) that correspond to $(A_1, ..., L_1)$, respectively. For example, $M_A = (p_n^* \cdot p_{\nu_e})\left(p_p^* \cdot p_{e-}\right)$ and $M_L = 1$. In a first step one integrates over the proton energy to reduce the four-momentum conservation δ^4 into momentum conservation δ^3. The inverse mean free path can then be expressed by

$$\frac{1}{\lambda(E_{\nu_e})} = \frac{G_F^2 V_{ud}^2}{4\pi^3} \frac{1}{E_{\nu_e}^2} \int\limits_{E_{n-}}^{\infty} dE_n \int\limits_{m_e}^{E_{e+}} dE_{e-} f_n \left[1 - f_{e-}\right] \left[1 - f_p\right] (A_1 I_{A1} + ... + L_1 I_{L1}) \Theta(P_{max} - P_{min}).$$

$$\tag{5.8}$$

Where the expressions I_{X1} combine all the angular integrals

$$I_{X1} \equiv \frac{\bar{p}_{\nu_e} \bar{p}_n \bar{p}_{e-} \bar{p}_p}{4\pi^2} \int d\Omega_n d\Omega_{e-} d\Omega_p M_X \delta^3(\vec{p}_{\nu_e} + \vec{p}_n - \vec{p}_{e-} - \vec{p}_p). \tag{5.9}$$

The integration limits for E_n and E_{e-} are given by

$$E_{n-} = \max\left\{m_e + m_p^* + U_p - E_{\nu_e}, m_n^* + U_n\right\} \qquad \text{and} \qquad E_{e+} = E_{\nu_e} + E_n - m_p^* - U_p. \tag{5.10}$$

Further, the heaviside function guarantees momentum conservation. The arguments of Θ are defined by

$$P_{min} = \max\left\{\left|\bar{p}_{\nu_e} - \bar{p}_n\right|, \left|\bar{p}_{e-} - \bar{p}_p\right|\right\} \qquad \text{and} \qquad P_{max} = \min\left\{\bar{p}_{\nu_e} + \bar{p}_n, \bar{p}_{e-} + \bar{p}_p\right\}. \tag{5.11}$$

The angular integrals I_{X1} can be solved analytically. In appendix D.1 all integrals are computed explicitly in a general notation I_X. The integrals I_{X1} for ν_e-capture can be obtained from the I_X by replacing the general indices according to

$$I_{X1} = I_X|_{\{1\to\nu_e, 2\to n, 3\to e^-, 4\to p\}}. \tag{5.12}$$

5.1.2. Absorption of Electron Antineutrinos

The matrix element in its basic form for $\bar{\nu}_e$-capture can be derived from the expression for ν_e-capture (equations (3.9)-(3.11), (3.17), (3.21), (3.22)) by simply renaming the indices $\langle \nu_e \to \bar{\nu}_e, e^- \to e^+ \rangle$ and applying an additional sign change for the vector-tensor and axialvector-tensor terms. However, the kinematic relation Eq.(5.1) does not hold here. Instead one has

$$p_n^* = p_n - (U_n, 0) = p_p^* + p_{\bar{\nu}_e} - p_{e+} + (-\Delta U, 0) \qquad \text{with} \qquad \Delta U = U_n - U_p. \tag{5.13}$$

Eq.(5.13) is connected to Eq.(5.1) by the replacement $\{n \to p, p \to n, \nu_e \to \bar{\nu}_e, e^- \to e^+\}$. Since all derivations for the weak magnetism matrix elements in section 5.1.1 were based on Eq.(5.1), one can now repeat the exact same steps but with the nucleon indices exchanged. As explained before, the vector-tensor element for $\bar{\nu}_e$ capture can be derived from Eq.(3.21) by changing the sign and replacing $\{\nu_e \to \bar{\nu}_e, e^- \to e^+\}$. However, as Eq.(3.21) is asymmetric under exchange of the nucleon indices, this is equivalent to transforming it by $\{n \to p, p \to n, \nu_e \to \bar{\nu}_e, e^- \to e^+\}$. Since the vector-tensor matrix elements and the kinematics of antineutrino absorption are connected to neutrino absorption by the same relation, so will be the result of the subsequent transformations and one consequently finds

$$\left\langle \left| M \left(\bar{\nu}_e + p \to n + e^+ \right) \right|^2 \right\rangle_{VF} = \left\langle \left| M \left(\nu_e + n \to p + e^- \right) \right|^2 \right\rangle_{VF} \bigg|_{n \to p, p \to n, \nu_e \to \bar{\nu}_e, e^- \to e^+} . \quad (5.14)$$

For the axialvector-tensor element a similar argumentation can be applied. It can also be constructed from Eq.(3.22) by $\{\nu_e \to \bar{\nu}_e, e^- \to e^+\}$ and an overall sign change. Further, it is symmetric under exchange of the nucleon indices. Thus the negative matrix element and the kinematics of antineutrino capture are related to the matrix element and the kinematics of neutrino capture by the same replacement $\{n \to p, p \to n, \nu_e \to \bar{\nu}_e, e^- \to e^+\}$. Consequently one finds

$$\left\langle \left| M \left(\bar{\nu}_e + p \to n + e^+ \right) \right|^2 \right\rangle_{AF} = -\left\langle \left| M \left(\nu_e + n \to p + e^- \right) \right|^2 \right\rangle_{AF} \bigg|_{n \to p, p \to n, \nu_e \to \bar{\nu}_e, e^- \to e^+} . \quad (5.15)$$

Eventually the tensor matrix element for $\bar{\nu}_e$-capture can be obtained from Eq.(3.17) simply by $\{\nu_e \to \bar{\nu}_e, e^- \to e^+\}$. Also, it is symmetric under exchange of the nucleon indices. Hence the replacement $\{n \to p, p \to n, \nu_e \to \bar{\nu}_e, e^- \to e^+\}$ describes again the relation between matrix elements and kinematics for neutrino and antineutrino capture. For the tensor element the same relation like the one for the vector-tensor element applies then

$$\left\langle \left| M \left(\bar{\nu}_e + p \to n + e^+ \right) \right|^2 \right\rangle_{FF} = \left\langle \left| M \left(\nu_e + n \to p + e^- \right) \right|^2 \right\rangle_{FF} \bigg|_{n \to p, p \to n, \nu_e \to \bar{\nu}_e, e^- \to e^+} . \quad (5.16)$$

It has to be noted that the exchange of nucleon indices implies $Q \to -Q$ and $\Delta U \to -\Delta U$. Summing up all contributions, the total matrix element for antineutrino capture on protons becomes

$$\begin{aligned}
\langle |M|^2 \rangle = 16 G_F^2 V_{ud}^2 \Big[&\left(p_n^* \cdot p_{\bar{\nu}_e} \right) \left(p_p^* \cdot p_{e^+} \right) A_2 + \left(p_n^* \cdot p_{e^+} \right) \left(p_p^* \cdot p_{\bar{\nu}_e} \right) B_2 + \left(p_p^* \cdot p_{\bar{\nu}_e} \right)^2 \left(p_{\bar{\nu}_e} \cdot p_{e^+} \right) C_2 \\
&+ \left(p_p^* \cdot p_{\bar{\nu}_e} \right) \left(p_{\bar{\nu}_e} \cdot p_{e^+} \right)^2 D_2 + \left(p_p^* \cdot p_{\bar{\nu}_e} \right)^2 E_2 + \left(p_{\bar{\nu}_e} \cdot p_{e^+} \right)^2 G_2 \\
&+ \left(p_p^* \cdot p_{\bar{\nu}_e} \right) \left(p_{\bar{\nu}_e} \cdot p_{e^+} \right) H_2 + \left(p_p^* \cdot p_{\bar{\nu}_e} \right) J_2 + \left(p_{\bar{\nu}_e} \cdot p_{e^+} \right) K_2 + L_2 \Big] .
\end{aligned} \quad (5.17)$$

Where the coefficients G_2-L_2 can be easily obtained from G_1-L_1 by

$$\begin{aligned}
(G_2, H_2, J_2, K_2, L_2) = (G_1, H_1, J_1, K_1, L_1)| \{ &n \to p, p \to n, \nu_e \to \bar{\nu}_e, e^- \to e^+, \quad (5.18) \\
&G_A \to -G_A, Q \to -Q, \Delta U \to -\Delta U \} ,
\end{aligned}$$

while for the remaining coefficients one simply has

$$(A_2, B_2, C_2, D_2, E_2) = (A_1, B_1, C_1, D_1, E_1) . \quad (5.19)$$

With the matrix element of Eq.(5.17) the inverse mean free path becomes eventually

$$\frac{1}{\lambda(E_{\bar{\nu}_e})} = \int \frac{d^3p_p}{(2\pi)^3} \frac{d^3p_{e+}}{(2\pi)^3} \frac{d^3p_n}{(2\pi)^3} 2G_F^2 V_{ud}^2 \frac{(A_2 M_A + ... + L_2 M_L)}{E_{\bar{\nu}_e} E_p^* E_{e+} E_n^*} (2\pi)^4 \delta^4(p_{\bar{\nu}_e} + p_p - p_{e+} - p_n)$$
$$\times f_p(E_p) \left[1 - f_{e+}(E_{e+})\right] \left[1 - f_n(E_n)\right]. \tag{5.20}$$

Since $\bar{\nu}_e$-capture has the same kinematic structure as ν_e-capture, the phase space integrals can be computed analogous as well. Similar to Eq.(5.8) one finds then

$$\frac{1}{\lambda(E_{\bar{\nu}_e})} = \frac{G_F^2 V_{ud}^2}{4\pi^3} \frac{1}{E_{\bar{\nu}_e}^2} \int\limits_{E_{p-}}^{\infty} dE_p \int\limits_{m_e}^{E_{e+}} dE_{e+} f_p \left[1 - f_{e+}\right] \left[1 - f_n\right] (A_2 I_{A2} + ... + L_2 I_{L2}) \Theta(P_{max} - P_{min}).$$
$$\tag{5.21}$$

The arguments of the heaviside function are defined through

$$P_{min} = \max\left\{|\bar{p}_{\bar{\nu}_e} - \bar{p}_p|, |\bar{p}_{e+} - \bar{p}_n|\right\} \qquad \text{and} \qquad P_{max} = \min\left\{\bar{p}_{\bar{\nu}_e} + \bar{p}_p, \bar{p}_{e+} + \bar{p}_n\right\}. \tag{5.22}$$

The limits for the energy integration are given by

$$E_{p-} = \max\left\{m_e + m_n^* + U_n - E_{\bar{\nu}_e}, m_p^* + U_p\right\} \qquad \text{and} \qquad E_{e+} = E_{\bar{\nu}_e} + E_p - m_n^* - U_n. \tag{5.23}$$

The angular integrals I_{X2} can be obtained from the general I_X in appendix D.1 by replacing the indices according to

$$I_{X2} = I_X|_{\{1 \to \bar{\nu}_e, 2 \to p, 3 \to e^+, 4 \to n\}}. \tag{5.24}$$

5.1.3. Inverse Neutron Decay

For inverse neutron decay the matrix elements that correspond to weak magnetism have to be transformed seperately from the other semileptonic reactions. First, the matrix elements from equations (3.23), (3.24), and (3.20) are inherently different to the capture reactions. Second, the kinematic relation between the four-momenta has a different structure as well. It can be described by the relation

$$p_p^* = p_p - (U_p, 0) = p_n^* - p_{\bar{\nu}_e} - p_{e-} + (\Delta U, 0) \qquad \text{with} \qquad \Delta U = U_n - U_p. \tag{5.25}$$

Putting this relation into the vector-tensor matrix element from Eq.(3.23) one obtains

$$\left\langle |M|^2 \right\rangle_{VF} = 4G_F^2 V_{ud}^2 G_V F_2 \frac{m_N^*}{m_N} \left\{ -4\left(p_{\nu_e} \cdot p_{e-}\right)^2 - 3\left(p_{\nu_e} \cdot p_{e-}\right) m_e^2 \right. \tag{5.26}$$
$$\left. + \Delta U \left[2\left(p_{\nu_e} \cdot p_{e-}\right)\left(E_{e-} + E_{\nu_e}\right) + m_e^2 E_{\nu_e}\right] \right\}.$$

For the axialvector-tensor matrix element the following expression can be derived (see app. B.3.2)

$$\left\langle |M|^2 \right\rangle_{AF} = 8G_F^2 V_{ud}^2 G_A F_2 \frac{m_N^*}{m_N} \left\{ 2\left(p_n^* \cdot p_{\bar{\nu}_e}\right)\left(p_p^* \cdot p_{e-}\right) - 2\left(p_n^* \cdot p_{e-}\right)\left(p_p^* \cdot p_{\bar{\nu}_e}\right) \right. \tag{5.27}$$
$$- 2\left(p_n^* \cdot p_{\bar{\nu}_e}\right)\left(E_{\bar{\nu}_e} + E_{e-}\right)\Delta U + \left(p_{\bar{\nu}_e} \cdot p_{e-}\right)\left(E_{\bar{\nu}_e + E_{e-}}\right)\Delta U$$
$$\left. + 2\Delta U E_{\bar{\nu}_e} Q + 2\Delta U^2 E_{\bar{\nu}_e} E_p^* - \Delta U^3 E_{\bar{\nu}_e} \right\}.$$

Likewise the tensor matrix element can be transformed

$$\left\langle |M|^2 \right\rangle_{FF} = \frac{4G_F^2 V_{ud}^2 F_2^2}{m_N^2} \left[2 \left(p_n^* \cdot p_{\nu_e}\right)^2 \left(p_{\nu_e} \cdot p_{e^-}\right) - 2 \left(p_n^* \cdot p_{\nu_e}\right) \left(p_{\nu_e} \cdot p_{e^-}\right)^2 \right. \tag{5.28}$$

$$- \left(p_n^* \cdot p_{\nu_e}\right)\left(p_{\nu_e} \cdot p_{e^-}\right)\left[2Q + m_e^2 + \Delta U \left(2E_p^* - E_{\nu_e} + E_{e^-}\right) - \Delta U^2\right] + \left(p_n^* \cdot p_{\nu_e}\right)^2 m_e^2$$

$$- \left(p_{\nu_e} \cdot p_{e^-}\right)^2 \left[m_n^* m_p^* - Q + \frac{m_e^2}{4} - \Delta U \left(E_p^* + E_{e^-}\right) + \frac{\Delta U^2}{2}\right] + \left(p_n^* \cdot p_{\nu_e}\right) m_e^2 \Delta U E_{\nu_e}$$

$$+ \left(p_{\nu_e} \cdot p_{e^-}\right) \left\{ -\left(3m_p^* + m_n^*\right) m_n^* \frac{m_e^2}{4} + Q^2 + Q\frac{m_e^2}{4} - \frac{m_e^4}{8} \right.$$

$$+ \Delta U \left[E_p^* \left(2Q + \frac{m_e^2}{4}\right) + E_{e^-}\left(Q + \frac{m_e^2}{2}\right) - E_n^* \frac{m_e^2}{4}\right]$$

$$\left. \left. + \Delta U^2 \left(E_p^{*2} + E_p^* E_{e^-} - Q - \frac{m_e^2}{8}\right) - \Delta U^3 \left(E_p^* + \frac{E_{e^-}}{2}\right) + \frac{\Delta U^4}{4} \right\} \right] .$$

Summing up equations (3.9)-(3.11) and (5.26)-(5.28) the total matrix element for inverse neutron decay becomes

$$\left\langle |M|^2 \right\rangle = 8G_F^2 V_{ud}^2 \left[\left(p_n^* \cdot p_{\bar{\nu}_e}\right)\left(p_p^* \cdot p_{e^-}\right) A_3 + \left(p_n^* \cdot p_{e^-}\right)\left(p_p^* \cdot p_{\bar{\nu}_e}\right) B_3 + \left(p_n^* \cdot p_{\bar{\nu}_e}\right)^2 \left(p_{\bar{\nu}_e} \cdot p_{e^-}\right) C_3 \right.$$

$$+ \left(p_n^* \cdot p_{\bar{\nu}_e}\right)\left(p_{\bar{\nu}_e} \cdot p_{e^-}\right)^2 D_3 + \left(p_n^* \cdot p_{\bar{\nu}_e}\right)^2 E_3 + \left(p_{\bar{\nu}_e} \cdot p_{e^-}\right)^2 G_3$$

$$\left. + \left(p_n^* \cdot p_{\bar{\nu}_e}\right)\left(p_{\bar{\nu}_e} \cdot p_{e^-}\right) H_3 + \left(p_n^* \cdot p_{\bar{\nu}_e}\right) J_3 + \left(p_{\bar{\nu}_e} \cdot p_{e^-}\right) K_3 + L_3 \right] . \tag{5.29}$$

where the coefficients $(E_3...K_3)$ are given in app. B.3.3, while the remaining coefficients simply follow

$$(A_3, B_3, C_3, D_3, L_3) = (A_1, B_1, C_1, D_1, L_1) . \tag{5.30}$$

With the matrix element Eq.(5.29) the inverse mean free path becomes eventually

$$\frac{1}{\lambda(E_{\bar{\nu}_e})} = \int \frac{d^3 p_p}{(2\pi)^3} \frac{d^3 p_{e^-}}{(2\pi)^3} \frac{d^3 p_n}{(2\pi)^3} 2G_F^2 V_{ud}^2 \frac{(A_2 M_A + ... + L_2 M_L)}{E_{\bar{\nu}_e} E_p^* E_{e^-} E_n^*} (2\pi)^4 \, \delta^4(p_{\bar{\nu}_e} + p_p + p_{e^-} - p_n)$$

$$\times f_p(E_p) f_{e^-}(E_{e^-}) \left[1 - f_n(E_n)\right] . \tag{5.31}$$

Similar to the neutrino capture reactions the angular integrals can be combined into one expression, so the inverse mean free path becomes

$$\frac{1}{\lambda(E_{\bar{\nu}_e})} = \frac{G_F^2 V_{ud}^2}{4\pi^3} \frac{1}{E_{\bar{\nu}_e}^2} \int\limits_{m_p^* + U_p}^{\infty} dE_p \int\limits_{E_{e^-}}^{\infty} dE_{e^-} \, f_p f_{e^-} \left[1 - f_n\right] \left(A_3 I_{A3} + ... + L_3 I_{L3}\right) \Theta(P_{max} - P_{min}).$$

$$\tag{5.32}$$

The angular integrals I_{X3} have the form

$$I_{X3} \equiv \frac{\bar{p}_{\bar{\nu}_e} \bar{p}_p \bar{p}_{e^-} \bar{p}_n}{4\pi^2} \int d\Omega_p d\Omega_{e^-} d\Omega_n M_X \delta^3(\vec{p}_{\bar{\nu}_e} + \vec{p}_p + \vec{p}_{e^-} - \vec{p}_n). \tag{5.33}$$

The arguments of the heaviside function are defined again through

$$P_{min} = \max\left\{ |\bar{p}_{\bar{\nu}_e} - \bar{p}_p| , |\bar{p}_{e^-} - \bar{p}_n| \right\} \qquad \text{and} \qquad P_{max} = \min\left\{ \bar{p}_{\bar{\nu}_e} + \bar{p}_p, \bar{p}_{e^-} + \bar{p}_n \right\} . \tag{5.34}$$

The lower integration limit for the electron energy equals

$$E_{e^-} = \max\left\{ m_n^* + U_n - E_{\bar{\nu}_e} - E_p; m_e \right\} . \tag{5.35}$$

Eventually the integrals I_{X3} are solved explicitly in appendix D.2.

5.1.4. Absorption of Muon Neutrinos

For the absorption of muon neutrinos one finds that the matrix element and the kinematic conditions are exactly the same as for absorption of electron neutrinos under the replacement $\{\nu_e \rightarrow \nu_\mu, e \rightarrow \mu\}$. Consequently the total matrix element for ν_μ-absorption can be described by

$$
\begin{aligned}
\langle |M|^2 \rangle = 16 G_F^2 V_{ud}^2 \Big[& \left(p_n^* \cdot p_{\nu_\mu}\right) \left(p_p^* \cdot p_{\mu^-}\right) A_4 + \left(p_n^* \cdot p_{\mu^-}\right) \left(p_p^* \cdot p_{\nu_\mu}\right) B_4 + \left(p_n^* \cdot p_{\nu_\mu}\right)^2 \left(p_{\nu_\mu} \cdot p_{\mu^-}\right) C_4 \\
& + \left(p_n^* \cdot p_{\nu_\mu}\right) \left(p_{\nu_\mu} \cdot p_{\mu^-}\right)^2 D_4 + \left(p_n^* \cdot p_{\nu_\mu}\right)^2 E_4 + \left(p_{\nu_\mu} \cdot p_{\mu^-}\right)^2 G_4 \\
& + \left(p_n^* \cdot p_{\nu_\mu}\right) \left(p_{\nu_\mu} \cdot p_{\mu^-}\right) H_4 + \left(p_n^* \cdot p_{\nu_\mu}\right) J_4 + \left(p_{\nu_\mu} \cdot p_{\mu^-}\right) K_4 + L_4 \Big].
\end{aligned}
\tag{5.36}
$$

where the coefficients E_4-L_4 can be obtained from E_1-L_1 by

$$
(E_4, G_4, H_4, J_4, K_4, L_4) = (E_1, G_1, H_1, J_1, K_1, L_1)|\{\nu_e \rightarrow \nu_\mu, e \rightarrow \mu\}.
\tag{5.37}
$$

while for the remaining coefficients one simply has

$$
(A_4, B_4, C_4, D_4) = (A_1, B_1, C_1, D_1).
\tag{5.38}
$$

Since the matrix element and the kinematics are exactly the same as for ν_e-capture, the inverse mean free path can analogously be expressed.

$$
\frac{1}{\lambda\left(E_{\nu_\mu}\right)} = \frac{G_F^2 V_{ud}^2}{4\pi^3} \frac{1}{E_{\nu_\mu}^2} \int\limits_{E_{n-}}^{\infty} dE_n \int\limits_{m_\mu}^{E_{\mu+}} dE_{\mu^-} f_n \left[1 - f_{\mu^-}\right] \left[1 - f_p\right] \left(A_4 I_{A4} + ... + L_4 I_{L4}\right) \Theta(P_{max} - P_{min}).
\tag{5.39}
$$

The angular integrals, the integration limits, and the arguments of the heaviside function can be obtained from equations (5.9)-(5.11) simply by replacing $\{e \rightarrow \mu\}$. Likewise, the integrals I_{X4} can be obtained from the I_X by

$$
I_{X4} = I_X|_{\{1 \rightarrow \nu_\mu, 2 \rightarrow n, 3 \rightarrow \mu^-, 4 \rightarrow p\}}
\tag{5.40}
$$

5.2. Nonrelativistic Interacting Nucleons

For nuclear matter in a PNS at densities significantly below the nuclear saturation density and temperatures of several $10\,\mathrm{MeV}$, it is a reasonable lowest order approximation to consider the nucleons as nonrelativstic particles. The dispersion relation of the quasiparticles is then approximated by

$$
E_{n,p} = \sqrt{p_{n,p}^2 + m_{n,p}^{*2}} + U_{n,p} \simeq \frac{p_N^2}{2m_N^*} + m_N^* + U_N = \frac{p_N^2}{2m_N^*} + m_N + \tilde{U}_N.
\tag{5.41}
$$

Here $\tilde{U}_N$ denotes the so called nonrelativistic interaction potential. From Eq.(5.41) it is clear that $\tilde{U}_N$ relates to the relativistic interaction potential U_N by

$$
\tilde{U}_N = U_N + m_N^* - m_N = U_N - g_\sigma S.
\tag{5.42}
$$

Both notations are used in the literature on calculations of neutrino opacities. For the derivations of opacities it does not matter which notation is chosen, both will lead to the same result. For this work the notation with the effective mass and the relativistic potentials is chosen. The following calculations of neutrino opacities on nonrelativistic nucleons are strongly based on the work in [124], more recently revisited in [63, 61]. In the case of ν_e-capture and $\bar{\nu}_e$-capture their results are reproduced. However, the approach is modified to take the finite lepton mass into account, which is very important for the absorption of ν_μ. Also, the calculation of inverse neutron decay requires some adjustments of the formalism.

5.2.1. Absorption of Electron Neutrinos

Under the assumption of nonrelativistic nucleons one can simplify the matrix element for neutrino capture on neutrons significantly. Therefore it is assumed that all particle momenta are much smaller than the nucleon mass, $p/m_N^* \ll 1$. All contributions to the normalized matrix element that are of order (p/m_N^*) or higher are then neglected. Under this approximation, only the terms $A_1 M_A$, $B_1 M_B$, and $C_1 M_C$ do not vanish. For these one finds

$$
\begin{aligned}
\frac{A_1 M_A}{E_{\nu_e} E_n^* E_{e^-} E_p^*} &= \left[(G_V + G_A)^2 + 2 G_A F_2 \frac{m_N^*}{m_N} \right] \frac{(p_n^* \cdot p_{\nu_e})(p_p^* \cdot p_{e^-})}{E_{\nu_e} E_n^* E_{e^-} E_p^*} \\
&= \left[(G_V + G_A)^2 + 2 G_A F_2 \frac{m_N^*}{m_N} \right] \left(1 - \cos\theta_{\nu,n} \frac{\bar{p}_n}{E_n^*} \right) \left(1 - \cos\theta_{e^-,p} \frac{\bar{p}_{e^-} \bar{p}_p}{E_{e^-} E_p^*} \right) \\
&\simeq (G_V + G_A)^2 + 2 G_A F_2 \frac{m_N^*}{m_N},
\end{aligned}
\tag{5.43}
$$

$$
\begin{aligned}
\frac{B_1 M_B}{E_{\nu_e} E_n^* E_{e^-} E_p^*} &= \left[(G_V - G_A)^2 - 2 G_A F_2 \frac{m_N^*}{m_N} \right] \frac{(p_p^* \cdot p_{\nu_e})(p_n^* \cdot p_{e^-})}{E_{\nu_e} E_n^* E_{e^-} E_p^*} \\
&= \left[(G_V + G_A)^2 + 2 G_A F_2 \frac{m_N^*}{m_N} \right] \left(1 - \cos\theta_{\nu,p} \frac{\bar{p}_p}{E_p^*} \right) \left(1 - \cos\theta_{e^-,n} \frac{\bar{p}_{e^-} \bar{p}_n}{E_{e^-} E_n^*} \right) \\
&\simeq (G_V - G_A)^2 - 2 G_A F_2 \frac{m_N^*}{m_N},
\end{aligned}
\tag{5.44}
$$

$$
\begin{aligned}
\frac{C_1 M_C}{E_{\nu_e} E_n^* E_{e^-} E_p^*} &= \left[G_A^2 - G_V^2 + O\left(\frac{p^2}{m_N^{*2}} \right) \right] m_n^* m_p^* \frac{(p_{\nu_e} \cdot p_{e^-})}{E_{\nu_e} E_n^* E_{e^-} E_p^*} \\
&= \left[G_A^2 - G_V^2 + O\left(\frac{p^2}{m_N^{*2}} \right) \right] \left(1 - \cos\theta_{\nu,e^-} \frac{\bar{p}_{e^-}}{E_{e^-}} \right) \\
&\simeq \left(G_A^2 - G_V^2 \right) \left(1 - \cos\theta_{\nu,e^-} \frac{\bar{p}_{e^-}}{E_{e^-}} \right).
\end{aligned}
\tag{5.45}
$$

Summing these terms up, the total normalized matrix element takes the form

$$
\frac{\langle |M|^2 \rangle}{E_{\nu_e} E_n^* E_{e^-} E_p^*} = 16 G_F^2 V_{ud}^2 \left[G_V^2 \left(1 + \cos\theta_{\nu,e^-} \frac{\bar{p}_{e^-}}{E_{e^-}} \right) + G_A^2 \left(3 - \cos\theta_{\nu,e^-} \frac{\bar{p}_{e^-}}{E_{e^-}} \right) \right].
\tag{5.46}
$$

The cross section for electron neutrino absorption on neutrons can then be expressed by

$$
\begin{aligned}
\frac{1}{\lambda(E_{\nu_e})} = \int & \frac{d^3 p_n}{(2\pi)^3} \frac{d^3 p_{e^-}}{(2\pi)^3} \frac{d^3 p_p}{(2\pi)^3} 2 G_F^2 V_{ud}^2 \left[G_V^2 \left(1 + \cos\theta_{\nu,e^-} \frac{\bar{p}_{e^-}}{E_{e^-}} \right) + G_A^2 \left(3 - \cos\theta_{\nu,e^-} \frac{\bar{p}_{e^-}}{E_{e^-}} \right) \right] \\
& \times (2\pi)^4 \delta^4(p_{\nu_e} + p_n - p_{e^-} - p_p) f_n(E_n) \left[1 - f_{e^-}(E_{e^-}) \right] \left[1 - f_p(E_p) \right].
\end{aligned}
\tag{5.47}
$$

Now one can define the structure function $S(q_0, \vec{q})$. It contains all terms that are connected to the nucleons and thus characterizes the response of the nucleon system. It is given by

$$S(q_0, \vec{q}) \equiv 2 \int \frac{d^3 p_n}{(2\pi)^3} \frac{d^3 p_p}{(2\pi)^3} (2\pi)^4 \delta^4(p_{\nu_e} + p_n - p_{e^-} - p_p) f_n(E_n) [1 - f_p(E_p)]. \tag{5.48}$$

Here q_0 and $\vec{q}$ are the energy and momentum part of the four-momentum transfer $q = p_{\nu_e} - p_{e^-}$, respectively. It is then convenient to substitute the integration over electron phase space $d^3 p_{e^-}$ by integration over energy and momentum transfer (see appendix E.1)

$$\int d^3 p_{e^-} = 2\pi \int\limits_{-\infty}^{E_{\nu_e} - m_e} dq_0 \frac{E_{e^-}}{E_{\nu_e}} \int\limits_{E_{\nu_e} - \bar{p}_{e^-}}^{E_{\nu_e} + \bar{p}_{e^-}} d\bar{q}\, \bar{q}. \tag{5.49}$$

Combining equations (5.48) and (5.49) the inverse mean free path becomes

$$\frac{1}{\lambda(E_{\nu_e})} = \frac{G_F^2 V_{ud}^2}{4\pi^2} \int\limits_{-\infty}^{E_{\nu_e} - m_e} dq_0 \frac{E_{e^-}}{E_{\nu_e}} [1 - f_{e^-}(E_{e^-})]$$

$$\times \int\limits_{E_{\nu_e} - \bar{p}_{e^-}}^{E_{\nu_e} + \bar{p}_{e^-}} d\bar{q} \left[G_V^2 \left(1 + \cos\theta_{\nu,e^-} \frac{\bar{p}_{e^-}}{E_{e^-}}\right) + G_A^2 \left(3 - \cos\theta_{\nu,e^-} \frac{\bar{p}_{e^-}}{E_{e^-}}\right) \right] \bar{q} S(q_0, \vec{q}). \tag{5.50}$$

The structure function can be solved analytically (see appendix E.1). It becomes eventually

$$S(q_0, \vec{q}) = \frac{m_n^* m_p^* T}{\pi \bar{q}} \frac{\xi_- - \xi_+}{1 - \exp(-z)} \qquad \text{with} \tag{5.51}$$

$$\xi_\pm = \ln\left[\frac{1 + \exp\left((E_{n\pm} - \mu_n)/T\right)}{1 + \exp\left((E_{n\pm} + q_0 - \mu_p)/T\right)} \right], \qquad z = \frac{\mu_n - \mu_p + q_0}{T}, \qquad E_{n\pm} = \frac{\bar{p}_{n\pm}^2}{2m_n^*} + m_n^* + U_n,$$

$$\bar{p}_{n\pm}^2 = \frac{2\bar{q}^2}{\chi^2} \left[\left(1 + \frac{\chi m_p^* c}{\bar{q}^2}\right) \pm \sqrt{1 + \frac{2\chi m_p^* c}{\bar{q}^2}} \right], \quad \chi = 1 - \frac{m_p^*}{m_n^*},$$

$$c = q_0 + U_n - U_p + m_n^* - m_p^* - \frac{\bar{q}^2}{2m_p^*}.$$

In the special case of equal effective nucleon masses $m_n^* = m_p^* = m^*$ this expressions simplifies to (see appendix E.1)

$$S(q_0, \vec{q}) = \frac{m^{*2} T}{\pi \bar{q}} \frac{z + \xi_-}{1 - \exp(-z)}. \tag{5.52}$$

Here z and ξ_- are defined as before. However, $\bar{p}_{n-}$ is given by

$$\bar{p}_{n-}^2 = \frac{m^{*2}}{\bar{q}^2} \left(q_0 + \Delta U - \frac{\bar{q}^2}{2m_p^*} \right)^2. \tag{5.53}$$

5.2.2. Absorption of Electron Antineutrinos

It can be shown that the matrix element for $\bar{\nu}_e$-capture in the nonrelativistic approximation is the same as for ν_e-capture. Also the kinematics are the same for both reactions. Consequently the cross sections for absorption on nonrelativstic nucleons for neutrinos and antineutrinos are connected by a simple replacement of indices.

$$\frac{1}{\lambda(E_{\bar{\nu}_e})} = \frac{1}{\lambda(E_{\nu_e})}\bigg|_{\{\nu_e \to \bar{\nu}_e, e^- \to e^+, n \to p, p \to n\}}. \tag{5.54}$$

Mind again that this implies $\Delta U = U_n - U_p \to -\Delta U = U_p - U_n$.

5.2.3. Inverse Neutron Decay

For inverse neutron decay, the terms of the matrix element that do not vanish for nonrelativistic nucleons are exactly the same as for capture of electron neutrinos. Consequently the inverse mean free path for inverse neutron decay differs only in the statistical factor and with respect to the four-momentum conservation in the δ^4-function. It is given by

$$\frac{1}{\lambda(E_{\bar{\nu}_e})} = \int \frac{d^3 p_p}{(2\pi)^3} \frac{d^3 p_{e^-}}{(2\pi)^3} \frac{d^3 p_n}{(2\pi)^3} 2G_F^2 V_{ud}^2 \left[G_V^2 \left(1 + \cos\theta_{\nu,e^-} \frac{\bar{p}_{e^-}}{E_{e^-}}\right) + G_A^2 \left(3 - \cos\theta_{\nu,e^-} \frac{\bar{p}_{e^-}}{E_{e^-}}\right) \right]$$
$$\times (2\pi)^4 \delta^4(p_{\bar{\nu}_e} + p_p + p_{e^-} - p_n) f_p(E_p) f_{e^-}(E_{e^-}) \left[1 - f_n(E_n)\right]. \tag{5.55}$$

The integration over electron phase space can be be substituted again by integration over energy transfer q_0 and momentum transfer $\vec{q}$ (see appendix E.2)

$$d^3 p_{e^-} = 2\pi \int\limits_{E_{\bar{\nu}_e} + m_e}^{\infty} dq_0 \frac{E_{e^-}}{E_{\bar{\nu}_e}} \int\limits_{E_{\bar{\nu}_e} - \bar{p}_{e^-}}^{E_{\bar{\nu}_e} + \bar{p}_{e^-}} d\bar{q}\, \bar{q}. \tag{5.56}$$

Now the inverse mean free path can again be expressed as integration over a structure function

$$\frac{1}{\lambda(E_{\bar{\nu}_e})} = \frac{G_F^2 V_{ud}^2}{4\pi^2} \int\limits_{E_{\bar{\nu}_e} + m_e}^{\infty} dq_0 \frac{E_{e^-}}{E_{\bar{\nu}_e}} \left[1 - f_{e^-}(E_{e^-})\right] \tag{5.57}$$

$$\times \int\limits_{E_{\bar{\nu}_e} - \bar{p}_{e^-}}^{E_{\bar{\nu}_e} + \bar{p}_{e^-}} d\bar{q} \left[G_V^2 \left(1 + \cos\theta_{\bar{\nu},e^-} \frac{\bar{p}_{e^-}}{E_{e^-}}\right) + G_A^2 \left(3 - \cos\theta_{\bar{\nu},e^-} \frac{\bar{p}_{e^-}}{E_{e^-}}\right) \right] \bar{q} S(q_0, \vec{q}).$$

Integrating over neutron phase space, the structure function for inverse neutron decay is given by

$$S(q_0, \vec{q}) = \frac{1}{2\pi^2} \int d^3 p_p \delta(q_0 + E_p - E_n) f_p(E_p) \left[1 - f_n(E_n)\right]. \tag{5.58}$$

Comparing this with the structure function for ν_e-capture (equation E.1) the only difference is the exchange of nucleon indices. Hence the result for the structure function can be obtained by the same exchange of indices.

$$S(q_0, \vec{q}) \left(\bar{\nu}_e + p + e^- \to n\right) = S(q_0, \vec{q}) \left(\nu_e + n \to p + e^-\right)\big|_{\{n \to p, p \to n\}}. \tag{5.59}$$

It is then clear that the structure functions for inverse neutron decay and $\bar{\nu}_e$-absorption are the same. This is intuitively clear, as the structure function represents the nucleon response and in both reactions a proton is converted into a neutron after receiving energy.

5.2.4. Absorption of Muon Neutrinos

For the absorption of muon neutrinos everything is analogous to the absorption of electron neutrinos. The only difference is the mass m_μ and the chemical potential μ_μ of the muons. However, since no assumptions were made in the derivation about the size of these quantities, the inverse mean free paths of both reactions are simply related by

$$\frac{1}{\lambda(E_{\nu_\mu})} = \frac{1}{\lambda(E_{\nu_e})}\bigg|_{\{\nu_e \to \nu_\mu, e^- \to \mu^-\}}. \tag{5.60}$$

5.3. Elastic Approximation for Nonrelativistic Nucleons

5.3.1. Absorption of Electron Neutrinos

In the elastic approximation for capture reactions [139] one assumes that the momentum transfer between leptons and nucleons does not lead to a change in absolute momentum of the nucleon. Hence, $\bar{p}_n = \bar{p}_p$. This is a reasonable approximation if the energy of the lepton is considerably smaller than the mass of the nucleons. In this approximation the structure function reduces to (see appendix E.1)

$$\begin{aligned}
S(q_0, \vec{q}) &= 4\pi\delta\big(q_0 - U_n + U_p - m_n^* + m_p^*\big)\frac{n_n - n_p}{1 - \exp\left[\big(m_n^* - m_p^* + U_n - U_p - \mu_n + \mu_p\big)/T\right]} \\
&= 4\pi\delta\big(q_0 - U_n + U_p - m_n^* + m_p^*\big)\frac{n_n - n_p}{1 - \exp\left[\left(\eta_p - \eta_n\right)/T\right]}.
\end{aligned} \tag{5.61}$$

In the elastic approximation it is more convenient to write the electron phase space integral in the following form

$$\int d^3 p_{e^-} = 2\pi \int\limits_{-\infty}^{E_{\nu_e} - m_e} dq_0\, E_{e^-}\bar{p}_{e^-} \int\limits_{-1}^{1} d\cos(\theta).$$

The inverse mean free path becomes then

$$\begin{aligned}
\frac{1}{\lambda(E_{\nu_e})} =& \frac{G_F^2 V_{ud}^2}{\pi}\frac{n_n - n_p}{1 - \exp\left[\left(\eta_p - \eta_n\right)/T\right]} \int\limits_{-\infty}^{E_{\nu_e} - m_e} dq_0\, E_{e^-} p_{e^-}\left[1 - f_{e^-}(E_{e^-})\right]\delta\big(q_0 - U_n + U_p - m_n^* + m_p^*\big) \\
&\times \int\limits_{-1}^{1} d\cos\theta_{\nu,e^-}\left[G_V^2\left(1 + \cos\theta_{\nu,e^-}\frac{\bar{p}_{e^-}}{E_{e^-}}\right) + G_A^2\left(3 - \cos\theta_{\nu,e^-}\frac{\bar{p}_{e^-}}{E_{e^-}}\right)\right].
\end{aligned} \tag{5.62}$$

The terms proportional to $\cos\theta_{\nu,e^-}$ vanish after integration. The q_0-integral fixes the electron energy to

$$E_{e^-} = E_{\nu_e} + m_n^* - m_p^* + U_n - U_p. \tag{5.63}$$

The inverse mean free path becomes eventually

$$\frac{1}{\lambda(E_{\nu_e})} = \frac{2G_F^2 V_{ud}^2}{\pi}\left(G_V^2 + 3G_A^2\right)E_{e^-} p_{e^-}\left[1 - f_{e^-}(E_{e^-})\right]\frac{n_n - n_p}{1 - \exp\left[\left(\eta_p - \eta_n\right)/T\right]}\Theta(E_{e^-} - m_e). \tag{5.64}$$

5.3.2. Absorption of Electron Antineutrinos

Proceeding analogous to electron neutrino capture the inverse mean free path results into

$$\frac{1}{\lambda(E_{\bar{\nu}_e})} = \frac{2G_F^2 V_{ud}^2}{\pi} \left(G_V^2 + 3G_A^2\right) E_{e^+} p_{e^+} \left[1 - f_{e^+}(E_{e^+})\right] \frac{n_p - n_n}{1 - \exp\left[(\eta_n - \eta_p)/T\right]} \Theta(E_{e^+} - m_e),$$
(5.65)

with the positron energy E_{e^+} as function of the incoming antineutrino energy $E_{\bar{\nu}_e}$

$$E_{e^+} = E_{\bar{\nu}_e} + m_p^* - m_n^* + U_p - U_n.$$
(5.66)

5.3.3. Inverse Neutron Decay

The inverse mean free path for inverse neutron decay in the elastic approximation becomes

$$\frac{1}{\lambda(E_{\bar{\nu}_e})} = \frac{2G_F^2 V_{ud}^2}{\pi} \left(G_V^2 + 3G_A^2\right) E_{e^-} p_{e^-} f_{e^-}(E_{e^-}) \frac{n_p - n_n}{1 - \exp\left[(\eta_n - \eta_p)/T\right]} \Theta(E_{e^-} - m_e),$$
(5.67)

with the electron energy E_{e^-} as function of the incoming neutrino energy E_{ν_e}

$$E_{e^-} = m_n^* - m_p^* + U_n - U_p - E_{\nu_e}.$$
(5.68)

5.3.4. Absorption of Muon Neutrinos

The inverse mean free path for absorption of muon neutrinos can be derived form the expression for electron neutrinos simply by renaming $\{e \to \mu\}$. This is possible since up to now there were no assumptions made with respect to the mass of the charged lepton.

$$\frac{1}{\lambda(E_{\nu_\mu})} = \frac{2G_F^2 V_{ud}^2}{\pi} \left(G_V^2 + 3G_A^2\right) E_{\mu^-} p_{\mu^-} \left[1 - f_{\mu^-}(E_{\mu^-})\right] \frac{n_n - n_p}{1 - \exp\left[(\eta_p - \eta_n)/T\right]} \Theta(E_{\mu^-} - m_\mu),$$
(5.69)

with the muon energy E_{μ^-} as function of the incoming neutrino energy E_{ν_μ}

$$E_{\mu^-} = E_{\nu_\mu} + m_n^* - m_p^* + U_n - U_p.$$
(5.70)

6. Neutrino Transport Properties

6.1. Standard Set of Reactions

In this chapter it will be discussed how the new reactions affect neutrino transport in a hot PNS during the first 100 milliseconds to seconds. For this purpose, transport properties such as opacities and neutrinospheres will be calculated on the basis of the expressions that have been derived in the previous chapters. The results will be compared against what is called here a standard set of neutrino reactions for transport in core collapse supernovae. This standard set consists of most of the reactions that are included in current CCSN simulations and are considered to be the dominant contributions for neutrino transport. An overview over the standard set is given in Table 6.1.

standard reactions	reference
$\nu/\bar{\nu} + e^-/e^+ \rightarrow \nu/\bar{\nu} + e^-/e^+$	[135]
$\nu/\bar{\nu} + n/p \rightarrow \nu/\bar{\nu} + n/p$	[139]
$\nu_e + n \rightarrow e^- + p$	[124, 137], this work
$\bar{\nu}_e + p \rightarrow e^+ + n$	[124, 137], this work
$\nu + \bar{\nu} + NN \rightarrow NN$	[140]
$\nu + \bar{\nu} \rightarrow e^- + e^+$	[139]

Table 6.1.: Standard reactions for $\bar{\nu}_e$ and ν_μ for neutrino transport in PNS.

For electron neutrinos, transport is dominated by the charged-current absorption on neutrons and the corresponding emission through electron captures on protons. The inverse mean free path of these reactions is significantly larger than of any other reaction for practically all relevant neutrino energies, temperatures, and matter densities. However, this reaction will only be studied to asses the impact of the improved treatment of weak magnetism and nucleon relativity from section 5.1.1. The transport of ν_e as such will not be investigated, as no changes are expected. Even though the new reaction $\nu_\mu + e^- \rightarrow \nu_e + \mu^-$ does emit an electron neutrino

and the inverse reaction is a source of opacity, there is no reason to believe that its contribution can come close to be significant compared to the standard charged-current channel. Nevertheless these calculations where performed and the result confirmed the intuition.

For electron antineutrinos the charged-current absorption on protons and its inverse is one of the important reactions, but not the dominating one. PNS matter is initially neutron rich and becomes even more so over time. There are then less absorption targets for $\bar{\nu}_e$ than for ν_e. Also, absorption on protons has to overcome the mass (energy) difference to the neutron, while absorption on neutrons releases this energy. This is further reducing the opacity for $\bar{\nu}_e$, especially for low neutrino energies. Also, this effect becomes even stronger at high densities when the difference in the strong interaction potentials adds up to the mass difference between the nucleons. When assessing the role of inverse neutron decay for $\bar{\nu}_e$-transport, absorption on protons will be calculated based on the derivations in section 5.1.2 although this is strictly speaking not part of a standard reaction set. However, for the overall comparison of different reaction channels, the difference between the approach in this work to the ones in e.g. [139, 124] is not of major relevance. Also, these modifications will be studied in a separate section.

Another reaction that is very important for $\bar{\nu}_e$ is scattering on nucleons, in particular neutrons. For this reaction all nucleons are viable targets and there is no energy difference to be overcome, which is especially relevant at higher densities. In this chapter, scattering on nucleons is described as a purely elastic reaction [139], i.e. $E_\nu = E'_\nu$. The approximation is justified by the large mass of the nucleons compared to the neutrino energies. One can show that for such a kinematic combination, the response function and consequently the scattering kernel are strongly peaked around zero energy exchange. However, it was found years ago already that the energy exchange per reaction is actually not so small at all, and that even a small energy exchange eventually leads to a significant modification of the neutrino spectrum due to the large number of scatterings [141, 142, 19]. Hence, the simplification of elastic scattering is a noticeable shortcoming of the approach in this work. Given the present approximation, more recent improvement of the neutrino-nucleon scatterings are also left out of the discussion. The inelasticity of this reaction has two sources, nucleon recoil and nucleon-nucleon interactions. The precise nature of the nuclear interaction is still a topic of ongoing research. At the same time, the structure function of this reaction is much more dependent on the description of nuclear interaction than e.g. the charged-current reactions. Recent work on chiral effective field theory suggests that more sophisticated calculations of NN-interactions might be required than all the approaches discussed in this work [120]. Nuclear correlations will play a much larger role for scattering on nucleons even at comparably low densities. Beyond that, weak magnetism is relevant for scattering on nucleons, too [66, 130]. All these effects will be neglected in the elastic scattering approximation that is adopted in this work.

Scattering of neutrinos on electrons (and some positrons) is another reaction that is included in neutrino transport simulations for a long time. It is implemented here with the full inelastic and relativistic treatment [134, 139, 135]. The scattering kernel for muon neutrinos is reproduced in chapter 3 in this work to derive the muonic reactions in close analogy. Due to the large neutron fraction Y_n, scatterings on charged leptons are less frequent than scattering on nucleons. Still, it is argued that they are very important for downscattering of neutrino

energies and thus for the energetic equilibration especially of the heavy flavour neutrinos. μ- and τ-neutrinos experience no charged-current reactions in the standard picture of current simulations. In the frame of this work scattering on electrons is thus the main channel of energy exchange for ν_μ and all other heavy flavour neutrinos. Hence it is the main reaction against which the role of charged-current muonic reactions for muon neutrinos has to be compared. However, several studies suggest that the dominance of scattering on electrons is only true for certain conditions and especially for neutrino energies $E_\nu \lesssim 10\,\text{MeV}$, while for higher neutrino energies $E_\nu \gtrsim 20\,\text{MeV}$ scattering on nucleons is more important for energy exchange, too [141]. One should keep this in mind as in this work the relevance of scattering on nucleons cannot really be compared to the one of muonic charged-current reactions.

Eventually, bremsstrahlung $NN \rightarrow NN + \nu + \bar{\nu}$ and its inverse can be another dominant source of energy exchange for low energy $\bar{\nu}_e$. Especially for those neutrinos that are below the absorption threshold this reaction can become very relevant. Bremsstrahlung has a smaller inverse mean free path than scattering on nucleons but is much more efficient in equilibrating the neutrino spectrum with the matter. Yet again, when including the full inelastic treatment of nucleon scattering, it is under debate how relevant bremsstrahlung is for electron antineutrinos [142, 19]. In this work bremsstrahlung is computed based on an analytic interpolation formula from [140]. The same implementation is found in many state of the art CCSN simulations. For muon neutrinos and all other heavy flavour neutrinos bremsstrahlung is especially important as it is expected to be their main thermal production process.

Neutrino pair production from electron-positron annihilation and its inverse is also included in the standard reaction set [139]. This reaction channel competes with bremsstrahlung as it has a similar effect on the neutrino spectrum. It is initially crucial for the thermal production of neutrinos, especially for the heavy leptons flavours, where it dominates over bremsstrahlung. Yet it is predicted that, in terms of opacity, for the most relevant conditions this reaction is inferior to bremsstrahlung for neutrino energies below $50\,\text{MeV}$ [141].

There are several notable omissions from what is considered here the standard reaction set. Scattering of neutrinos from each other $\nu_x + \nu_y \rightarrow \nu'_x + \nu'_y$ is not included, as well as the flavour conversion of a neutrino-antineutrino pair into another one $\nu_{\mu,\tau} + \bar{\nu}_{\mu,\tau} \rightarrow \nu_e + \bar{\nu}_e$ [129]. These reactions were found to increase the number flux of μ- and τ-neutrinos [25]. Further we do not consider scattering [143, 144] or absorption [145] on nuclei. These reactions are very important during the collapse phase and later at lower densities where nucleons are mainly bound in nuclei. Also at high densities nuclei might form, although the extent of this depends strongly on the description of nuclear interactions at high densities and consequently on the choice of the EoS. Still, for the regions where neutrinos decouple after the bounce, nuclei are practically absent and the corresponding reactions are negligible. A notable exception to this statement could be scatterings and captures on light nuclei, especially deuterium [146, 147, 148].

6.2. Explosion Model

In order to study neutrino transport in a hot PNS one needs the chemical composition and thermodynamical condition of the matter. Also some neutrino reactions such as scatterings

and pair processes need actual neutrino spectra of reaction partner neutrinos. Thus, all results in this chapter will be based on matter profiles and neutrino spectra from an actual CCSN simulation. More precise, this input is obtained from a 1-dimensional (spherically symmetric) hydrodynamical CCSN simulation [37] of a $18\,M_\odot$ progenitor star [88]. The neutrino radiation field was evolved with full Boltzmann neutrino transport, based on the above standard set of neutrino reactions, plus additional reaction channels involving nuclei such as electron captures [139, 149]. The nuclear matter in nuclear statistical equilibrium (NSE) at temperatures $T > 0.5\,MeV$ is described by the baryon EoS from Shen et al.[43]. This supernova model, like all 1-D models except simulations of the O-Ne-Mg progenitor, does not develop a self consistent explosion. This is most likely due to the lack of hydrodynamical instabilities in 1-D which are understood to increase the neutrino heating efficiency. Therefore this model artificially increases charged-current electron flavour neutrino rates in the region between the neutrinosphere and the standing accretion shock (SAS). This increases the efficiency of energy deposition behind the SAS and eventually triggers an explosion.

For the present work it is important to note that the neutrino spectra from such an artificial explosion were found to be in relative good agreement with neutrino spectra from self consistent 2-D models [20]. The calculations in this work are based on radial profiles of the temperature T, the baryon mass density ρ, and the electron fraction Y_e at different times during the simulation. To obtain the chemical composition of the nuclear matter these profiles are used as input for an interpolation of the Shen-EoS [43]. Whenever neutrino profiles are required, they are taken from the simulation as well.

At this point one has to note that the calculations in this thesis are done in a post processing manner. In post processing one can show whether additional neutrino reactions should be important for matter profiles and neutrino spectra that are encountered in CCSN. One might also be able to hint at the direction of changes. But it is difficult to quantify possible changes as the actual effect upon implementation of new rates can only be shown by new dynamic simulations.

6.3. Concept of Neutrinospheres

When neutrinos diffuse out of a medium like a stellar surface, the matter usually becomes increasingly transparent and the mean free path of the radiation is gradually decreasing. In the deep interior, radiation is strongly coupled to the medium, both thermally and chemically. Far outside, the mean free path becomes so large that radiation can be considered as free streaming. In both cases the description of the radiation field and its evolution is rather straightforward. One does not need to consider the exact reaction rates, as they are either so large or so small that it does not matter. In contrast the description of the diffusion process in the transition region proves to be significantly more difficult. However the theory of radiative transport offers tools to simplify the diffusion problem, most notably the radiation sphere. Radiative transport predicts that the intensity and likewise the spectrum of radiation outside of a hot emitting source is approximately a thermal black body spectrum. Furthermore there exists a relation between the temperature of the radiation and the temperature of the source at a certain depth

below the surface. In particular, the effective radiation temperature is equal to the temperature of the medium at the region where the optical depth $\tau = 2/3$ [150]. The optical depth is defined as the space integral over the total inverse mean free path, coming from the vacuum where the inverse mean free path vanishes, up to a certain point in the medium. Assuming spherical symmetry one can define the optical depth as a function of the radius by

$$\tau(R) = \int_R^\infty dr \frac{1}{\lambda_{tot}(r)}. \tag{6.1}$$

Consequently the radius R_S of the effective decoupling region of radiation is defined by

$$\tau(R_S) = \int_{R_S}^\infty dr \frac{1}{\lambda_{tot}(r)} = \frac{2}{3}. \tag{6.2}$$

Using this expression, the diffusion problem can simply be approximated by emitting a black body spectrum from R_S according to the matter temperature $T(R_S)$. Applying this approach to the transport of neutrinos results in the concept of the neutrinosphere. However, the neutrino sphere is not perfect in that sense. It was already discussed in the previous chapters that the inverse mean free path is an energy dependent quantity, $1/\lambda(r) = 1/\lambda(r, E)$. Hence the neutrino sphere has a different position and a different temperature for varying neutrino energies. One finds that these differences can actually be quite large. As a result, the spectrum is not perfectly described by a single temperature. Nevertheless, calculations showed that the concept of the neutrinosphere can give reasonable estimates for neutrino spectra and luminosities. In this work it is especially useful as it roughly marks the region where neutrinos decouple from matter. Thus, when assessing whether a reaction is important for the formation of neutrino spectra, one has to ask whether it is important at the position of the neutrinosphere.

Later studies have discussed that in general one needs to distinguish two different kind of neutrino spheres [150, 140]. The transport or scattering sphere R_{tr} defines the region of last interaction with the medium, while the effective or energy sphere R_{eff} is the region of last energy exchange with the medium. For electron neutrinos where the charged-current channels are the dominating opacity source both regions are the same $R_{tr,\nu_e} = R_{eff,\nu_e}$. However, for $\bar{\nu}_e$ and even more so for all heavy lepton flavour neutrinos, the dominating reaction on the surface of the PNS is scattering on nucleons. As it was discussed before, this reaction can be considered as almost isoenergetic. Under this assumption, scattering on nucleons delays the time when neutrinos leave the surface, but cannot modify their energy. Instead, the spectrum of the neutrinos is determined by the energy exchanging reactions such as scattering on electrons deeper inside. The main effect of isoenergetic scatterings is to increase the time for additional non-isoenergetic reactions to take place. Comparing the two concepts of the transport and the effective neutrinosphere, they are defined via the total and the effective inverse mean free path, respectively. The total inverse mean free path $1/\lambda_{tot}$ is an equally weighted sum over the inverse mean free path of all possible reactions, including isoenergetic scatterings. The effective mean free path $1/\lambda_{eff}$ is composed of the energy inverse mean free path $1/\lambda_e$ and of $1/\lambda_{tot}$ according

to

$$\frac{1}{\lambda_{eff}} = \sqrt{\frac{1}{\lambda_{tot}} \cdot \frac{1}{\lambda_e}}. \tag{6.3}$$

Here, $1/\lambda_e$ is the sum over all reactions that are not isoenergetic. Thus one finds

$$\frac{1}{\lambda_{tot}} = \frac{1}{\lambda_e} + \frac{1}{\lambda_{iso}}. \tag{6.4}$$

Isoenergetic scattering reactions contribute less to $1/\lambda_{eff}$ than energy changing reactions. The transport and effective neutrino spheres are now given by

$$\tau_{tr}(R_{tr}) = \int\limits_{R_{tr}}^{\infty} dr \frac{1}{\lambda_{tot}(r)} = \frac{2}{3} \quad \text{and} \quad \tau_{eff}(R_{eff}) = \int\limits_{R_{eff}}^{\infty} dr \frac{1}{\lambda_{eff}(r)} = \frac{2}{3}. \tag{6.5}$$

For neutrino species where $R_{tr} \neq R_{eff}$, a reaction can be considered important for the formation of the neutrino spectrum when it is important at R_{eff}, compared to other non-isoenergetic reactions. The region between R_{eff} and R_{tr} is called the scattering atmosphere. However, it has to be noted that the neutrino spectrum will in fact be modified when crossing an extended scattering atmosphere. As it was explained before, scattering of neutrons is not isoenergetic. Even though the response function might be more sharp than for other reactions, there is still a relevant width to it. Since for μ- and τ-neutrinos the opacity of nucleon scattering is much larger than for any other channel, the neutrino spectrum does experience considerable modification between R_{tr} and R_{eff} [140, 142, 141, 19]. On the other hand, scatterings on nucleons are not energy changing enough that the effective neutrino temperature would be defined by the temperature at R_{tr} i.e. $T_\nu \neq T(R_{tr})$. Instead the effective neutrino temperature T_ν depends in a non-trivial way on the medium temperature at the effective neutrinosphere $T(R_{eff})$, on the development of the medium temperature between R_{eff} and R_{tr}, and on the transport optical depth at the effective neutrino sphere $\tau_{tr}(R_{eff})$ [142]. For the results in this chapter one must keep then in mind that the concept of the effective neutrino sphere is somewhat overestimated in its relevance compared to what happens in a dynamical simulation. Still, for a post processing calculation R_{eff} remains a major point of reference to determine the neutrino spectrum.

6.4. Spectral averages

In the previous section it was explained that concepts such as inverse mean free path and neutrinosphere depend on the neutrino energy. Beyond that, they depend also on the thermodynamical conditions and the chemical composition of the nuclear mater, which in turn depends on the density and the time of the PNS evolution. Studying energy dependent expressions gives accurate information on the progression of neutrino transport, but they are less helpful in giving an overview of neutrino transport over the whole PNS. Fur this purpose it is helpful to compute spectrally averaged quantities and study the density dependence for a given time. Particularly interesting is the spectrally averaged inverse mean free path $1/\langle\lambda\rangle$ which is

defined by

$$\frac{1}{\langle\lambda\rangle} = \frac{\int dE_\nu \, d\cos\theta \, E_\nu^2 f_\nu(E_\nu,\theta)\frac{1}{\lambda(E_\nu)}}{\int dE_\nu \, d\cos\theta \, E_\nu^2 f_\nu(E_\nu,\theta)}. \tag{6.6}$$

For the effective mean free path one defines

$$\frac{1}{\langle\lambda_{eff}\rangle} = \sqrt{\frac{1}{\langle\lambda_{tot}\rangle} \cdot \frac{1}{\langle\lambda_e\rangle}}. \tag{6.7}$$

These expressions can readily be extended to account for scattering reactions by replacing $1/\lambda(E_\nu) \to 1/\lambda(E_\nu,\theta)$. Based on $1/\langle\lambda\rangle$ one can likewise define a spectrally averaged neutrino sphere $\langle R_\nu\rangle$ by

$$\tau(\langle R_\nu\rangle) = \int\limits_{\langle R_\nu\rangle}^{\infty} dr \frac{1}{\langle\lambda(r)\rangle} = \frac{2}{3}. \tag{6.8}$$

One has to be careful not to overestimate the quantitative meaning of spectrally averaged expression, but they are of great use for qualitative discussion and comparison.

6.5. Transport of Electron Antineutrinos

6.5.1. Standard Scenario

This section will sketch the transport situation for $\bar\nu_e$ in a hot PNS after bounce. It will present the thermodynamical and chemical conditions, spectrally averaged inverse mean free paths and the position of the spectrally averaged neutrino spheres. All transport properties will be derived on the basis of the standard set of neutrino reactions. All quantities will be shown for the relevant density range for three different times, 150 ms, 500 ms, and 2 s post bounce. At 150 ms for this simulation one looks still at the early evolution before the shock is fully revived. After 500 ms one studies the situation shortly after the explosion is achieved. Eventually after 2 s one studies the cooling phase of the PNS. Figures 6.1 and 6.2 show the composition and the thermodynamical conditions for different densities in the PNS, 150 ms after bounce.

There, matter is significantly neutron rich. Up to 10^{13} g/cm^3 the neutron fraction Y_n reaches almost 0.9. This also manifests in a significant difference between neutron and proton chemical potentials μ_n and μ_p. At higher densities, matter is less deleptonized with $Y_n \sim 0.75$, which is due to the fact that neutrinos are still mostly trapped in this region. In the chemical potentials one has therefore a small dip in $\mu_n - \mu_p$ at $\rho \sim 2 \times 10^{13}$ g/cm^3. In general chemical potentials increase with density, as it is expected. This can be nicely seen from the electron chemical potential μ_e. At the surface of the PNS at $\rho = 10^{11}$ g/cm^3 the temperature is below 5 MeV. It increases up to more than 20 MeV above $\rho = 10^{13}$ g/cm^3. The difference in the strong interaction potentials is negligible up to several times 10^{12} g/cm^3, where it slowly starts to rise. Eventually, the effective mass does not deviate significantly from the rest mass below $\rho = 10^{13}$ g/cm^3. Also, in the considered density range it stays always above $0.8\,m_N$.
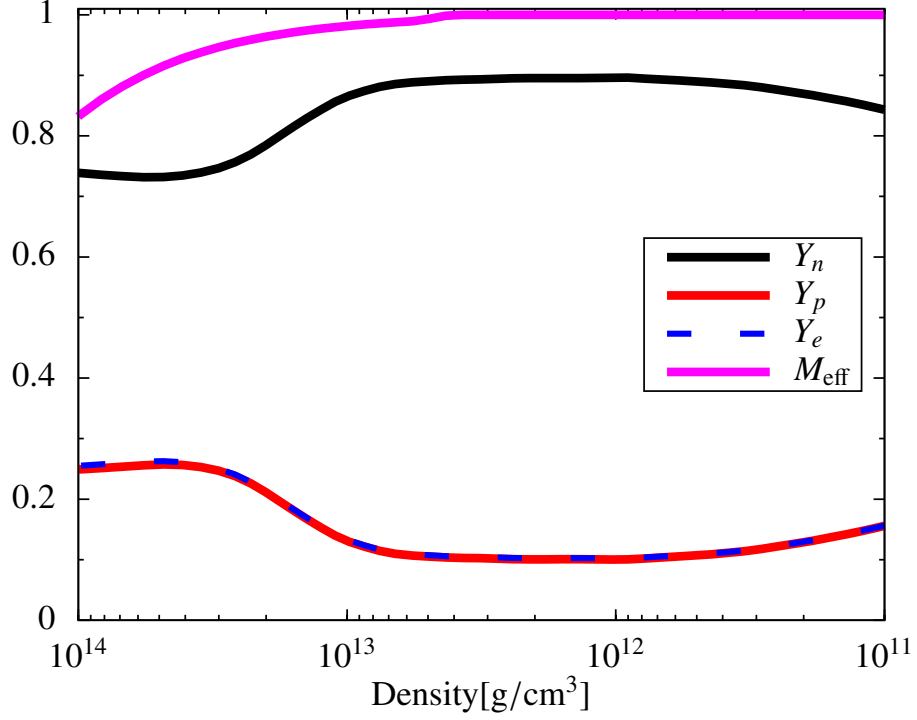
Figure 6.1.: Chemical abundances and effective nucleon mass over density, 150 ms post bounce. Y_n, Y_p, and Y_e denote neutron, proton, and electron fraction per baryon, respectively. The effective mass M_{eff} is shown in terms of the nucleon rest mass $m_N = 938\,\text{MeV}$.
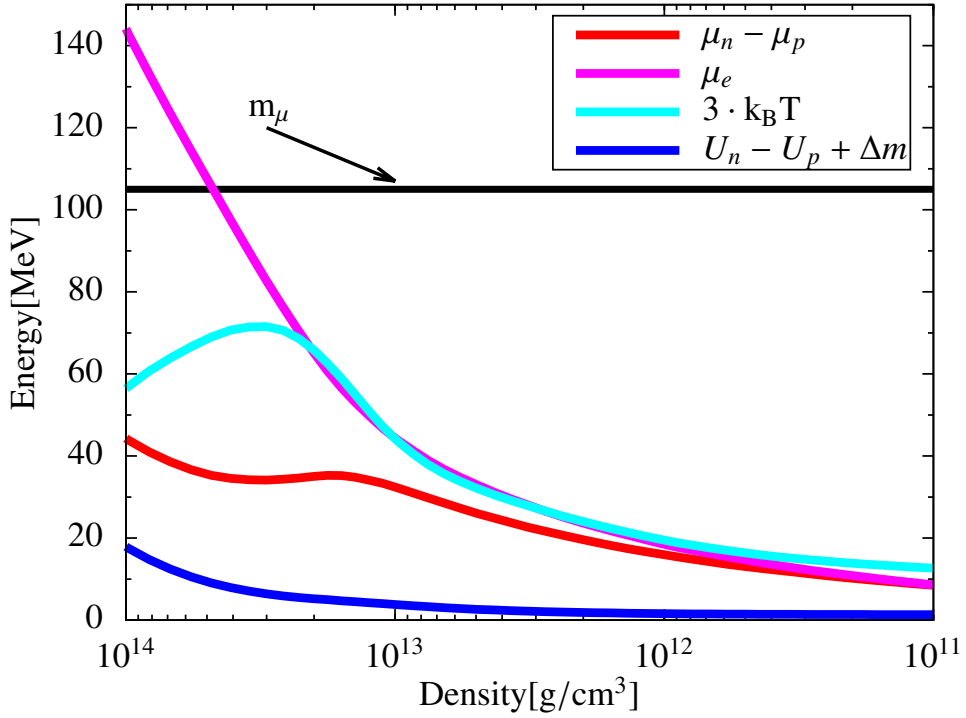

Figure 6.2.: Thermodynamical quantities over density, 150 ms post bounce. μ denotes chemical potentials and U denotes strong interaction potentials. The curve for $3\,\text{k}_B T$ denotes the average thermal energy of neutrinos.
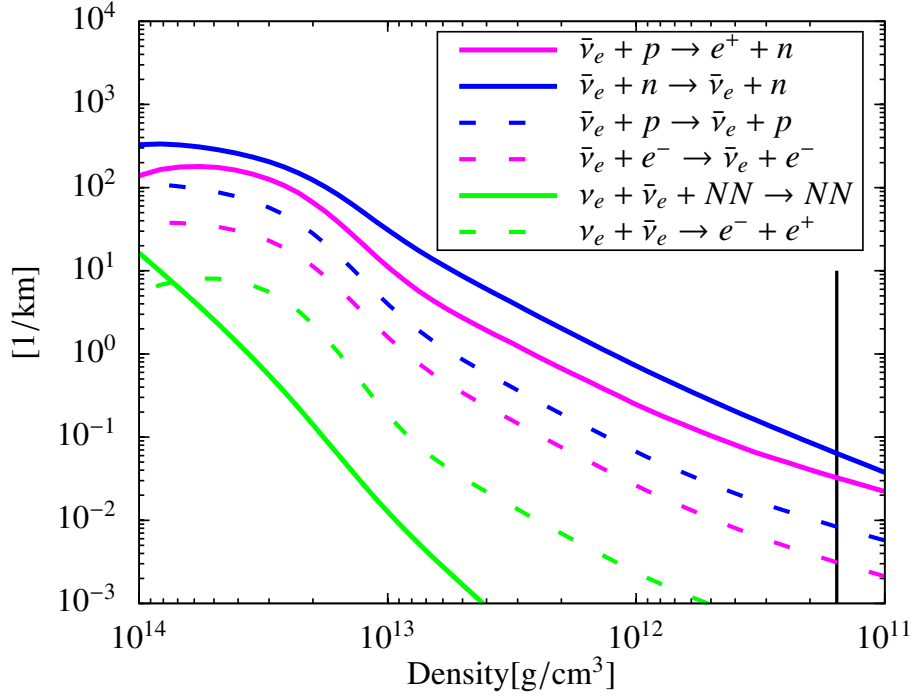
Figure 6.3.: Spectrally averaged inverse mean free path of $\bar{\nu}_e$ for various reactions, $150\,\mathrm{ms}$ post bounce. The black vertical line marks the density of the spectrally averaged effective neutrinosphere.

Now that the state of nuclear matter is known, one can study the corresponding neutrino interactions.

Figure 6.3 shows the spectrally averaged mean free paths for $\bar{\nu}_e$ over density. One can see that scattering on neutrons shows the largest rate followed by absorption on protons. It can be seen that the rate for absorption increases compared to the scattering, when the neutron fraction decreases at high density. For even higher densities the strong interaction potentials rises. This leads again to a relative decrease of the absorption inverse mean free path. The position of the spectrally averaged neutrinosphere is marked by the black line in Figure 6.3, it lies at $\langle R_{eff} \rangle \sim 1.6 \times 10^{11}\,\mathrm{g/cm^3}$. One expects then, that $\bar{\nu}_e$ decoupling is determined mainly by absorption on protons, as scattering on neutrons is less efficient in equilibrating. Also, one can conclude that strong interaction will not play a relevant role at this density. Therefore, one would not expect for muonic reactions or inverse neutron decay to contribute significantly in the decoupling region. However, as can be seen in Figure 6.2, at very large densities μ_e becomes larger then the muon mass, so one should expect muon production in this region already at this early time. Regarding the other standard reactions, scattering on protons and scattering on electrons have the next largest inverse mean free path. Thereby, scattering on protons is roughly 3 times larger for all densities. The two pair processes have even smaller opacities, with electron-positron pair creation dominating up to almost $10^{14}\,\mathrm{g/cm^3}$.

Next, Figures 6.4 and 6.5 show the thermodynamical and chemical composition of the matter at $500\,\mathrm{ms}$ post bounce.

One can see that the deleptonization has further progressed, as $Y_n > 0.9$ up to $3 \times 10^{13}\,\mathrm{g/cm^3}$. The temperature profile is lower and more flat at densities below $10^{13}\,\mathrm{g/cm^3}$. However further

Figure 6.4.: Chemical abundances and effective nucleon mass over density, 500 ms post bounce. Y_n, Y_p, and Y_e denote neutron, proton, and electron fraction per baryon, respectively. The effective mass M_{eff} is shown in terms of the nucleon rest mass $m_N = 938\,\text{MeV}$.
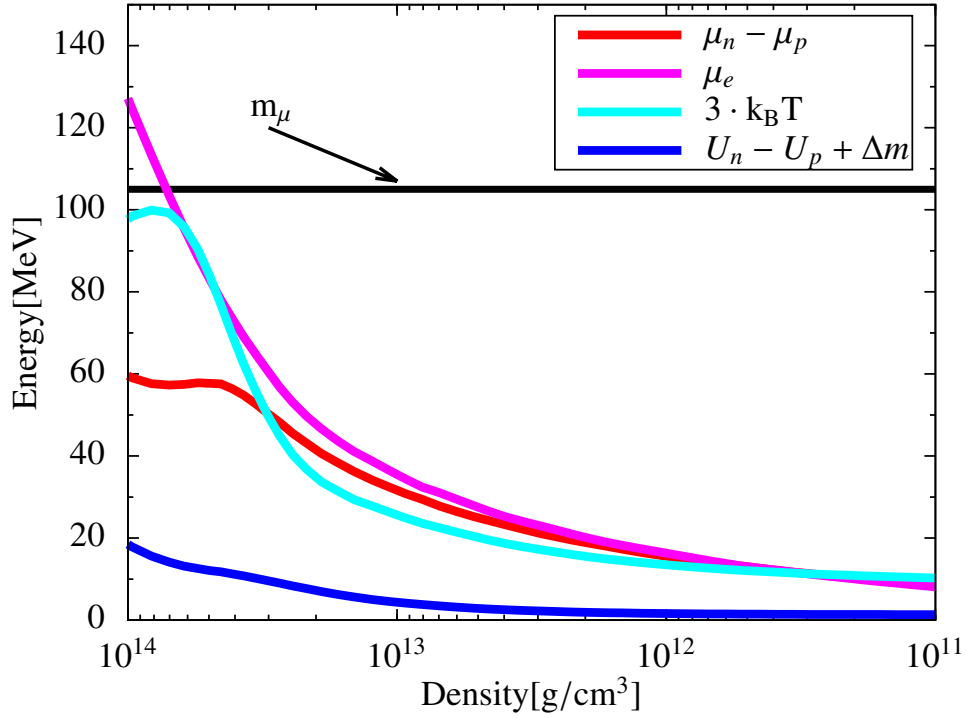
Figure 6.5.: Thermodynamical quantities over density, 500 ms post bounce. μ denotes chemical potentials and U denotes strong interaction potentials. The curve for $3\,\text{k}_B T$ denotes the average thermal energy of neutrinos.

inside it peaks higher than before, reaching a maximum of over $30\,\mathrm{MeV}$. This means that thermal neutrinos in this region will have energies similar to the muon mass. The rise in $U_n - U_p$ starts earlier, mainly due to the higher neutron fraction and therefore larger asymmetry at intermediate densities. Yet, it reaches roughly the same maximum value, as the neutron fraction close to $10^{14}\,\mathrm{g/cm^3}$ has not changed significantly since the earlier time. The larger intermediate Y_n translates intuitively also in a larger $\mu_n - \mu_p$ and smaller μ_e. The behaviour of the effective mass has not changed significantly. One can note that it only starts to deviate from the rest mass at even higher densities now.

Looking at the spectrally averaged transport properties in Figure 6.6 , one recognizes first that the effective neutrinosphere has moved up more than one order of magnitude in density to $\langle R_{eff} \rangle \sim 2 \times 10^{12}\,\mathrm{g/cm^3}$. The reason for this is not obvious from a comparison of the opacities. Opacities have indeed decreased at lower densities but not so much that they could explain the size of the shift in $\langle R_{eff} \rangle$. Instead the reason for this is the contraction of the PNS in the meantime. The density profile has become much stepper and therefore the radial extent of the PNS surface has shrinked. Also the radial position of the neutrinosphere has moved further inside, from $\sim 49\,\mathrm{km}$ after $150\,\mathrm{ms}$ to $\sim 25\,\mathrm{km}$ after $500\,\mathrm{ms}$. The size of the PNS surface can be approximately read from the size of the mean free path at the neutrinosphere. The size of the mean free path at decoupling should be similar to the extent of the region with significant opacity, i.e. the PNS surface. It has decreased from $\sim 20\,\mathrm{km}$ down to $\sim 1\,\mathrm{km}$ for scattering on neutrons and $\sim 8\,\mathrm{km}$ for absorption on protons.

Figure 6.6.: Spectrally averaged inverse mean free path of $\bar{\nu}_e$ for various reactions, $500\,\mathrm{ms}$ post bounce. The black vertical line marks the density of the spectrally averaged effective neutrinosphere.

When comparing the different reactions to each other, scattering on neutron has the largest inverse mean free path over all densities. At the position of the effective neutrino sphere it is
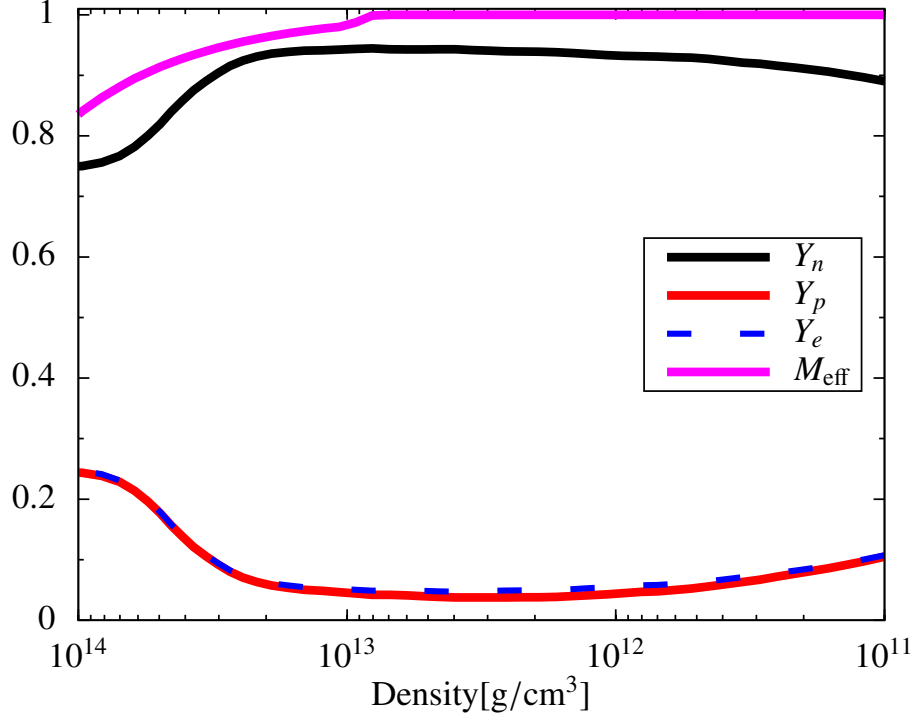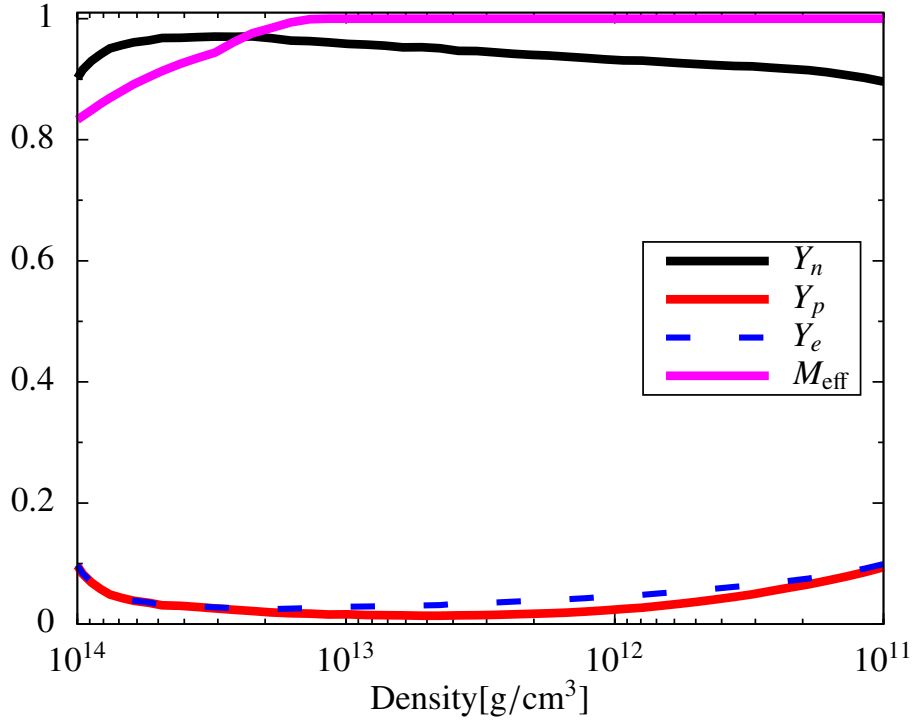
Figure 6.7.: Chemical abundances and effective nucleon mass over density, 2 s post bounce. Y_n, Y_p, and Y_e denote neutron, proton, and electron fraction per baryon, respectively. The effective mass M_{eff} is shown in terms of the nucleon rest mass $m_N = 938$ MeV.
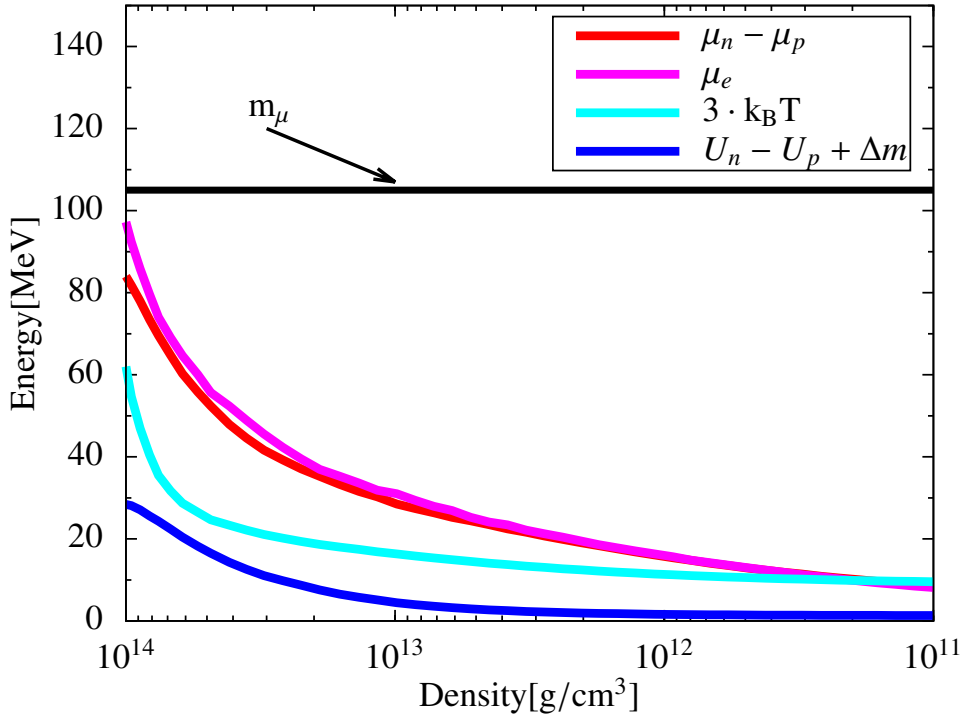
Figure 6.8.: Thermodynamical quantities over density, 2 s post bounce. μ denotes chemical potentials and U denotes strong interaction potentials. The curve for $3\,k_B T$ denotes the average thermal energy of neutrinos.

almost an order of magnitude larger than the one for absorption on neutrons. Consequently a scattering atmosphere emerges above the effective neutrinosphere, as the transport neutri-

nosphere lies at lower densities $\langle R_{tr} \rangle \sim 9 \times 10^{11}\,\mathrm{g/cm^3}$. Thus the neutrino spectrum will be determined by the interplay of absorption on protons and scattering on neutrons. While absorption on protons has the smaller opacity, it is still more inelastic than the scattering reaction. Beyond the leading order one finds again scattering on protons followed by scattering on electrons. Of those, scattering on electrons might be the more important reaction, as it is more inelastic and efficient in neutrino downscattering. The pair processes still seem to be less relevant, with electron-positron-pair creation dominating over inverse bremsstrahlung. Given the position of the effective neutrinosphere it is not expected that mean field effects or the new reactions investigated in this work might play a role.

Next, Figures 6.7 and 6.8 show the thermodynamical and chemical composition of the matter at 2 s post bounce. The deleptonization of matter has progressed much further, as $Y_n > 0.9$ for the whole density range. Close to $10^{14}\,\mathrm{g/cm^3}$ a decrease on Y_n can still be found, hinting that deleptonization is still ongoing. Additionally, the proton fraction decreases well below the electron fraction down to $Y_p < 0.02$ for intermediate densities as the EoS predicts an alpha mass fraction $X_\alpha = 0.045$ for $\rho = 10^{12}\,\mathrm{g/cm^3}$. The temperature profile is lower and flatter for all densities. At lower densities it has not decreased significantly, staying almost the same at the surface. Inside $10^{13}\,\mathrm{g/cm^3}$ the PNS has cooled significantly with a maximum temperature of 20 MeV. Below $10^{13}\,\mathrm{g/cm^3}$ the increase in Y_n does not translate in a significant change of the chemical potentials $\mu_n - \mu_p$ or μ_e. Above this density μ_e has decreased while $\mu_n - \mu_p$ has increased. At high density the difference in strong interaction potentials has notably increased, rising stronger and reaching almost up to 30 MeV. Eventually, the behaviour of the effective mass is the same as it was 500 ms post bounce.
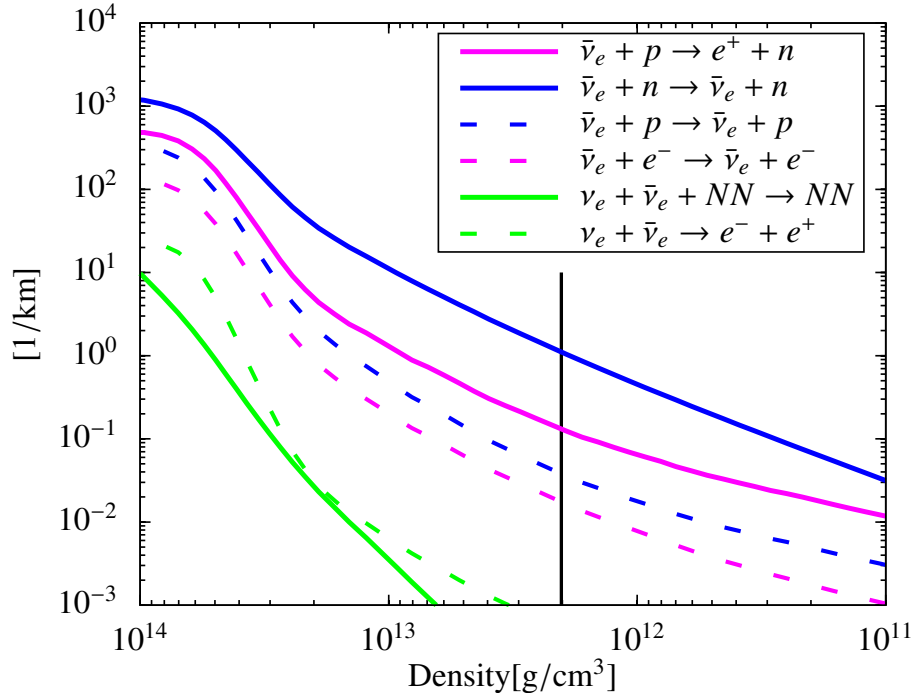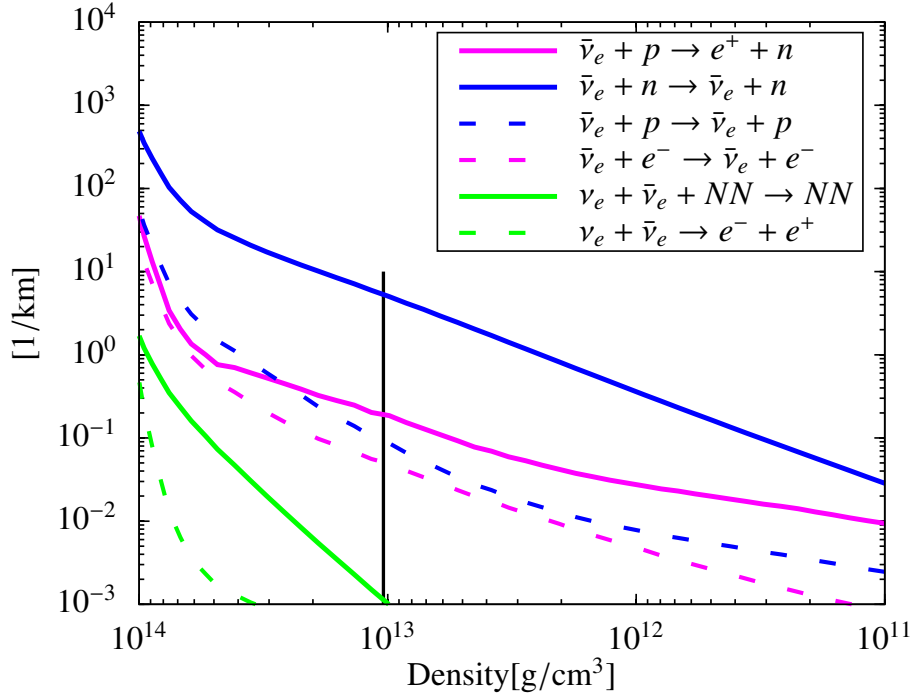

Figure 6.9.: Spectrally averaged inverse mean free path of $\bar{\nu}_e$ for various reactions, 2 s post bounce. The black vertical line marks the density of the spectrally averaged effective neutrinosphere.

The effective neutrinosphere has moved significantly higher in density $\langle R_{eff} \rangle \sim 10^{13}\,\mathrm{g/cm^3}$. This time the difference is also due to a decrease in the opacities, especially for absorption on protons. The PNS has contracted further indeed, with the effective neutrinosphere now sitting at a radius of $\sim 17.7\,\mathrm{km}$. Yet the mean free path for $\bar{\nu}_e$ absorption at this position is $\sim 5\,\mathrm{km}$, similar to the situation after 500 ms. However, the mean free path for scattering on neutrons is down to $\sim 200\,\mathrm{m}$ at $\langle R_{eff} \rangle$. Consequently the range of the scattering atmosphere increases as the transport mean free path lies significantly lower at $\langle R_{tr} \rangle \sim 2.8 \times 10^{12}\,\mathrm{g/cm^3}$.

The absorption on protons has still the largest inelastic opacity at the neutrinosphere. Yet considering how much larger the inverse mean free path for scattering on neutrons is, it can be assumed that even the small inelasticity of this reaction will lead to a modification of the neutrino spectrum that is emitted from $\langle R_{eff} \rangle$. Scattering on electrons and on protons are closer to the absorption than before, with scattering on protons becoming larger than absorption for $\rho > 3 \times 10^{13}\,\mathrm{g/cm^3}$. This is caused by the larger $U_n - U_p$, which decreases the rate for absorption on protons but not for scattering. The pair processes seem to be negligible. However it has to be noted that bremsstrahlung is now the clearly dominating pair process at high densities. Given that $U_n - U_p = 5\,\mathrm{MeV}$ at $\langle R_{eff} \rangle$ it is interesting to look at the relevance of inverse neutron decay.
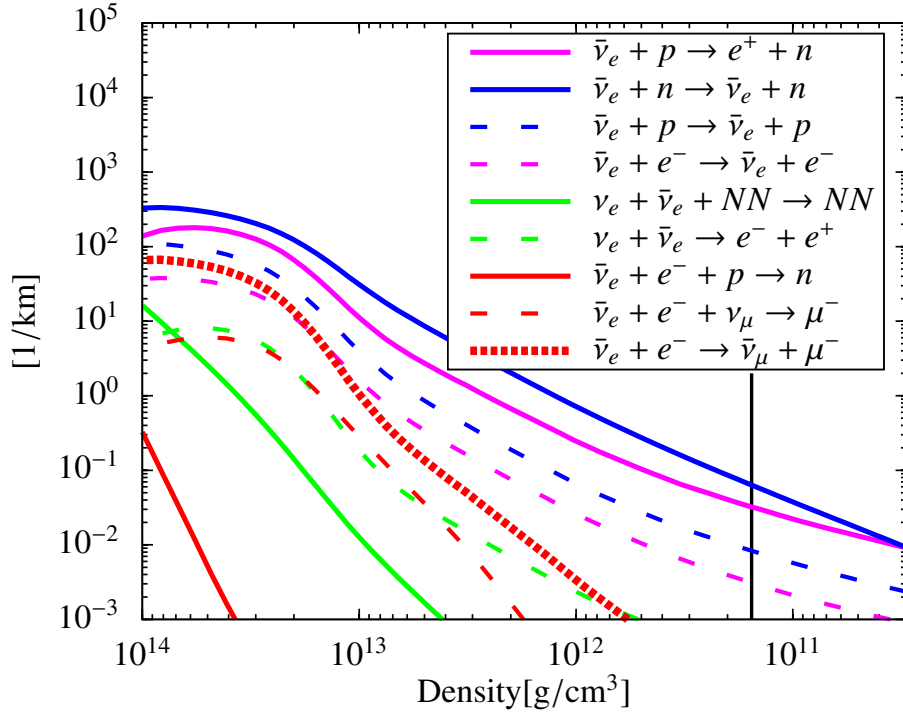
Figure 6.10.: Spectrally averaged inverse mean free path of $\bar{\nu}_e$ for extended reaction set, 150 ms post bounce. The black vertical line marks the density of the spectrally averaged effective neutrinosphere.

6.5.2. Role of New Reactions

Now the reaction set is extended to include inverse neutron decay $\bar{\nu}_e + p + e^- \to n$, inverse muon decay $\bar{\nu}_e + e^- + \nu_\mu \to \mu^-$, and the reaction $\bar{\nu}_e + e^- \to \bar{\nu}_\mu + \mu^-$. Figure 6.10 shows the

spectrally averaged inverse mean free paths and the spectrally averaged effective neutrinosphere 150 ms post bounce for the extended reaction set. The position of $\langle R_{eff} \rangle$ does not change upon inclusion of the additional reactions. All new reactions seem to be negligible in the decoupling region. The absorption on electrons $\bar{\nu}_e + e^- \rightarrow \bar{\nu}_\mu + \mu^-$ has the largest inverse mean free path among the new reactions, becoming similar to scattering on electrons above $10^{13}\,\mathrm{g/cm^3}$. Inverse muon decay comes close to electron-positron pair creation while inverse neutron decay has the smallest opacity of all reactions.

It was noted in the beginning, that the spectrally averaged quantities can be misleading if one is concerned with the transport of neutrinos with a particular energy. For this purpose, it is better to look at energy dependent transport properties. Figure 6.11 shows the energy dependent effective neutrino sphere $R_{eff}(E_\nu)$.
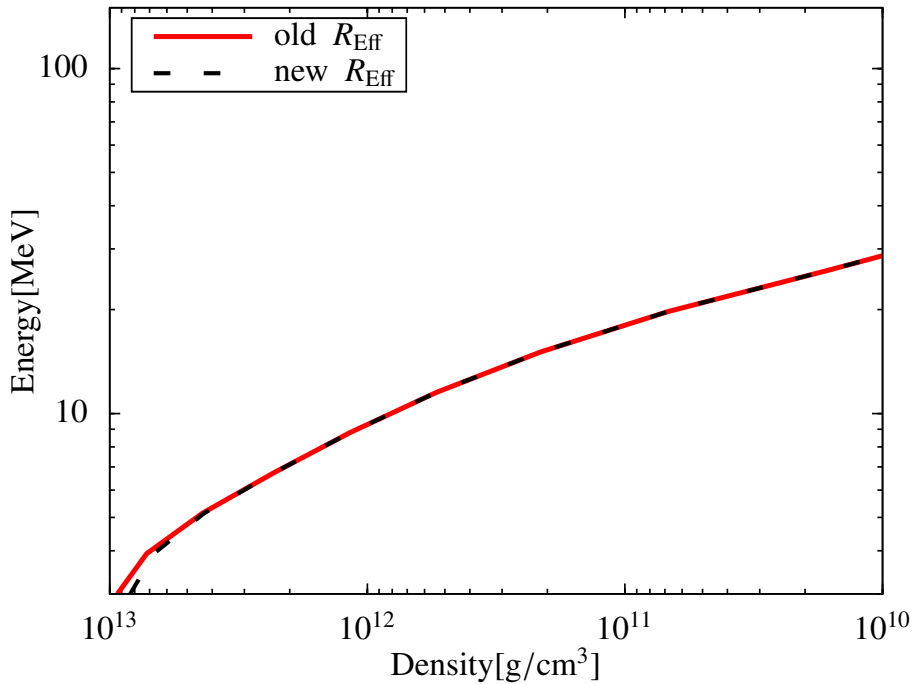
Figure 6.11.: Energy dependent effective neutrinosphere $R_{eff}(E_\nu)$ for $\bar{\nu}_e$, 150 ms post bounce. The red curve shows R_{eff} for the standard reaction set, the black dashed curve is computed for the extended reaction set.

The red curve shows R_{eff} for the standard reaction set while the black dashed curve is computed for the extended reaction set. One can see immediately that the effective neutrinosphere $\langle R_{eff} \rangle$ is in fact somewhat misleading, as all neutrinos with energy $E_\nu < 15\,\mathrm{MeV}$ decouple further inside. Neutrinos with energies $E_\nu < 10\,\mathrm{MeV}$ decouple at densities higher than $10^{12}\,\mathrm{g/cm^3}$, even going up to $10^{13}\,\mathrm{g/cm^3}$ for $E_\nu < 3\,\mathrm{MeV}$. Also it can be seen that for $E_\nu < 5\,\mathrm{MeV}$ there is actually a difference in R_{eff} between the standard and extended reaction sets. In order to understand this difference one needs to study energy dependent opacities. However, as the energy will be the dependent variable, one has to look at several discrete densities separately. Figure 6.12 shows the energy dependent opacities of $\bar{\nu}_e$ for $\rho \sim 1.6 \times 10^{11}\,\mathrm{g/cm^3}$, the position of the neutrino sphere. It has to be noted that for scatterings, opacities are defined as the phase space integral of the final state neutrino over the scattering kernel, as in eq. (2.22), averaged

over the angle of the initial state neutrino. In general the opacity is given as a rate, equal to the inverse mean free path times the speed of light.

At this density, neutrinos with $E_\nu \sim 15\,\mathrm{MeV}$ decouple from matter. As expected from the spectrally averaged opacity, the dominating reactions for these neutrinos are absorption on protons and scattering on neutrons. Also the new reactions are indeed negligible as expected from the energy dependent neutrino sphere.

Figure 6.12.: Energy dependent opacity of $\bar{\nu}_e$ for extended reaction set, $150\,\mathrm{ms}$ post bounce for $\rho = 1.60 \times 10^{11}\,\mathrm{g/cm^3}$. Rate is defined as inverse mean free path times c.

Next, Figure 6.13 shows the effective opacity for $\rho \sim 10^{12}\,\mathrm{g/cm^3}$ for the same time. At this density, neutrinos with $E_\nu \sim 10\,\mathrm{MeV}$ decouple according to Figure 6.11.

Again, the energy dependent opacities agree with the general statements from before. Scattering on neutrons and absorption on protons are the important reactions for the neutrinos that decouple here. Also, the additional reactions are negligible.

Eventually, Figure 6.14 shows the energy dependent opacities for $\rho \sim 10^{13}\,\mathrm{g/cm^3}$, $150\,\mathrm{ms}$ post bounce. Here low energy neutrinos with $E_\nu \sim 3\,\mathrm{MeV}$ should decouple. This energy is at the left border of Figure 6.14. One finds that for these low neutrino energies the inverse muon decay is the reaction with the largest opacity. More than a factor of 2 smaller are scattering on neutrons, scattering on electrons and inverse bremsstrahlung. Also, the rate for absorption on protons is vanishing for these energies. None of this was indicated in Figure 6.10 by the spectrally averaged opacities. Yet, it is in agreement with the observation from Figure 6.11 that the effective neutrinosphere moves outwards upon inclusion of the additional reactions. Hence, for the decoupling of $\bar{\nu}_e$ with $E_\nu \sim 3\,\mathrm{MeV}$ the inverse muon decay should be considered in neutrino transport as it has the largest opacity. Interestingly, the absorption on electrons is not

Figure 6.13.: Energy dependent opacity of $\bar{\nu}_e$ for extended reaction set, $150\,\mathrm{ms}$ post bounce for $\rho = 10^{12}\,\mathrm{g/cm^3}$. Rate is defined as inverse mean free path times c.

Figure 6.14.: Energy dependent opacity of $\bar{\nu}_e$ for extended reaction set, $150\,\mathrm{ms}$ post bounce for $\rho = 1.1 \times 10^{13}\,\mathrm{g/cm^3}$. Rate is defined as inverse mean free path times c.

important for any neutrino energy, even though it showed the largest average opacity of the new reactions in Figure 6.10. Also, in the standard scenario one finds that inverse bremsstrahlung and inelastic scattering on electrons are the most important reactions for the decoupling of low energy neutrinos. Eventually it is notable that at 150 ms post bounce there is no scattering atmosphere for $\bar{\nu}_e$ for any energy.

The same study as before is then repeated at 500 ms post bounce. One first looks at the spectrally averaged opacities including the new reactions in Figure 6.15. The position of the averaged neutrinosphere does not change noticeably as the new reactions are negligible at the corresponding density. Of the new reactions, the inverse mean free path for the absorption on electrons surpasses those of scattering on electrons and comes close to scattering on protons for very high densities. However, one should keep in mind that this was similar for the earlier time. There the reaction turned out to be irrelevant for the decoupling of all neutrino energies.

Figure 6.15.: Spectrally averaged inverse mean free path of $\bar{\nu}_e$ for extended reaction set, 500 ms post bounce. The black vertical line marks the density of the spectrally averaged effective neutrinosphere.

One therefore studies next the energy dependent effective neutrinosphere in Figure 6.16. As expected $R_{eff}(E_\nu)$ moves to higher densities for all neutrino energies. It is especially notable that now neutrinos up to energies $E_\nu \sim 10 \, \text{MeV}$ decouple inside $10^{13} \, \text{g/cm}^3$ where mean field effects are relevant. The position of R_{eff} changes with the extended reaction set for $E_\nu < 7 \, \text{MeV}$.

Figure 6.17 shows the energy dependent opacity for $\rho \sim 10^{12} \, \text{g/cm}^3$ where neutrinos with $E_\nu \sim 25 \, \text{MeV}$ decouple. One can see that for these neutrinos the situation is well described by the spectrally averaged properties. Scattering on neutrons has the largest opacity while absorption on protons has the largest inelastic rate. Also the new reactions are in fact negligible.

Next Figure 6.18 shows the energy dependent opacity for $\rho \sim 10^{13} \, \text{g/cm}^3$ after 500 ms where

Figure 6.16.: Energy dependent effective neutrinosphere $R_{eff}(E_\nu)$ for $\bar{\nu}_e$, 500 ms post bounce. The red curve shows R_{eff} for the standard reaction set, the black dashed curve is computed for the extended reaction set.
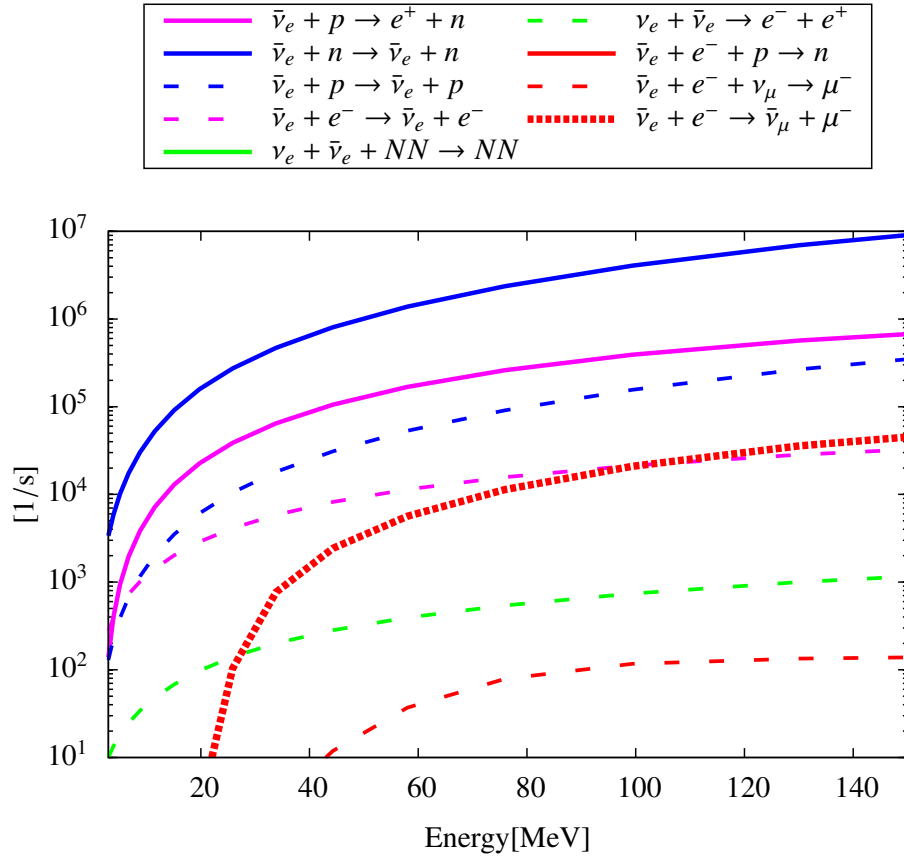
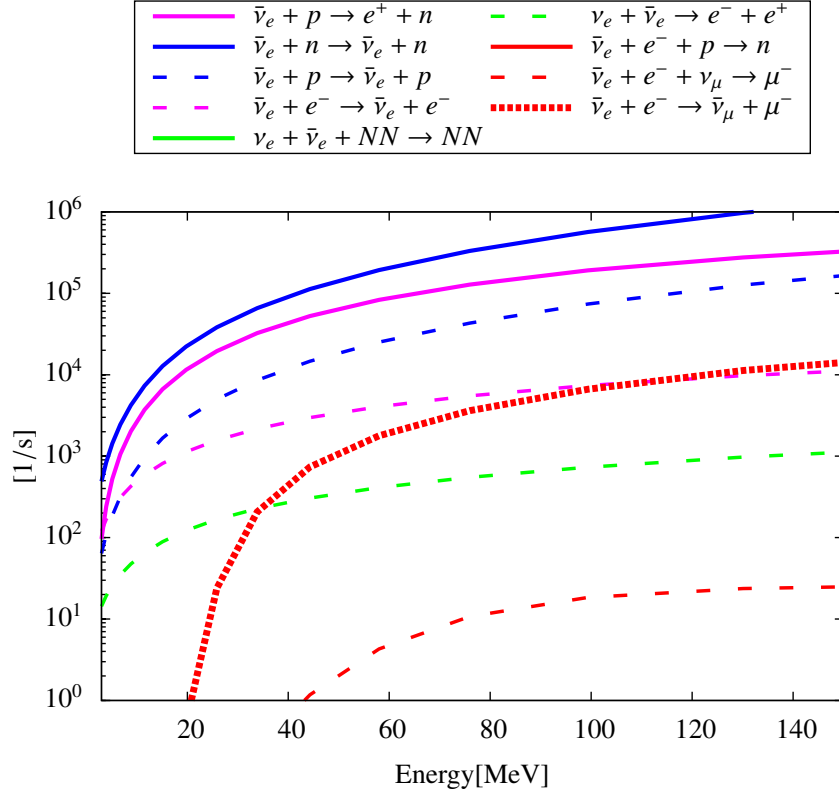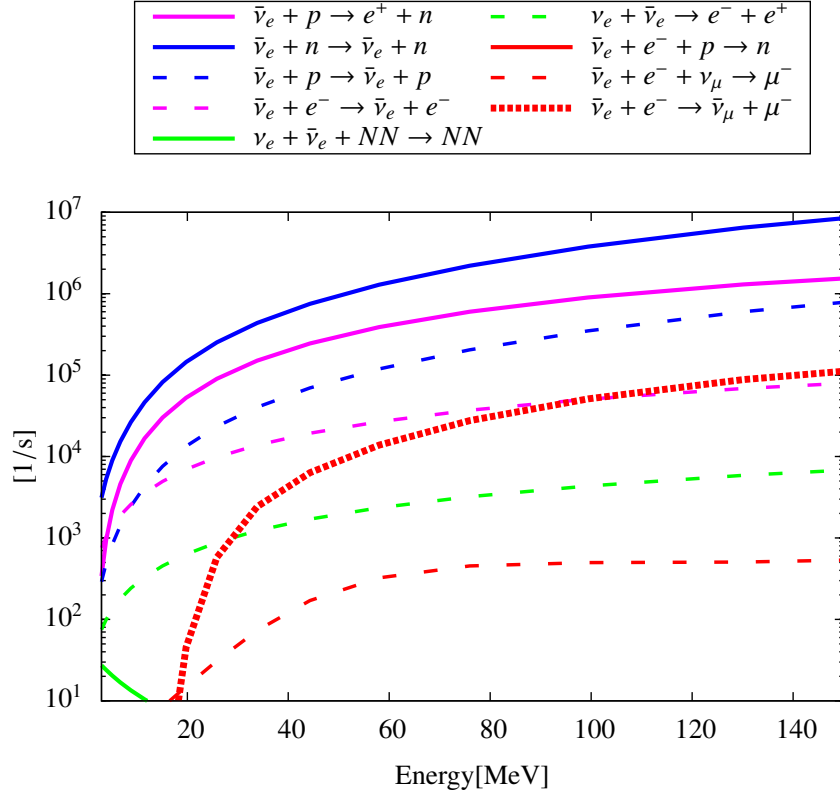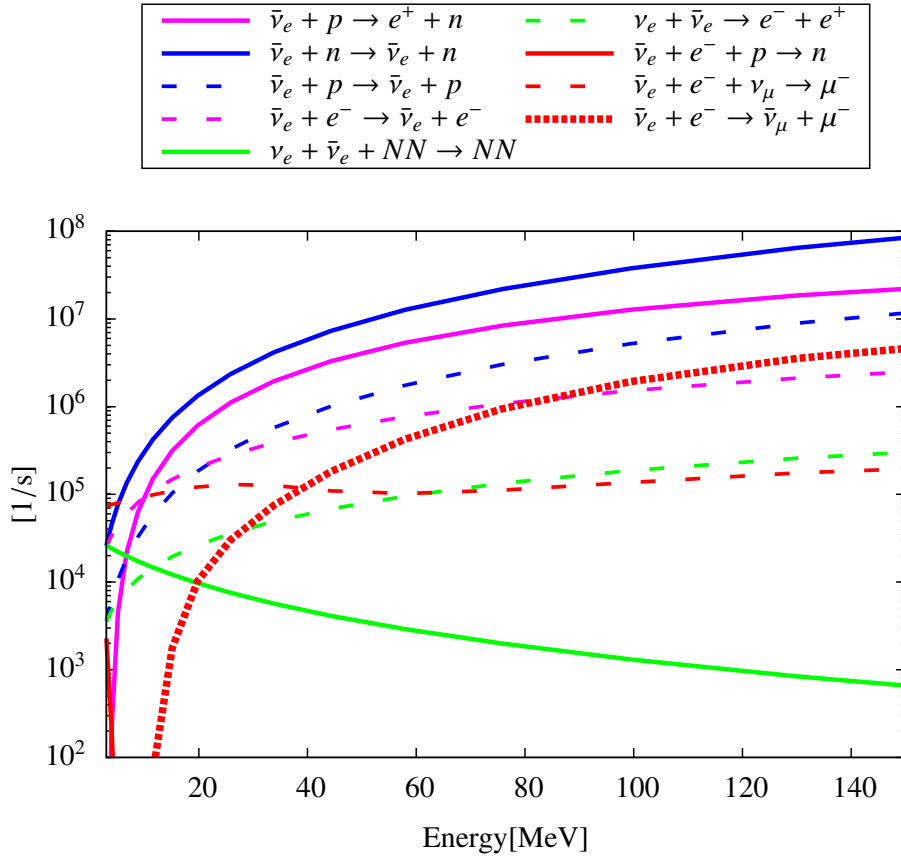Figure 6.17.: Energy dependent opacity of $\bar{\nu}_e$ for extended reaction set, 500 ms post bounce for $\rho = 1.1 \times 10^{12}$ g/cm^3. Rate is defined as inverse mean free path times c.

Figure 6.18.: Energy dependent opacity of $\bar{\nu}_e$ for extended reaction set, 500 ms post bounce for $\rho = 1.1 \times 10^{13} \, \text{g/cm}^3$. Rate is defined as inverse mean free path times c.

Figure 6.19.: Energy dependent opacity of $\bar{\nu}_e$ for extended reaction set, 500 ms post bounce for $\rho = 2.2 \times 10^{13} \, \text{g/cm}^3$. Rate is defined as inverse mean free path times c.

neutrinos with $E_\nu \sim 10\,\text{MeV}$ decouple. Scattering on neutrons is again the largest opacity, resulting in a scattering atmosphere above R_{eff}. For the inelastic reactions one finds that scattering on electrons has almost the same rate as absorption on protons. Still, the new reactions are not contributing significantly.

Eventually the situation at $\rho \sim 2 \times 10^{13}\,\text{g/cm}^3$ is studied in Figure 6.19. Here neutrinos with energies $E_\nu < 7\,\text{MeV}$ decouple from matter. The elastic scattering on neutrons is still the largest opacity source for $E_\nu \sim 7\,\text{MeV}$. However for the equilibration of low energy neutrinos the most important reactions are scattering on electrons, inverse bremsstrahlung, and inverse muon decay. For neutrino energies below $3\,\text{MeV}$ the rate of inverse neutron decay rises sharply and becomes the largest opacity.

It can be concluded that at later times $500\,\text{ms}$ after bounce inverse muon decay is an important opacity source for electron antineutrinos with energies less than $7\,\text{MeV}$. Also, for even lower energies less then $3\,\text{MeV}$ inverse neutron decay becomes the dominant reaction. Both these findings are not affected by the elastic treatment of scattering on nucleons but should also hold in a more general approach. Also it should be noted that again spectrally averaged transport properties are not suited to describe the transport of relatively low energetic neutrinos. In the standard scenario one finds again that inverse bremsstrahlung and scattering on electrons are the most important reactions for $\bar{\nu}_e$ with $E_\nu < 7\,\text{MeV}$.
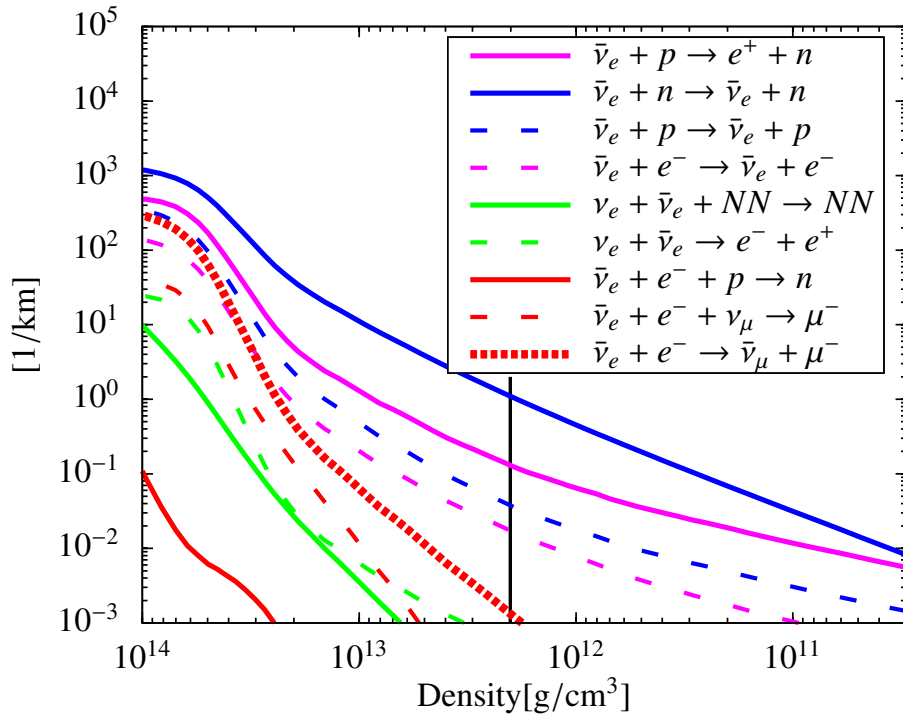

Figure 6.20.: Spectrally averaged inverse mean free path of $\bar{\nu}_e$ for extended reaction set, $2\,\text{s}$ post bounce. The black vertical line marks the density of the spectrally averaged effective neutrinosphere.

To conclude the study on electron antineutrinos the influence of the extended reaction set on energy dependent transport properties is performed for even later times, $2\,\text{s}$ after bounce. First the spectrally averaged opacities are shown in Figure 6.20. Even though the effective neutrinosphere is now located at $\rho > 10^{13}\,\text{g/cm}^3$ where strong interaction potentials are relevant,

the new reactions seem to be irrelevant in the decoupling region. Inverse muon decay has eventually one of the largest spectrally averaged inverse mean free paths of all inelastic reactions, but only for densities higher than $5 \times 10^{13}\,\mathrm{g/cm^3}$.
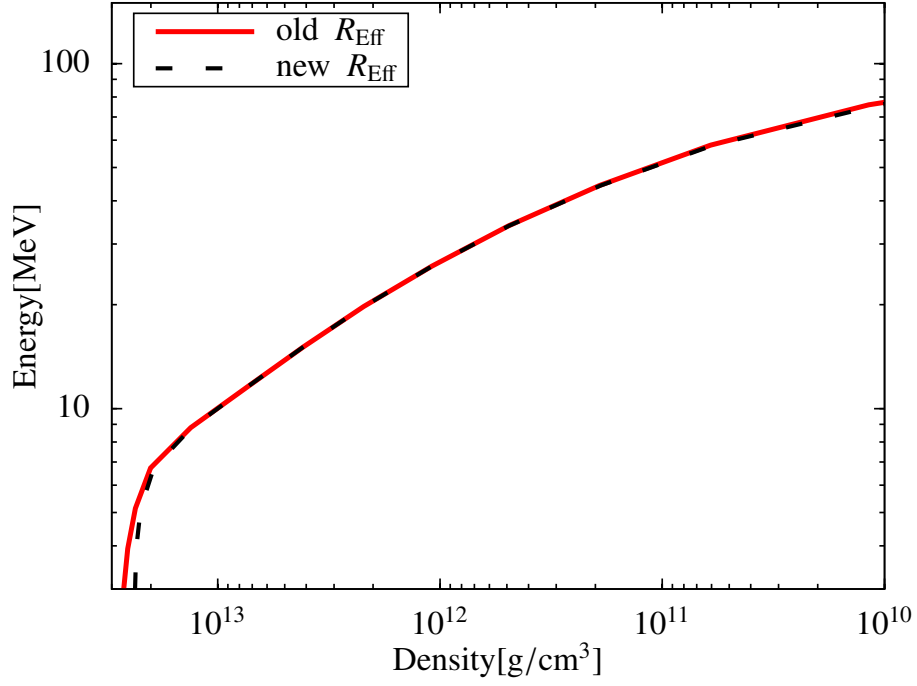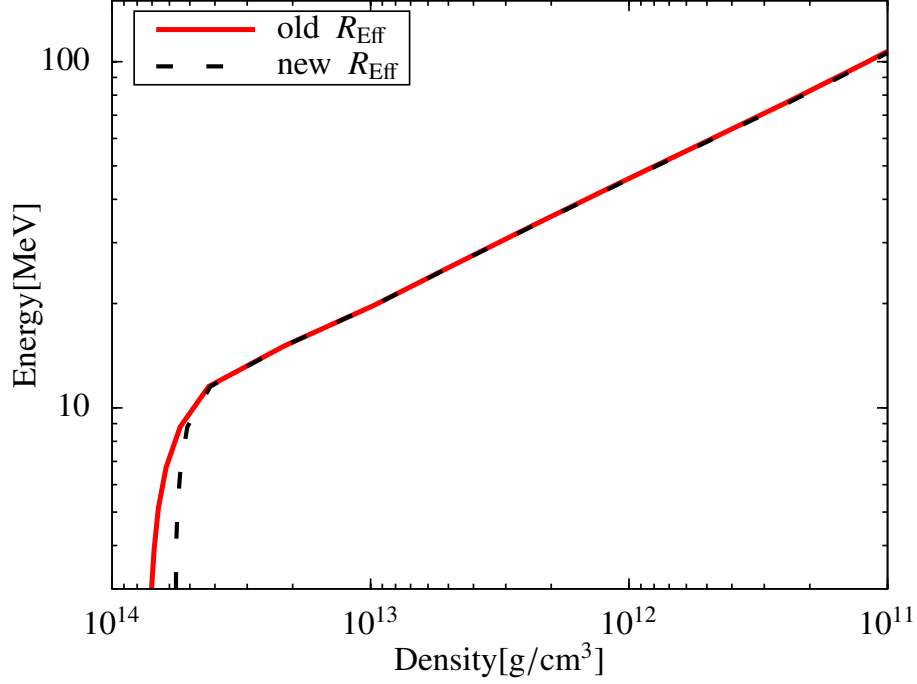

Figure 6.21.: Energy dependent effective neutrinosphere $R_{eff}(E_\nu)$ for $\bar\nu_e$, 2 s post bounce. The red curve shows R_{eff} for the standard reaction set, the black dashed curve is computed for the extended reaction set.

Looking at the energy dependent effective neutrinosphere in Figure 6.21 one finds that there is a difference between the standard and the extended reaction set. For neutrino energies around $E_\nu \sim 10\,\mathrm{MeV}$ and less, R_{eff} is clearly shifted to lower densities. As $R_{eff}(10\,\mathrm{MeV})$ at $5 \times 10^{13}\,\mathrm{g/cm^3}$ this seems plausible also from the spectrally averaged opacities.

In Figure 6.22 the energy dependent opacities are shown for $\rho \sim 10^{13}\,\mathrm{g/cm^3}$. This is were neutrinos with an energy of 20 MeV should decouple at 2 s after bounce. It can be seen that the rate for scattering on neutrons is an order of magnitude larger than any other reaction for this neutrino energy. This will probably result in a significant scattering atmosphere above R_{eff}. The largest inelastic contribution is absorption on protons which is about 3 times as large as scattering on electrons. The new reactions are not relevant, indeed.

This picture changes significantly for neutrinos with $E_\nu \sim 10\,\mathrm{MeV}$ and less. They decouple above $5 \times 10^{13}\,\mathrm{g/cm^3}$ and the corresponding opacities are depicted in Figure 6.23. The largest inelastic opacities are those of inverse neutron decay and inverse bremsstrahlung. The lower the neutrino energy, the larger is especially the rate for inverse neutron decay. For neutrino energies of 5 MeV it becomes the reaction with the largest rate. Consequently, the phenomenon of the scattering atmosphere is less relevant if not completely absent for low energy $\bar\nu_e$. In contrast to the situation for earlier times, the muonic reactions are not contributing much for any neutrino energy at 2 s post bounce.
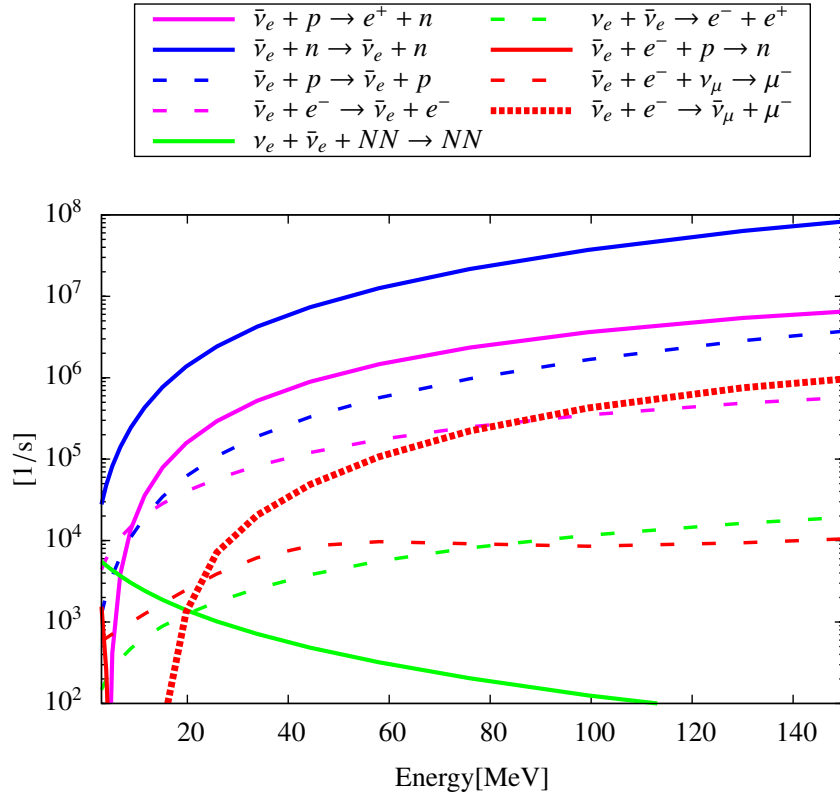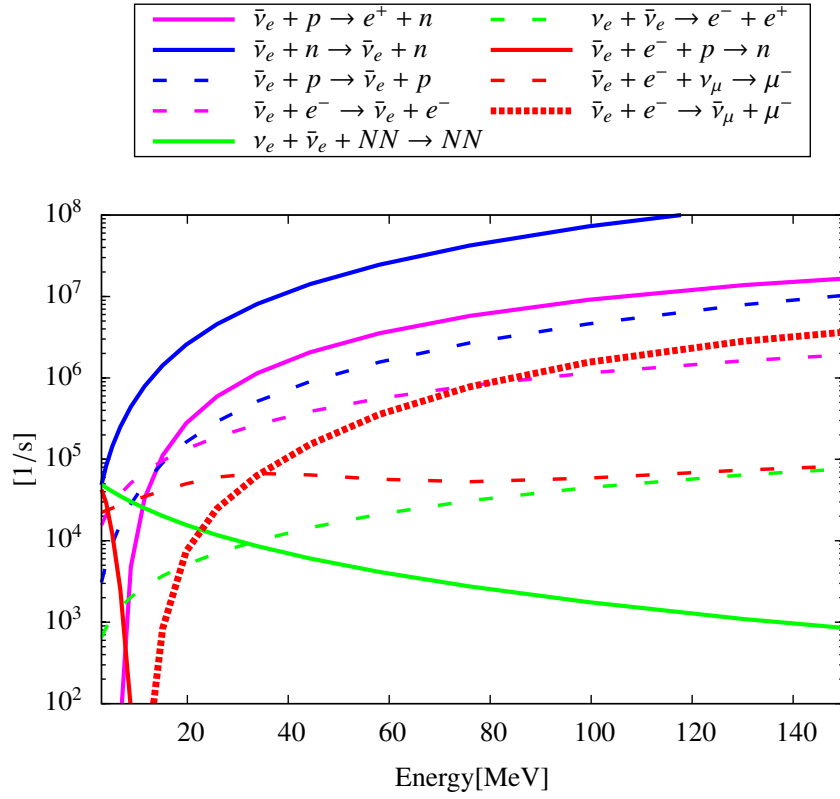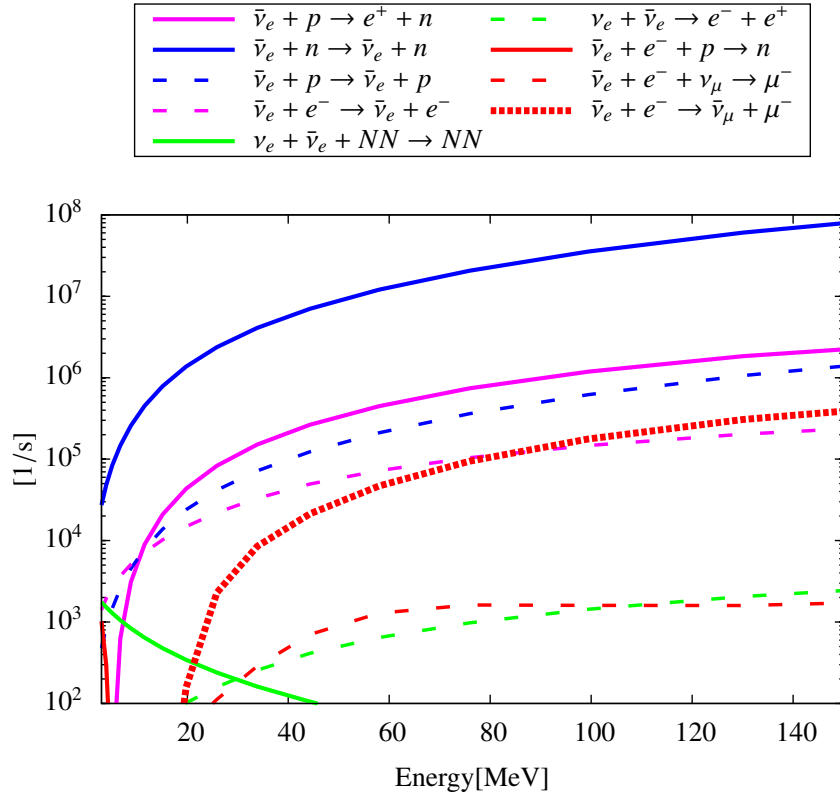
Figure 6.22.: Energy dependent opacity of $\bar{\nu}_e$ for extended reaction set, $2\,\mathrm{s}$ post bounce for $\rho = 1.2 \times 10^{13}\,\mathrm{g/cm^3}$. Rate is defined as inverse mean free path times c.

Figure 6.23.: Energy dependent opacity of $\bar{\nu}_e$ for extended reaction set, $2\,\mathrm{s}$ post bounce for $\rho = 5.4 \times 10^{13}\,\mathrm{g/cm^3}$. Rate is defined as inverse mean free path times c.

6.5.3. Summary

For the standard reaction set it is found that for all times up to several seconds post bounce scattering on neutrons and absorption on protons are the reactions with the largest inverse mean free path for electron antineutrinos. As time progresses, the opacity for scattering on neutrons grows relative to the one for absorption on protons because of the ongoing deleptonization of the PNS. As a result, a scattering atmosphere emerges outside of R_{eff}. These findings hold for all neutrino energies except for the lowest one. Absorption on protons decreases strongly for neutrino energies that are close to or less than the energy difference between protons on neutrons. R_{eff} moves to higher densities over time for all energies, due to the contraction and cooling of the PNS. Consequently, the neutrino energies for which absorption on neutrons is suppressed rise over time, as the strong interaction potentials add to the energy difference between the nucleons. To be precise, this study finds the transition to be at roughly $3\,\mathrm{MeV}$ after $150\,\mathrm{ms}$, growing to $7\,\mathrm{MeV}$ after $500\,\mathrm{ms}$, and reaching $10\,\mathrm{MeV}$ at $2\,\mathrm{sc}$. Below these threshold energies, inelastic scattering on electrons and inverse bremsstrahlung are the major energy equilibrating opacity sources. It is further noteworthy that electron-positron pair creation has no significant inverse mean free path for any neutrino energy at any time.

The additional reactions of the extended reaction set are likewise only important for the low neutrino energies. Until $500\,\mathrm{ms}$ post bounce inverse muon decay is a significant contribution to the inelastic opacity of these neutrinos. As it is strongly temperature dependent it vanishes later. In contrast, inverse neutron decay does not become important even for lowest energies before $500\,\mathrm{ms}$. However, after $2\,\mathrm{s}$ it is the most important reaction for neutrino energies below $10\,\mathrm{MeV}$. It can be expected that for later times, when R_{eff} moves to even higher densities, inverse neutron decay might become the most important reaction of $\bar{\nu}_e$ for all relevant neutrino energies.

The effect of the increased opacity for low energy $\bar{\nu}_e$ is difficult to estimate in post processing. On one side it could be argued that less low energy neutrinos emitted should result in relatively more high energy neutrinos, increasing the average energy of electron antineutrinos $\langle \epsilon_{\bar{\nu}_e} \rangle$. On the other hand experience suggests that every increase in opacity leads to a decrease in average energies. Hence the outcome can only be evaluated by dynamic simulations.

6.6. Transport of Muon Neutrinos

For muon neutrinos the standard reaction set will not be discussed separately. Instead it will be discussed along with the extended reaction set by spectrally averaged as well as energy dependent opacities and effective neutrinospheres. The matter profiles are the same as in the previous section for $\bar{\nu}_e$. Again the transport problem is investigated for the same three different times, i.e. $150\,\mathrm{ms}$, $500\,\mathrm{ms}$, and $2\,\mathrm{s}$ post bounce. To begin with, Figure 6.24 shows the spectrally averaged opacities and the corresponding effective neutrinosphere at $150\,\mathrm{ms}$ post bounce. For the standard reaction set, scattering on neutrons clearly shows the largest inverse mean free path of all reactions. Scattering on electrons is the major inelastic reaction for all densities, yet its opacity is always more than an order of magnitude below scattering on neutrons. Therefore

a significant scattering atmosphere emerges. The spectrally averaged effective neutrinosphere lies for the standard set at $\langle R_{eff} \rangle = 1.04 \times 10^{12} \, \mathrm{g/cm^3}$, while the transport sphere is located further outside at $\langle R_{tr} \rangle = 1.21 \times 10^{11} \, \mathrm{g/cm^3}$.
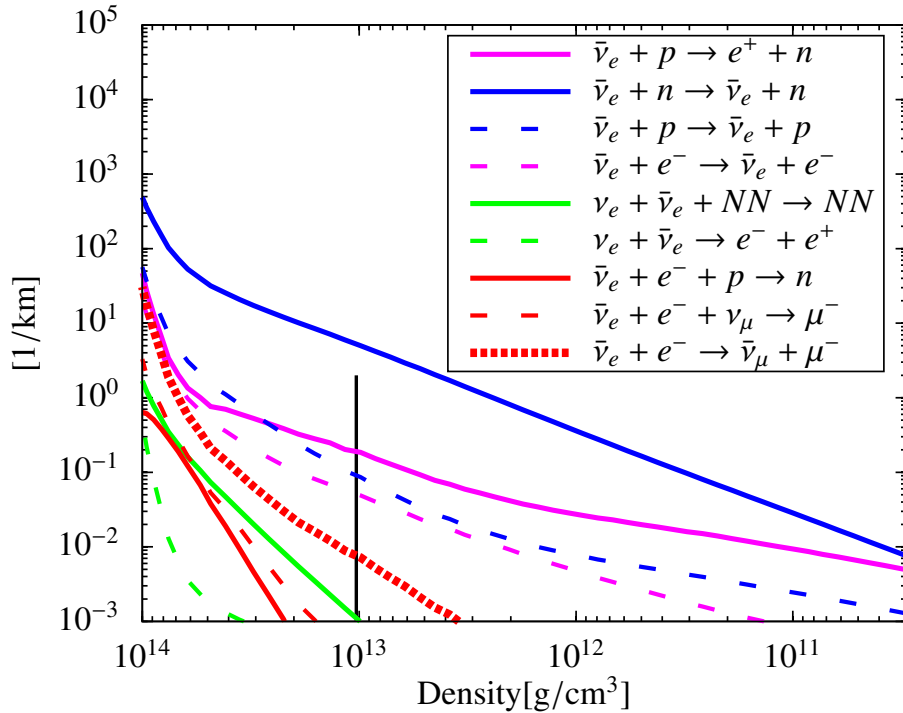

Figure 6.24.: Spectrally averaged inverse mean free path of ν_μ for extended reaction set, 150 ms post bounce. The black vertical line marks the density of the spectrally averaged effective neutrinosphere.

Further, the pair processes seem to be irrelevant, as they are more than an order of magnitude smaller than scattering on electrons. The inclusion of the additional reactions leads to an outward shift of the effective neutrinosphere, $\langle R_{eff} \rangle = 9.5 \times 10^{11} \, \mathrm{g/cm^3}$. One notices that the absorption on electrons $\nu_\mu + e^- \rightarrow \nu_e + \mu^-$ shows the second largest inelastic opacity at R_{eff} behind scattering on electrons, followed by the absorption on neutrons $\nu_\mu + n \rightarrow p + \mu^-$. Also, both of these reactions eventually grow above scattering on electrons further inside, with absorption on neutrons becoming the reaction with the largest inverse mean free path of all reactions for densities higher than $10^{13} \, \mathrm{g/cm^3}$.

Figure 6.25 shows the energy dependent neutrinosphere, both for the standard and extended reaction set. One can see that the additional reactions shift $R_{eff}(E_\nu)$ to lower densities for $E_\nu \lesssim 10 \, \mathrm{MeV}$ and $E_\nu \gtrsim 25 \, \mathrm{MeV}$. Especially for high neutrino energies this shift grows and becomes eventually very large.

Figure 6.26 depicts the energy dependent opacities a $\rho \sim 3 \times 10^{11} \, \mathrm{g/cm^3}$ where neutrinos with $E_\nu \lesssim 50 \, \mathrm{MeV}$ decouple from matter. For these neutrinos one finds that the inelastic opacities due to scattering on electrons and absorption on electrons are almost equally large. This explains the shift observed in Figure 6.25. One can also see that the absorption on neutrons is probably only relevant for very large ν_μ energies above 90 MeV. Beyond that one finds that scatterings on neutrons and even on protons have a much larger rate than any inelastic reaction, both in the standard and extended scenario. Pair process or the inverse muon decay have no significant impact on the transport of high energy neutrinos.

Figure 6.25.: Energy dependent effective neutrinosphere $R_{eff}(E_\nu)$ for ν_μ, 150 ms post bounce. The red curve shows R_{eff} for the standard reaction set, the black dashed curve is computed for the extended reaction set.

Figure 6.26.: Energy dependent opacity of ν_μ for extended reaction set, 150 ms post bounce for $\rho = 3.3 \times 10^{11}\,\mathrm{g/cm^3}$. Rate is defined as inverse mean free path times c.
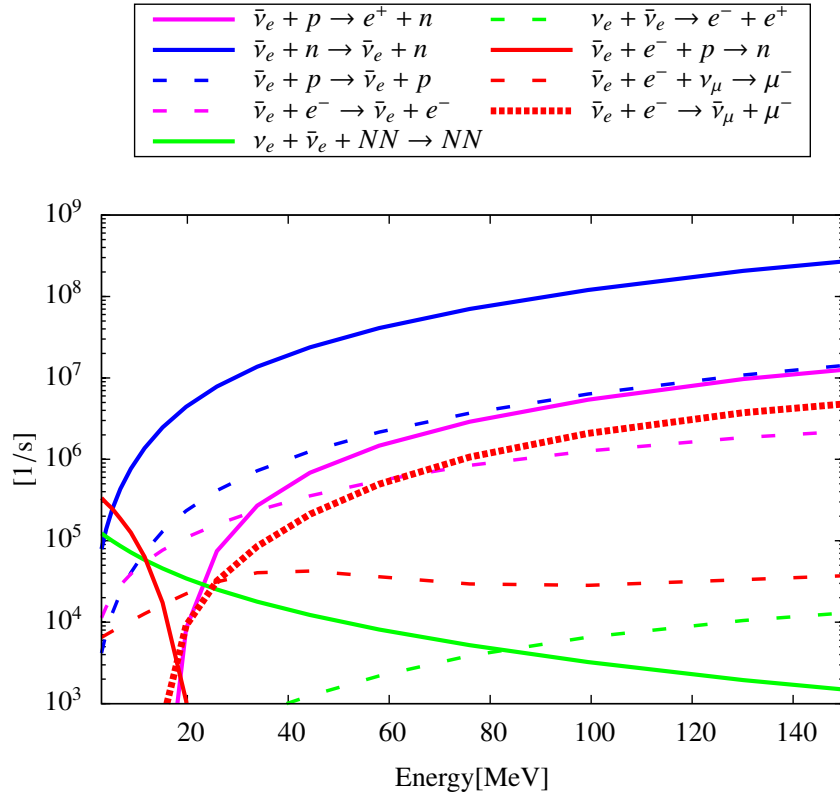
Figure 6.27.: Energy dependent opacity of ν_μ for extended reaction set, $150\,\mathrm{ms}$ post bounce for $\rho = 7.6 \times 10^{12}\,\mathrm{g/cm^3}$. Rate is defined as inverse mean free path times c.

Figure 6.27 shows the energy dependent opacities at $\rho \sim 7.6 \times 10^{12}\,\mathrm{g/cm^3}$ where ν_μ with $E_\nu \lesssim 8\,\mathrm{MeV}$ decouple. In the standard scenario, scattering on electrons is still the dominant inelastic reaction with elastic scattering on neutrons being significantly more frequent. However, in the extended reaction set inverse muon decay is equally as important as scattering on electrons for equilibrating ν_μ. By studying opacities for $\rho \sim 10^{13}\,\mathrm{g/cm^3}$ where neutrinos with energy less than $5\,\mathrm{MeV}$ decouple, one even finds that inverse muon decay has the largest opacity for all reactions. It becomes even larger than scattering on neutrons. In the standard scenario inverse bremsstrahlung becomes similar frequent as scattering on electrons for these lowest neutrino energies. Summing it up, at $150\,\mathrm{ms}$ after core bounce, scattering on electrons is the largest inelastic opacity source for almost all energies. Only for neutrino energies below $5\,\mathrm{MeV}$ is inverse bremsstrahlung a relevant reaction, too. Elastic scattering on neutrons shows always a much larger opacity, leading to a wide scattering atmosphere above R_{eff}. In the extended scenario, one finds that all new reactions are important at some neutrino energy. Absorption of ν_μ is important only for neutrinos with $E_\nu > 90\,\mathrm{MeV}$. Below this limit and down to $E_\nu \sim 40\,\mathrm{MeV}$ absorption on electrons is as important as scattering on electrons. Eventually for energies less than $10\,\mathrm{MeV}$ inverse muon decay has a similar rate to scattering on electrons, even becoming the largest rate for $E_\nu < 5\,\mathrm{MeV}$. Therefore the scattering atmosphere vanishes for these ν_μ.

Next the spectrally averaged transport properties are studied at $500\,\mathrm{ms}$ post bounce in Figure 6.28. For the standard scenario the picture looks similar to the earlier time. Scattering on neutrons has by far the largest inverse mean free path while scattering on electrons is the most important inelastic reaction for all densities. The effective neutrinosphere is now at
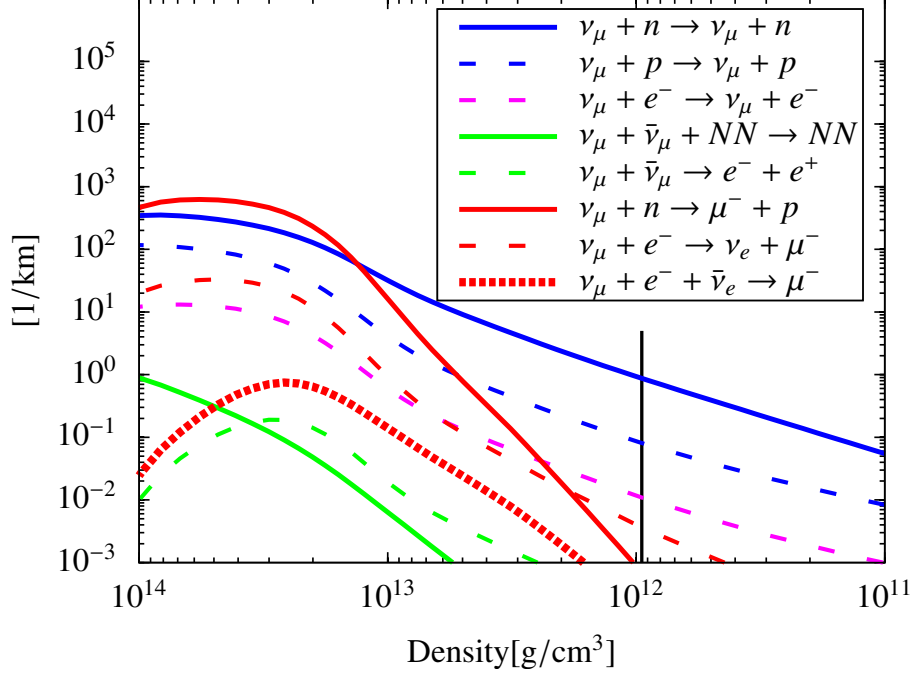
Figure 6.28.: Spectrally averaged inverse mean free path of ν_μ for extended reaction set, $500\,\mathrm{ms}$ post bounce. The black vertical line marks the density of the spectrally averaged effective neutrinosphere.

higher densities due to ongoing contraction, cooling, and deleptonization of the PNS, $\langle R_{eff} \rangle = 6.0 \times 10^{12}\,\mathrm{g/cm^3}$. In the extended scenario, the neutrinosphere moves outwards to $\langle R_{eff} \rangle = 5.2 \times 10^{12}\,\mathrm{g/cm^3}$. Absorption on neutrons and on electrons are comparable to scattering on electrons in the decoupling region and become larger than the latter deeper inside. Also, absorption on neutrons shows the largest opacity of all reactions for $\rho > 3 \times 10^{13}\,\mathrm{g/cm^3}$.

Looking then at the energy dependent effective neutrinosphere in Figure 6.29 the situation is similar to the earlier time. The neutrinospheres have overall moved to higher densities. The extended reaction set causes an outward shift of of R_{eff} for energies less than $\sim 10\,\mathrm{MeV}$ and more than $\sim 30\,\mathrm{MeV}$. This shift becomes very large for the most energetic neutrinos with $E_\nu > 70 - 80\,\mathrm{MeV}$.

Figure 6.30 shows the energy dependent opacities at $\rho = 3.4 \times 10^{12}\,\mathrm{g/cm^3}$ where neutrinos with $E_\nu \lesssim 40\,\mathrm{MeV}$ decouple. In the standard scenario the situation is as before. Scattering on electrons is the only relevant inelastic reaction while the rate for scattering on neutrons is two orders of magnitude larger. For the extended reaction set one finds that the opacity for absorption on electrons is almost as large as for scattering on electrons. For higher neutrino energies, absorption on electrons even becomes the major inelastic reaction, until absorption on neutrons dominates for energies above $\sim 95\,\mathrm{MeV}$.

Figure 6.31 depicts then the energy dependent opacity at $\rho \sim 2 \times 10^{13}\,\mathrm{g/cm^3}$ where neutrinos with $E_\nu \sim 10\,\mathrm{MeV}$ decouple. In the standard scenario the inelastic opacity comes mainly from inverse bremsstrahlung and scattering on electrons. Elastic scattering on neutrons has the overall largest rate. When included, inverse muon decay is equally important as the other main inelastic reactions, which results in the observed shift of R_{eff}. For neutrino energies of $5\,\mathrm{MeV}$
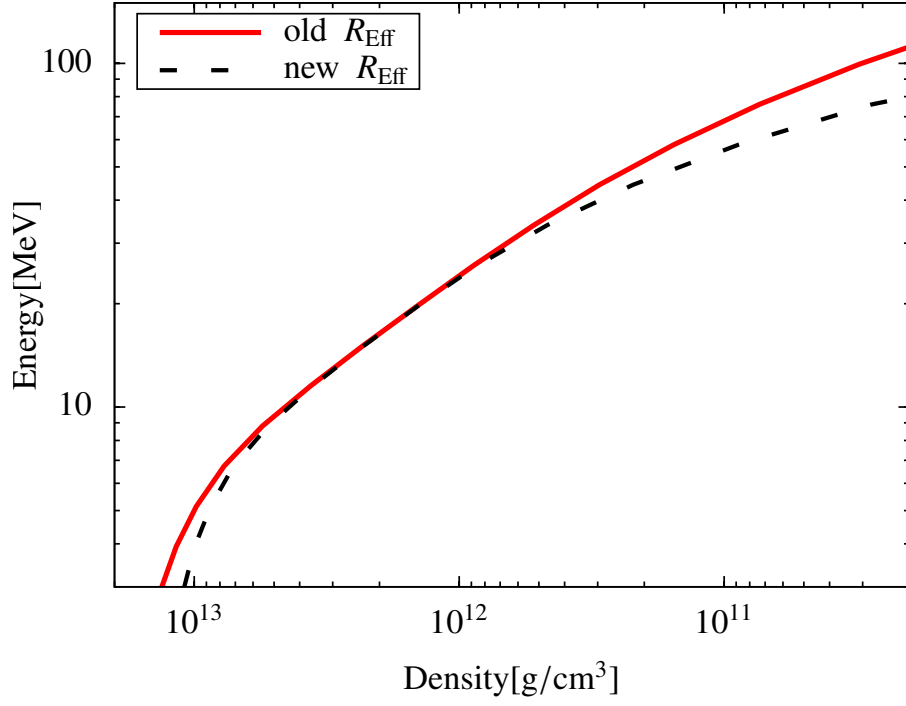
Figure 6.29.: Energy dependent effective neutrinosphere $R_{eff}(E_\nu)$ for ν_μ, $500\,\text{ms}$ post bounce. The red curve shows R_{eff} for the standard reaction set, the black dashed curve is computed for the extended reaction set.
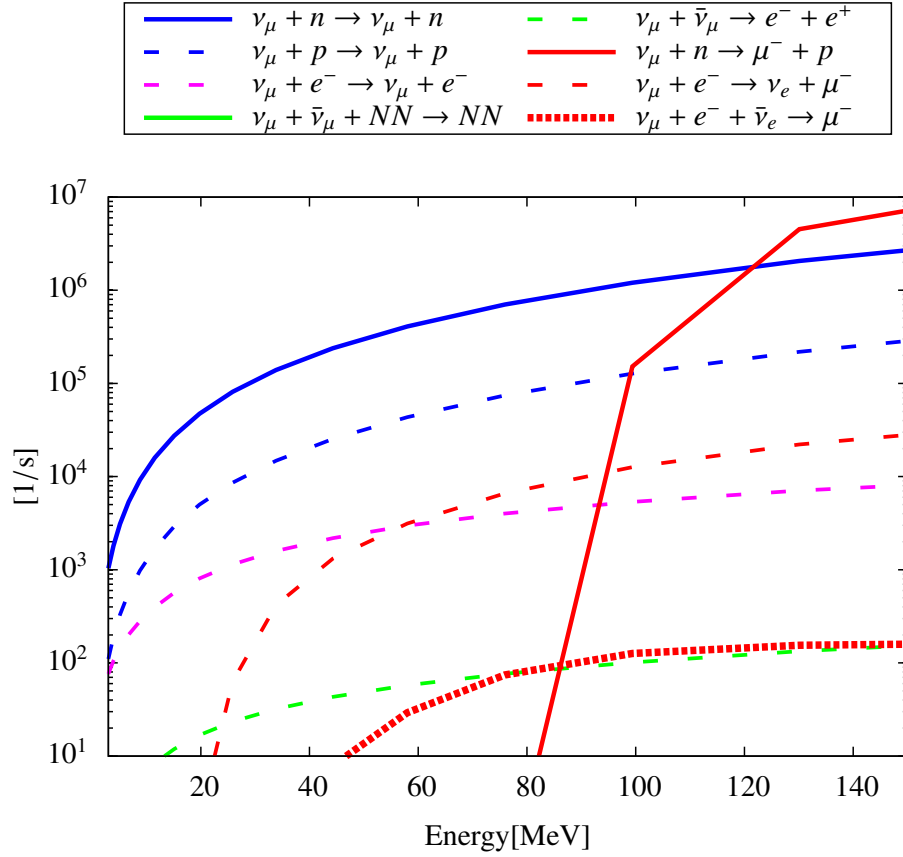

Figure 6.30.: Energy dependent opacity of ν_μ for extended reaction set, $500\,\text{ms}$ post bounce for $\rho = 3.4 \times 10^{12}\,\text{g/cm}^3$. Rate is defined as inverse mean free path times c.
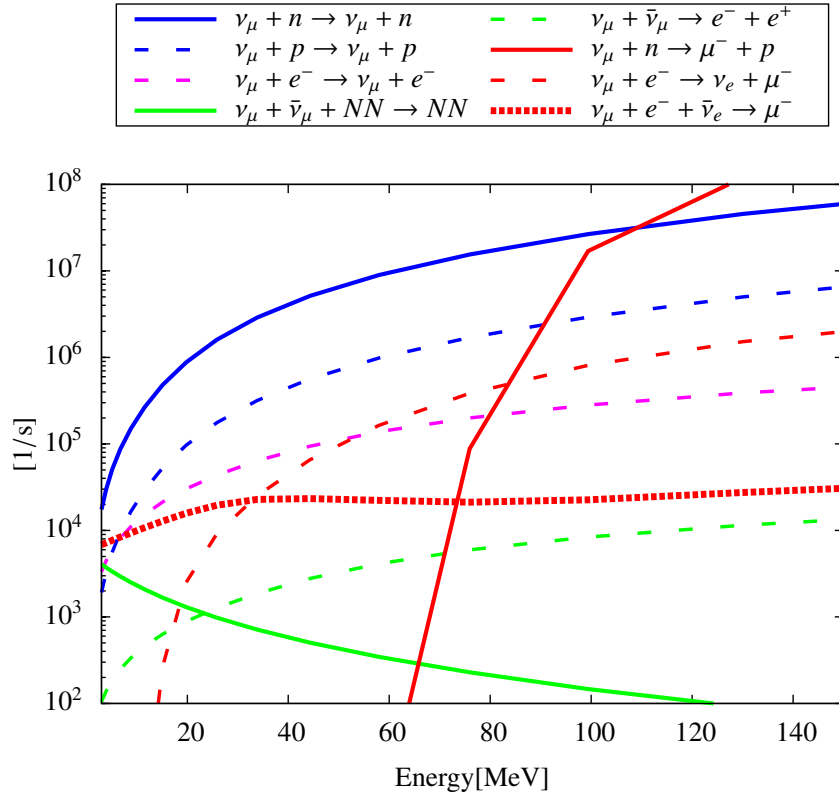
Figure 6.31.: Energy dependent opacity of ν_μ for extended reaction set, $500\,\mathrm{ms}$ post bounce for $\rho = 2.2 \times 10^{13}\,\mathrm{g/cm^3}$. Rate is defined as inverse mean free path times c.

and less, inverse bremsstrahlung is the dominant inelastic reaction in the standard set and the scattering atmosphere vanishes. The opacity for inverse muon decay surpasses even the one for bremsstrahlung for these low energies.

Summing up the findings, the transport situation after $500\,\mathrm{ms}$ is almost the same as the one after $150\,\mathrm{ms}$ except that the decoupling in general takes place at higher densities. Inelastic scattering in the standard scenario is dominated by scattering on electrons down to $E_\nu = 10\,\mathrm{MeV}$, below this point inverse bremsstrahlung takes over. Elastic scattering on neutrons has a much larger opacity than the inelastic reactions down to $E_\nu = 5\,\mathrm{MeV}$ resulting in a scattering atmosphere above R_{eff}. For the muonic reactions, absorption on neutrons has the largest inelastic opacity for $E_\nu > 95\,\mathrm{MeV}$, absorption on electrons is an important opacity source down to $E_\nu = 40\,\mathrm{MeV}$, and inverse muon decay becomes the most important inelastic reaction below $E_\nu = 10\,\mathrm{MeV}$.

To conclude the study on the transport of ν_μ the situation at $2\,\mathrm{s}$ after bounce is looked at. The spectrally averaged opacities and effective neutrinosphere are plotted in Figure 6.32. The standard scenario is straightforward again. Scattering on neutrons has by far the largest inverse mean free path of all reactions. Scattering on electrons is the most important inelastic reaction. Inverse bremsstrahlung comes close for very high densities only. The averaged effective neutrinosphere lies for the standard reactions at $\langle R_{eff} \rangle = 3.0 \times 10^{13}\,\mathrm{g/cm^3}$. A scattering atmosphere reaches up to $\langle R_{tr} \rangle = 2.4 \times 10^{12}\,\mathrm{g/cm^3}$. When including the additional reactions, the effective neutrinosphere moves outwards to $\langle R_{eff} \rangle = 2.3 \times 10^{13}\,\mathrm{g/cm^3}$. Opacity for absorption on neutrons is a little larger than scattering on electrons at $\langle R_{eff} \rangle$, while absorption on electrons
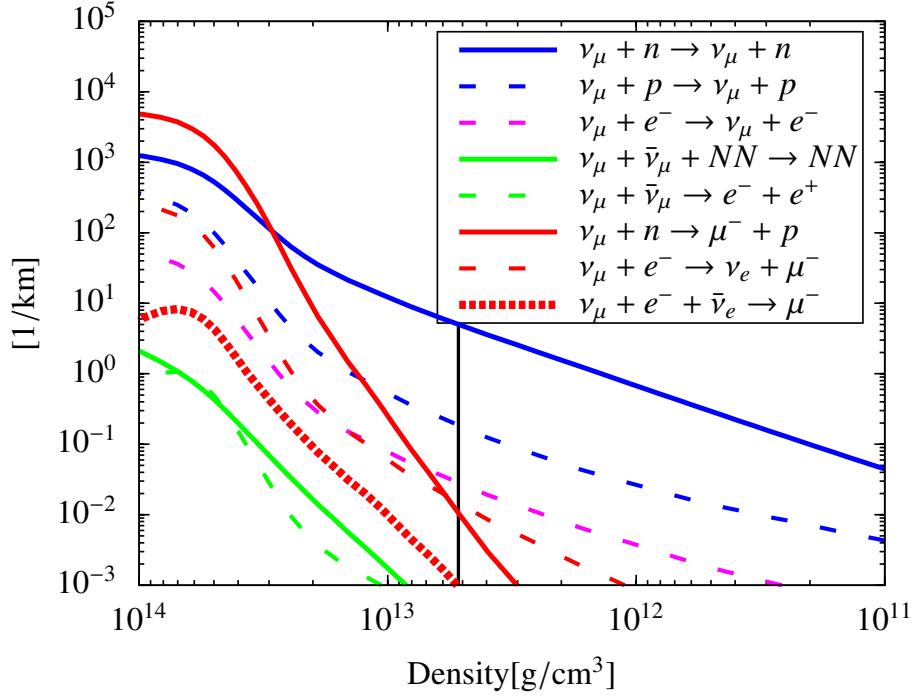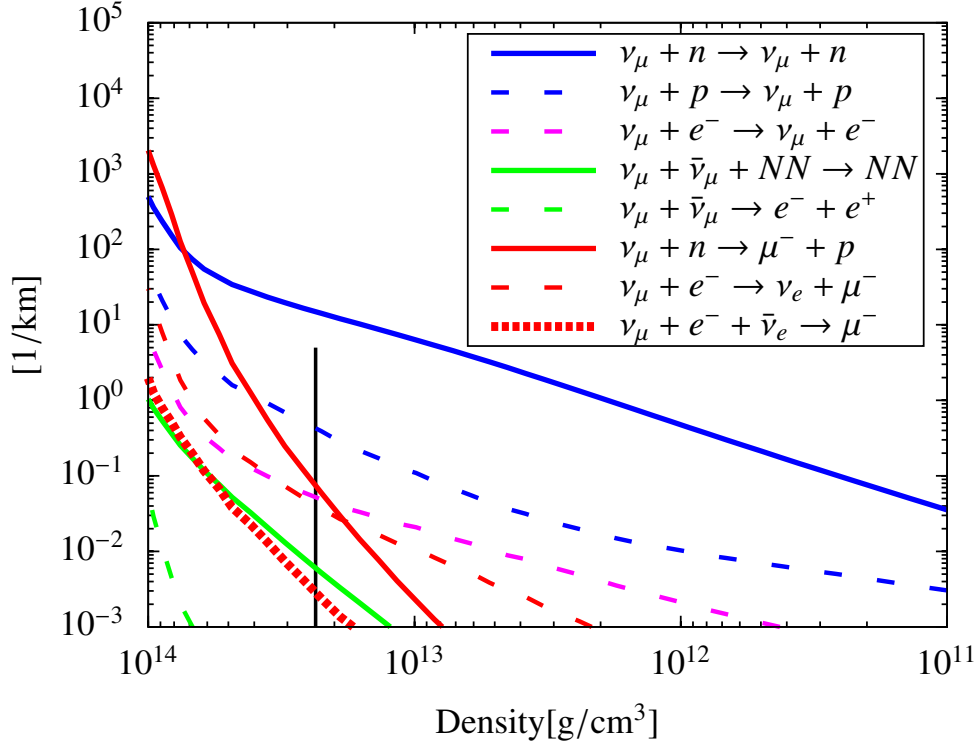
Figure 6.32.: Spectrally averaged inverse mean free path of ν_μ for extended reaction set, 2 s post bounce. The black vertical line marks the density of the spectrally averaged effective neutrinosphere.
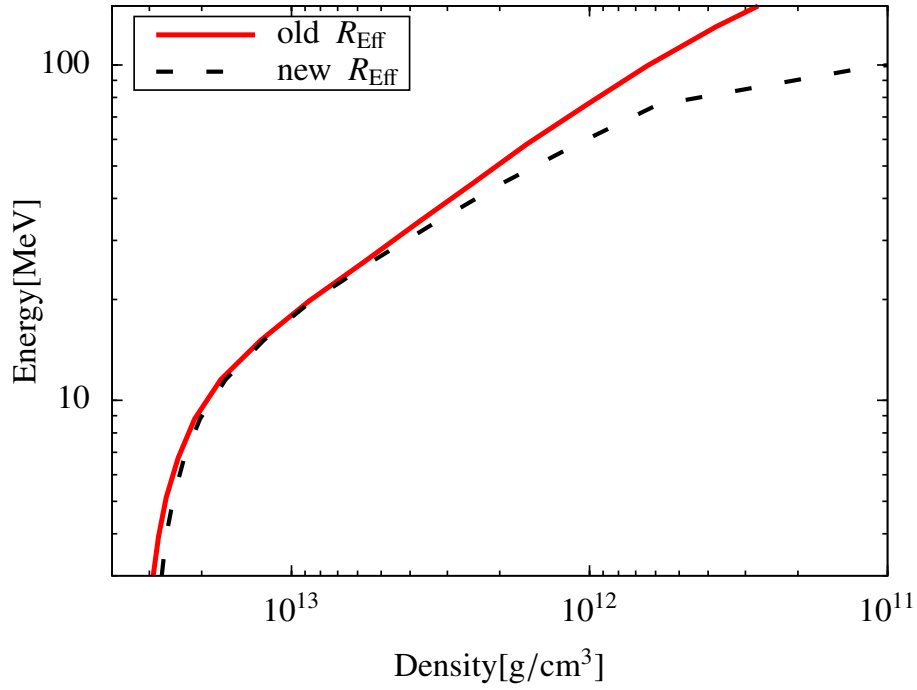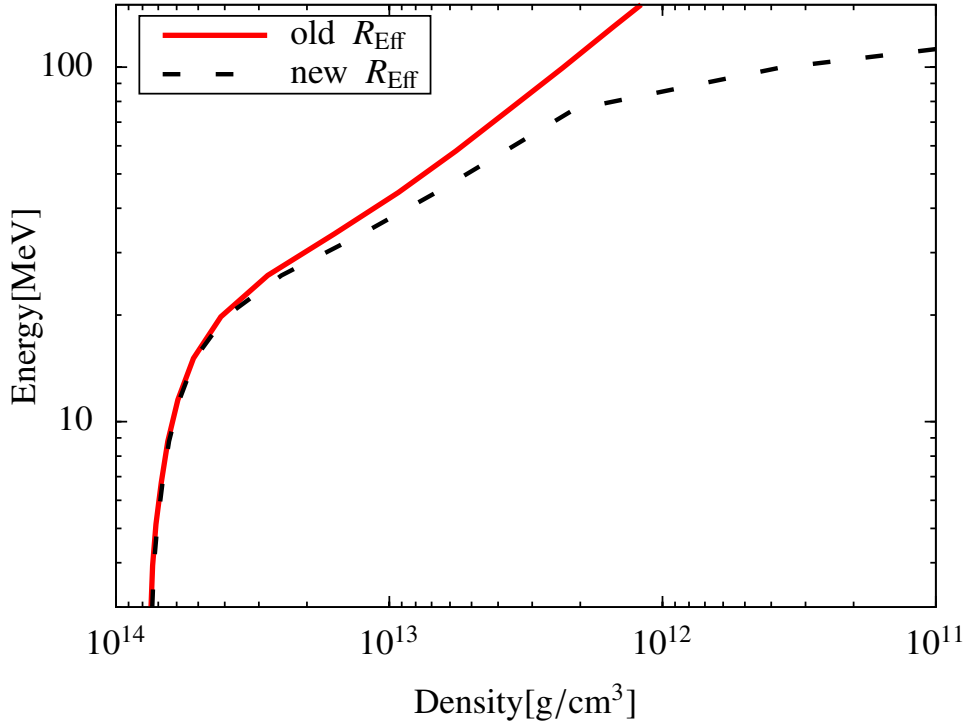

Figure 6.33.: Energy dependent effective neutrinosphere $R_{eff}(E_\nu)$ for ν_μ, 2 s post bounce. The red curve shows R_{eff} for the standard reaction set, the black dashed curve is computed for the extended reaction set.

is almost equal to the latter.

Figure 6.33 shows the energy dependent effective neutrinosphere $2\,$s post bounce. For the extended reaction set, $R_{eff}(E_\nu)$ is shifted to lower densities for $E_\nu > 25\,$MeV. However, for low energy neutrinos there is no change between the standard and the extended scenario. This is a notable difference to earlier times.

To investigate this, first the energy dependent opacities are studied for $\rho \sim 3 \times 10^{13}\,$g/cm^3 where neutrinos with $E_\nu =< 30\,$MeV decouple from matter. This is shown in Figure 6.34. Like at earlier times it is found that in the standard case the scattering on electrons is the single most important inelastic reaction for these neutrinos while scattering on neutrons has the largest overall opacity.
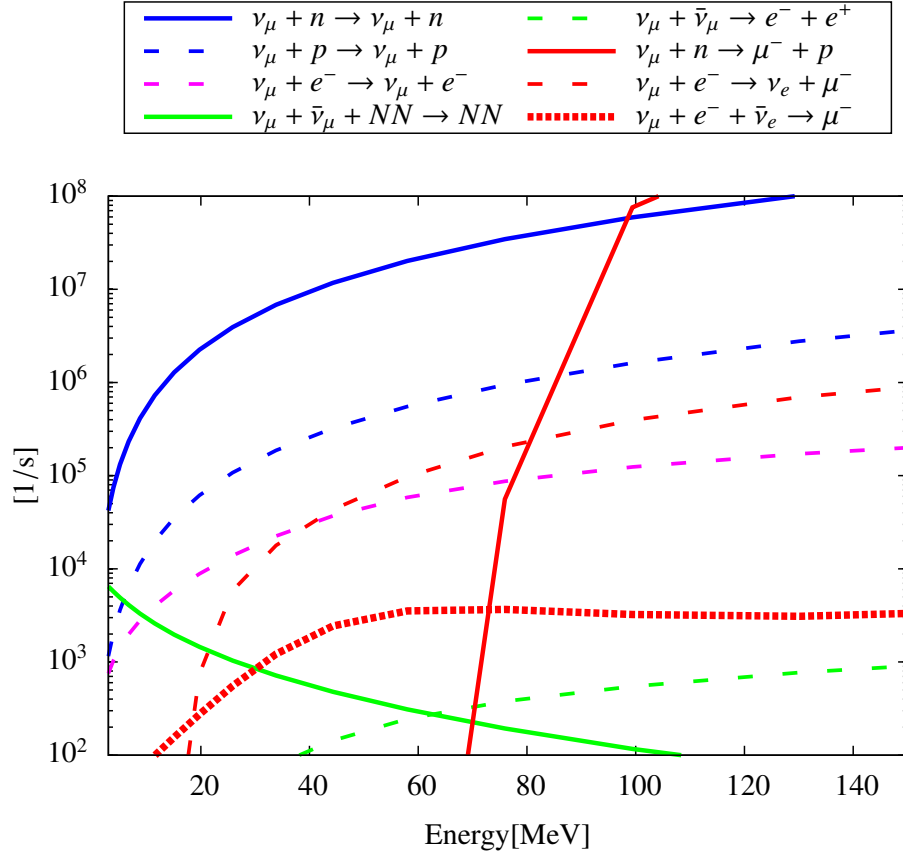
Figure 6.34.: Energy dependent opacity of ν_μ for extended reaction set, $2\,$s post bounce for $\rho = 3.1 \times 10^{13}\,$g/cm^3. Rate is defined as inverse mean free path times c.

When including the charged-current muonic reactions, one finds that absorption of ν_μ on electrons is equally as relevant as scattering on electrons. Looking at opacities for lower densities one finds further, that absorption on electrons becomes relatively more important for decoupling as the neutrino energy grows. It is then the most frequent inelastic reaction in the decoupling region up to $E_\nu = 95\,$MeV. Only for these very high energy neutrinos is absorption on neutrons more important.

Next Figure 6.35 shows the energy dependent opacity for $\rho \sim 7.6 \times 10^{13}\,$g/cm^3. This is roughly where neutrinos with $E_\nu < 10\,$MeV should decouple. In the standard scenario one finds that inverse bremsstrahlung is the most important inelastic reaction for these energies. For $E_\nu < 5\,$MeV it is even larger than scattering on neutrons. When including the charged-
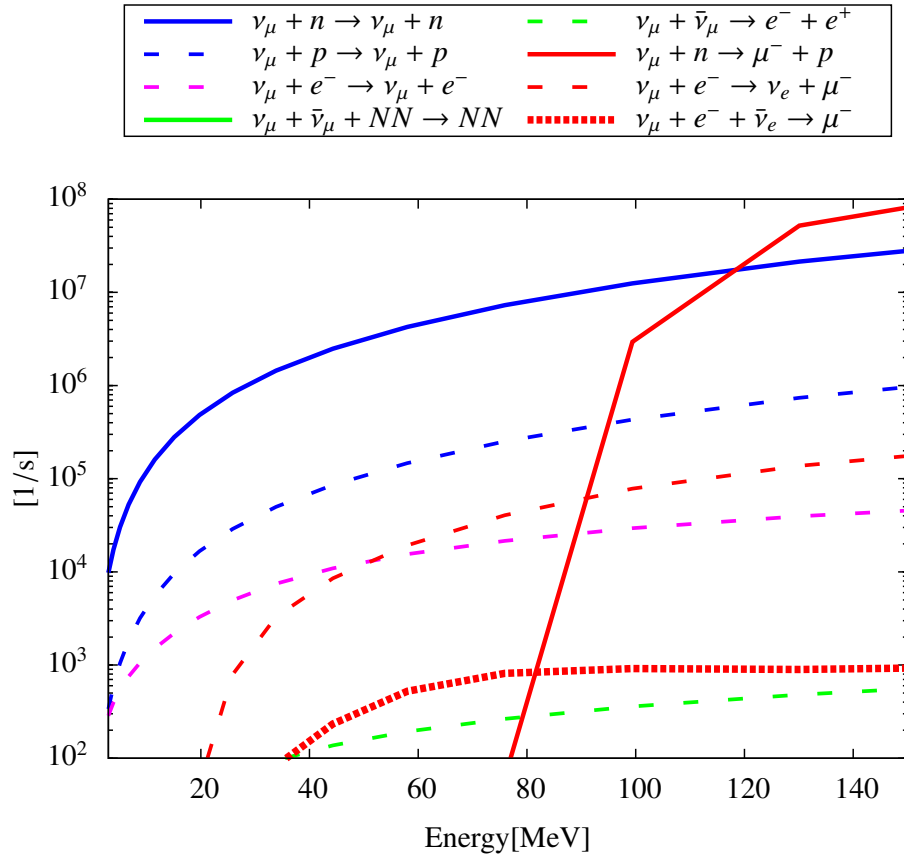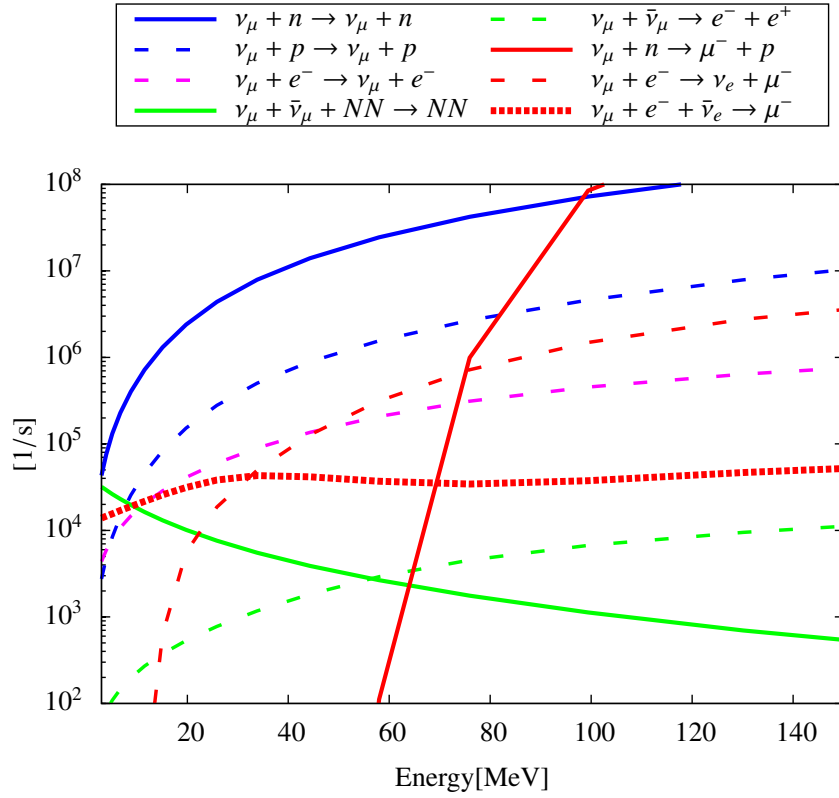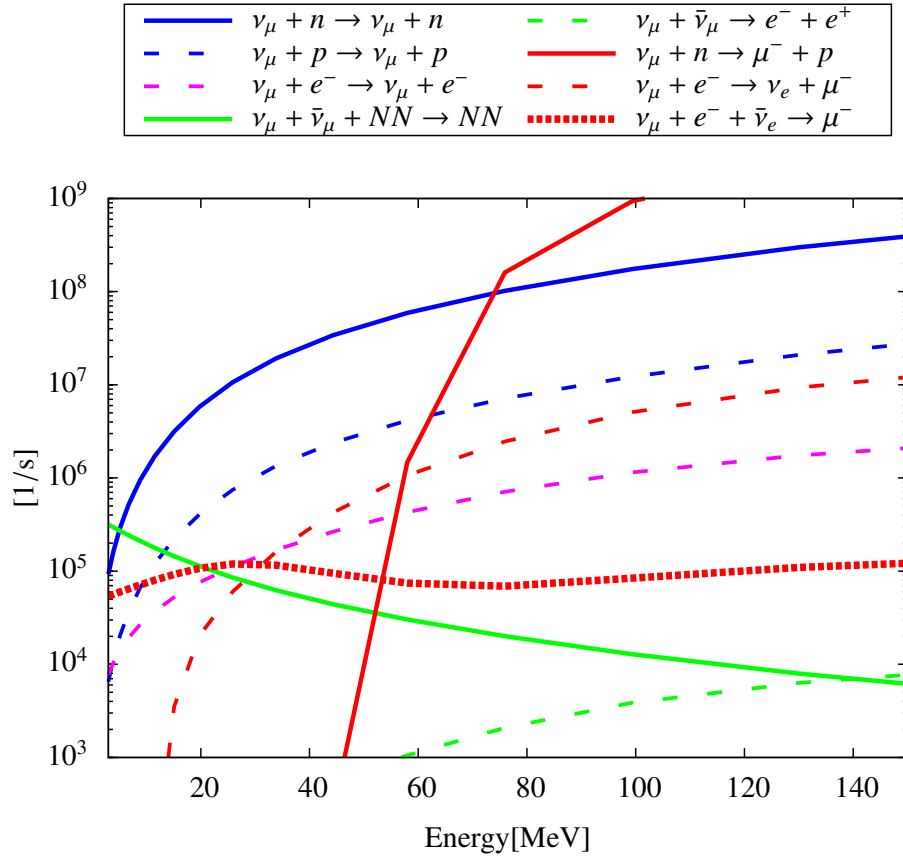
Figure 6.35.: Energy dependent opacity of ν_μ for extended reaction set, $2\,\text{s}$ post bounce for $\rho = 7.6 \times 10^{13}\,\text{g/cm}^3$. Rate is defined as inverse mean free path times c.

current muonic reactions, inverse muon decay is more important than scattering on electrons but it stays below inverse bremsstrahlung unlike earlier times. Therefore R_{eff} does not differ much between standard and extended reaction set.

6.6.1. Summary

For the standard reaction set scattering on electrons has by far the largest inverse mean free path in the decoupling region for all inelastic neutrino energies and all times down to $E_\nu < 10\,\text{MeV}$. Likewise scattering on neutrons has the largest opacity of all reactions, resulting in an extended scattering atmosphere between R_{eff} and R_{tr}. For the lowest neutrino energies the scattering atmosphere becomes thinner and vanishes eventually. This transition always coincides with the rise of inverse bremsstrahlung. The exact energy at which this takes place grows slowly with time.

When including the extended reaction set, the charged-current muonic reactions shift R_{eff} to lower densities for several distinct ranges in neutrino energy. Absorption on neutrons is by far the most important reaction for $E_\nu > 95\,\text{MeV}$ for all times. However, as few of these neutrinos are emitted in the first place, the additional reaction effectively suppresses them completely. Also, the influence of ν_μ absorption on neutrons on overall ν_μ-transport might probably be rather small. Absorption of ν_μ on electrons is a major inelastic reaction down to an energy $E_\nu \sim 50\,\text{MeV}$ at $150\,\text{ms}$ post bounce, $E_\nu \sim 40\,\text{MeV}$ at $500\,\text{ms}$ post bounce, and

$E_\nu \sim 30\,\mathrm{MeV}$ at 2 s. The influence of this reaction on ν_μ-transport could indeed be significant and dynamic simulations should be performed to test this. Eventually, inverse muon decay is a very important reaction for $E_\nu < 10\,\mathrm{MeV}$, probably within the first second post bounce. In this time it surpasses inverse bremsstrahlung and also scattering on neutrons for lowest neutrino energies. It is then expected that this reaction will clearly impact transport of low energy neutrinos. However, at later times this reaction is less relevant than inverse bremsstrahlung, probably because the temperature dependence of inverse muon decay is stronger.

When including the charged-current reactions for ν_μ in a dynamic CCSN simulation this will probably lead to a decrease of the average neutrino energy $\langle \epsilon_{\nu_\mu} \rangle$. This is insofar interesting, as it leads to a difference in the spectra between ν_μ and all other heavy lepton flavour neutrinos. The changes could even affect ν_τ via neutrino oscillations. In state of the art CCSN simulations, neutrino transport and consequently spectra of ν_μ and ν_τ are exactly the same. The inclusion of the extended reaction set will changes the spectrum of ν_μ compared to ν_τ and neutrino oscillations are very sensitive to differences between spectra and changes in spectra.

An additional effect is the appearance of a positive net muon leptonic abundance. As $\bar{\nu}_\mu$ diffuse faster out of the PNS than ν_μ, a net flux of muon antineutrinos leaves the PNS, at least for some time. This leads to a growth of the net muon neutrino number and therefore the net muon number.

Based on all of the above arguments, the implementation of charged-current reactions for muon neutrinos in CCSN simulations is strongly recommended.

6.6.2. Muon Production

It is argued in this work that for certain neutrino energies, charged-current reactions for ν_μ are comparable to standard inelastic reactions in the region of the effective neutrinosphere. Moreover, the charged-current reactions show a stronger density and temperature dependence. Therefore their rate is even larger inside the region where neutrinos are trapped. While this might not affect the emitted neutrino spectra in the first place, these reactions will certainly produce muons.

Muons are expected to appear in a neutron star after the first cooling phase and deleptonization have settled down. This is based on the argument that the electron chemical potential μ_e in the deep interior of a NS is larger than the muon mass. In chemical equilibrium the muon abundance should thus be non-vanishing. However, it can be asked whether charged-current muonic reactions might lead already to an earlier production of μ^-. To study this question the total rate of muon production was calculated for early times. The total rate of muon production is equal to the total reaction rate i.e. "absorption" rate of muon neutrinos for reactions that produce muons. To derive this rate one has to compute the integral of the inverse mean free path over the initial muon neutrino phase space. Figure 6.36 shows the total production rate of muons, per baryon and per second, for the respective charged-current reactions. The rates are computed at 150 ms post bounce and plotted over density. The black line denotes again the position of the spectrally averaged effective neutrinosphere. The production rates of muons are relatively high indeed. At the position of the neutrinosphere the production rate is $\sim 3\,\mathrm{s}^{-1}$
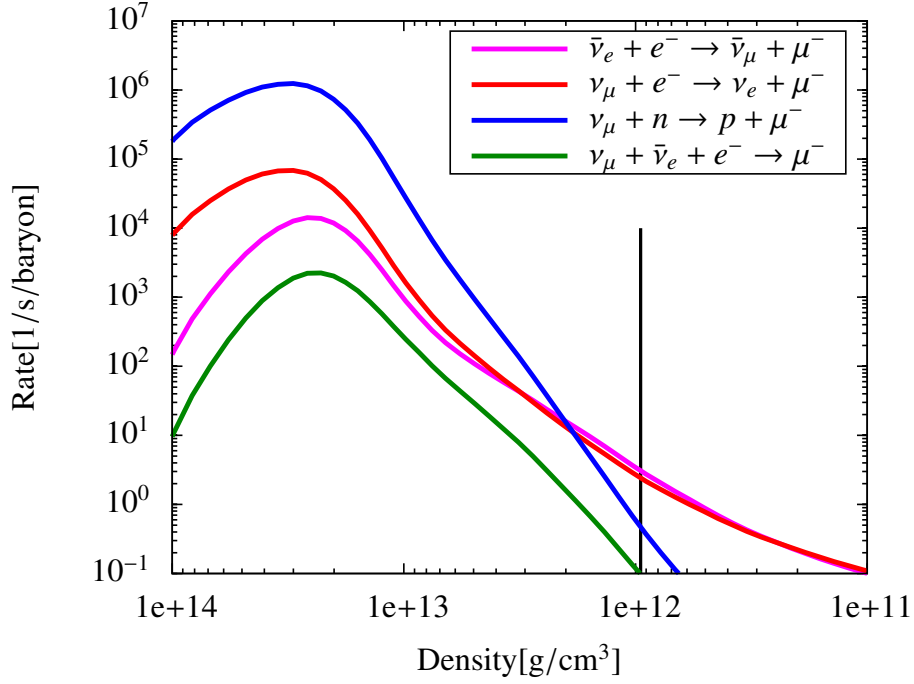
Figure 6.36.: Production rate of μ^- for various charged-current reactions over density at $150\,\mathrm{ms}$ post bounce. Rate is number of μ^- produced per baryon per second. The black vertical line denotes the position of the spectrally averaged effective neutrinosphere $\langle R_{eff} \rangle >$.

per baryon, and further inside it becomes as large $\sim 10^6\,\mathrm{s}^{-1}$ per baryon. The equilibrium muon fraction must be less than the electron fraction Y_e before equilibration, and Y_e is mostly in the range $0.1 - 0.25$. Hence, one can assume that the muon abundance inside the effective muon neutrinosphere will be equilibrated within milliseconds. Muons will then be present int the PNS directly after bounce, maybe even already at bounce.

In order to investigate the effect of muon production on chemical composition of the PNS, it is computed in this work how the overall equilibrium distribution differs when including muons. Figure 6.37 shows the abundance as it is from the simulation at $150\,\mathrm{ms}$ post bounce. The black dashed line marks the position of $\langle R_{eff} \rangle$ for the extended reaction set.

The abundance of ν_e is larger than the one of $\bar{\nu}_e$ for all densities. This difference becomes monotonously bigger with increasing density. The reason for this is the ongoing deleptonization of the star. As mentioned before, after the transition to the high temperature NSE, chemical equilibrium favours a higher neutron abundance in the matter. This leads to net electron captures and to net emission of electron neutrinos. Yet as these neutrinos are trapped, they cannot escape immediately and form a positive net Y_{ν_e}. In contrast, for muon neutrinos the abundances Y_{ν_μ} and $Y_{\bar{\nu}_\mu}$ are exactly the same so the curves lie on top of each other. This is because the CCSN simulation does not distinguish between the transport of ν_μ and $\bar{\nu}_\mu$. They are only produced and destroyed together via neutral current pair processes and all their neutral current opacities are the same. To include muons into the PNS, a new equilibrium distribution was computed. First it was assumed that all μ- and e-flavour neutrinos are trapped inside $\langle R_{eff} \rangle$.

Then the composition inside $\langle R_{eff} \rangle$ was updated to fulfill the following set of equations:

(1) $Y_n + Y_p - 1 = 0$ baryon number conservation

(2) $Y_p - Y_e - Y_\mu = 0$ charge neutrality

(3) $Y_{l_e} = Y_{e^-} - Y_{e^+} + Y_{\nu_e} - Y_{\bar{\nu}_e} = $ constant   electron lepton flavour conservation

(4) $Y_{l_\mu} = Y_{\mu^-} - Y_{\mu^+} + Y_{\nu_\mu} - Y_{\bar{\nu}_\mu} = 0$ muon lepton flavour conservation

(5) $\mu_n - \mu_p = \mu_{e^-} - \mu_{\nu_e}$

(6) $\mu_n - \mu_p = \mu_{\mu^-} - \mu_{\nu_\mu}$
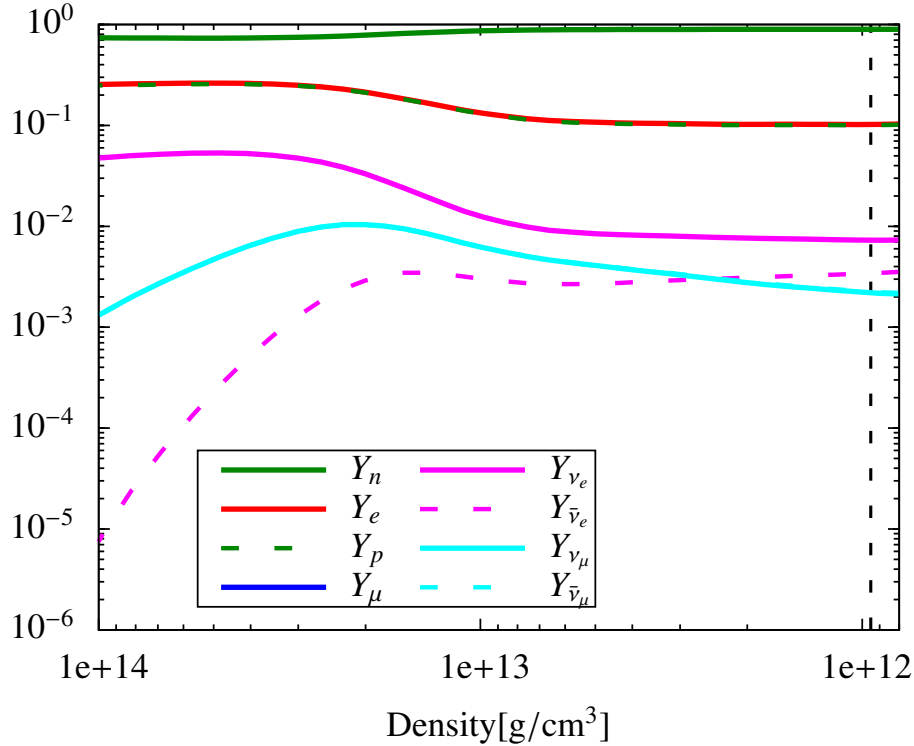
Figure 6.37.: Particle abundances in terms of particles per baryon at 150 ms post bounce. The vertical black dashed line marks the position of $\langle R_{eff} \rangle$ for the extended reaction set

A special choice is the demand that $Y_\mu = 0$. It cannot be derived in post processing how the net muon number might evolve, even though arguments were given why it should grow to a positive non-vanishing value. Therefore it appears most reasonable to leave it at the original value. The result can therefore suggest how the abundances will look like before the difference in the transport of ν_μ and $\bar{\nu}_\mu$ leads to $Y_\mu > 0$. The result for this, for the same time 150 ms post bounce is shown in Figure 6.38. The muon abundance reaches a maximum of $Y_{\mu^-} = 0.6\%$. This is more than an order of magnitude lower than Y_e. Also at the position of the effective neutrinosphere the muon abundance is negligible with $Y_{\mu^-} < 10^{-6}$. When performing the same calculations for different times, the maximum muon abundance to be found is $Y_{\mu^-} \sim 1\%$ roughly 1 second after bounce. One can conclude then that the inclusion of muons will not affect the dynamics of the CCSN, as the small muon fraction does not result in significant changes of thermodynamical variables such as pressure. Further, comparing the equilibrium abundances from Figure 6.38 with the production rates from 6.36 it can be assumed that inside the effective
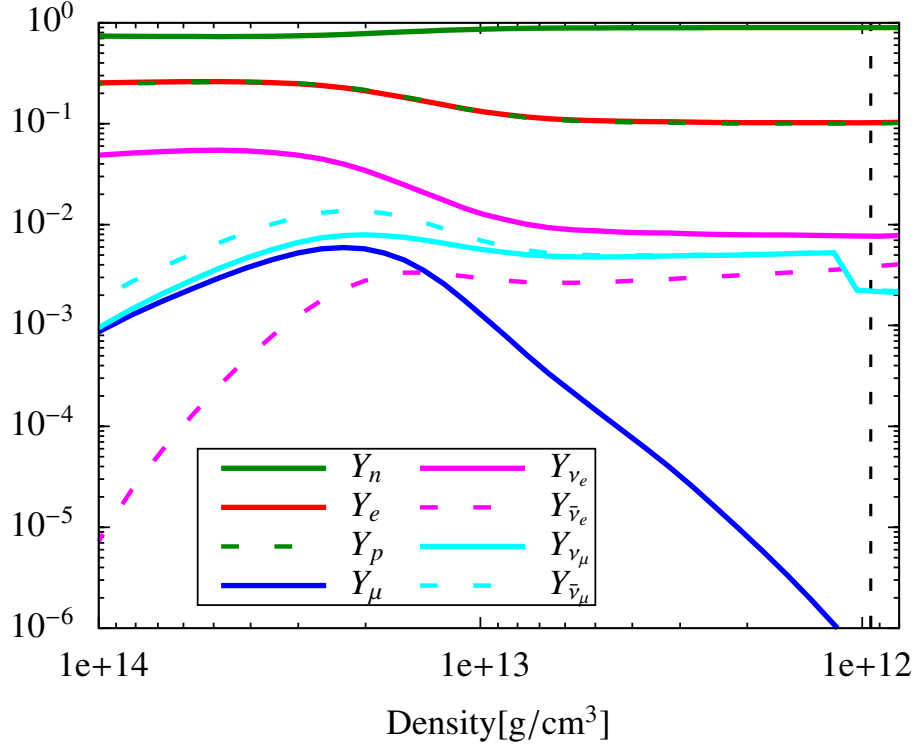
Figure 6.38.: Particle abundances in terms of particles per baryon at $150\,\text{ms}$ post bounce, for new equilibrium including muons. The vertical black dashed line marks the position of $\langle R_{eff} \rangle$ for the extended reaction set

neutrinosphere muons will be in equilibrium on timescales less than milliseconds i.e. faster than the dynamical timescale of the CCSN.

To give a reliable assessment of the effect of muons in equilibrium on the neutrino spectra and the deleptonization of the PNS one needs to perform dynamical simulations. With all the feedback effects that are involved in a PNS intuitive conclusions are difficult to make. However, the findings in this section certainly serve as an additional argument to actually include charged-current muonic reactions into dynamical CCSN simulations.

6.7. Weak Magnetism Correction

This section will compare the treatment of weak magnetism as done in this work with weak magnetism correction factors from the literature that are commonly used in CCSN simulations. The relevant correction factors were derived in [130]. The idea there was to calculate the effect of weak magnetism in the limit of infinitely heavy nucleons, somewhat corresponding to the limit of nonrelativistic nucleons. For this purpose it was assumed that the initial state nucleon is at rest. However, while this approach should be reasonable in the non-relativistic, non-interacting limit, one can argue that it misses the correct kinematics, the effect of strong interaction potentials (which were not included) and of thermal nucleon motion at high temperatures. In order to asses the validity of the correction factors at high densities and temperatures in a PNS we proceed as follows: First the rates for ν_e absorption on neutrons and $\bar{\nu}_e$ absorption on protons will be calculated without weak magnetism, i.e. $F_2 = 0$, but with the full relativistic

kinematics and strong interaction potentials. This is the base against which to compare the different treatments of weak magnetism. One option is to simply calculate the rates according to the full formalism in this work. The other is to multiply the base rate with the analytic correction factor obtained at [130]. However, the appropriate factor is actually not given in [130]. Instead that work gives a factor R_{Rec} that corrects for nucleon recoil and one that corrects for nucleon recoil and weak magnetism $R_{\text{Rec+WM}}$. Yet, the base rate in this work contains nucleon recoil already as it considers the full relativistic kinematics without approximations. One can still derive a factor that only corrects for weak magnetism R_{WM} by

$$R_{\text{WM}} = \frac{R_{\text{Rec+WM}}}{R_{\text{Rec}}} \tag{6.9}$$

This was proposed in [19]. The factors in particular are given by

$$R_{\text{Rec}} = \left\{ G_V^2 \left(1 + 4e + \frac{16}{3}e^2\right) + 3G_A^2 \left(1 + \frac{4}{3}e\right)^2 \pm 4G_V G_A \left(e + \frac{4}{3}e^2\right) \right\}$$
$$\times \left[G_V^2 + 3G_A^2 \left(1 + 2e\right)^3\right]^{-1} \tag{6.10}$$

$$R_{\text{Rec+WM}} = \left\{ G_V^2 \left(1 + 4e + \frac{16}{3}e^2\right) + 3G_A^2 \left(1 + \frac{4}{3}e\right)^2 \pm 4G_A \left(G_V + F_2\right) \left(e + \frac{4}{3}e^2\right) + \frac{8}{3}G_V F_2 e^2 \right.$$
$$\left. + F_2^2 \left(\frac{5}{3}e^2 + \frac{2}{3}e^3\right) \right\} \times \left[G_V^2 + 3G_A^2 \left(1 + 2e\right)^3\right]^{-1} \tag{6.11}$$

Here, $e = E_\nu/m_N$ and the plus-sign is for absorption of ν_e while the minus-sign is for absorption of $\bar{\nu}_e$.
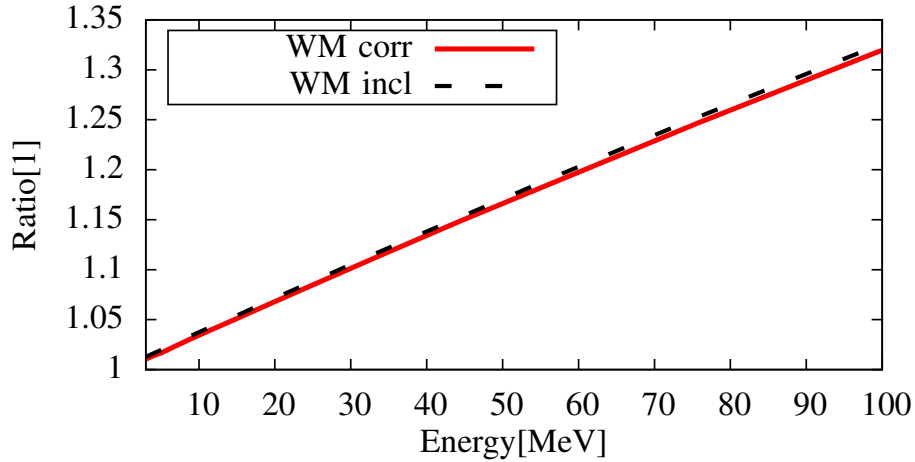
Figure 6.39.: Relative weak magnetism corrections for ν_e absorption on neutron. $T = 5.0\,\text{MeV}$, $\rho = 10^{11}\,\text{g/cm}^3$, $Y_e = 0.1$. "corr" shows the analytic correction factor from [130], "incl" is based on the derivations in this work.

Figure 6.39 shows the comparison of the different approaches for ν_e absorption on neutrons, for $T = 5.0\,\text{MeV}$, $\rho = 10^{11}\,\text{g/cm}^3$, and $Y_e = 0.1$. At this condition the non-relativistic non-interacting approximation is expected to work properly. Indeed the two curves for the analytic correction factor and for the inclusion of weak magnetism as done in this work lie almost on top.
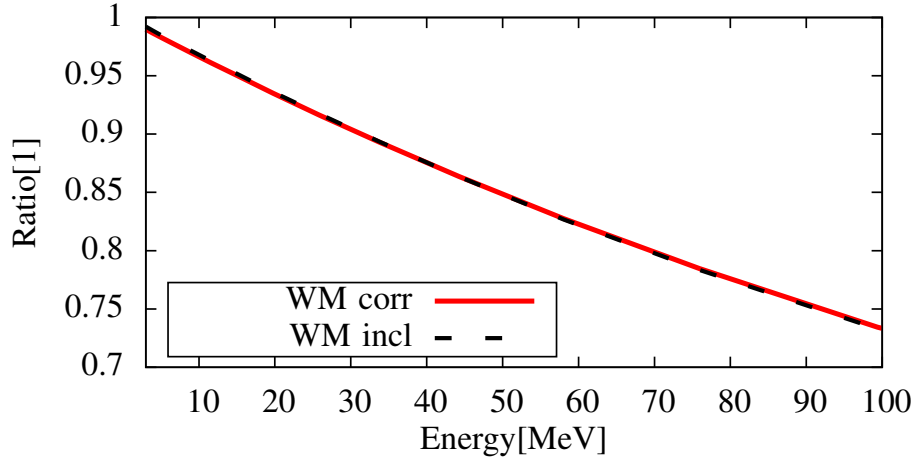
Figure 6.40.: Relative weak magnetism corrections for $\bar{\nu}_e$ absorption on proton. $T = 5.0\,\mathrm{MeV}$, $\rho = 10^{11}\,\mathrm{g/cm^3}$, $Y_e = 0.1$. "corr" shows the analytic correction factor from [130], "incl" is based on the derivations in this work.

Figure 6.40 shows the same comparison for $\bar{\nu}_e$ absorption on protons for the same thermodynamical conditions. Again, both curves lie on top of each other. Both results hold in general also for similar conditions but lower densities. This is especially interesting for nucleosynthesis in the neutrino driven wind. Since the weak magnetism correction factors are not density dependent, they also apply at the region of the NDW. Their inclusion is important to achieve the correct Y_e in the NDW, because they affect ν_e and $\bar{\nu}_e$ in different ways.

Besides, the results in Figures 6.39 and 6.40 are a good cross check for the expressions that were derived in this work
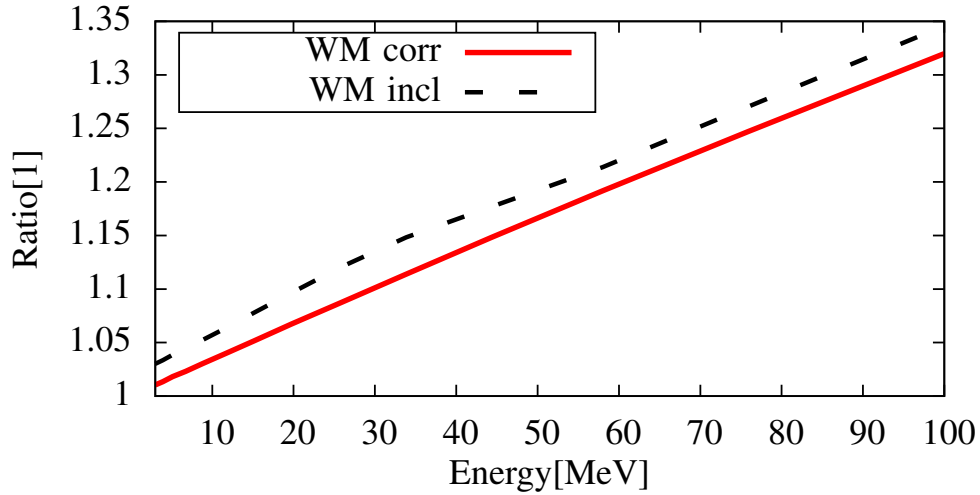
Figure 6.41.: Relative weak magnetism corrections for ν_e absorption on neutron. $T = 7.0\,\mathrm{MeV}$, $\rho = 3 \times 10^{13}\,\mathrm{g/cm^3}$, $Y_e = 0.05$. "corr" shows the analytic correction factor from [130], "incl" is based on the derivations in this work.

The same comparison for ν_e absorption but with different thermodynamical conditions is shown in Figure 6.41. There it is $T = 7.0\,\mathrm{MeV}$, $\rho = 3 \times 10^{13}\,\mathrm{g/cm^3}$, $Y_e = 0.05$. One can see that the analytic correction factor is underestimating the impact of weak magnetism by a few percent of the base rate.
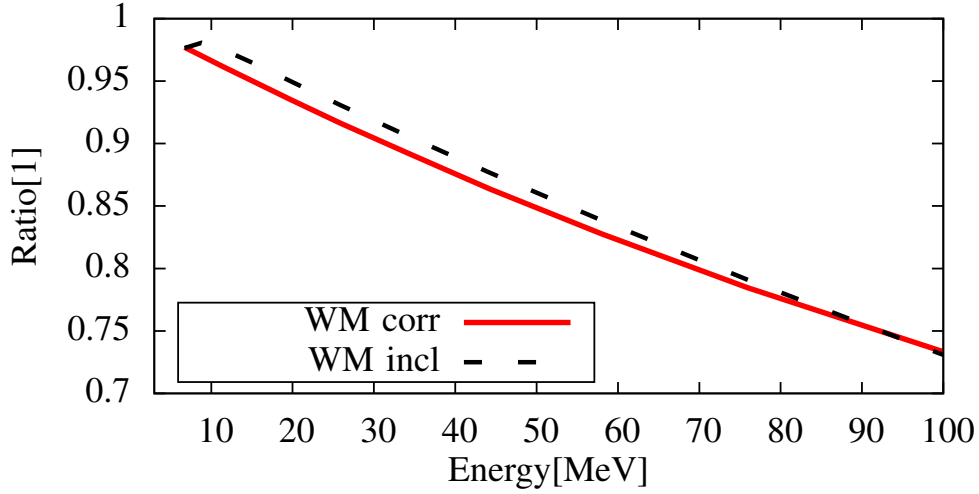
Figure 6.42.: Relative weak magnetism corrections for $\bar{\nu}_e$ absorption on proton. $T = 7.0\,\mathrm{MeV}$, $\rho = 3 \times 10^{13}\,\mathrm{g/cm^3}$, $Y_e = 0.05$. "corr" shows the analytic correction factor from [130], "incl" is based on the derivations in this work.

Therefore one can see that the weak magnetism factor does indeed start to deviate from the correct result when strong interactions become important and the approximation of non-relativistic nucleons becomes worse. Hence, for precise rates at high densities above $10^{13}\,\mathrm{g/cm^3}$ these analytic factors should be used with caution. Especially, since the relative mistake is the largest for low energy neutrinos, which in return are those that decouple at the highest densities. Again, the same comparison is repeated at large densities for $\bar{\nu}_e$ absorption on protons in Figure 6.42. Here, the two approaches differ, too. Yet, the deviation is smaller and not as constant as for ν_e absorption. The two curves even cross at one point. Hence, the statements for ν_e can in principle be repeated for $\bar{\nu}_e$ yet the problems with the analytic correction factor at large densities appear not as significant.

One can conclude, that the analytic correction factors for weak magnetism from [130] and [19] work very well at the PNS surface and in lower density environments as the neutrino driven wind. However, above densities of $10^{13}\,\mathrm{g/cm^3}$ they have to be used with care as they are the less correct, the larger the role of strong interactions and the worse the non-relativistic nucleon approximation. This is especially true for low energy electron neutrinos.

7. Summary

In this thesis, neutrino interactions in hot and dense matter are studied. In particular, this work is concerned with neutrino matter interactions that are relevant for neutrino transport in core-collapse supernovae (CCSNe). It is known that the core collapse of a massive star and the subsequent explosion release the gravitational binding energy, about 10^{53} erg, mostly in the form of neutrinos. Consequently, such large neutrino fluxes play are a major factor in a variety of processes that are related with the supernova explosion. Simulations of CCSNe agree that the initial shock, which forms due to a bounce of the core after contracting to supranuclear density, stalls on the way out due to energy loss by heating the ongoing mass accretion flow. Hence, there is no prompt explosion. Most studies find that the eventual explosion proceeds in the so called delayed neutrino-heating mechanism. It predicts that neutrinos which are emitted from deeper inside heat the region below the stalled shock front. Thereby they deposit enough energy to revive the shock and eventually produce an explosion. In order to achieve a reliable explosion model in the delayed neutrino-heating mechanism, accurate treatment of neutrino interactions in the hot and dense protoneutron star (PNS) is required.

Beyond the explosion itself there are various other processes that depend on the precise spectra of the emitted neutrinos. For example, neutrino absorption on the PNS surface is expected to result in a considerable mass outflow. This outflow is the so called neutrino driven wind and it is considered as a possible site of heavy element production via the r-process nucleosynthesis. The possible path of nucleosynthesis in this scenario depends sensitively on the thermodynamical conditions and the chemical composition of the neutrino driven wind. These conditions are in return mostly determined by the spectral properties of the emitted neutrinos. Further, the direct measurement of neutrino spectra from a next nearby supernova with modern detectors is expected to give detailed information on the evolution of a CCSN but also on the state of matter at extremely high densities. This is particularly interesting as such matter is very difficult to reproduce in a laboratory on Earth, even in the most modern heavy ion accelerators, if it is possible at all. However, the information that is contained in the neutrino spectra will only be obtained, if theory is also able to produce reliable models for neutrino emission. Another very interesting aspect of neutrino emission is the possibility of neutrino oscillations in the vicinity of a protoneutron star. If oscillations take place, they could for example change the outcome of nucleosynthesis or modify the neutrino signal that is received on earth. However, the predictions for neutrino oscillations are naturally based on the exact properties of the initial neutrino spectra.

Neutrino transport in a PNS is a unique problem insofar, as neutrinos are trapped at high densities and cannot simply leave the object after their production. In general, neutrinos interact only via the weak interaction (and gravity). Neutrinos are therefore only very weakly

coupled to all other particles and reaction probabilities are extremely low. In most environments, the mean free path of neutrinos is significantly larger than the size of any relevant object. However, the core of a PNS in a CCSN is so dense and hot that inside a certain region the mean free path for neutrinos becomes smaller than the size of the PNS. These neutrinos are then in a thermal and chemical equilibrium with the matter. At lower densities the mean free path becomes larger and the neutrinos can leave freely. In the transition region between both regimes neutrino transport is a nontrivial problem. The spectrum of emitted neutrinos depends on the conditions of the region where they decouple from matter. Yet, the position of this region is determined by the size of neutrino interactions with matter. In general, the position of the decoupling region varies for different neutrino energies and different neutrino flavours. Usually, neutrinos with lower energy decouple further inside as the mean free path decreases with increasing energy. Electron neutrinos are expected to have the shortest mean free path of all neutrino types in the neutron rich matter of a protoneutron star, followed by electron antineutrinos. The μ- and τ-flavour neutrinos are predicted to have the longest mean free path and consequently to decouple at the highest densities.

Modeling of neutrino transport in a CCSN has then to deal among other things with two issues. The first question is which neutrino reactions are relevant in a PNS. One has to make sure that all reactions which contribute significantly to a neutrino of any particular energy or flavour are considered in the transport problem. The second question is how the corresponding transport properties should be evaluated numerically. Simulations of neutrino transport can be very computationally demanding. As limited computational resources are among the main constraints of state of the art supernova simulations, a trade of between accuracy and complexity has to be made. Therefore one tries to use reasonable approximations in the description of neutrino interactions which greatly reduce the computational effort. Such approximations are e.g. simplified treatment of strong interactions in the baryonic matter or simplified kinematics by assuming neutrons and protons to be non-relativistic. All these approximations have to be used with care, as they work very well in some regimes, yet might fail in others. As neutrino interactions are very sensitive to e.g. the description of nuclear interactions at high densities, this can lead to significant shortcomings in the predicted neutrino spectra and all dependent processes.

It is precisely these questions with which the present work is concerned. First it tries to asses the relevance of charged-current weak interactions that include muon neutrinos or muons, as well as the role of inverse neutron decay for neutrino transport in CCSNe. Charged-current muonic reactions are not implemented in current simulations as they are expected to have negligibly small rates. It is argued that because of the large muon mass $m_\mu = 105.7\,\mathrm{MeV}$ the production of a muon is almost impossible at the thermodynamical conditions in a PNS or at least it is significantly suppressed compared to other reaction channels. This thesis questions these arguments as the particle energies at densities above $10^{12}\,\mathrm{g/cm^3}$ in a PNS can in principle be high enough for muon production. Inverse neutron decay is neglected for the transport of electron antineutrinos, as the reaction rate is expected to be significantly lower than the rate for absorption on protons and scattering on neutrons. However at large densities in neutron rich matter, nuclear interactions effectively increase the energy difference between neutrons and

protons. Consequently, absorption of $\bar{\nu}_e$ is strongly suppressed for low neutrino energies. In contrast, inverse neutron decay is not affected by this problem.

The second project of this work is to improve the description of interactions between neutrinos and nucleons in neutrino transport. The idea is to derive semi-analytic expressions for these reactions that are not based on the assumption of nonrelativistic nucleons, and to have a more accurate treatment of the hadronic weak current including weak magnetism corrections, while at the same time not increasing the computational demand.

In the first part of this work, semi-analytic expressions for transport properties, in particular the inverse mean free path, of various neutrino interactions are derived. To be precise, the following reactions are studied: Absorption of ν_e on neutrons; absorption of $\bar{\nu}_e$ on protons; inverse neutron decay; inverse muon decay; conversion of $\bar{\nu}_e$ and electrons into $\bar{\nu}_\mu$ and muons; absorption of ν_μ on neutrons; conversion of ν_μ and electrons into ν_e and muons. First the corresponding matrix elements were derived analytically. The momentum transfer dependence of the weak coupling and of hadronic coupling constants is ignored, due to the comparably low energy scale in PNSs. Strong interactions at high densities are implemented on the level of relativistic mean field theory via strong interaction potentials and effective nucleon masses. Also, the hadron weak magnetism coupling is explicitly included. These derivations reproduce previous findings in the literature, but also generalize them to include finite mass corrections and strong interaction potentials. Next, the transport properties such as inverse mean free path for absorption reactions and scattering kernels for scattering reactions are derived from the matrix elements. These derivations consider the full relativistic kinematics of all participating particles without further approximations. Also the weak magnetism terms of the matrix elements are explicitly included to all orders. The resulting expressions are either derived for the first time explicitly or more precisely than most expressions that are used in state of the art simulations, while being similarly demanding in terms of computational effort. This part of the work is structured in two different problems, one for purely leptonic reactions and one for interactions between neutrinos and nucleons.

After these purely analytic derivations, the transport properties are then evaluated numerically for PNS conditions. Therefore matter and neutrino profiles from a 1-dimensional general relativistic hydrodynamic CCSN simulation with full Boltzmann neutrino transport are used to determine the relevant thermodynamical variables and the chemical composition. The impact of the new reactions is compared to a standard set of neutrino reactions which is representative for state of the art supernova simulations. It is found that for $\bar{\nu}_e$ inverse muon decay is an important contribution to the inverse mean free path for neutrino energies less than $5 - 10\,\mathrm{MeV}$ during the first second after core bounce. Likewise, inverse neutron decay is important in the neutrino decoupling region for the same neutrino energies after the first seconds post bounce. This is due to the decoupling region eventually moving to densities above $10^{13}\,\mathrm{g/cm^3}$ as the PNS cools and deleptonizes. At these densities, the energy difference between neutrons and protons grows significantly because of nuclear interactions. Therefore inverse neutron decay is favoured above absorption on protons for low energy $\bar{\nu}_e$. For ν_μ it is found that absorption on neutrons is important only for the decoupling of neutrinos with extremely high energies above $95\,\mathrm{MeV}$. Below this value and down to energies between $30 - 50\,\mathrm{MeV}$ the conversion of ν_μ and

electrons into ν_e and muons is a major inelastic reaction channel, comparable to scattering of ν_μ on electrons. Eventually for small neutrino energies below $5 - 10 \, \text{MeV}$, inverse muon decay is an important reaction during the first second after bounce for ν_μ, as it is for $\bar{\nu}_e$. It is concluded that the charged-current weak muonic reactions and inverse neutron decay should be included in dynamical simulations of core collapse supernovae. It is expected that they will modify the spectra of $\bar{\nu}_e$ and ν_μ. Furthermore, these reactions couple different neutrino flavours in a rather asymmetric way. For example, high energy $\bar{\nu}_e$ can be converted into low energy $\bar{\nu}_\mu$ deep in the PNS. The latter can easily leave the core and consequently affect deleptonization rates. Similar arguments can be made for the conversion of high energy ν_μ into low energy ν_e. However, due to the various feedback mechanisms that are active in supernovae, it is nigh impossible to assess the spectral changes in the post-processing manner of this thesis.

The relevance of muonic reactions also emphasizes that muons will be present in the stellar core early on during the supernova evolution. The exact amount and possible consequences on neutrino emissions are again difficult to predict without performing dynamical simulations.

The approach to include weak magnetism that is chosen in this work is compared to analytic approximations from the literature. It is found that for neutrino transport at high densities in a PNS weak magetism is not properly described by such a simplifying approximation.

Concluding the overall study, it is strongly recommended to implement both the new reactions and the improved semi-analytic transport expressions from this work into dynamical CCSN simulations. Only then can the possible impact on explosion dynamics, PNS deleptonization and cooling, and neutrino spectra really be evaluated.

A natural yet nontrivial extension of this work is the derivation of scattering kernels for neutrino scattering on nucleons, including relativistic nucleon kinematics, strong interaction potenials, and weak magnetism corrections. Another interesting project is the inclusion of pseudoscalar coupling for muonic reactions with nucleons.

A. Traces of γ-Matrices

All traces over odd numbers of γ-matrices vanish. For traces over even numbers one can find the following rules

$$\mathrm{Tr}\left[\gamma_\alpha \gamma_\beta\right] = 4g_{\alpha\beta}, \tag{A.1}$$

$$\mathrm{Tr}\left[\gamma_\alpha \gamma_\beta \gamma_\delta \gamma_\epsilon\right] = 4\left(g_{\alpha\beta}g_{\delta\epsilon} - g_{\alpha\delta}g_{\beta\epsilon} + g_{\alpha\epsilon}g_{\beta\delta}\right), \tag{A.2}$$

$$\mathrm{Tr}\left[\gamma_\alpha \gamma_\beta \gamma_\delta \gamma_\epsilon \gamma_\kappa \gamma_\rho\right] = 4\left[g_{\alpha\beta}\left(g_{\delta\epsilon}g_{\kappa\rho} - g_{\delta\kappa}g_{\epsilon\rho} + g_{\delta\rho}g_{\epsilon\kappa}\right) - g_{\alpha\delta}\left(g_{\beta\epsilon}g_{\kappa\rho} - g_{\beta\kappa}g_{\epsilon\rho} + g_{\beta\rho}g_{\epsilon\kappa}\right)\right. \tag{A.3}$$
$$+ g_{\alpha\epsilon}\left(g_{\beta\delta}g_{\kappa\rho} - g_{\beta\kappa}g_{\delta\rho} + g_{\beta\rho}g_{\delta\kappa}\right) - g_{\alpha\kappa}\left(g_{\beta\delta}g_{\epsilon\rho} - g_{\beta\epsilon}g_{\delta\rho} + g_{\beta\rho}g_{\delta\epsilon}\right)$$
$$\left.+ g_{\alpha\rho}\left(g_{\beta\delta}g_{\epsilon\kappa} - g_{\beta\epsilon}g_{\delta\kappa} + g_{\beta\kappa}g_{\delta\epsilon}\right)\right],$$

$$\mathrm{Tr}\left[\gamma_5\right] = 0, \tag{A.4}$$

$$\mathrm{Tr}\left[\gamma_5 \gamma_\alpha \gamma_\beta\right] = 0, \tag{A.5}$$

$$\mathrm{Tr}\left[\gamma_5 \gamma_\alpha \gamma_\beta \gamma_\delta \gamma_\epsilon\right] = 4i\epsilon_{\alpha\beta\delta\epsilon}. \tag{A.6}$$

For matrix elements that correspond to weak magnetism one has to calculate traces that include $\sigma^{\alpha\beta}$, the commutator of the γ-matrices.

$$\sigma_{\alpha\beta} = \frac{i}{2}\left[\gamma_\alpha, \gamma\beta\right] = \frac{i}{2}\left(\gamma_\alpha\gamma_\beta - \gamma_\beta\gamma_\alpha\right). \tag{A.7}$$

One can then derive the following rules

$$\mathrm{Tr}\left[\sigma_{\alpha\beta}\gamma_\delta\gamma_\epsilon\right] = \frac{i}{2}\left(\mathrm{Tr}\left[\gamma_\alpha\gamma_\beta\gamma_\delta\gamma_\epsilon\right] - \mathrm{Tr}\left[\gamma_\beta\gamma_\alpha\gamma_\delta\gamma_\epsilon\right]\right) = 4i\left(-g_{\alpha\delta}g_{\beta\epsilon} + g_{\alpha\epsilon}g_{\beta\delta}\right), \tag{A.8}$$

$$\mathrm{Tr}\left[\sigma_{\alpha\beta}\sigma_{\delta\epsilon}\right] = \frac{i}{2}\left(\mathrm{Tr}\left[\sigma_{\alpha\beta}\gamma_\delta\gamma_\epsilon\right] - \mathrm{Tr}\left[\sigma_{\alpha\beta}\gamma_\epsilon\gamma_\delta\right]\right) = 4\left(g_{\alpha\delta}g_{\beta\epsilon} - g_{\alpha\epsilon}g_{\beta\delta}\right), \tag{A.9}$$

$$\mathrm{Tr}\left[\gamma_5\sigma_{\alpha\beta}\gamma_\delta\gamma_\epsilon\right] = \frac{i}{2}\left(\mathrm{Tr}\left[\gamma_5\gamma_\alpha\gamma_\beta\gamma_\delta\gamma_\epsilon\right] - \mathrm{Tr}\left[\gamma_5\gamma_\beta\gamma_\alpha\gamma_\delta\gamma_\epsilon\right]\right) = -4\epsilon_{\alpha\beta\delta\epsilon}, \tag{A.10}$$

$$\mathrm{Tr}\left[\gamma_5\sigma_{\alpha\beta}\gamma_\delta\gamma_\epsilon\right] = \mathrm{Tr}\left[\gamma_5\gamma_\alpha\sigma_{\beta\delta}\gamma_\epsilon\right] = \mathrm{Tr}\left[\gamma_5\gamma_\alpha\gamma_\beta\sigma_{\delta\epsilon}\right], \tag{A.11}$$

$$\mathrm{Tr}\left[\sigma_{\alpha\beta}\gamma_\delta\sigma_{\epsilon\kappa}\gamma_\rho\right] = -\frac{1}{4}\left(\mathrm{Tr}\left[\gamma_\alpha\gamma_\beta\gamma_\delta\gamma_\epsilon\gamma_\kappa\gamma_\rho\right] - \mathrm{Tr}\left[\gamma_\beta\gamma_\alpha\gamma_\delta\gamma_\epsilon\gamma_\kappa\gamma_\rho\right]\right. \tag{A.12}$$
$$\left.-\mathrm{Tr}\left[\gamma_\alpha\gamma_\beta\gamma_\delta\gamma_\kappa\gamma_\epsilon\gamma_\rho\right] + \mathrm{Tr}\left[\gamma_\beta\gamma_\alpha\gamma_\delta\gamma_\kappa\gamma_\epsilon\gamma_\rho\right]\right)$$
$$= 4\left[g_{\alpha\delta}\left(g_{\beta\epsilon}g_{\kappa\rho} - g_{\beta\kappa}g_{\epsilon\rho}\right) - g_{\alpha\epsilon}\left(g_{\beta\delta}g_{\kappa\rho} - g_{\beta\kappa}g_{\delta\rho} + g_{\beta\rho}g_{\delta\kappa}\right)\right.$$
$$\left.+g_{\alpha\kappa}\left(g_{\beta\delta}g_{\epsilon\rho} - g_{\beta\epsilon}g_{\delta\rho} + g_{\beta\rho}g_{\delta\epsilon}\right) + g_{\alpha\rho}\left(g_{\beta\epsilon}g_{\delta\kappa} - g_{\beta\kappa}g_{\delta\epsilon}\right)\right].$$

For the fully antisymmetric tensor $\epsilon_{\alpha\beta\delta\epsilon}$ the following relations are usefull

$$\epsilon_{\alpha\beta\delta\epsilon}\epsilon^{\alpha\beta\kappa\rho} = -2\left(\delta_\delta^\kappa\delta_\epsilon^\rho - \delta_\delta^\rho\delta_\epsilon^\kappa\right), \tag{A.13}$$

$$\epsilon_{\alpha\beta\delta\epsilon}\epsilon^{\alpha\beta\delta\kappa} = -6\delta_\epsilon^\kappa. \tag{A.14}$$

B. Derivation of $\left\langle |M|^2 \right\rangle$

B.1. Leptonic Reactions

$$\boxed{\nu_\mu / \bar{\nu}_\mu + e^- \rightarrow \nu_\mu / \bar{\nu}_\mu + e^-}$$

Calculation of the Electron Tensor

$$\sum_{t,t'} E_{\alpha\beta}(t,t') = \sum_{t,t'} \left[\bar{u}^{t'}_{e^-} \gamma_\alpha \left(-1 + 4s_W^2 + \gamma_5 \right) u^t_{e^-} \right] \left[\bar{u}^t_{e^-} \gamma_\beta \left(-1 + 4s_W^2 + \gamma_5 \right) u^{t'}_{e^-} \right]$$

$$= \sum_{t'} \left[\bar{u}^{t'}_{e^-} \gamma_\alpha \left(-1 + 4s_W^2 + \gamma_5 \right) \left(\gamma_\delta p^\delta_{e^-} + m_e \right) \gamma_\beta \left(-1 + 4s_W^2 + \gamma_5 \right) u^{t'}_{e^-} \right]$$

$$= Tr \left[\gamma_\alpha \left(-1 + 4s_W^2 + \gamma_5 \right) \left(\gamma_\delta p^\delta_{e^-} + m_e \right) \gamma_\beta \left(-1 + 4s_W^2 + \gamma_5 \right) \left(\gamma_\epsilon p'^\epsilon_{e^-} + m_e \right) \right]$$

$$= p^\delta_{e^-} p'^\epsilon_{e^-} Tr \left[\gamma_\alpha \left(-1 + 4s_W^2 + \gamma_5 \right) \gamma_\delta \gamma_\beta \left(-1 + 4s_W^2 + \gamma_5 \right) \gamma_\epsilon \right]$$

$$+ m_e^2 Tr \left[\gamma_\alpha \left(-1 + 4s_W^2 + \gamma_5 \right) \gamma_\beta \left(-1 + 4s_W^2 + \gamma_5 \right) \right].$$

Define $V \equiv -1 + 4s_W^2$.

$$\sum_{t,t'} E_{\alpha\beta}(t,t') = p^\delta_{e^-} p'^\epsilon_{e^-} Tr \left[\left(V^2 + 1 - 2V\gamma_5 \right) \gamma_\alpha \gamma_\delta \gamma_\beta \gamma_\epsilon \right] + m_e^2 Tr \left[\left(V^2 - 1 \right) \gamma_\alpha \gamma_\beta \right]$$

$$= p^\delta_{e^-} p'^\epsilon_{e^-} \left[\left(V^2 + 1 \right) Tr \left[\gamma_\alpha \gamma_\delta \gamma_\beta \gamma_\epsilon \right] - 2V Tr \left[\gamma_5 \gamma_\alpha \gamma_\delta \gamma_\beta \gamma_\epsilon \right] \right] + m_e^2 \left(V^2 - 1 \right) Tr \left[\gamma_\alpha \gamma_\beta \right]$$

$$= 4 \left(V^2 + 1 \right) \left[p_{e^-,\alpha} p'_{e^-,\beta} + p_{e^-,\beta} p'_{e^-,\alpha} - g_{\alpha\beta} \left(p_{e^-} \cdot p'_{e^-} \right) \right]$$

$$+ i8V \epsilon_{\alpha\beta\delta\epsilon} p^\delta_{e^-} p'^\epsilon_{e^-} + 4m_e^2 \left(V^2 - 1 \right) g_{\alpha\beta}$$

$$= 8 \left\{ \left(1 - 4s_W^2 + 8s_W^4 \right) \left[p_{e^-,\alpha} p'_{e^-,\beta} + p_{e^-,\beta} p'_{e^-,\alpha} - g_{\alpha\beta} \left(p_{e^-} \cdot p'_{e^-} \right) \right] \right.$$

$$\left. -i \left(1 - 4s_W^2 \right) \epsilon_{\alpha\beta\delta\epsilon} p^\delta_{e^-} p'^\epsilon_{e^-} - m_e^2 \left(4s_W^2 - 8s_W^4 \right) g_{\alpha\beta} \right\}.$$

Piecewise Contraction of Neutrino Tensor and Electron Tensor

$$8 \left(p^\alpha_{\nu_\mu} p'^\beta_{\nu_\mu} \right) \times 8 \left(1 - 4s_W^2 + 8s_W^4 \right) \left[p_{e^-,\alpha} p'_{e^-,\beta} + p_{e^-,\beta} p'_{e^-,\alpha} - g_{\alpha\beta} \left(p_{e^-} \cdot p'_{e^-} \right) \right]$$

$$= 64 \left(1 - 4s_W^2 + 8s_W^4 \right) \left[\left(p_{\nu_\mu} \cdot p_{e^-} \right) \left(p'_{\nu_\mu} \cdot p'_{e^-} \right) + \left(p_{\nu_\mu} \cdot p'_{e^-} \right) \left(p'_{\nu_\mu} \cdot p_{e^-} \right) - \left(p_{\nu_\mu} \cdot p'_{\nu_\mu} \right) \left(p_{e^-} \cdot p'_{e^-} \right) \right],$$

$$8 \left(p^\beta_{\nu_\mu} p'^\alpha_{\nu_\mu} \right) \times 8 \left(1 - 4s_W^2 + 8s_W^4 \right) \left[p_{e^-,\alpha} p'_{e^-,\beta} + p_{e^-,\beta} p'_{e^-,\alpha} - g_{\alpha\beta} \left(p_{e^-} \cdot p'_{e^-} \right) \right]$$

$$= 64 \left(1 - 4s_W^2 + 8s_W^4 \right) \left[\left(p_{\nu_\mu} \cdot p_{e^-} \right) \left(p'_{\nu_\mu} \cdot p'_{e^-} \right) + \left(p_{\nu_\mu} \cdot p'_{e^-} \right) \left(p'_{\nu_\mu} \cdot p_{e^-} \right) - \left(p_{\nu_\mu} \cdot p'_{\nu_\mu} \right) \left(p_{e^-} \cdot p'_{e^-} \right) \right],$$

$$-8g^{\alpha\beta} \left(p_{\nu_\mu} \cdot p'_{\nu_\mu} \right) \times 8 \left(1 - 4s_W^2 + 8s_W^4 \right) \left[p_{e^-,\alpha} p'_{e^-,\beta} + p_{e^-,\beta} p'_{e^-,\alpha} - g_{\alpha\beta} \left(p_{e^-} \cdot p'_{e^-} \right) \right]$$

$$= 64 \left(1 - 4s_W^2 + 8s_W^4 \right) \left[2 \left(p_{\nu_\mu} \cdot p'_{\nu_\mu} \right) \left(p_{e^-} \cdot p'_{e^-} \right) \right],$$

$$-i8 \left(\epsilon^{\alpha\beta\delta\epsilon} p_{\nu_\mu,\delta} p'_{\nu_\mu,\epsilon} \right) \times 8 \left(1 - 4s_W^2 + 8s_W^4 \right) \left[p_{e^-,\alpha} p'_{e^-,\beta} + p_{e^-,\beta} p'_{e^-,\alpha} - g_{\alpha\beta} \left(p_{e^-} \cdot p'_{e^-} \right) \right]$$
$$= 0,$$

$$-8 \left[p^\alpha_{\nu_\mu} p'^\beta_{\nu_\mu} + p^\beta_{\nu_\mu} p'^\alpha_{\nu_\mu} - g^{\alpha\beta} \left(p_{\nu_\mu} \cdot p'_{\nu_\mu} \right) \right] \times i8 \left(1 - 4s_W^2 \right) \epsilon_{\alpha\beta\kappa\rho} p^\kappa_{e^-} p'^\rho_{e^-}$$
$$= 0,$$

$$i8 \left(\epsilon^{\alpha\beta\delta\epsilon} p_{\nu_\mu,\delta} p'_{\nu_\mu,\epsilon} \right) \times i8 \left(1 - 4s_W^2 \right) \epsilon_{\alpha\beta\kappa\rho} p^\kappa_{e^-} p'^\rho_{e^-}$$
$$= -64 \left(1 - 4s_W^2 \right) \left[-2 \left(\delta^\delta_\kappa \delta^\epsilon_\rho - \delta^\delta_\rho \delta^\epsilon_\kappa \right) \right] p_{\nu_\mu,\delta} p'_{\nu_\mu,\epsilon} p^\kappa_{e^-} p'^\rho_{e^-}$$
$$= 64 \left(1 - 4s_W^2 \right) \left[2 \left(p_{\nu_\mu} \cdot p_{e^-} \right) \left(p'_{\nu_\mu} \cdot p'_{e^-} \right) - 2 \left(p_{\nu_\mu} \cdot p'_{e^-} \right) \left(p'_{\nu_\mu} \cdot p_{e^-} \right) \right],$$

$$-8 \left[p^\alpha_{\nu_\mu} p'^\beta_{\nu_\mu} + p^\beta_{\nu_\mu} p'^\alpha_{\nu_\mu} - g^{\alpha\beta} \left(p_{\nu_\mu} \cdot p'_{\nu_\mu} \right) \right] \times 8m_e^2 \left(4s_W^2 - 8s_W^4 \right) g_{\alpha\beta}$$
$$= 64m_e^2 \left(4s_W^2 - 8s_W^4 \right) \left[2 \left(p_{\nu_\mu} \cdot p'_{\nu_\mu} \right) \right].$$

$$\boxed{\nu_\mu + e^- \rightarrow \nu_e + \mu^-}$$

Piecewise Contraction of Muon Tensor and Electron Tensor

$$8 \left(p^\alpha_{\nu_\mu} p'^\beta_{\mu^-} \right) \times 8 \left[p_{e^-,\alpha} p'_{\nu_e,\beta} + p_{e^-,\beta} p'_{\nu_e,\alpha} - g_{\alpha\beta} \left(p_{e^-} \cdot p'_{\nu_e} \right) \right]$$
$$= 64 \left[\left(p_{\nu_\mu} \cdot p_{e^-} \right) \left(p'_{\mu^-} \cdot p'_{\nu_e} \right) + \left(p_{\nu_\mu} \cdot p'_{\nu_e} \right) \left(p'_{\mu^-} \cdot p_{e^-} \right) - \left(p_{\nu_\mu} \cdot p'_{\mu^-} \right) \left(p_{e^-} \cdot p'_{\nu_e} \right) \right],$$

$$8 \left(p^\beta_{\nu_\mu} p'^\alpha_{\mu^-} \right) \times 8 \left[p_{e^-,\alpha} p'_{\nu_e,\beta} + p_{e^-,\beta} p'_{\nu_e,\alpha} - g_{\alpha\beta} \left(p_{e^-} \cdot p'_{\nu_e} \right) \right]$$
$$= 64 \left[\left(p_{\nu_\mu} \cdot p_{e^-} \right) \left(p'_{\mu^-} \cdot p'_{\nu_e} \right) + \left(p_{\nu_\mu} \cdot p'_{\nu_e} \right) \left(p'_{\mu^-} \cdot p_{e^-} \right) - \left(p_{\nu_\mu} \cdot p'_{\mu^-} \right) \left(p_{e^-} \cdot p'_{\nu_e} \right) \right],$$

$$-8g^{\alpha\beta} \left(p_{\nu_\mu} \cdot p'_{\mu^-} \right) \times 8 \left[p_{e^-,\alpha} p'_{\nu_e,\beta} + p_{e^-,\beta} p'_{\nu_e,\alpha} - g_{\alpha\beta} \left(p_{e^-} \cdot p'_{\nu_e} \right) \right]$$
$$= 64 \left[2 \left(p_{\nu_\mu} \cdot p'_{\mu^-} \right) \left(p_{e^-} \cdot p'_{\nu_e} \right) \right],$$

$$-i8 \left(\epsilon^{\alpha\beta\delta\epsilon} p_{\nu_\mu,\delta} p'_{\mu^-,\epsilon} \right) \times 8 \left[p_{e^-,\alpha} p'_{\nu_e,\beta} + p_{e^-,\beta} p'_{\nu_e,\alpha} - g_{\alpha\beta} \left(p_{e^-} \cdot p'_{\nu_e} \right) \right]$$
$$= 0,$$

$$-i8 \left[p^\alpha_{\nu_\mu} p'^\beta_{\mu^-} + p^\beta_{\nu_\mu} p'^\alpha_{\mu^-} - g^{\alpha\beta} \left(p_{\nu_\mu} \cdot p'_{\mu^-} \right) \right] \times 8 \left(\epsilon_{\alpha\beta\kappa\rho} p^\kappa_{e^-} p'^\rho_{\nu_e} \right)$$
$$= 0,$$

$$i8 \left(\epsilon^{\alpha\beta\delta\epsilon} p_{\nu_\mu,\delta} p'_{\mu^-,\epsilon} \right) \times i8 \epsilon_{\alpha\beta\kappa\rho} p^\kappa_{e^-} p'^\rho_{\nu_e}$$
$$= -64 \left[-2 \left(\delta^\delta_\kappa \delta^\epsilon_\rho - \delta^\delta_\rho \delta^\epsilon_\kappa \right) \right] p_{\nu_\mu,\delta} p'_{\mu^-,\epsilon} p^\kappa_{e^-} p'^\rho_{\nu_e}$$
$$= 64 \left[2 \left(p_{\nu_\mu} \cdot p_{e^-} \right) \left(p'_{\mu^-} \cdot p'_{\nu_e} \right) - 2 \left(p_{\nu_\mu} \cdot p'_{\nu_e} \right) \left(p'_{\mu^-} \cdot p_{e^-} \right) \right].$$

B.2. Semileptonic Reactions

$$\boxed{\nu_e + n \to p + e^-}$$

Vector Element $H_{VV}^{\alpha\beta}$

$$
\begin{aligned}
\sum_{s,s'} H_{VV}^{\alpha\beta} &= G_V^2 Tr\left[\gamma^\alpha \left(\gamma^\delta p_{n,\delta}^* + m_n^*\right)\gamma^\beta \left(\gamma^\epsilon p_{p,\epsilon}^* + m_p^*\right)\right] \\
&= G_V^2 p_{n,\delta}^* p_{p,\epsilon}^* Tr\left[\gamma^\alpha\gamma^\delta\gamma^\beta\gamma^\epsilon\right] + G_V^2 m_n^* m_p^* Tr\left[\gamma^\alpha\gamma^\beta\right] \\
&= 4G_V^2 \left[p_n^{*\alpha}p_p^{*\beta} + p_n^{*\beta}p_p^{*\alpha} - g^{\alpha\beta}\left(p_n^* \cdot p_p^*\right) + g^{\alpha\beta}m_n^* m_p^*\right].
\end{aligned}
$$

Axialvector Element $H_{AA}^{\alpha\beta}$

$$
\begin{aligned}
\sum_{s,s'} H_{AA}^{\alpha\beta} &= G_A^2 Tr\left[\gamma^\alpha\gamma_5 \left(\gamma^\delta p_{n,\delta}^* + m_n^*\right)\gamma^\beta\gamma_5 \left(\gamma^\epsilon p_{p,\epsilon}^* + m_p^*\right)\right] \\
&= G_A^2 p_{n,\delta}^* p_{p,\epsilon}^* Tr\left[\gamma^\alpha\gamma^\delta\gamma^\beta\gamma^\epsilon\right] - G_A^2 m_n^* m_p^* Tr\left[\gamma^\alpha\gamma^\beta\right] \\
&= 4G_A^2 \left[p_n^{*\alpha}p_p^{*\beta} + p_n^{*\beta}p_p^{*\alpha} - g^{\alpha\beta}\left(p_n^* \cdot p_p^*\right) - g^{\alpha\beta}m_n^* m_p^*\right].
\end{aligned}
$$

Vector-Axialvector Element $H_{VA}^{\alpha\beta}$

$$
\begin{aligned}
\sum_{s,s'} H_{VA}^{\alpha\beta} &= -G_V G_A Tr\left[\gamma^\alpha \left(\gamma^\delta p_{n,\delta}^* + m_n^*\right)\gamma^\beta\gamma_5 \left(\gamma^\epsilon p_{p,\epsilon}^* + m_p^*\right)\right] \\
&\quad - G_V G_A Tr\left[\gamma^\alpha\gamma_5 \left(\gamma^\delta p_{n,\delta}^* + m_n^*\right)\gamma^\beta \left(\gamma^\epsilon p_{p,\epsilon}^* + m_p^*\right)\right] \\
&= G_V G_A Tr\left[\gamma_5\gamma^\alpha \left(\gamma^\delta p_{n,\delta}^* - m_n^*\right)\gamma^\beta \left(\gamma^\epsilon p_{p,\epsilon}^* + m_p^*\right)\right] \\
&\quad G_V G_A Tr\left[\gamma_5\gamma^\alpha \left(\gamma^\delta p_{n,\delta}^* + m_n^*\right)\gamma^\beta \left(\gamma^\epsilon p_{p,\epsilon}^* + m_p^*\right)\right] \\
&= 2G_V G_A p_{n,\delta}^* p_{p,\epsilon}^* Tr\left[\gamma_5\gamma^\alpha\gamma^\delta\gamma^\beta\gamma^\epsilon\right] = 8iG_V G_A p_{n,\delta}^* p_{p,\epsilon}^* \epsilon^{\alpha\delta\beta\epsilon} = -8iG_V G_A p_{n,\delta}^* p_{p,\epsilon}^* \epsilon^{\alpha\beta\delta\epsilon}.
\end{aligned}
$$

Vector-Tensor Element $H_{VF}^{\alpha\beta}$

$$
\begin{aligned}
\sum_{s,s'} H_{VF}^{\alpha\beta} &= \frac{iG_V F_2}{2m_N}\left\{-Tr\left[\gamma^\alpha \left(\gamma^\delta p_{n,\delta}^* + m_n^*\right)\sigma^{\beta\lambda}q_\lambda \left(\gamma^\epsilon p_{p,\epsilon}^* + m_p^*\right)\right]\right. \\
&\quad \left. + Tr\left[\sigma^{\alpha\eta}q_\eta \left(\gamma^\delta p_{n,\delta}^* + m_n^*\right)\gamma^\beta \left(\gamma^\epsilon p_{p,\epsilon}^* + m_p^*\right)\right]\right\} \\
&= \frac{iG_V F_2}{2m_N}\left\{-p_{n,\delta}^* q_\lambda m_p^* Tr\left[\gamma^\alpha\gamma^\delta\sigma^{\beta\lambda}\right] - p_{p,\epsilon}^* q_\lambda m_n^* Tr\left[\gamma^\alpha\sigma^{\beta\lambda}\gamma^\epsilon\right]\right. \\
&\quad \left. + p_{n,\delta}^* q_\eta m_p^* Tr\left[\sigma^{\alpha\eta}\gamma^\delta\gamma^\beta\right] + p_{p,\epsilon}^* q_\eta m_n^* Tr\left[\sigma^{\alpha\eta}\gamma^\beta\gamma^\epsilon\right]\right\} \\
&= \frac{iG_V F_2}{2m_N}\left\{p_{n,\delta}^* q_\lambda m_p^* \left(Tr\left[\sigma^{\alpha\lambda}\gamma^\delta\gamma^\beta\right] - Tr\left[\gamma^\alpha\gamma^\delta\sigma^{\beta\lambda}\right]\right)\right. \\
&\quad \left. + p_{p,\delta}^* q_\lambda m_n^* \left(Tr\left[\sigma^{\alpha\lambda}\gamma^\beta\gamma^\delta\right] - Tr\left[\gamma^\alpha\sigma^{\beta\lambda}\gamma^\delta\right]\right)\right\}.
\end{aligned}
$$

By permutation of arguments in the traces and applying the corresponding rules for traces from sec.A one finds then

$$
\sum_{s,s'} H_{VF}^{\alpha\beta} = \frac{iG_V F_2}{2m_N} \left\{ p_{n,\delta}^* q_\lambda m_p^* \left(Tr\left[\sigma^{\alpha\lambda} \gamma^\delta \gamma^\beta \right] - Tr\left[\sigma^{\beta\lambda} \gamma^\alpha \gamma^\delta \right] \right) \right.
$$
$$
\left. + p_{p,\delta}^* q_\lambda m_n^* \left(Tr\left[\sigma^{\alpha\lambda} \gamma^\beta \gamma^\delta \right] - Tr\left[\sigma^{\beta\lambda} \gamma^\delta \gamma^\alpha \right] \right) \right\}
$$
$$
= -\frac{2G_V F_2}{m_N} \left\{ p_{n,\delta}^* q_\lambda m_p^* \left(-g^{\alpha\delta} g^{\beta\lambda} + g^{\alpha\beta} g^{\delta\lambda} + g^{\alpha\beta} g^{\delta\lambda} - g^{\alpha\lambda} g^{\beta\delta} \right) \right.
$$
$$
\left. + p_{p,\delta}^* q_\lambda m_n^* \left(-g^{\alpha\beta} g^{\delta\lambda} + g^{\alpha\delta} g^{\beta\lambda} + g^{\alpha\lambda} g^{\beta\delta} - g^{\alpha\beta} g^{\delta\lambda} \right) \right\}
$$
$$
= -\frac{2G_V F_2}{m_N} \left\{ q_\lambda \left(p_{n,\delta}^* m_p^* - p_{p,\delta}^* m_n^* \right) \left(2g^{\alpha\beta} g^{\delta\lambda} - g^{\alpha\delta} g^{\beta\lambda} - g^{\alpha\lambda} g^{\beta\delta} \right) \right\}
$$
$$
= \frac{2G_V F_2}{m_N} \left\{ 2g^{\alpha\beta} \left[m_n^* (q\cdot p_p^*) - m_p^* (q\cdot p_n^*) \right] + q^\beta \left(p_n^{*\alpha} m_p^* - p_p^{*\alpha} m_n^* \right) + q^\alpha \left(p_n^{*\beta} m_p^* - p_p^{*\beta} m_n^* \right) \right\}.
$$

Axialvector-Tensor Element $H_{AF}^{\alpha\beta}$

$$
\sum_{s,s'} H_{AF}^{\alpha\beta} = -\frac{iG_A F_2}{2m_N} \left\{ -Tr\left[\gamma^\alpha \gamma_5 \left(\gamma^\delta p_{n,\delta}^* + m_n^* \right) \sigma^{\beta\lambda} q_\lambda \left(\gamma^\epsilon p_{p,\epsilon}^* + m_p^* \right) \right] \right.
$$
$$
\left. + Tr\left[\sigma^{\alpha\eta} q_\eta \left(\gamma^\delta p_{n,\delta}^* + m_n^* \right) \gamma^\beta \gamma_5 \left(\gamma^\epsilon p_{p,\epsilon}^* + m_p^* \right) \right] \right\}.
$$

Proceeding analogous to $H_{VF}^{\alpha\beta}$ one finds

$$
\sum_{s,s'} H_{AF}^{\alpha\beta} = -\frac{iG_A F_2}{2m_N} \left\{ p_{n,\delta}^* q_\lambda m_p^* \left(Tr\left[\sigma^{\alpha\lambda} \gamma^\delta \gamma^\beta \gamma_5 \right] - Tr\left[\gamma^\alpha \gamma_5 \gamma^\delta \sigma^{\beta\lambda} \right] \right) \right.
$$
$$
\left. + p_{p,\delta}^* q_\lambda m_n^* \left(Tr\left[\sigma^{\alpha\lambda} \gamma^\beta \gamma_5 \gamma^\delta \right] - Tr\left[\gamma^\alpha \gamma_5 \sigma^{\beta\lambda} \gamma^\delta \right] \right) \right\}
$$
$$
= -\frac{iG_A F_2}{2m_N} \left\{ p_{n,\delta}^* q_\lambda m_p^* \left(Tr\left[\gamma_5 \sigma^{\alpha\lambda} \gamma^\delta \gamma^\beta \right] + Tr\left[\gamma_5 \gamma^\alpha \gamma^\delta \sigma^{\beta\lambda} \right] \right) \right.
$$
$$
\left. + p_{p,\delta}^* q_\lambda m_n^* \left(-Tr\left[\gamma_5 \sigma^{\alpha\lambda} \gamma^\beta \gamma^\delta \right] + Tr\left[\gamma_5 \gamma^\alpha \sigma^{\beta\lambda} \gamma^\delta \right] \right) \right\}
$$
$$
= \frac{2iG_A F_2}{m_N} \left\{ p_{n,\delta}^* q_\lambda m_p^* \left(\epsilon^{\alpha\lambda\delta\beta} + \epsilon^{\alpha\delta\beta\lambda} \right) + p_{p,\delta}^* q_\lambda m_n^* \left(-\epsilon^{\alpha\lambda\beta\delta} + \epsilon^{\alpha\beta\lambda\delta} \right) \right\}
$$
$$
= -\frac{4iG_A F_2}{m_N} \left(p_{n,\delta}^* q_\lambda m_p^* + p_{p,\delta}^* q_\lambda m_n^* \right) \epsilon^{\alpha\beta\delta\lambda}.
$$

Tensor Element $H_{FF}^{\alpha\beta}$

$$
\sum_{s,s'} H_{FF}^{\alpha\beta} = \frac{F_2^2}{4m_N^2} q_\eta q_\lambda Tr\left[\sigma^{\alpha\eta} \left(\gamma^\delta p_{n,\delta}^* + m_n^* \right) \sigma^{\beta\lambda} \left(\gamma^\epsilon p_{p,\epsilon}^* + m_p^* \right) \right]
$$
$$
= \frac{F_2^2}{4m_N^2} q_\eta q_\lambda \left\{ m_n^* m_p^* Tr\left[\sigma^{\alpha\eta} \sigma^{\beta\lambda} \right] + p_{n,\delta}^* p_{p,\epsilon}^* Tr\left[\sigma^{\alpha\eta} \gamma^\delta \sigma^{\beta\lambda} \gamma^\epsilon \right] \right\}
$$
$$
= \frac{F_2^2}{m_N^2} q_\eta q_\lambda \left\{ m_n^* m_p^* \left(g^{\alpha\beta} g^{\eta\lambda} - g_{\alpha\lambda} g_{\beta\eta} \right) + p_{n,\delta}^* p_{p,\epsilon}^* \times \right.
$$
$$
\left[g^{\alpha\delta} \left(g^{\beta\eta} g^{\epsilon\lambda} - g^{\eta\lambda} g^{\beta\epsilon} \right) - g^{\alpha\beta} \left(g^{\delta\eta} g^{\epsilon\lambda} - g^{\eta\lambda} g^{\delta\epsilon} + g^{\epsilon\eta} g^{\delta\lambda} \right) \right.
$$
$$
\left. \left. + g^{\alpha\lambda} \left(g^{\delta\eta} g^{\beta\epsilon} - g^{\beta\eta} g^{\delta\epsilon} + g^{\epsilon\eta} g^{\beta\delta} \right) + g^{\alpha\epsilon} \left(g^{\beta\eta} g^{\delta\lambda} - g^{\eta\lambda} g^{\beta\delta} \right) \right] \right\},
$$

$$\sum_{s,s'} H_{FF}^{\alpha\beta} = \frac{F_2^2}{m_N^2} \left\{ m_n^* m_p^* \left(g^{\alpha\beta} q^2 - q^\alpha q^\beta \right) + \left[p_n^{*\alpha} q^\beta \left(p_p^* \cdot q \right) - p_n^{*\alpha} p_p^{*\beta} q^2 - g^{\alpha\beta} \left(p_n^* \cdot q \right) \left(p_p^* \cdot q \right) \right. \right.$$

$$+ g^{\alpha\beta} \left(p_n^* \cdot p_p^* \right) q^2 - g^{\alpha\beta} \left(p_n^* \cdot q \right) \left(p_p^* \cdot q \right) + q^\alpha p_p^{*\beta} \left(p_n^* \cdot q \right) - q^\alpha q^\beta \left(p_n^* \cdot p_p^* \right)$$

$$\left. \left. + q^\alpha p_n^{*\beta} \left(p_p^* \cdot q \right) + p_p^{*\alpha} q^\beta \left(p_n^* \cdot q \right) - p_p^{*\alpha} p_n^{*\beta} q^2 \right] \right\}$$

$$= \frac{F_2^2}{m_N^2} \left\{ m_n^* m_p^* \left(g^{\alpha\beta} q^2 - q^\alpha q^\beta \right) + \left(g^{\alpha\beta} \left[\left(p_n^* \cdot p_p^* \right) q^2 - 2 \left(p_n^* \cdot q \right) \left(p_p^* \cdot q \right) \right] \right. \right.$$

$$+ p_n^{*\alpha} \left[q^\beta \left(p_p^* \cdot q \right) - p_p^{*\beta} q^2 \right] + p_p^{*\alpha} \left[q^\beta \left(p_n^* \cdot q \right) - p_n^{*\beta} q^2 \right]$$

$$\left. \left. + q^\alpha \left[p_n^{*\beta} \left(p_p^* \cdot q \right) + p_p^{*\beta} \left(p_n^* \cdot q \right) - q^\beta \left(p_n^* \cdot p_p^* \right) \right] \right) \right\} .$$

Piecewise Contraction of Vector Matrix Element $\left\langle |M|^2 \right\rangle_{VV}$ and Axialvector Matrix Element $\left\langle |M|^2 \right\rangle_{AA}$

$$4 G_V^2 p_n^{*\alpha} p_p^{*\beta} \times 8 \left[p_{\nu_e,\alpha} p_{e^-,\beta} + p_{\nu_e,\beta} p_{e^-,\alpha} - g_{\alpha\beta} \left(p_{\nu_e} \cdot p_{e^-} \right) - i \epsilon_{\alpha\beta\kappa\rho} p_{\nu_e}^\kappa p_{e^-}^\rho \right]$$

$$= 32 G_V^2 \left[\left(p_n^* \cdot p_{\nu_e} \right) \left(p_p^* \cdot p_{e^-} \right) + \left(p_n^* \cdot p_{e^-} \right) \left(p_p^* \cdot p_{\nu_e} \right) - \left(p_n^* \cdot p_p^* \right) \left(p_{\nu_e} \cdot p_{e^-} \right) \right] ,$$

$$4 G_V^2 p_p^{*\alpha} p_n^{*\beta} \times 8 \left[p_{\nu_e,\alpha} p_{e^-,\beta} + p_{\nu_e,\beta} p_{e^-,\alpha} - g_{\alpha\beta} \left(p_{\nu_e} \cdot p_{e^-} \right) - i \epsilon_{\alpha\beta\kappa\rho} p_{\nu_e}^\kappa p_{e^-}^\rho \right]$$

$$= 32 G_V^2 \left[\left(p_n^* \cdot p_{\nu_e} \right) \left(p_p^* \cdot p_{e^-} \right) + \left(p_n^* \cdot p_{e^-} \right) \left(p_p^* \cdot p_{\nu_e} \right) - \left(p_n^* \cdot p_p^* \right) \left(p_{\nu_e} \cdot p_{e^-} \right) \right] ,$$

$$- 4 G_V^2 g^{\alpha\beta} \left(p_n^* \cdot p_p^* \right) \times 8 \left[p_{\nu_e,\alpha} p_{e^-,\beta} + p_{\nu_e,\beta} p_{e^-,\alpha} - g_{\alpha\beta} \left(p_{\nu_e} \cdot p_{e^-} \right) - i \epsilon_{\alpha\beta\kappa\rho} p_{\nu_e}^\kappa p_{e^-}^\rho \right]$$

$$= 64 G_V^2 \left(p_n^* \cdot p_p^* \right) \left(p_{\nu_e} \cdot p_{e^-} \right) ,$$

$$4 G_V^2 g^{\alpha\beta} m_n^* m_p^* \times 8 \left[p_{\nu_e,\alpha} p_{e^-,\beta} + p_{\nu_e,\beta} p_{e^-,\alpha} - g_{\alpha\beta} \left(p_{\nu_e} \cdot p_{e^-} \right) - i \epsilon_{\alpha\beta\kappa\rho} p_{\nu_e}^\kappa p_{e^-}^\rho \right]$$

$$= - 64 G_V^2 m_n^* m_p^* \left(p_{\nu_e} \cdot p_{e^-} \right) .$$

Summing all terms up, the matrix element becomes

$$\frac{4 \left\langle |M|^2 \right\rangle_{VV}}{G_F^2 V_{ud}^2} = 64 G_V^2 \left[\left(p_n^* \cdot p_{\nu_e} \right) \left(p_p^* \cdot p_{e^-} \right) + \left(p_n^* \cdot p_{e^-} \right) \left(p_p^* \cdot p_{\nu_e} \right) - m_n^* m_p^* \left(p_{\nu_e} \cdot p_{e^-} \right) \right] .$$

For the element $\left\langle |M|^2 \right\rangle_{AA}$ the only difference arises from the sign of the $m_n^* m_p^*$-term.

$$\frac{4 \left\langle |M|^2 \right\rangle_{AA}}{G_F^2 V_{ud}^2} = 64 G_A^2 \left[\left(p_n^* \cdot p_{\nu_e} \right) \left(p_p^* \cdot p_{e^-} \right) + \left(p_n^* \cdot p_{e^-} \right) \left(p_p^* \cdot p_{\nu_e} \right) + m_n^* m_p^* \left(p_{\nu_e} \cdot p_{e^-} \right) \right] .$$

Contraction of Vector-Axialvector Matrix Element $\left\langle |M|^2 \right\rangle_{VA}$

$$\frac{4 \left\langle |M|^2 \right\rangle_{AA}}{G_F^2 V_{ud}^2} = - 8 i G_V G_A p_{n,\delta}^* p_{p,\epsilon}^* \epsilon^{\alpha\beta\delta\epsilon} \times 8 \left[p_{\nu_e,\alpha} p_{e^-,\beta} + p_{\nu_e,\beta} p_{e^-,\alpha} - g_{\alpha\beta} \left(p_{\nu_e} \cdot p_{e^-} \right) - i \epsilon_{\alpha\beta\kappa\rho} p_{\nu_e}^\kappa p_{e^-}^\rho \right]$$

$$= - 64 G_V G_A p_{n,\delta}^* p_{p,\epsilon}^* p_{\nu_e}^\kappa p_{e^-}'^\rho \left[-2 \left(\delta_\delta^\kappa \delta_\epsilon^\rho - \delta_\delta^\rho \delta_\epsilon^\kappa \right) \right]$$

$$= 128 G_V G_A \left[\left(p_n^* \cdot p_{\nu_e} \right) \left(p_p^* \cdot p_{e^-} \right) - \left(p_n^* \cdot p_{e^-} \right) \left(p_p^* \cdot p_{\nu_e} \right) \right] .$$

Piecewise Contraction of Vector-Tensor Matrix Element $\left\langle |M|^2 \right\rangle_{VF}$

$$\frac{4G_V F_2}{m_N} g^{\alpha\beta} \left[m_n^* \left(q \cdot p_p^* \right) - m_p^* \left(q \cdot p_n^* \right) \right] \times 8 \left[p_{\nu_e,\alpha} p_{e^-,\beta} + p_{\nu_e,\beta} p_{e^-,\alpha} - g_{\alpha\beta} \left(p_{\nu_e} \cdot p_{e^-} \right) - i\epsilon_{\alpha\beta\kappa\rho} p_{\nu_e}^\kappa p_{e^-}^\rho \right]$$

$$= \frac{64 G_V F_2}{m_N} \left(p_{\nu_e} \cdot p_{e^-} \right) \left[m_p^* \left(q \cdot p_n^* \right) - m_n^* \left(q \cdot p_p^* \right) \right],$$

$$\frac{2G_V F_2}{m_N} q^\beta \left(p_n^{*\alpha} m_p^* - p_p^{*\alpha} m_n^* \right) \times 8 \left[p_{\nu_e,\alpha} p_{e^-,\beta} + p_{\nu_e,\beta} p_{e^-,\alpha} - g_{\alpha\beta} \left(p_{\nu_e} \cdot p_{e^-} \right) - i\epsilon_{\alpha\beta\kappa\rho} p_{\nu_e}^\kappa p_{e^-}^\rho \right]$$

$$= \frac{16 G_V F_2}{m_N} \left\{ \left[\left(p_n^* \cdot p_{\nu_e} \right) m_p^* - \left(p_p^* \cdot p_{\nu_e} \right) m_n^* \right] \left(p_{e^-} \cdot q \right) + \left[\left(p_n^* \cdot p_{e^-} \right) m_p^* - \left(p_p^* \cdot p_{e^-} \right) m_n^* \right] \left(p_{\nu_e} \cdot q \right) \right.$$

$$\left. + \left[\left(p_p^* \cdot q \right) m_n^* - \left(p_n^* \cdot q \right) m_p^* \right] \left(p_{\nu_e} \cdot p_{e^-} \right) \right\},$$

$$\frac{2G_V F_2}{m_N} q^\alpha \left(p_n^{*\beta} m_p^* - p_p^{*\beta} m_n^* \right) \times 8 \left[p_{\nu_e,\alpha} p_{e^-,\beta} + p_{\nu_e,\beta} p_{e^-,\alpha} - g_{\alpha\beta} \left(p_{\nu_e} \cdot p_{e^-} \right) - i\epsilon_{\alpha\beta\kappa\rho} p_{\nu_e}^\kappa p_{e^-}^\rho \right]$$

$$= \frac{16 G_V F_2}{m_N} \left\{ \left[\left(p_n^* \cdot p_{\nu_e} \right) m_p^* - \left(p_p^* \cdot p_{\nu_e} \right) m_n^* \right] \left(p_{e^-} \cdot q \right) + \left[\left(p_n^* \cdot p_{e^-} \right) m_p^* - \left(p_p^* \cdot p_{e^-} \right) m_n^* \right] \left(p_{\nu_e} \cdot q \right) \right.$$

$$\left. + \left[\left(p_p^* \cdot q \right) m_n^* - \left(p_n^* \cdot q \right) m_p^* \right] \left(p_{\nu_e} \cdot p_{e^-} \right) \right\}.$$

Summing all terms up, the matrix element becomes

$$\frac{4 \left\langle |M|^2 \right\rangle_{VF}}{G_F^2 V_{ud}^2} = \frac{32 G_V F_2}{m_N} \left\{ \left[\left(p_n^* \cdot p_{\nu_e} \right) m_p^* - \left(p_p^* \cdot p_{\nu_e} \right) m_n^* \right] \left(p_{e^-} \cdot q \right) \right.$$

$$\left. + \left[\left(p_n^* \cdot p_{e^-} \right) m_p^* - \left(p_p^* \cdot p_{e^-} \right) m_n^* \right] \left(p_{\nu_e} \cdot q \right) + \left[\left(p_n^* \cdot q \right) m_p^* - \left(p_p^* \cdot q \right) m_n^* \right] \left(p_{\nu_e} \cdot p_{e^-} \right) \right\}.$$

Replacing further the momentum transfer by $q = p_{\nu_e} - p_{e^-}$ this can be transformed into.

$$\frac{4 \left\langle |M|^2 \right\rangle_{VF}}{G_F^2 V_{ud}^2} = \frac{32 G_V F_2}{m_N} \left\{ 2 \left[\left(p_n^* \cdot p_{\nu_e} \right) m_p^* - \left(p_p^* \cdot p_{\nu_e} \right) m_n^* - \left(p_n^* \cdot p_{e^-} \right) m_p^* + \left(p_p^* \cdot p_{e^-} \right) m_n^* \right] \left(p_{\nu_e} \cdot p_{e^-} \right) \right.$$

$$\left. - \left[\left(p_n^* \cdot p_{\nu_e} \right) m_p^* - \left(p_p^* \cdot p_{\nu_e} \right) m_n^* \right] m_e^2 \right\}.$$

Contraction of Axialvector-Tensor Matrix Element $\left\langle |M|^2 \right\rangle_{AF}$

$$\frac{4 \left\langle |M|^2 \right\rangle_{AF}}{G_F^2 V_{ud}^2}$$

$$= \frac{-4i G_A F_2}{m_N} \left(p_{n,\delta}^* q_\lambda m_p^* + p_{p,\delta}^* q_\lambda m_n^* \right) \epsilon^{\alpha\beta\delta\lambda} \times 8 \left[p_{\nu_e,\alpha} p_{e^-,\beta} + p_{\nu_e,\beta} p_{e^-,\alpha} - g_{\alpha\beta} \left(p_{\nu_e} \cdot p_{e^-} \right) - i\epsilon_{\alpha\beta\kappa\rho} p_{\nu_e}^\kappa p_{e^-}^\rho \right]$$

$$= \frac{-32 G_A F_2}{m_N} \left(p_{n,\delta}^* m_p^* + p_{p,\delta}^* m_n^* \right) q_\lambda p_{\nu_e}^\kappa p_{e^-}^{\prime\rho} \left[-2 \left(\delta_\delta^\kappa \delta_\lambda^\rho - \delta_\delta^\rho \delta_\lambda^\kappa \right) \right]$$

$$= \frac{64 G_A F_2}{m_N} \left\{ \left[\left(p_n^* \cdot p_{\nu_e} \right) m_p^* + \left(p_p^* \cdot p_{\nu_e} \right) m_n^* \right] \left(p_{e^-} \cdot q \right) - \left[\left(p_n^* \cdot p_{e^-} \right) m_p^* + \left(p_p^* \cdot p_{e^-} \right) m_n^* \right] \left(p_{\nu_e} \cdot q \right) \right\}.$$

Replacing again $q = p_{\nu_e} - p_{e^-}$ the alternative notation reads

$$\frac{4 \left\langle |M|^2 \right\rangle_{AF}}{G_F^2 V_{ud}^2} = \frac{64 G_A F_2}{m_N} \left\{ \left[\left(p_n^* \cdot p_{\nu_e} \right) m_p^* + \left(p_p^* \cdot p_{\nu_e} \right) m_n^* + \left(p_n^* \cdot p_{e^-} \right) m_p^* + \left(p_p^* \cdot p_{e^-} \right) m_n^* \right] \left(p_{\nu_e} \cdot p_{e^-} \right) \right.$$

$$\left. - \left[\left(p_n^* \cdot p_{\nu_e} \right) m_p^* + \left(p_p^* \cdot p_{\nu_e} \right) m_n^* \right] m_e^2 \right\}.$$

Piecewise Contraction of Tensor Matrix Element $\left\langle |M|^2 \right\rangle_{FF}$

$$\frac{F_2^2}{m_N^2} m_n^* m_p^* \left(g^{\alpha\beta} q^2 - q^\alpha q^\beta \right) \times 8 \left[p_{\nu_e,\alpha} p_{e^-,\beta} + p_{\nu_e,\beta} p_{e^-,\alpha} - g_{\alpha\beta} \left(p_{\nu_e} \cdot p_{e^-} \right) - i\epsilon_{\alpha\beta\kappa\rho} p_{\nu_e}^\kappa p_{e^-}^\rho \right]$$

$$= -\frac{8F_2^2}{m_N^2} m_n^* m_p^* \left[q^2 \left(p_{\nu_e} \cdot p'_{e^-} \right) + 2 \left(p_{\nu_e} \cdot q \right) \left(p_{e^-} \cdot q \right) \right],$$

$$\frac{F_2^2}{m_N^2} g^{\alpha\beta} \left[\left(p_n^* \cdot p_p^* \right) q^2 - 2 \left(p_n^* \cdot q \right) \left(p_p^* \cdot q \right) \right] \times 8 \left[p_{\nu_e,\alpha} p_{e^-,\beta} + p_{\nu_e,\beta} p_{e^-,\alpha} - g_{\alpha\beta} \left(p_{\nu_e} \cdot p_{e^-} \right) - i\epsilon_{\alpha\beta\kappa\rho} p_{\nu_e}^\kappa p_{e^-}^\rho \right]$$

$$= \frac{16F_2^2}{m_N^2} \left[2 \left(p_n^* \cdot q \right) \left(p_p^* \cdot q \right) - \left(p_n^* \cdot p_p^* \right) q^2 \right] \left(p_{\nu_e} \cdot p_{e^-} \right),$$

$$\frac{F_2^2}{m_N^2} p_n^{*\alpha} \left[q^\beta \left(p_p^* \cdot q \right) - p_p^{*\beta} q^2 \right] \times 8 \left[p_{\nu_e,\alpha} p_{e^-,\beta} + p_{\nu_e,\beta} p_{e^-,\alpha} - g_{\alpha\beta} \left(p_{\nu_e} \cdot p_{e^-} \right) - i\epsilon_{\alpha\beta\kappa\rho} p_{\nu_e}^\kappa p_{e^-}^\rho \right]$$

$$= \frac{8F_2^2}{m_N^2} \left[\left(p_n^* \cdot p_{\nu_e} \right) \left(p_p^* \cdot q \right) \left(p_{e^-} \cdot q \right) - \left(p_n^* \cdot p_{\nu_e} \right) \left(p_p^* \cdot p_{e^-} \right) q^2 + \left(p_n^* \cdot p_{e^-} \right) \left(p_p^* \cdot q \right) \left(p_{\nu_e} \cdot q \right) \right.$$

$$\left. - \left(p_n^* \cdot p_{e^-} \right) \left(p_p^* \cdot p_{\nu_e} \right) q^2 - \left(p_n^* \cdot q \right) \left(p_p^* \cdot q \right) \left(p_{\nu_e} \cdot p_{e^-} \right) + \left(p_n^* \cdot p_p^* \right) \left(p_{\nu_e} \cdot p_{e^-} \right) q^2 \right],$$

$$\frac{F_2^2}{m_N^2} p_p^{*\alpha} \left[q^\beta \left(p_n^* \cdot q \right) - p_n^{*\beta} q^2 \right] \times 8 \left[p_{\nu_e,\alpha} p_{e^-,\beta} + p_{\nu_e,\beta} p_{e^-,\alpha} - g_{\alpha\beta} \left(p_{\nu_e} \cdot p_{e^-} \right) - i\epsilon_{\alpha\beta\kappa\rho} p_{\nu_e}^\kappa p_{e^-}^\rho \right]$$

$$= \frac{8F_2^2}{m_N^2} \left[\left(p_p^* \cdot p_{\nu_e} \right) \left(p_n^* \cdot q \right) \left(p_{e^-} \cdot q \right) - \left(p_p^* \cdot p_{\nu_e} \right) \left(p_n^* \cdot p_{e^-} \right) q^2 + \left(p_p^* \cdot p_{e^-} \right) \left(p_n^* \cdot q \right) \left(p_{\nu_e} \cdot q \right) \right.$$

$$\left. - \left(p_p^* \cdot p_{e^-} \right) \left(p_n^* \cdot p_{\nu_e} \right) q^2 - \left(p_p^* \cdot q \right) \left(p_n^* \cdot q \right) \left(p_{\nu_e} \cdot p_{e^-} \right) + \left(p_p^* \cdot p_n^* \right) \left(p_{\nu_e} \cdot p_{e^-} \right) q^2 \right],$$

$$\frac{F_2^2}{m_N^2} q^\alpha \left[p_n^{*\beta} \left(p_p^* \cdot q \right) + p_p^{*\beta} \left(p_n^* \cdot q \right) - q^\beta \left(p_n^* \cdot p_p^* \right) \right] \times 8 \left[p_{\nu_e,\alpha} p_{e^-,\beta} + p_{\nu_e,\beta} p_{e^-,\alpha} - g_{\alpha\beta} \left(p_{\nu_e} \cdot p_{e^-} \right) \right.$$

$$\left. - i\epsilon_{\alpha\beta\kappa\rho} p_{\nu_e}^\kappa p_{e^-}^\rho \right]$$

$$= \frac{8F_2^2}{m_N^2} \left[\left(p_n^* \cdot p_{e^-} \right) \left(p_p^* \cdot q \right) \left(p_{\nu_e} \cdot q \right) + \left(p_p^* \cdot p_{e^-} \right) \left(p_n^* \cdot q \right) \left(p_{\nu_e} \cdot q \right) - \left(p_n^* \cdot p_p^* \right) \left(p_{\nu_e} \cdot q \right) \left(p_{e^-} \cdot q \right) \right.$$

$$+ \left(p_n^* \cdot p_{\nu_e} \right) \left(p_p^* \cdot q \right) \left(p_{e^-} \cdot q \right) + \left(p_p^* \cdot p_{\nu_e} \right) \left(p_n^* \cdot q \right) \left(p_{e^-} \cdot q \right) - \left(p_n^* \cdot p_p^* \right) \left(p_{\nu_e} \cdot q \right) \left(p_{e^-} \cdot q \right)$$

$$\left. - 2 \left(p_n^* \cdot q \right) \left(p_p^* \cdot q \right) \left(p_{\nu_e} \cdot p_{e^-} \right) + \left(p_n^* \cdot p_p^* \right) \left(p_{\nu_e} \cdot p_{e^-} \right) q^2 \right].$$

Summing up all terms the tensor matrix element becomes

$$\frac{4 \left\langle |M|^2 \right\rangle_{FF}}{G_F^2 V_{ud}^2} = \frac{8F_2^2}{m_N^2} \left[\left(p_n^* \cdot p_p^* \right) \left(p_{\nu_e} \cdot p_{e^-} \right) q^2 + 2 \left(p_n^* \cdot p_{\nu_e} \right) \left(p_p^* \cdot q \right) \left(p_{e^-} \cdot q \right) \right.$$

$$- 2 \left(p_n^* \cdot p_p^* \right) \left(p_{\nu_e} \cdot q \right) \left(p_{e^-} \cdot q \right) - 2 \left(p_n^* \cdot p_{\nu_e} \right) \left(p_p^* \cdot p_{e^-} \right) q^2 + 2 \left(p_n^* \cdot p_{e^-} \right) \left(p_p^* \cdot q \right) \left(p_{\nu_e} \cdot q \right)$$

$$- 2 \left(p_n^* \cdot p_{e^-} \right) \left(p_p^* \cdot p_{\nu_e} \right) q^2 + 2 \left(p_n^* \cdot q \right) \left(p_p^* \cdot p_{\nu_e} \right) \left(p_{e^-} \cdot q \right) + 2 \left(p_n^* \cdot q \right) \left(p_p^* \cdot p_{e^-} \right) \left(p_{\nu_e} \cdot q \right)$$

$$\left. - m_n^* m_p^* \left[\left(p_{\nu_e} \cdot p_{e^-} \right) q^2 + 2 \left(p_{\nu_e} \cdot q \right) \left(p_{e^-} \cdot q \right) \right] \right].$$

Replacing $q = p_{\nu_e} - p_{e^-}$ and $q^2 = m_e^2 - 2 \left(p_{\nu_e} \cdot p_{e^-} \right)$ an alternative notation reads

$$\frac{4 \left\langle |M|^2 \right\rangle_{FF}}{G_F^2 V_{ud}^2} = \frac{8F_2^2}{m_N^2} \left\{ 4 \left(p_{e^-} \cdot p_{\nu_e} \right) \left[\left(p_n^* \cdot p_{\nu_e} \right) \left(p_p^* \cdot p_{\nu_e} \right) + \left(p_n^* \cdot p_{e^-} \right) \left(p_p^* \cdot p_{e^-} \right) \right] \right.$$

$$\left. - m_e^2 \left[4 \left(p_n^* \cdot p_{\nu_e} \right) \left(p_p^* \cdot p_{\nu_e} \right) + \left(p_n^* \cdot p_p^* \right) \left(p_{\nu_e} \cdot p_{e^-} \right) \right] + m_n^* m_p^* \left[4 \left(p_{\nu_e} \cdot p_{e^-} \right)^2 - 3 \left(p_{\nu_e} \cdot p_{e^-} \right) m_e^2 \right] \right\}.$$

B.3. Semileptonic Matrix Elements for Cross Sections

B.3.1. Capture of Electron Neutrinos

Axialvector-Tensor Matrix Element

First one needs to derive several simple relations between the four-momenta that will then be used to transform the matrix element. The effective proton four momentum p_p^* is given through the four momenta of the other particles by

$$p_p^* = p_p - (U_p, 0) = p_n^* + p_{\nu_e} - p_{e^-} + (\Delta U, 0) \qquad \text{with} \qquad \Delta U = U_n - U_p. \tag{B.1}$$

Using this relation to replace p_p^* one can derive the following equation

$$(p_n^* \cdot p_{\nu_e})(p_p^* \cdot p_{e^-}) - (p_n^* \cdot p_{e^-})(p_p^* \cdot p_{\nu_e}) = [p_n^* \cdot (p_{\nu_e} + p_{e^-})](p_{\nu_e} \cdot p_{e^-}) + (p_n^* \cdot p_{\nu_e})(\Delta U E_e - m_e^2)$$
$$- (p_n^* \cdot p_{e^-}) \Delta U E_{\nu_e}. \tag{B.2}$$

Next one defines the constant Q by

$$Q \equiv \frac{1}{2}\left(m_n^{*2} - m_p^{*2}\right). \tag{B.3}$$

Then the following relation can be derived through four momentum conservation

$$(p_n^* - p_{e^-})^2 = \left[p_p^* - p_{\nu_e} - (\Delta U, 0)\right]^2,$$
$$\Rightarrow (p_n^* \cdot p_{e^-}) = (p_p^* \cdot p_{\nu_e}) + Q + \frac{m_e^2}{2} - \frac{\Delta U^2}{2} + \Delta U\left(E_p^* - E_{\nu_e}\right). \tag{B.4}$$

Using again (B.1) in (B.4) one gets

$$(p_n^* \cdot p_{e^-}) = (p_n^* \cdot p_{\nu_e}) - (p_{\nu_e} \cdot p_{e^-}) + Q + \frac{m_e^2}{2} - \frac{\Delta U^2}{2} + \Delta U\, E_p^*. \tag{B.5}$$

Plugging (B.5) into the RHS of (B.2) one gets

$$(p_n^* \cdot p_{\nu_e})(p_p^* \cdot p_{e^-}) - (p_n^* \cdot p_{e^-})(p_p^* \cdot p_{\nu_e}) = [p_n^* \cdot (p_{\nu_e} + p_{e^-})](p_{\nu_e} \cdot p_{e^-}) \tag{B.6}$$
$$- (p_n^* \cdot p_{\nu_e})\left[m_e^2 + \Delta U\left(E_{\nu_e} - E_{e^-}\right)\right] + (p_{\nu_e} \cdot p_{e^-}) \Delta U E_{\nu_e} - \Delta U E_{\nu_e}\left(Q + \frac{m_e^2}{2} + \Delta U E_p^* - \frac{\Delta U^2}{2}\right).$$

The axialvector-tensor matrix element is given in Eq.(5.3) by

$$\left\langle |M|^2 \right\rangle_{AF} = 16 G_F^2 V_{ud}^2 G_A F_2 \frac{m_N^*}{m_N}\left\{2\left[p_n^* \cdot (p_{\nu_e} + p_{e^-})\right](p_{\nu_e} \cdot p_{e^-}) - 2\left(p_n^* \cdot p_{\nu_e}\right) m_e^2 \right.$$
$$\left. + \Delta U\left[(p_{\nu_e} \cdot p_{e^-})\left(E_{\nu_e} + E_{e^-}\right) - m_e^2 E_{\nu_e}\right]\right\}.$$

Solving (B.6) for $[p_n^* \cdot (p_{\nu_e} + p_{e^-})](p_{\nu_e} \cdot p_{e^-})$ and using the result in $\left\langle |M|^2 \right\rangle_{AF}$, the matrix element becomes

$$\left\langle |M|^2 \right\rangle_{AF} = 16 G_F^2 V_{ud}^2 G_A F_2 \frac{m_N^*}{m_N}\left\{2\left(p_n^* \cdot p_{\nu_e}\right)\left(p_p^* \cdot p_{e^-}\right) - 2\left(p_n^* \cdot p_{e^-}\right)\left(p_p^* \cdot p_{\nu_e}\right)\right. \tag{B.7}$$
$$\left. + 2\left(p_n^* \cdot p_{\nu_e}\right)\left(E_{\nu_e} - E_{e^-}\right)\Delta U + (p_{\nu_e} \cdot p_{e^-})\left(E_{e^-} - E_{\nu_e}\right)\Delta U + \Delta U E_{\nu_e}\left(2Q + 2\Delta U E_p^* + \Delta U^2\right)\right\}.$$

Tensor Matrix Element

The tensor matrix element is given by Eq.(3.17)

$$\frac{\left\langle |M|^2 \right\rangle_{FF}}{2G_F^2 V_{ud}^2 F_2^2 m_N^{-2}} = 4\left(p_{\nu_e} \cdot p_{e-}\right) \left[\left(p_n^* \cdot p_{\nu_e}\right)\left(p_p^* \cdot p_{\nu_e}\right) + \left(p_n^* \cdot p_{e-}\right)\left(p_p^* \cdot p_{e-}\right)\right]$$
$$-m_e^2 \left[4\left(p_n^* \cdot p_{\nu_e}\right)\left(p_p^* \cdot p_{\nu_e}\right) + \left(p_n^* \cdot p_p^*\right)\left(p_{\nu_e} \cdot p_{e-}\right)\right] + m_n^* m_p^* \left[4\left(p_{\nu_e} \cdot p_{e-}\right)^2 - 3\left(p_{\nu_e} \cdot p_{e-}\right)m_e^2\right].$$

To transform it into a more suitable form it is helpfull to derive some additional relations. With (B.1) one finds

$$\left(p_p^* \cdot p_{\nu_e}\right) = \left(p_n^* \cdot p_{\nu_e}\right) - \left(p_{\nu_e} \cdot p_{e-}\right) + \Delta U E_{\nu_e}. \tag{B.8}$$

Another relation that follows from (B.1) is

$$\left(p_n^* \cdot p_p^*\right) = m_n^{*2} + \left(p_n^* \cdot p_{\nu_e}\right) - \left(p_n^* \cdot p_{e-}\right) + \Delta U E_n^*.$$

Now (B.5) can be used on this expression to yield

$$\left(p_n^* \cdot p_p^*\right) = \left(p_{\nu_e} \cdot p_{e-}\right) + \left[m_n^{*2} - Q - \frac{m_e^2}{2} + \frac{\Delta U^2}{2} + \Delta U\left(E_n^* - E_p^*\right)\right]. \tag{B.9}$$

One can derive yet another relation from (B.1)

$$\left(p_p^* \cdot p_{e-}\right) = \left(p_n^* \cdot p_{e-}\right) + \left(p_{\nu_e} \cdot p_{e-}\right) - m_e^2 + \Delta U E_{e-}.$$

Using (B.5) again this transforms into

$$\left(p_p^* \cdot p_{e-}\right) = \left(p_n^* \cdot p_{\nu_e}\right) + Q - \frac{m_e^2}{2} - \frac{\Delta U^2}{2} + \Delta U\left(E_p^* + E_{e-}\right). \tag{B.10}$$

In order to transform the tensor matrix element we define the term A by

$$A \equiv \frac{\left\langle |M|^2 \right\rangle_{FF}}{2G_F^2 V_{ud}^2 F_2^2 m_N^{-2}} - m_n^* m_p^* \left[4\left(p_{\nu_e} \cdot p_{e-}\right)^2 - 3\left(p_{\nu_e} \cdot p_{e-}\right)m_e^2\right]$$
$$= 4\left(p_n^* \cdot p_{\nu_e}\right)\left(p_{\nu_e} \cdot p_{e-}\right)\left(p_p^* \cdot p_{\nu_e}\right) + 4\left(p_{\nu_e} \cdot p_{e-}\right)\left(p_n^* \cdot p_{e-}\right)\left(p_p^* \cdot p_{e-}\right) \tag{B.11}$$
$$- 4\left(p_n^* \cdot p_{\nu_e}\right)\left(p_p^* \cdot p_{\nu_e}\right)m_e^2 - \left(p_{\nu_e} \cdot p_{e-}\right)\left(p_n^* \cdot p_p^*\right)m_e^2.$$

Using (B.8) on A yields

$$A = 4\left(p_n^* \cdot p_{\nu_e}\right)^2\left(p_{\nu_e} \cdot p_{e-}\right) - 4\left(p_n^* \cdot p_{\nu_e}\right)\left(p_{\nu_e} \cdot p_{e-}\right)^2 + 4\left(p_n^* \cdot p_{\nu_e}\right)\left(p_{\nu_e} \cdot p_{e-}\right)\left(\Delta U E_{\nu_e} + m_e^2\right)$$
$$+ 4\left(p_{\nu_e} \cdot p_{e-}\right)\left(p_n^* \cdot p_{e-}\right)\left(p_p^* \cdot p_{e-}\right) - 4\left(p_n^* \cdot p_{\nu_e}\right)^2 m_e^2 - 4\left(p_n^* \cdot p_{\nu_e}\right)m_e^2 \Delta U E_{\nu_e} - \left(p_{\nu_e} \cdot p_{e-}\right)\left(p_n^* \cdot p_p^*\right)m_e^2.$$

Next use (B.9) on A to get

$$A = 4\left(p_n^* \cdot p_{\nu_e}\right)^2\left(p_{\nu_e} \cdot p_{e-}\right) - 4\left(p_n^* \cdot p_{\nu_e}\right)\left(p_{\nu_e} \cdot p_{e-}\right)^2 + 4\left(p_n^* \cdot p_{\nu_e}\right)\left(p_{\nu_e} \cdot p_{e-}\right)\left(\Delta U E_{\nu_e} + m_e^2\right)$$
$$+ 4\left(p_{\nu_e} \cdot p_{e-}\right)\left(p_n^* \cdot p_{e-}\right)\left(p_p^* \cdot p_{e-}\right) - 4\left(p_n^* \cdot p_{\nu_e}\right)^2 m_e^2 - 4\left(p_n^* \cdot p_{\nu_e}\right)m_e^2 \Delta U E_{\nu_e} - \left(p_{\nu_e} \cdot p_{e-}\right)^2 m_e^2$$
$$+ \left(p_{\nu_e} \cdot p_{e-}\right)m_e^2 \left[-m_n^{*2} + Q + \frac{m_e^2}{2} - \frac{\Delta U^2}{2} + \Delta U\left(E_p^* - E_n^*\right)\right].$$

Now one defines B, which is a part of A

$$B \equiv \left(p_{\nu_e} \cdot p_{e-}\right)\left(p_n^* \cdot p_{e-}\right)\left(p_p^* \cdot p_{e-}\right). \tag{B.12}$$

Applying (B.10) on B yields

$$B = (p_n^* \cdot p_{\nu_e})\,(p_{\nu_e} \cdot p_{e^-})\,(p_n^* \cdot p_{e^-}) + (p_{\nu_e} \cdot p_{e^-})\,(p_n^* \cdot p_{e^-})\left[Q - \frac{m_e^2}{2} - \frac{\Delta U^2}{2} + \Delta U\left(E_p^* + E_{e^-}\right)\right].$$

Eventually using (B.5) on B one finds

$$B = (p_n^* \cdot p_{\nu_e})^2\,(p_{\nu_e} \cdot p_{e^-}) - (p_n^* \cdot p_{\nu_e})(p_{\nu_e} \cdot p_{e^-})^2 + (p_n^* \cdot p_{\nu_e})(p_{\nu_e} \cdot p_{e^-})\left[2Q - \Delta U^2 + \Delta U\left(2E_p^* + E_{e^-}\right)\right]$$

$$- (p_{\nu_e} \cdot p_{e^-})^2\left[Q - \frac{m_e^2}{2} - \frac{\Delta U^2}{2} + \Delta U\left(E_p^* + E_{e^-}\right)\right] + (p_{\nu_e} \cdot p_{e^-})\left[Q^2 - \frac{m_e^4}{4}\right.$$

$$\left. + \Delta U\left(2E_p^*Q + E_{e^-}Q + E_{e^-}\frac{m_e^2}{2}\right) + \Delta U^2\left(E_p^{*2} + E_p^*E_{e^-} - Q\right) - \Delta U^3\left(E_p^* + \frac{E_{e^-}}{2}\right) + \frac{\Delta U^4}{4}\right].$$

Plugging B into A and A into $\left\langle|M|^2\right\rangle_{FF}$, the tensor matrix element eventually becomes

$$\frac{\left\langle|M|^2\right\rangle_{FF}}{8G_F^2 V_{ud}^2 F_2^2 m_N^{-2}} = 2\,(p_n^* \cdot p_{\nu_e})^2\,(p_{\nu_e} \cdot p_{e^-}) - 2\,(p_n^* \cdot p_{\nu_e})\,(p_{\nu_e} \cdot p_{e^-})^2 \tag{B.13}$$

$$+ (p_n^* \cdot p_{\nu_e})\,(p_{\nu_e} \cdot p_{e^-})\left[2Q + m_e^2 + \Delta U\left(2E_p^* + E_{\nu_e} + E_{e^-}\right) - \Delta U^2\right] - (p_n^* \cdot p_{\nu_e})^2\,m_e^2$$

$$+ (p_{\nu_e} \cdot p_{e^-})^2\left[m_n^*m_p^* - Q + \frac{m_e^2}{4} - \Delta U\left(E_p^* + E_{e^-}\right) + \frac{\Delta U^2}{2}\right] - (p_n^* \cdot p_{\nu_e})\,m_e^2\Delta U E_{\nu_e}$$

$$+ (p_{\nu_e} \cdot p_{e^-})\left\{-\left(3m_p^* + m_n^*\right)m_n^*\frac{m_e^2}{4} + Q^2 + Q\frac{m_e^2}{4} - \frac{m_e^4}{8}\right.$$

$$+ \Delta U\left[E_p^*\left(2Q + \frac{m_e^2}{4}\right) + E_{e^-}\left(Q + \frac{m_e^2}{2}\right) - E_n^*\frac{m_e^2}{4}\right]$$

$$\left. + \Delta U^2\left(E_p^{*2} + E_p^*E_{e^-} - Q - \frac{m_e^2}{8}\right) - \Delta U^3\left(E_p^* + \frac{E_{e^-}}{2}\right) + \frac{\Delta U^4}{4}\right\}.$$

B.3.2. Inverse Neutron Decay

Axialvector-Tensor Matrix Element

The kinematic relation between four-momenta for inverse neutron decay is given by

$$p_p^* = p_p - (U_p, 0) = p_n^* - p_{\bar{\nu}_e} - p_{e^-} + (\Delta U, 0) \qquad \text{with} \qquad \Delta U = U_n - U_p. \tag{B.14}$$

Plugging this into Eq.(3.24) results in

$$\left\langle|M|^2\right\rangle_{AF} = 8G_F^2 V_{ud}^2 G_A F_2 \frac{m_N^*}{m_N}\left\{2\left[p_n^* \cdot (p_{e^-} - p_{\bar{\nu}_e})\right](p_{\bar{\nu}_e} \cdot p_{e^-}) - 2\,(p_n^* \cdot p_{\bar{\nu}_e})\,m_e^2 \right. \tag{B.15}$$

$$\left. + (p_{\bar{\nu}_e} \cdot p_{e^-})\,(E_{e^-} - E_{\bar{\nu}_e})\,\Delta U - \Delta U E_{\bar{\nu}_e}m_e^2\right\}.$$

Further using (B.14), one can derive the following relation

$$(p_n^* \cdot p_{\bar{\nu}_e})\left(p_p^* \cdot p_{e^-}\right) - (p_n^* \cdot p_{e^-})\left(p_p^* \cdot p_{\bar{\nu}_e}\right) = \left[p_n^* \cdot (p_{e^-} - p_{\bar{\nu}_e})\right](p_{\bar{\nu}_e} \cdot p_{e^-}) + (p_n^* \cdot p_{\bar{\nu}_e})\left(\Delta U E_{e^-} - m_e^2\right)$$

$$- (p_n^* \cdot p_{e^-})\,\Delta U E_{\bar{\nu}_e}. \tag{B.16}$$

Again the constant Q is defined as in (B.3). Another relation can then be obtained from rewriting the kinematics (B.14).

$$\left(p_n^* - p_{e^-}\right)^2 = \left(p_p^* + p_{\bar{\nu}_e} - (\Delta U, 0)\right)^2,$$

$$\Rightarrow (p_n^* \cdot p_{e^-}) = -\left(p_p^* \cdot p_{\bar{\nu}_e}\right) + Q + \frac{m_e^2}{2} - \frac{\Delta U^2}{2} + \Delta U\left(E_p^* + E_{\bar{\nu}_e}\right)$$

$$= -(p_n^* \cdot p_{\bar{\nu}_e}) + (p_{\bar{\nu}_e} \cdot p_{e^-}) + Q + \frac{m_e^2}{2} - \frac{\Delta U^2}{2} + \Delta U E_p^*. \tag{B.17}$$

Using (B.17) on the RHS of (B.16) yields

$$\left(p_n^* \cdot p_{\bar{\nu}_e}\right)\left(p_p^* \cdot p_{e-}\right) - \left(p_n^* \cdot p_{e-}\right)\left(p_p^* \cdot p_{\bar{\nu}_e}\right) = \left[p_n^* \cdot \left(p_{e-} - p_{\bar{\nu}_e}\right)\right]\left(p_{\bar{\nu}_e} \cdot p_{e-}\right) - \left(p_{\bar{\nu}_e} \cdot p_{e-}\right)\Delta U E_{\bar{\nu}_e} \quad \text{(B.18)}$$

$$+ \left(p_n^* \cdot p_{\bar{\nu}_e}\right)\left[\Delta U\left(E_{\bar{\nu}_e} + E_{e-}\right) - m_e^2\right] - \Delta U E_{\bar{\nu}_e}\left(Q + \frac{m_e^2}{2} + \Delta U E_p^* - \frac{\Delta U^2}{2}\right).$$

Solving this equation for $\left[p_n^* \cdot \left(p_{e-} - p_{\bar{\nu}_e}\right)\right]\left(p_{\bar{\nu}_e} \cdot p_{e-}\right)$ and inserting it into the matrix element (B.15), it transforms eventually into

$$\left\langle |M|^2 \right\rangle_{AF} = 8 G_F^2 V_{ud}^2 G_A F_2 \frac{m_N^*}{m_N} \left\{ 2\left(p_n^* \cdot p_{\bar{\nu}_e}\right)\left(p_p^* \cdot p_{e-}\right) - 2\left(p_n^* \cdot p_{e-}\right)\left(p_p^* \cdot p_{\bar{\nu}_e}\right) \right. \quad \text{(B.19)}$$

$$\left. -2\left(p_n^* \cdot p_{\bar{\nu}_e}\right)\left(E_{\bar{\nu}_e} + E_{e-}\right)\Delta U + \left(p_{\bar{\nu}_e} \cdot p_{e-}\right)\left(E_{\bar{\nu}_e + E_{e-}}\right)\Delta U + 2\Delta U E_{\bar{\nu}_e} Q + 2\Delta U^2 E_{\bar{\nu}_e} E_p^* - \Delta U^3 E_{\bar{\nu}_e} \right\}.$$

Tensor Matrix Element

The tensor matrix element for inverse neutron decay is given in Eq.(3.20) by

$$\left\langle |M|^2 \right\rangle_{FF} = \frac{G_F^2 V_{ud}^2 F_2^2}{m_N^2} \left\{ 4\left(p_{e-} \cdot p_{\bar{\nu}_e}\right)\left[\left(p_n^* \cdot p_{\bar{\nu}_e}\right)\left(p_p^* \cdot p_{\bar{\nu}_e}\right) + \left(p_n^* \cdot p_{e-}\right)\left(p_p^* \cdot p_{e-}\right)\right] \right. \quad \text{(B.20)}$$

$$\left. + m_e^2\left[4\left(p_n^* \cdot p_{\bar{\nu}_e}\right)\left(p_p^* \cdot p_{\bar{\nu}_e}\right) - \left(p_n^* \cdot p_p^*\right)\left(p_{\bar{\nu}_e} \cdot p_{e-}\right)\right] - m_n^* m_p^* \left[4\left(p_{\bar{\nu}_e} \cdot p_{e-}\right)^2 + 3\left(p_{\bar{\nu}_e} \cdot p_{e-}\right)m_e^2\right] \right\}.$$

In order to transform it into a more suitable expression several helpfull relations can be derived. By applying (B.14) one finds

$$\left(p_p^* \cdot p_{\bar{\nu}_e}\right) = \left(p_n^* \cdot p_{\bar{\nu}_e}\right) - \left(p_{\bar{\nu}_e} \cdot p_{e-}\right) + \Delta U E_{\bar{\nu}_e}. \quad \text{(B.21)}$$

Also from (B.14) it can be shown that

$$\left(p_n^* \cdot p_p^*\right) = m_n^{*2} - \left(p_n^* \cdot p_{\nu_e}\right) - \left(p_n^* \cdot p_{e-}\right) + \Delta U E_n^*.$$

Now (B.17) can be used on this expression. Doing so results in

$$\left(p_n^* \cdot p_p^*\right) = -\left(p_{\bar{\nu}_e} \cdot p_{e-}\right) + \left[m_n^{*2} - Q - \frac{m_e^2}{2} + \Delta U\left(E_n^* - E_p^*\right) + \frac{\Delta U^2}{2}\right]. \quad \text{(B.22)}$$

A third relation that follows from (B.14) is

$$\left(p_p^* \cdot p_{e-}\right) = \left(p_n^* \cdot p_{e-}\right) - \left(p_{\bar{\nu}_e} \cdot p_{e-}\right) - m_e^2 + \Delta U E_{e-}.$$

Using again (B.17) this transforms into

$$\left(p_p^* \cdot p_{e-}\right) = -\left(p_n^* \cdot p_{\nu_e}\right) + Q - \frac{m_e^2}{2} - \frac{\Delta U^2}{2} + \Delta U\left(E_p^* + E_{e-}\right). \quad \text{(B.23)}$$

Next one defines C which is the part of the matrix element that is to be transformed

$$C \equiv \frac{\left\langle |M|^2 \right\rangle_{FF}}{2 G_F^2 V_{ud}^2 F_2^2 m_N^{-2}} + m_n^* m_p^* \left[4\left(p_{\nu_e} \cdot p_{e-}\right)^2 + 3\left(p_{\nu_e} \cdot p_{e-}\right)m_e^2\right]$$

$$= 4\left(p_n^* \cdot p_{\nu_e}\right)\left(p_{\nu_e} \cdot p_{e-}\right)\left(p_p^* \cdot p_{\nu_e}\right) + 4\left(p_{\nu_e} \cdot p_{e-}\right)\left(p_n^* \cdot p_{e-}\right)\left(p_p^* \cdot p_{e-}\right) \quad \text{(B.24)}$$

$$+ 4\left(p_n^* \cdot p_{\nu_e}\right)\left(p_p^* \cdot p_{\nu_e}\right)m_e^2 - \left(p_{\nu_e} \cdot p_{e-}\right)\left(p_n^* \cdot p_p^*\right)m_e^2.$$

Using (B.21) on C yields

$$C = 4\left(p_n^* \cdot p_{\nu_e}\right)^2\left(p_{\nu_e} \cdot p_{e-}\right) - 4\left(p_n^* \cdot p_{\nu_e}\right)\left(p_{\nu_e} \cdot p_{e-}\right)^2 + 4\left(p_n^* \cdot p_{\nu_e}\right)\left(p_{\nu_e} \cdot p_{e-}\right)\left(\Delta U E_{\bar{\nu}_e} - m_e^2\right)$$

$$+ 4\left(p_{\nu_e} \cdot p_{e-}\right)\left(p_n^* \cdot p_{e-}\right)\left(p_p^* \cdot p_{e-}\right) + 4\left(p_n^* \cdot p_{\nu_e}\right)^2 m_e^2 + 4\left(p_n^* \cdot p_{\nu_e}\right)\Delta U E_{\bar{\nu}_e} m_e^2 - \left(p_{\nu_e} \cdot p_{e-}\right)\left(p_n^* \cdot p_p^*\right)m_e^2.$$

Next use (B.22) on C

$$
\begin{aligned}
C = {} & 4 \left(p_n^* \cdot p_{\nu_e}\right)^2 \left(p_{\nu_e} \cdot p_{e-}\right) - 4 \left(p_n^* \cdot p_{\nu_e}\right) \left(p_{\nu_e} \cdot p_{e-}\right)^2 + 4 \left(p_n^* \cdot p_{\nu_e}\right) \left(p_{\nu_e} \cdot p_{e-}\right) \left(\Delta U E_{\bar{\nu}_e} - m_e^2\right) \\
& + 4 \left(p_{\nu_e} \cdot p_{e-}\right) \left(p_n^* \cdot p_{e-}\right) \left(p_p^* \cdot p_{e-}\right) + 4 \left(p_n^* \cdot p_{\nu_e}\right)^2 m_e^2 + 4 \left(p_n^* \cdot p_{\nu_e}\right) \Delta U E_{\bar{\nu}_e} m_e^2 + \left(p_{\nu_e} \cdot p_{e-}\right)^2 m_e^2 \\
& + \left(p_{\nu_e} \cdot p_{e-}\right) m_e^2 \left[-m_n^{*2} + Q + \frac{m_e^2}{2} + \Delta U \left(E_p^* - E_n^*\right) - \frac{\Delta U^2}{2}\right].
\end{aligned}
$$

Now one defines D which is a part of C

$$
D \equiv \left(p_{\nu_e} \cdot p_{e-}\right) \left(p_n^* \cdot p_{e-}\right) \left(p_p^* \cdot p_{e-}\right). \tag{B.25}
$$

Applying (B.23) on D yields

$$
D = -\left(p_n^* \cdot p_{\nu_e}\right) \left(p_{\nu_e} \cdot p_{e-}\right) \left(p_n^* \cdot p_{e-}\right) + \left(p_{\nu_e} \cdot p_{e-}\right) \left(p_n^* \cdot p_{e-}\right) \left[Q - \frac{m_e^2}{2} - \frac{\Delta U^2}{2} + \Delta U \left(E_p^* + E_{e-}\right)\right].
$$

Eventually using (B.17) on D one finds

$$
\begin{aligned}
D = {} & \left(p_n^* \cdot p_{\nu_e}\right)^2 \left(p_{\nu_e} \cdot p_{e-}\right) - \left(p_n^* \cdot p_{\nu_e}\right) \left(p_{\nu_e} \cdot p_{e-}\right)^2 - \left(p_n^* \cdot p_{\nu_e}\right) \left(p_{\nu_e} \cdot p_{e-}\right) \left[2Q + \Delta U \left(2E_p^* + E_{e-}\right) - \Delta U^2\right] \\
& + \left(p_{\nu_e} \cdot p_{e-}\right)^2 \left[Q - \frac{m_e^2}{2} - \frac{\Delta U^2}{2} + \Delta U \left(E_p^* + E_{e-}\right)\right] + \left(p_{\nu_e} \cdot p_{e-}\right) \left[Q^2 - \frac{m_e^4}{4}\right. \\
& \left. + \Delta U \left(2E_p^* Q + E_{e-} Q + E_{e-} \frac{m_e^2}{2}\right) + \Delta U^2 \left(E_p^{*2} + E_p^* E_{e-} - Q\right) - \Delta U^3 \left(E_p^* + \frac{E_{e-}}{2}\right) + \frac{\Delta U^4}{4}\right].
\end{aligned}
$$

Inserting D into C and C into $\left\langle |M|^2 \right\rangle_{FF}$, the matrix element eventually becomes

$$
\begin{aligned}
\frac{\left\langle |M|^2 \right\rangle_{FF}}{4 G_F^2 V_{ud}^2 F_2^2 m_N^{-2}} = {} & 2 \left(p_n^* \cdot p_{\nu_e}\right)^2 \left(p_{\nu_e} \cdot p_{e-}\right) - 2 \left(p_n^* \cdot p_{\nu_e}\right) \left(p_{\nu_e} \cdot p_{e-}\right)^2 \tag{B.26} \\
& - \left(p_n^* \cdot p_{\nu_e}\right) \left(p_{\nu_e} \cdot p_{e-}\right) \left[2Q + m_e^2 + \Delta U \left(2E_p^* - E_{\nu_e} + E_{e-}\right) - \Delta U^2\right] + \left(p_n^* \cdot p_{\nu_e}\right)^2 m_e^2 \\
& - \left(p_{\nu_e} \cdot p_{e-}\right)^2 \left[m_n^* m_p^* - Q + \frac{m_e^2}{4} - \Delta U \left(E_p^* + E_{e-}\right) + \frac{\Delta U^2}{2}\right] + \left(p_n^* \cdot p_{\nu_e}\right) m_e^2 \Delta U E_{\nu_e} \\
& + \left(p_{\nu_e} \cdot p_{e-}\right) \left\{ -\left(3 m_p^* + m_n^*\right) m_n^* \frac{m_e^2}{4} + Q^2 + Q \frac{m_e^2}{4} - \frac{m_e^4}{8} \right. \\
& \left. + \Delta U \left[E_p^* \left(2Q + \frac{m_e^2}{4}\right) + E_{e-} \left(Q + \frac{m_e^2}{2}\right) - E_n^* \frac{m_e^2}{4}\right] \right. \\
& \left. + \Delta U^2 \left(E_p^{*2} + E_p^* E_{e-} - Q - \frac{m_e^2}{8}\right) - \Delta U^3 \left(E_p^* + \frac{E_{e-}}{2}\right) + \frac{\Delta U^4}{4} \right\}.
\end{aligned}
$$

B.3.3. Coefficients of Matrix Element

Electron Capture on Neutrons

$$A_1 = (G_V + G_A)^2 + 2G_A F_2 \frac{m_N^*}{m_N}, \tag{B.27}$$

$$B_1 = (G_V - G_A)^2 - 2G_A F_2 \frac{m_N^*}{m_N}, \tag{B.28}$$

$$C_1 = \frac{F_2^2}{m_N^2}, \tag{B.29}$$

$$D_1 = -\frac{F_2^2}{m_N^2}, \tag{B.30}$$

$$E_1 = -\frac{F_2^2}{2m_N^2} m_e^2, \tag{B.31}$$

$$G_1 = 2G_V F_2 \frac{m_N^*}{m^*} + \frac{F_2^2}{2m_N^2} \left[m_n^* m_p^* - Q + \frac{m_e^2}{4} - \Delta U \left(E_p^* + E_{e^-} \right) + \frac{\Delta U^2}{2} \right], \tag{B.32}$$

$$H_1 = \frac{F_2^2}{2m_N^2} \left[2Q + m_e^2 + \Delta U \left(2E_p^* + E_{\nu_e} + E_{e^-} \right) - \Delta U^2 \right], \tag{B.33}$$

$$J_1 = 2G_A F_2 \Delta U \left(E_{\nu_e} - E_{e^-} \right) - \frac{F_2^2}{2m_N^2} m_e^2 \Delta U E_{\nu_e}, \tag{B.34}$$

$$K_1 = \left(G_A^2 - G_V^2 \right) m_n^* m_p^* + G_A F_2 \frac{m_N^*}{m_N} \Delta U \left(E_{e^-} - E_{\nu_e} \right) + G_V F_2 \frac{m_N^*}{m_N} \left[\Delta U \left(E_{e^-} - E_{\nu_e} \right) - \frac{3}{2} m_e^2 \right] \tag{B.35}$$

$$+ \frac{F_2^2}{2m_N^2} \left\{ - \left(3m_p^* + m_n^* \right) m_n^* \frac{m_e^2}{4} + Q^2 + Q \frac{m_e^2}{4} - \frac{m_e^4}{8} + \Delta U^2 \left(E_p^{*2} + E_p^* E_{e^-} - Q - \frac{m_e^2}{8} \right) \right.$$

$$\left. + \Delta U \left[E_p^* \left(2Q + \frac{m_e^2}{4} \right) + E_{e^-} \left(Q + \frac{m_e^2}{2} \right) - E_n^* \frac{m_e^2}{4} \right] - \Delta U^3 \left(E_p^* + \frac{E_{e^-}}{2} \right) + \frac{\Delta U^4}{4} \right\},$$

$$L_1 = G_V F_2 \frac{m_N^*}{m_N} \Delta U E_{\nu_e} \frac{m_e^2}{2} + G_A F_2 \frac{m_N^*}{m_N} \Delta U E_{\nu_e} \left(2Q + 2\Delta U E_p^* + \Delta U^2 \right). \tag{B.36}$$

The terms Q and ΔU are defined by

$$Q \equiv \frac{1}{2} \left(m_n^{*2} - m_p^{*2} \right) \qquad \text{and} \qquad \Delta U = U_n - U_p.$$

Inverse Neutron Decay

$$E_3 = \frac{F_2^2}{2m_N^2} m_e^2 = -E_1, \tag{B.37}$$

$$G_3 = -2G_V F_2 \frac{m_N^*}{m^*} - \frac{F_2^2}{2m_N^2} \left[m_n^* m_p^* - Q + \frac{m_e^2}{4} - \Delta U \left(E_p^* + E_{e^-} \right) + \frac{\Delta U^2}{2} \right] = -G_1, \tag{B.38}$$

$$H_3 = -\frac{F_2^2}{2m_N^2} \left[2Q + m_e^2 + \Delta U \left(2E_p^* - E_{\bar{\nu}_e} + E_{e^-} \right) - \Delta U^2 \right] = -H_1 + \frac{F_2^2}{m_N^2} \Delta U E_{\bar{\nu}_e}, \tag{B.39}$$

$$J_3 = -2G_A F_2 \Delta U \left(E_{\bar{\nu}_e} + E_{e^-} \right) + \frac{F_2^2}{2m_N^2} m_e^2 \Delta U E_{\bar{\nu}_e} = -J_1 - 2G_A F_2 \Delta U E_{e^-}, \tag{B.40}$$

$$K_3 = \left(G_A^2 - G_V^2\right) m_n^* m_p^* + G_A F_2 \frac{m_N^*}{m_N} \Delta U \left(E_{\bar{\nu}_e} + E_{e^-}\right) + G_V F_2 \frac{m_N^*}{m_N} \left[\Delta U \left(E_{\bar{\nu}_e} + E_{e^-}\right) - \frac{3}{2} m_e^2\right] \quad \text{(B.41)}$$

$$+ \frac{F_2^2}{2 m_N^2} \left\{ - \left(3 m_p^* + m_n^*\right) m_n^* \frac{m_e^2}{4} + Q^2 + Q \frac{m_e^2}{4} - \frac{m_e^4}{8} + \Delta U^2 \left(E_p^{*2} + E_p^* E_{e^-} - Q - \frac{m_e^2}{8}\right)\right.$$

$$+ \Delta U \left[E_p^* \left(2Q + \frac{m_e^2}{4}\right) + E_{e^-} \left(Q + \frac{m_e^2}{2}\right) - E_n^* \frac{m_e^2}{4}\right] - \Delta U^3 \left(E_p^* + \frac{E_{e^-}}{2}\right) + \frac{\Delta U^4}{4} \left.\right\}$$

$$= K_1 + 2 \left(G_V + G_A\right) F_2 \frac{m_N^*}{m_N} \Delta U E_{\bar{\nu}_e}.$$

C. Derivation of Scattering Kernels

C.1. General Scattering Kernel

Usefull Kinematic Relations

The four momenta of the particles are connected by

$$p_1 + p_2 = p_3 + p_4. \tag{C.1}$$

Particles "1" and "3" are massless. The constant Q is defined by

$$Q = \frac{1}{2}\left(m_4^2 - m_2^2\right). \tag{C.2}$$

Consequently one can show

$$
\begin{aligned}
(p_3 \cdot p_4) &= [p_3 \cdot (p_1 + p_2 - p_3)] \\
&= (p_1 \cdot p_3) + (p_2 \cdot p_3),
\end{aligned} \tag{C.3}
$$

$$
\begin{aligned}
(p_1 + p_2)^2 &= (p_3 + p_4)^2 \\
\Rightarrow (p_1 \cdot p_2) &= (p_3 \cdot p_4) + Q \\
&= (p_1 \cdot p_3) + (p_2 \cdot p_3) + Q,
\end{aligned} \tag{C.4}
$$

$$
\begin{aligned}
(p_4 - p_1)^2 &= (p_2 - p_3)^2 \\
\Rightarrow (p_1 \cdot p_4) &= (p_2 \cdot p_3) + Q.
\end{aligned} \tag{C.5}
$$

Further the angles between the particles are denoted in the following way. α is the angle between $\vec{p_3}$ and $\vec{p_2}$, θ is the angle between $\vec{p_1}$ and $\vec{p_3}$, and γ is the angle between $\vec{p_1}$ and $\vec{p_2}$. Eventually, ϕ is the polar angle between $\vec{p_1}$ and $\vec{p_2}$ around the axis of $\vec{p_3}$. Then one can use the relation

$$\cos\gamma = \cos\alpha\cos\beta + \sin\alpha\sin\beta\cos\phi. \tag{C.6}$$

Integral R_1

The integral R_1 is given by

$$R_1 = \int d^3p_2 d^3p_4 \frac{(p_1 \cdot p_2)(p_3 \cdot p_4)}{E_1 E_2 E_3 E_4} \delta^4(p_1 + p_2 - p_3 - p_4) f_2(E_2)\left[1 - f_4(E_4)\right]. \tag{C.7}$$

Using (C.3) and (C.4) the four-momentum product can be transformed into

$$
\begin{aligned}
(p_1 \cdot p_2)(p_3 \cdot p_4) &= [p_3 \cdot (p_1 + p_2) + Q][p_3 \cdot (p_1 + p_2)] \\
&= E_3^2\left(E_2 - \bar{p}_2\cos\alpha + E_1 - E_1\cos\theta\right)^2 + E_3 Q\left(E_2 - \bar{p}_2\cos\alpha + E_1 - E_1\cos\theta\right) \\
&= \frac{E_3}{\bar{p}_2}\left[A_1 + B_1\cos\alpha + C_1\cos^2\alpha\right]. \tag{C.8}
\end{aligned}
$$

The expressions A_1, B_1, and C_1 are given by

$$A_1 = \bar{p}_2 \left(E_2 + E_1 - E_1 \cos\theta\right) \left[E_3 \left(E_2 + E_1 - E_1 \cos\theta\right) + Q\right], \tag{C.9}$$

$$B_1 = -\bar{p}_2^2 \left[2E_3 \left(E_2 + E_1 - E_1 \cos\theta\right) + Q\right], \tag{C.10}$$

$$C_1 = E_3 \bar{p}_2^3. \tag{C.11}$$

Writing the phase space integral over particle 2 in the form

$$d^3 p_2 = d\phi dy dE_2 \bar{p}_2 E_2 \qquad \text{with} \qquad y \equiv \cos\alpha.$$

R_1 transforms into

$$R_1 = \frac{1}{E_1} \int \frac{d^3 p_4}{E_4} d\phi dy dE_2 \left[A_1 + B_1 y + C_1 y^2\right] \delta^4(p_1 + p_2 - p_3 - p_4) f_2(E_2) \left[1 - f_4(E_4)\right]. \tag{C.12}$$

Now one consideres the identity

$$\frac{1}{2E_4} = \int dE_4 \delta\left(p_4^2 - m_4^2\right). \tag{C.13}$$

With the help of (C.13) the phase space integration over p_4 can be used to transform the δ^4-function

$$\int \frac{d^3 p_4}{E_4} \delta^4(p_1 + p_2 - p_3 - p_4) = 2 \int d^4 p_4 \delta^4(p_1 + p_2 - p_3 - p_4)\delta\left(p_4^2 - m_4^2\right)$$
$$= 2\delta\left[(p_1 + p_2 - p_3)^2 - m_4^2\right]$$
$$= \delta\left[\frac{m_4^2 - (p_1 + p_2 - p_3)^2}{2}\right]. \tag{C.14}$$

The argument of the δ-function can be expressed as a function of ϕ by using (C.6)

$$f(\phi) = \frac{1}{2}\left[m_4^2 - (p_1 + p_2 - p_3)^2\right]$$
$$= Q + E_1 E_3 \left(1 - \cos\theta\right) + E_3 \left(E_2 - \bar{p}_2 y\right) - E_1 \left(E_2 - \bar{p}_2 \cos\gamma\right)$$
$$= E_1 \bar{p}_2 \sin\alpha \sin\theta \cos\phi + Q + E_1 E_3 \left(1 - \cos\theta\right) + E_3 \left(E_2 - \bar{p}_2 y\right) - E_1 \left(E_2 - \bar{p}_2 \cos\alpha \cos\theta\right). \tag{C.15}$$

Now one can write the integral R_1 in the form

$$R_1 = \frac{1}{E_1} \int dy dE_2 \left[A_1 + B_1 y + C_1 y^2\right] f_2(E_2) \left[1 - f_4(E_4)\right] \int_0^{2\pi} d\phi \delta(f(\phi)). \tag{C.16}$$

The derivative of $f(\phi)$ with respect to ϕ is given by

$$f'(\phi) = -E_1 \bar{p}_2 \sin\alpha \sin\theta \sqrt{1 - \cos^2\phi}. \tag{C.17}$$

The angle ϕ_0 is defined by $f(\phi_0) = 0$. One finds then

$$\cos\phi_0 = \frac{E_1 \left(E_2 - \bar{p}_2 \cos\alpha \cos\theta\right) - Q - E_1 E_3 \left(1 - \cos\theta\right) - E_3 \left(E_2 - \bar{p}_2 y\right)}{E_1 \bar{p}_2 \sin\alpha \sin\theta}. \tag{C.18}$$

The integration over ϕ can then be handled in the following way

$$\int_0^{2\pi} d\phi \delta(f(\phi)) = 2 \int_0^{\pi} d\phi \delta(f(\phi)) = 2 \int_0^{\pi} d\phi \frac{\delta(\phi - \phi_0)}{|f'(\phi)|_{\phi=\phi_0}} = 2\frac{\Theta\left(1 - \cos^2\phi_0\right)}{E_1 \bar{p}_2 \sin\alpha \sin\theta \sqrt{1 - \cos^2\phi}}. \tag{C.19}$$

The heaviside function is necessary to prevent configurations that are kinematically not possible and would thus force $\cos\phi_0$ to take unphysical values. The heaviside function can be transformed by

$$\Theta\big(1 - \cos^2\phi_0\big) = \Theta\left[\Big(E_1\bar{p}_2\sin\alpha\sin\theta\sqrt{1-\cos^2\phi}\Big)^2\right]. \tag{C.20}$$

The integration over ϕ becomes then

$$\int_0^{2\pi} d\phi\,\delta(f(\phi)) = 2\frac{\Theta\left[\Big(E_1\bar{p}_2\sin\alpha\sin\theta\sqrt{1-\cos^2\phi}\Big)^2\right]}{E_1\bar{p}_2\sin\alpha\sin\theta\sqrt{1-\cos^2\phi}}. \tag{C.21}$$

This can be transformed into

$$2\frac{\Theta\left[\Big(E_1\bar{p}_2\sin\alpha\sin\theta\sqrt{1-\cos^2\phi}\Big)^2\right]}{E_1\bar{p}_2\sin\alpha\sin\theta\sqrt{1-\cos^2\phi}} = 2\frac{\Theta\big(ay^2+by+c\big)}{\sqrt{ay^2+by+c}}. \tag{C.22}$$

with the expressions a, b, and c given by

$$a = -\bar{p}_2^2\left(E_1^2 + E_3^2 - 2E_1E_3\cos\theta\right), \tag{C.23}$$

$$b = 2\bar{p}_2\left(E_3 - E_1\cos\theta\right)\left[Q + E_2\left(E_3 - E_1\right) + E_1E_3\left(1 - cos\theta\right)\right], \tag{C.24}$$

$$c = E_1^2\bar{p}_2^2\sin^2\theta - \left[Q + E_2\left(E_3 - E_1\right) + E_1E_3\left(1 - cos\theta\right)\right]^2. \tag{C.25}$$

Deriving (C.22)-(C.25) from (C.21) requires tedious but simple algebra. It will not be shown here in detail. Summing all up, the intgral R_1 can now be written in the form

$$R_1 = \frac{2}{E_1}\int dE_2 f_2(E_2)\left[1 - f_4(E_4)\right]\int_{-1}^{1} dy\left[A_1 + B_1 y + C_1 y^2\right]\frac{\Theta\big(ay^2+by+c\big)}{\sqrt{ay^2+by+c}}. \tag{C.26}$$

The limits for y that are imposed by the heaviside function are in fact the roots of the radical

$$0 = ay^2 + by + c \qquad \Rightarrow \qquad y = \pm\sqrt{\frac{b^2}{4a^2} - \frac{c}{a}} - \frac{b}{2a}.$$

Consequently the integral over y can be transformed into

$$\int_{-1}^{1} dy\,\frac{f(y)}{\sqrt{ay^2+by+c}}\Theta\big(ay^2+by+c\big) = \frac{1}{\sqrt{-a}}\int_{-\sqrt{\frac{b^2}{4a^2}-\frac{c}{a}}-\frac{b}{2a}}^{+\sqrt{\frac{b^2}{4a^2}-\frac{c}{a}}-\frac{b}{2a}} dy\,\frac{f(y)}{\sqrt{-\left(y+\frac{b}{2a}\right)^2+\frac{b^2}{4a^2}-\frac{c}{a}}}\Theta\big(b^2-4ac\big). \tag{C.27}$$

The heaviside function arises from the requirement for the integrand to be integrable. As a first step to solve this integral, define the expressions $\bar{b}$ and $\bar{c}$ by

$$\bar{b} = \frac{b}{2a} \qquad \text{and} \qquad \bar{c} = \frac{c}{a}. \tag{C.28}$$

The integral becomes then

$$\int_{-\sqrt{\frac{b^2}{4a^2}-\frac{c}{a}}-\frac{b}{2a}}^{+\sqrt{\frac{b^2}{4a^2}-\frac{c}{a}}-\frac{b}{2a}} dy\,\frac{f(y)}{\sqrt{-\left(y+\frac{b}{2a}\right)^2+\frac{b^2}{4a^2}-\frac{c}{a}}} = \int_{-\sqrt{\bar{b}^2-\bar{c}}-\bar{b}}^{+\sqrt{\bar{b}^2-\bar{c}}-\bar{b}} dy\,\frac{f(y)}{\sqrt{-\left(y+\bar{b}\right)^2+\bar{b}^2-\bar{c}}}. \tag{C.29}$$

Now it is helpfull to introduce several identities that will be needed soon

$$\int\limits_{-1}^{1} dx \frac{1}{\sqrt{1-x^2}} = \pi, \qquad \int\limits_{-1}^{1} dx \frac{x}{\sqrt{1-x^2}} = 0, \qquad \int\limits_{-1}^{1} dx \frac{x^2}{\sqrt{1-x^2}} = \frac{\pi}{2}. \tag{C.30}$$

In the next step one substitutes y by y^* according to

$$y^* \equiv \frac{y+\bar{b}}{\sqrt{\bar{b}^2-\bar{c}}} \qquad \Rightarrow \qquad dy = dy^*\sqrt{\bar{b}^2-\bar{c}}. \tag{C.31}$$

The whole integral over y becomes then

$$\int\limits_{-\sqrt{\bar{b}^2-\bar{c}}-\bar{b}}^{+\sqrt{\bar{b}^2-\bar{c}}-\bar{b}} dy \frac{A_1 + B_1 y + C_1 y^2}{\sqrt{-\left(y+\bar{b}\right)^2+\bar{b}^2-\bar{c}}} = \int\limits_{-1}^{1} dy^{*2} \frac{\left(A_1-\bar{b}B_1+\bar{b}^2 C_1\right)+\sqrt{\bar{b}^2-\bar{c}}\left(B_1-2\bar{b}C_1\right)y^*+\left(\bar{b}^2-c\right)C_1 y^2}{\sqrt{1-y^{*2}}}$$

$$= \pi\left(A_1 - \bar{b}B_1 + \frac{3\bar{b}^2}{2}C_1 - \frac{\bar{c}}{2}C_1\right)$$

$$= \frac{\pi}{\sqrt{-a}^4}\left[a^2 A_1 - \frac{ab}{2}B_1 + \left(\frac{3b^2}{8}-\frac{ca}{2}\right)C_1\right]. \tag{C.32}$$

Then the whole integral R_1 becomes

$$R_1 = \frac{2\pi}{E_1}\int dE_2 f_2(E_2)\left[1-f_4(E_4)\right]\frac{1}{\sqrt{-a}^5}\left[a^2 A_1 - \frac{ab}{2}B_1 + \left(\frac{3b^2}{8}-\frac{ca}{2}\right)C_1\right]\Theta\left(b^2-4ac\right). \tag{C.33}$$

The heaviside function can be transformed into boundaries for the remaining energy integral. In the limiting case the condition gives

$$0 = b^2 - 4ac. \tag{C.34}$$

By plugging (C.23)-(C.25) into (C.34) and solving for positive solutions of E_2, the heaviside function can be transformed into a lower limit on E_2

$$\int\limits_{m_2}^{\infty} dE_2 \Theta\left(b^2-4ac\right) = \int\limits_{E_-}^{\infty} dE_2. \tag{C.35}$$

This lower limit is given by

$$E_- = \frac{1}{2}\left[\left(E_3-E_1\right)\left(1+k\right)+\sqrt{\left(E_1^2+E_3^2-2E_1 E_3\cos\theta\right)\left[\left(1+k\right)^2+\frac{2m_2^2}{E_1 E_3\left(1-\cos\theta\right)}\right]}\right]. \tag{C.36}$$

where the coefficient k is defined by

$$k \equiv \frac{Q}{E_1 E_3\left(1-\cos\theta\right)}. \tag{C.37}$$

Now one has to sort the integrand in (C.33) by powers of E_2. Therefore one must make use of $\bar{p}_2^2 = E_2^2 - m_2^2$. This step requires several pages of tedious but straightforward algebra. Eventually one arrives at the following solution.

$$R_1 = \frac{2\pi}{\Delta^5}\int\limits_{E_-}^{\infty} dE_2 f_2(E_2)\left[1-f_4(E_4)\right]\left(\widetilde{A}_1 E_2^2 + \widetilde{B}_1 E_2 + \widetilde{C}_1\right). \tag{C.38}$$

150

The coefficients $\widetilde{A}_1$, $\widetilde{B}_1$, $\widetilde{C}_1$, and Δ are given by

$$\widetilde{A}_1 = E_1 E_3 \left(1 - \cos\theta\right)^2 \left[E_1^2 + E_1 E_3 \left(3 + \cos\theta\right) + E_3^2\right], \tag{C.39}$$

$$\widetilde{B}_1 = E_1^2 E_3 \left(1 - \cos\theta\right)^2 \left[2E_1^2 + E_1 E_3 \left(3 - \cos\theta\right) - E_3^2 \left(1 + 3\cos\theta\right)\right] \tag{C.40}$$
$$+ Q\left(1 - \cos\theta\right)\left[E_1^3 + E_1^2 E_3 \left(2 + \cos\theta\right) - E_1 E_3^2 \left(2 + \cos\theta\right) - E_3^3\right],$$

$$\widetilde{C}_1 = E_1^3 E_3 \left(1 - \cos\theta\right)^2 \left[E_1^2 - 2E_1 E_3 \cos\theta + E_3^2 \left(-\frac{1}{2} + \frac{3}{2}\cos^2\theta\right)\right] \tag{C.41}$$
$$+ QE_1 \left(1 - \cos\theta\right)\left[E_1^3 - E_1^2 E_3 \cos\theta + E_1 E_3^2 \left(-2 + \cos^2\theta\right) + E_3^3 \cos\theta\right]$$
$$+ Q^2 \left[E_1^2 \cos\theta - E_1 E_3 \left(\frac{3}{2} + \frac{1}{2}\cos^2\theta\right) + E_3^2 \cos\theta\right] + \frac{1}{2}E_1 E_3 \left(1 - \cos^2\theta\right)\Delta^2 m_2^2,$$

$$\Delta = \sqrt{E_1^2 - 2E_1 E_3 \cos\theta + E_3^2}. \tag{C.42}$$

Integral R_2

The integral R_2 is given by

$$R_2 = \int d^3 p_2 d^3 p_4 \frac{\left(p_1 \cdot p_4\right)\left(p_2 \cdot p_3\right)}{E_1 E_2 E_3 E_4} \delta^4(p_1 + p_2 - p_3 - p_4) f_2(E_2) \left[1 - f_4(E_4)\right]. \tag{C.43}$$

Using (C.5) the four-momentum product can be transformed into

$$\left(p_1 \cdot p_4\right)\left(p_2 \cdot p_3\right) = \left(p_2 \cdot p_3\right)\left[\left(p_2 \cdot p_3\right) + Q\right]$$
$$= E_3^2 \left(E_2 - \bar{p}_2 \cos\alpha\right)^2 + E_3 Q \left(E_2 - \bar{p}_2 \cos\alpha\right)$$
$$= \frac{E_3}{\bar{p}_2} \left[A_2 + B_2 \cos\alpha + C_2 \cos^2\alpha\right]. \tag{C.44}$$

The expressions A_2, B_2, and C_2 are given by

$$A_2 = \bar{p}_2 E_2 \left(E_3 E_2 + Q\right), \tag{C.45}$$

$$B_2 = -\bar{p}_2^2 \left(2E_3 E_2 + Q\right), \tag{C.46}$$

$$C_2 = E_3 \bar{p}_2^3. \tag{C.47}$$

The subsequent derivation is exactly the same as for R_1. Therefore R_2 eventually becomes.

$$R_2 = \frac{2\pi}{E_1} \int\limits_{E_-}^{\infty} dE_2 f_2(E_2) \left[1 - f_4(E_4)\right] \frac{1}{\sqrt{-a}^5} \left[a^2 A_2 - \frac{ab}{2}B_2 + \left(\frac{3b^2}{8} - \frac{ca}{2}\right)C_2\right]. \tag{C.48}$$

Sorting again by (tedious) ordering for powers of E_2 one finds

$$R_2 = \frac{2\pi}{\Delta^5} \int\limits_{E_-}^{\infty} dE_2 f_2(E_2) \left[1 - f_4(E_4)\right] \left(\widetilde{A}_2 E_2^2 + \widetilde{B}_2 E_2 + \widetilde{C}_2\right). \tag{C.49}$$

The coefficient Δ is given in (C.42), E_- is defined in (C.36), while $\widetilde{A}_2$, $\widetilde{B}_2$, and $\widetilde{C}_2$ are given by

$$\widetilde{A}_2 = E_1 E_3 \left(1 - \cos\theta\right)^2 \left[E_1^2 + E_1 E_3 \left(3 + \cos\theta\right) + E_3^2\right], \tag{C.50}$$

$$\widetilde{B}_2 = E_1 E_3^2 \left(1 - \cos\theta\right)^2 \left[E_1^2 \left(1 + 3\cos\theta\right) + E_1 E_3 \left(-3 + \cos\theta\right) - 2E_3^2\right] \tag{C.51}$$
$$+ Q\left(1 - \cos\theta\right)\left[E_1^3 + E_1^2 E_3 \left(2 + \cos\theta\right) - E_1 E_3^2 \left(2 + \cos\theta\right) - E_3^3\right],$$

$$\widetilde{C}_2 = E_1 E_3^3 \left(1 - \cos\theta\right)^2 \left[E_1^2 \left(-\frac{1}{2} + \frac{3}{2}\cos^2\theta\right) - 2E_1 E_3 \cos\theta + E_3^2\right] \tag{C.52}$$
$$+ QE_3 \left(1 - \cos\theta\right)\left[E_1^3 \cos\theta + E_1^2 E_3 \left(-2 + \cos^2\theta\right) - E_1 E_3^2 \cos\theta + E_3^3\right]$$
$$+ Q^2 \left[E_1^2 \cos\theta - E_1 E_3 \left(\frac{3}{2} + \frac{1}{2}\cos^2\theta\right) + E_3^2 \cos\theta\right] + \frac{1}{2}E_1 E_3 \left(1 - \cos^2\theta\right)\Delta^2 m_2^2.$$

Integral R_3

The integral R_3 is given by

$$R_3 = \int d^3p_2 d^3p_4 \frac{(p_1 \cdot p_3)}{E_1 E_2 E_3 E_4} \delta^4(p_1 + p_2 - p_3 - p_4) f_2(E_2) \left[1 - f_4(E_4)\right]. \tag{C.53}$$

The four-momentum product can be transformed into

$$(p_1 \cdot p_3) = E_1 E_3^2 \left(1 - \cos\theta\right) \tag{C.54}$$

$$= \frac{E_3}{\bar{p}_2} A_3. \tag{C.55}$$

The expressions A_3 is given by

$$A_3 = \bar{p}_2 E_1 \left(1 - \cos\theta\right). \tag{C.56}$$

The subsequent derivation is again completely analogous to R_1, so one eventually arrives at

$$R_3 = \frac{2\pi}{\Delta^5} \int dE_2 f_2(E_2) \left[1 - f_4(E_4)\right] \widetilde{C}_3. \tag{C.57}$$

The coefficient Δ is defined in (C.42), E_- is defined in (C.36), while $\widetilde{C}_3$ is given by

$$\widetilde{C}_3 = \left(1 - \cos\theta\right) \Delta^4 m_2 m_4. \tag{C.58}$$

Integral over E_2

For the scattering kernels, an energy integration over the distribution functions remains. The corresponding expressions are of the form

$$\int\limits_{E_-}^{\infty} dE_2 E_2^n f_2(E_2) \left[1 - f_4(E_2 + E_1 - E_3)\right], \qquad n = \{0, 1, 2\}. \tag{C.59}$$

Under the assumption of Fermi-Dirac-distributions for particles "2" and "4" it was shown in [133] that these expressions can be transformed into standard Fermi-Dirac-integrals. The latter can themselves be expressed in terms of polylogarithm functions which are numerically convenient to handel and for which good approximation formulas exist. To be precise, [133] discussed the special cas of $f_2 = f_4$. The more general case for different chemical potentials $\mu_2 \neq \mu_4$ is but a minor extension. Writing out the distribution functions (C.59) is given by

$$\int\limits_{E_-}^{\infty} dE_2 E_2^n \frac{1}{\exp\left(\frac{E_2 - \mu_2}{T}\right) + 1} \left[\frac{\exp\left(\frac{E_2 + E_1 - E_3 + \Delta\mu - \mu_2}{T}\right)}{\exp\left(\frac{E_2 + E_1 - E_3 + \Delta\mu - \mu_2}{T}\right) + 1}\right]. \tag{C.60}$$

where $\Delta\mu = \mu_2 - \mu_4$. Defining the following coefficients

$$y \equiv \frac{E_-}{T}, \qquad \eta = \frac{\mu_2}{T}, \qquad \eta' = \eta - \frac{E_1 - E_3 + \Delta\mu}{T}. \tag{C.61}$$

one can transform (C.60) into

$$\int\limits_{yT}^{\infty} dE_2 E_2^n \frac{1}{\exp\left(\frac{E_2}{T} - \eta\right) + 1} \left[\frac{\exp\left(\frac{E_2}{T} - \eta'\right)}{\exp\left(\frac{E_2}{T} - \eta'\right) + 1}\right]. \tag{C.62}$$

Substituting E_2 by x according to

$$x = \frac{E}{T} - y \qquad \Rightarrow \qquad \int\limits_{yT}^{\infty} dE_2 = \int\limits_{0}^{\infty} dx\, T. \qquad (C.63)$$

the integral becomes then

$$\int\limits_{0}^{\infty} dx\, T^{n+1} (x+y)^n \frac{1}{\exp(x+y-\eta)+1} \left[\frac{\exp(x+y-\eta')}{\exp(x+y-\eta')+1}\right] \qquad (C.64)$$

$$= \int\limits_{0}^{\infty} dx\, T^{n+1} (x+y)^n \frac{\exp(x+y+\eta)}{[\exp(x+y)+\exp(\eta)][\exp(x+y)+\exp(\eta')]}$$

$$= \int\limits_{0}^{\infty} dx\, T^{n+1} (x+y)^n \frac{\exp(\eta)}{\exp(\eta')-\exp(\eta)} \frac{\exp(x+y)[\exp(\eta')-\exp(\eta)]}{[\exp(x+y)+\exp(\eta)][\exp(x+y)+\exp(\eta')]}$$

$$= \int\limits_{0}^{\infty} dx\, T^{n+1} (x+y)^n \frac{1}{\exp(\eta'-\eta)-1} \frac{\exp(x+y+\eta')-\exp(x+y+\eta)}{[\exp(x+y)+\exp(\eta)][\exp(x+y)+\exp(\eta')]}$$

$$= \int\limits_{0}^{\infty} dx\, T^{n+1} (x+y)^n \frac{1}{\exp(\eta'-\eta)-1} \frac{\exp(x+y+\eta')+\exp(\eta'+\eta)-\exp(x+y+\eta)-\exp(\eta'+\eta)}{[\exp(x+y)+\exp(\eta)][\exp(x+y)+\exp(\eta')]}$$

$$= \int\limits_{0}^{\infty} dx\, T^{n+1} (x+y)^n \frac{1}{\exp(\eta'-\eta)-1} \left[\frac{\exp(\eta')}{\exp(x+y)+\exp(\eta')} - \frac{\exp(\eta)}{\exp(x+y)+\exp(\eta)}\right]$$

$$= \int\limits_{0}^{\infty} dx\, T^{n+1} (x+y)^n \frac{1}{\exp(\eta'-\eta)-1} \left[\frac{1}{\exp(x+y-\eta')+1} - \frac{1}{\exp(x+y-\eta)+1}\right].$$

Now the Fermi-Dirac integrals $F_n(z)$ and the Boltzman-Distribution $f_\gamma(z)$ are given by

$$F_n(z) = \int\limits_{0}^{\infty} dx \frac{x^n}{\exp(x-z)+1} \qquad \text{and} \qquad f_\gamma(z) = \frac{1}{\exp(z)-1}. \qquad (C.65)$$

Plugging this into the integral (C.64) one finds eventually

$$I_0 = \int\limits_{E_-}^{\infty} dE_2 f_2(E_2) \left[1 - f_4(E_2 + E_1 - E_3)\right]$$

$$= \int\limits_{0}^{\infty} dx\, T \frac{1}{\exp(x+y-\eta)+1} \left[\frac{\exp(x+y-\eta')}{\exp(x+y-\eta')+1}\right]$$

$$= T f_\gamma(\eta'-\eta) \left[F_0(\eta'-y) - F_0(\eta-y)\right]. \qquad (C.66)$$

$$I_1 = \int\limits_{E_-}^{\infty} dE_2 E_2 f_2(E_2) \left[1 - f_4(E_2 + E_1 - E_3)\right]$$

$$= \int\limits_{0}^{\infty} dx\, T^2 (x+y) \frac{1}{\exp(x+y-\eta)+1} \left[\frac{\exp(x+y-\eta')}{\exp(x+y-\eta')+1}\right]$$

$$= T^2 f_\gamma(\eta'-\eta) \left\{\left[F_1(\eta'-y) - F_1(\eta-y)\right] + y\left[F_0(\eta'-y) - F_0(\eta-y)\right]\right\}. \qquad (C.67)$$

$$I_2 = \int\limits_{E_-}^{\infty} dE_2 E_2^2 f_2(E_2) \left[1 - f_4(E_2 + E_1 - E_3) \right]$$

$$= \int\limits_0^{\infty} dx \, T^3 \, (x+y)^2 \, \frac{1}{\exp\left(x+y-\eta\right)+1} \left[\frac{\exp\left(x+y-\eta'\right)}{\exp\left(x+y-\eta'\right)+1} \right]$$

$$= T^3 f_\gamma(\eta' - \eta) \left\{ \left[F_2(\eta' - y) - F_2(\eta - y) \right] + 2y \left[F_1(\eta' - y) - F_1(\eta - y) \right] \right. \tag{C.68}$$

$$\left. + y^2 \left[F_0(\eta' - y) - F_0(\eta - y) \right] \right\}.$$

C.2. Scattering Kernel for Inverse Decay

Usefull Kinematic Relations

The four momenta of the particles are connected by

$$p_1 + p_2 = p_4 - p_3. \tag{C.69}$$

Particles "1" and "3" are massless. The constant Q is defined by

$$Q = \frac{1}{2} \left(m_4^2 - m_2^2 \right). \tag{C.70}$$

Consequently one can show

$$(p_3 \cdot p_4) = \left[p_3 \cdot (p_1 + p_2 + p_3) \right]$$
$$= (p_1 \cdot p_3) + (p_2 \cdot p_3), \tag{C.71}$$

$$(p_1 + p_2)^2 = (p_3 - p_4)^2$$
$$\Rightarrow (p_1 \cdot p_2) = -(p_3 \cdot p_4) + Q$$
$$= -(p_1 \cdot p_3) - (p_2 \cdot p_3) + Q, \tag{C.72}$$

$$(p_4 - p_1)^2 = (p_2 + p_3)^2$$
$$\Rightarrow (p_1 \cdot p_4) = -(p_2 \cdot p_3) + Q. \tag{C.73}$$

The angles between particles 1, 2, and 3 are denoted as for scattering. In particular, (C.6) applies.

Integral R_{D1}

The integral R_{D1} is given by

$$R_{D1} = \int d^3 p_2 d^3 p_4 \frac{(p_1 \cdot p_2)\,(p_3 \cdot p_4)}{E_1 E_2 E_3 E_4} \delta^4(p_1 + p_2 + p_3 - p_4) f_2(E_2) \left[1 - f_4(E_4) \right]. \tag{C.74}$$

Using (C.71) and (C.72) the four-momentum product can be transformed into

$$(p_1 \cdot p_2)\,(p_3 \cdot p_4) = \left[-p_3 \cdot (p_1 + p_2) + Q \right] \left[p_3 \cdot (p_1 + p_2) \right]$$
$$= -E_3^2 \left(E_2 - \bar{p}_2 \cos\alpha + E_1 - E_1 \cos\theta \right)^2 + E_3 Q \left(E_2 - \bar{p}_2 \cos\alpha + E_1 - E_1 \cos\theta \right)$$
$$= \frac{E_3}{\bar{p}_2} \left[A_{D1} + B_{D1} \cos\alpha + C_{D1} \cos^2\alpha \right]. \tag{C.75}$$

The expressions A_{D1}, B_{D1}, and C_{D1} are given by

$$A_{D1} = \bar{p}_2 \left(E_2 + E_1 - E_1 \cos\theta\right) \left[-E_3 \left(E_2 + E_1 - E_1 \cos\theta\right) + Q\right], \tag{C.76}$$

$$B_{D1} = -\bar{p}_2^2 \left[-2E_3 \left(E_2 + E_1 - E_1 \cos\theta\right) + Q\right], \tag{C.77}$$

$$C_{D1} = -E_3 \bar{p}_2^3. \tag{C.78}$$

Writing the phase space integral over particle 2 in the form

$$d^3 p_2 = d\phi dy dE_2 \bar{p}_2 E_2 \qquad \text{with} \qquad y \equiv \cos\alpha.$$

R_{D1} transforms into

$$R_{D1} = \frac{1}{E_1} \int \frac{d^3 p_4}{E_4} d\phi dy dE_2 \left[A_1 + B_1 y + C_1 y^2\right] \delta^4(p_1 + p_2 + p_3 - p_4) f_2(E_2) \left[1 - f_4(E_4)\right]. \tag{C.79}$$

Now one consideres the identity

$$\frac{1}{2E_4} = \int dE_4 \delta\left(p_4^2 - m_4^2\right). \tag{C.80}$$

With the help of (C.80) the phase space integration over p_4 can be used to transform the δ^4-function

$$\int \frac{d^3 p_4}{E_4} \delta^4(p_1 + p_2 + p_3 - p_4) = 2 \int d^4 p_4 \delta^4(p_1 + p_2 + p_3 - p_4) \delta\left(p_4^2 - m_4^2\right)$$

$$= 2\delta\left[(p_1 + p_2 + p_3)^2 - m_4^2\right]$$

$$= \delta\left[\frac{m_4^2 - (p_1 + p_2 + p_3)^2}{2}\right]. \tag{C.81}$$

The argument of the δ-function can be expressed as a function of ϕ by using (C.6)

$$f(\phi) = \frac{1}{2}\left[m_4^2 - (p_1 + p_2 + p_3)^2\right]$$

$$= Q - E_1 E_3 (1 - \cos\theta) - E_3 (E_2 - \bar{p}_2 y) - E_1 (E_2 - \bar{p}_2 \cos\gamma)$$

$$= E_1 \bar{p}_2 \sin\alpha \sin\theta \cos\phi + Q - E_1 E_3 (1 - \cos\theta) - E_3 (E_2 - \bar{p}_2 y) - E_1 (E_2 - \bar{p}_2 \cos\alpha \cos\theta). \tag{C.82}$$

Now one can write the integral R_{D1} in the form

$$R_{D1} = \frac{1}{E_1} \int dy dE_2 \left[A_{D1} + B_{D1} y + C_{D1} y^2\right] f_2(E_2) \left[1 - f_4(E_4)\right] \int_0^{2\pi} d\phi \delta(f(\phi)). \tag{C.83}$$

Comparing (C.76)-(C.78) with (C.9)-(C.11) and (C.82) with (C.15), it can be seen that at this point the difference between R_1 and R_{D1} comes down to replacing E_3 by $-E_3$. Consequently one can repeat the derivation for R_1 analogously. The integral R_{D1} becomes then

$$R_{D1} = \frac{2\pi}{E_1} \int dE_2 f_2(E_2) \left[1 - f_4(E_4)\right] \frac{1}{\sqrt{-a_D}^5} \left[a_D^2 A_{D1} - \frac{a_D b_D}{2} B_{D1} + \left(\frac{3b_D^2}{8} - \frac{c_D a_D}{2}\right) C_{D1}\right] \tag{C.84}$$

$$\times \Theta\left(b_D^2 - 4 a_D c_D\right).$$

with the expressions a_D, b_D, and c_D given by

$$a_D = -\bar{p}_2^2 \left(E_1^2 + E_3^2 + 2E_1 E_3 \cos\theta\right), \tag{C.85}$$

$$b_D = -2\bar{p}_2 \left(E_3 + E_1 \cos\theta\right) \left[Q - E_2 \left(E_3 + E_1\right) - E_1 E_3 \left(1 - cos\theta\right)\right], \tag{C.86}$$

$$c_D = E_1^2 \bar{p}_2^2 \sin^2\theta - \left[Q - E_2 \left(E_3 + E_1\right) - E_1 E_3 \left(1 - cos\theta\right)\right]^2. \tag{C.87}$$

However, special care has to be taken for the heaviside function. Even though the condition is the same as for the scattering reactions, except for a sign change of E_3, one cannot just do the same to derive the limit of E_2. The reason here is that the condition equates to a quadratic function of E_3. By replacing $E_3 \to -E_3$, instead of one lower limit that is physical one gets either a lower and an upper limit, or no solution at all. In particular the integral over E_2 becomes

$$\int_{m_2}^{\infty} dE_2 \Theta\left(b_D^2 - 4a_D c_D\right) = \int_{E_{D-}}^{E_{D+}} dE_2 \Theta(k - 1). \tag{C.88}$$

The coefficient k is defined in (C.37) while the integration limits $E_{D\pm}$ are given by

$$E_{D\pm} = \frac{1}{2}\left[(E_3 + E_1)(k - 1) \pm \sqrt{\left(E_1^2 + E_3^2 + 2E_1 E_3 \cos\theta\right)\left[(1 - k)^2 - \frac{2m_2^2}{E_1 E_3 (1 - \cos\theta)}\right]}\right]. \tag{C.89}$$

The meaning of the remaining heaviside function is that certain kinematic configurations of E_1, E_3, and $\cos\theta$ are in general not possible for given masses m_2 and m_4. As part of that it states that a particle can never decay into a heavier particle. Sorting now R_{D1} by powers of E_2 one finds

$$R_{D1} = \frac{2\pi}{\Delta_D^5} \int_{E_{D-}}^{E_{D+}} dE_2 f_2(E_2) \left[1 - f_4(E_4)\right] \left(\widetilde{A}_{D1} E_2^2 + \widetilde{B}_{D1} E_2 + \widetilde{C}_{D1}\right) \Theta(k - 1). \tag{C.90}$$

The coefficients $\widetilde{A}_{D1}$, $\widetilde{B}_{D1}$, $\widetilde{C}_{D1}$, and Δ_D are given by

$$\widetilde{A}_{D1} = E_1 E_3 (1 - \cos\theta)^2 \left[-E_1^2 + E_1 E_3 (3 + \cos\theta) - E_3^2\right], \tag{C.91}$$

$$\widetilde{B}_{D1} = E_1^2 E_3 (1 - \cos\theta)^2 \left[-2E_1^2 + E_1 E_3 (3 - \cos\theta) + E_3^2 (1 + 3\cos\theta)\right] \tag{C.92}$$
$$+ Q(1 - \cos\theta)\left[E_1^3 - E_1^2 E_3 (2 + \cos\theta) - E_1 E_3^2 (2 + \cos\theta) + E_3^3\right],$$

$$\widetilde{C}_{D1} = -E_1^3 E_3 (1 - \cos\theta)^2 \left[E_1^2 + 2E_1 E_3 \cos\theta + E_3^2 \left(-\frac{1}{2} + \frac{3}{2}\cos^2\theta\right)\right] \tag{C.93}$$
$$+ Q E_1 (1 - \cos\theta)\left[E_1^3 + E_1^2 E_3 \cos\theta + E_1 E_3^2 \left(-2 + \cos^2\theta\right) - E_3^3 \cos\theta\right]$$
$$+ Q^2 \left[E_1^2 \cos\theta + E_1 E_3 \left(\frac{3}{2} + \frac{1}{2}\cos^2\theta\right) + E_3^2 \cos\theta\right] - \frac{1}{2} E_1 E_3 (1 - \cos^2\theta) \Delta^2 m_2^2,$$

$$\Delta = \sqrt{E_1^2 + 2E_1 E_3 \cos\theta + E_3^2}. \tag{C.94}$$

Integral R_{D2}

The integral R_{D2} is given by

$$R_{D2} = \int d^3 p_2 d^3 p_4 \frac{(p_1 \cdot p_4)(p_2 \cdot p_3)}{E_1 E_2 E_3 E_4} \delta^4(p_1 + p_2 + p_3 - p_4) f_2(E_2) \left[1 - f_4(E_4)\right]. \tag{C.95}$$

Using (C.73) the four-momentum product can be transformed into

$$\begin{aligned}(p_1 \cdot p_4)(p_2 \cdot p_3) &= (p_2 \cdot p_3)\left[-(p_2 \cdot p_3) + Q\right] \\ &= -E_3^2 \left(E_2 - \bar{p}_2 \cos\alpha\right)^2 + E_3 Q \left(E_2 - \bar{p}_2 \cos\alpha\right) \\ &= \frac{E_3}{\bar{p}_2}\left[A_{D2} + B_{D2} \cos\alpha + C_{2D} \cos^2\alpha\right]. \end{aligned} \tag{C.96}$$

The expressions A_{D2}, B_{D2}, and C_{D2} are given by

$$A_{D2} = \bar{p}_2 E_2 \left(-E_3 E_2 + Q\right), \tag{C.97}$$

$$B_{D2} = -\bar{p}_2^2 \left(-2E_3 E_2 + Q\right), \tag{C.98}$$

$$C_{D2} = -E_3 \bar{p}_2^3. \tag{C.99}$$

Analogous to the relation between R_1 and R_{D1}, one can derive R_{D2} from R_2 by replacing E_3 with $-E_3$.

$$R_{D2} = \frac{2\pi}{\Delta_D^5} \int\limits_{E_{D-}}^{E_{D+}} dE_2 f_2(E_2) \left[1 - f_4(E_4)\right] \left(\widetilde{A}_{D2} E_2^2 + \widetilde{B}_{D2} E_2 + \widetilde{C}_{D2}\right) \Theta(k-1). \tag{C.100}$$

The coefficients Δ, $E_{D\pm}$, and k are given in (C.94), (C.89), and (C.37), respectively. $\widetilde{A}_{D2}$, $\widetilde{B}_{D2}$, and $\widetilde{C}_{D2}$ are given by

$$\widetilde{A}_{D2} = E_1 E_3 \left(1 - \cos\theta\right)^2 \left[-E_1^2 + E_1 E_3 \left(3 + \cos\theta\right) - E_3^2\right], \tag{C.101}$$

$$\begin{aligned}\widetilde{B}_{D2} = &E_1 E_3^2 \left(1 - \cos\theta\right)^2 \left[E_1^2 \left(1 + 3\cos\theta\right) - E_1 E_3 \left(-3 + \cos\theta\right) - 2E_3^2\right] \\ &+ Q \left(1 - \cos\theta\right) \left[E_1^3 - E_1^2 E_3 \left(2 + \cos\theta\right) - E_1 E_3^2 \left(2 + \cos\theta\right) + E_3^3\right],\end{aligned} \tag{C.102}$$

$$\begin{aligned}\widetilde{C}_{D2} = &- E_1 E_3^3 \left(1 - \cos\theta\right)^2 \left[E_1^2 \left(-\frac{1}{2} + \frac{3}{2}\cos^2\theta\right) + 2E_1 E_3 \cos\theta + E_3^2\right] \\ &+ QE_3 \left(1 - \cos\theta\right) \left[-E_1^3 \cos\theta + E_1^2 E_3 \left(-2 + \cos^2\theta\right) + E_1 E_3^2 \cos\theta + E_3^3\right] \\ &+ Q^2 \left[E_1^2 \cos\theta + E_1 E_3 \left(\frac{3}{2} + \frac{1}{2}\cos^2\theta\right) + E_3^2 \cos\theta\right] - \frac{1}{2} E_1 E_3 \left(1 - \cos^2\theta\right) \Delta^2 m_2^2.\end{aligned} \tag{C.103}$$

Integral R_{D3}

The integral R_{D3} is given by

$$R_{D3} = \int d^3 p_2 d^3 p_4 \frac{(p_1 \cdot p_3)}{E_1 E_2 E_3 E_4} \delta^4(p_1 + p_2 + p_3 - p_4) f_2(E_2) \left[1 - f_4(E_4)\right]. \tag{C.104}$$

The four-momentum product can be transformed into

$$(p_1 \cdot p_3) = E_1 E_3^2 \left(1 - \cos\theta\right) \tag{C.105}$$

$$= \frac{E_3}{\bar{p}_2} A_{D3}. \tag{C.106}$$

The expressions A_{D3} is given by

$$A_{D3} = \bar{p}_2 E_1 \left(1 - \cos\theta\right). \tag{C.107}$$

The subsequent derivation is completely analogous to R_{D1}, so one finds that R_{D3} is connected to R_3 by replacing E_3 with $-E_3$.

$$R_{D3} = \frac{2\pi}{\Delta_D^5} \int\limits_{E_{D-}}^{E_{D+}} dE_2 f_2(E_2) \left[1 - f_4(E_4)\right] \widetilde{C}_{D3} \Theta(k-1). \tag{C.108}$$

Again the coefficient Δ_D, $E_{D\pm}$, and k are given in (C.94), (C.89), and (C.37), respectively. $\widetilde{C}_{D3}$ is defined by

$$\widetilde{C}_{D3} = \left(1 - \cos\theta\right) \Delta_D^4 m_2 m_4. \tag{C.109}$$

157

Integral over E_2

The main difference between the dE_2 integration for scattering and inverse decay reactions is that inverse decay reactions also have an upper limit. Also the argument of f_4 changes due to the different kinematics. Consequently one can express it by

$$\int\limits_{E_{D-}}^{E_{D+}} dE_2 E_2^n f_2(E_2) \left[1 - f_4(E_2 + E_1 + E_3)\right] \qquad n = \{0, 1, 2\} \tag{C.110}$$

$$= \left(\int\limits_{E_{D-}}^{\infty} - \int\limits_{E_{D+}}^{\infty}\right) dE_2 E_2^n f_2(E_2) \left[1 - f_4(E_2 + E_1 + E_3)\right]. \tag{C.111}$$

Proceeding then analogous to the scattering reactions the derivation yields

$$I_{D0} = \int\limits_{E_{D-}}^{E_{D+}} dE_2 f_2(E_2) \left[1 - f_4(E_2 + E_1 + E_3)\right]$$
$$= T f_\gamma\big(\eta_D' - \eta\big) \left[F_0\big(\eta_D' - y_-\big) - F_0(\eta - y_-) - F_0\big(\eta_D' - y_+\big) + F_0(\eta - y_+)\right], \tag{C.112}$$

$$I_{D1} = \int\limits_{E_{D-}}^{E_{D+}} dE_2 E_2 f_2(E_2) \left[1 - f_4(E_2 + E_1 + E_3)\right]$$
$$= T^2 f_\gamma\big(\eta_D' - \eta\big) \left\{\left[F_1\big(\eta_D' - y_-\big) - F_1(\eta - y_-) - F_1\big(\eta_D' - y_+\big) + F_1(\eta - y_+)\right]\right.$$
$$\left. + y_- \left[F_0\big(\eta_D' - y_-\big) - F_0(\eta - y_-)\right] - y_+ \left[F_0\big(\eta_D' - y_+\big) - F_0(\eta - y_+)\right]\right\}, \tag{C.113}$$

$$I_{D2} = \int\limits_{E_{D-}}^{E_{D+}} dE_2 E_2^2 f_2(E_2) \left[1 - f_4(E_2 + E_1 + E_3)\right]$$
$$= T^3 f_\gamma\big(\eta_D' - \eta\big) \left\{\left[F_2\big(\eta_D' - y_-\big) - F_2(\eta - y_-) - F_2\big(\eta_D' - y_+\big) + F_2(\eta - y_+)\right]\right.$$
$$+ 2y_- \left[F_1\big(\eta_D' - y_-\big) - F_1(\eta - y_-)\right] - 2y_+ \left[F_1\big(\eta_D' - y_+\big) - F_1(\eta - y_+)\right]$$
$$\left. + y_-^2 \left[F_0\big(\eta_D' - y_-\big) - F_0(\eta - y_-)\right] - y_+^2 \left[F_0\big(\eta_D' - y_+\big) - F_0(\eta - y_+)\right]\right\}. \tag{C.114}$$

Here, $F_n(z)$ and $f_\gamma(z)$ are given in (C.65), η is given in (C.61), and y and η_D' determined by

$$y_\pm \equiv \frac{E_{D\pm}}{T}, \qquad \eta_D' = \eta - \frac{E_1 + E_3 + \mu_2 - \mu_4}{T}. \tag{C.115}$$

D. Cross Sections for Relativistic and Interacting Nucleons

D.1. Phasespace Integrals for Absorption Reactions

From the respective matrix elements (5.6), (5.17), (5.36) it can be seen that the cross sections have the same kinematic structure for all three neutrino capture reactions. In the following one denotes the incoming neutrino by "1", the incoming nucleon by "2", the outgoing charged lepton by "3" and the outgoing nucleon by "4". With this notation the cross section for all neutrino capture reactions can be written the following way

$$d\lambda^{-1}(E_1) = \int \frac{d^3p_2}{(2\pi)^3} \frac{d^3p_3}{(2\pi)^3} \frac{d^3p_4}{(2\pi)^3} 2G_F^2 V_{ud}^2 \frac{(A_j M_A + ... + L_j M_L)}{E_1 E_2^* E_3 E_4^*} (2\pi)^4 \delta^4(p_1 + p_2 - p_3 - p_4) \quad \text{(D.1)}$$
$$\times f_2(E_2) \left[1 - f_3(E_3)\right] \left[1 - f_4(E_4)\right].$$

In a first step one separates the phase space integrals into an angular integral and an integral over absolute momentum $\bar{p} = \sqrt{\vec{p}^2}$

$$d^3p_3 = \bar{p}_3^2 d\Omega_3 d\bar{p}_3 = \bar{p}_3 E_3 d\Omega_3 dE_3 \qquad \text{and} \qquad d^3p_{2,4} = \bar{p}_{2,4}^2 d\Omega_{2,4} d\bar{p}_{2,4} = \bar{p}_{2,4} E_{2,4}^* d\Omega_{2,4} dE_{2,4}. \quad \text{(D.2)}$$

Next the four-momentum conserving δ^4 is reduced to δ^3 by integration over dE_4

$$\int dE_4 \, \delta^4(p_1 + p_2 - p_3 - p_4) = \delta^3(\vec{p}_1 + \vec{p}_2 - \vec{p}_3 - \vec{p}_4)\Theta(E_4^* - m_4^*). \quad \text{(D.3)}$$

From here on the energy E_4 is given by $E_4 = E_1 + E_2 - E_3$. For convenience this relation will not be explicitly written out. With D.2 and D.3 the cross section becomes

$$d\lambda^{-1}(E_1) = \frac{2G_F^2 V_{ud}^2}{(2\pi)^5} \int\limits_{E_{2-}}^{\infty} dE_2 \int\limits_{m_3}^{E_{3+}} dE_3 \frac{\bar{p}_2 \bar{p}_3 \bar{p}_4}{E_1} f_2(E_2) \left[1 - f_3(E_3)\right] \left[1 - f_4(E_4)\right] \quad \text{(D.4)}$$
$$\int d\Omega_2 d\Omega_3 d\Omega_4 \left(A_j M_A + ... + L_j M_L\right) \delta^3(\vec{p}_1 + \vec{p}_2 - \vec{p}_3 - \vec{p}_4).$$

The limits for the two remaining energy integrals dE_2 and dE_3 are set by the following conditions. E_2 must be so large that for a given E_1 it is at least possible to produce final state particles with their respective minimal energy

$$E_{2-} \geq E_{3,\text{min}} + E_{4,\text{min}} - E_1 = m_3 + m_4^* + U_4 - E_1. \quad \text{(D.5)}$$

Also E_2 must be at least its own minimal energy. Hence the lower limit E_{2-} is given by

$$E_{2-} = \max\left\{m_3 + m_4^* + U_4 - E_1, m_2^* + U_2\right\}. \quad \text{(D.6)}$$

The lower limit for E_3 is trivially its mass m_3. The upper limit E_{3+} is set by the condition that for a given energy E_1 and E_2 the remaining energy E_4 is at least equal to the minimum energy of this particles

$$E_{3+} = E_1 + E_2 - E_{4,\text{min}} = E_1 + E_2 - m_4^* - U_4. \tag{D.7}$$

The three angular integrals can be solved analytically for all terms. For this purpose the integrals $(I_A, ..., I_L)$ are defined by

$$I_X \equiv \frac{\bar{p}_1 \bar{p}_2 \bar{p}_3 \bar{p}_4}{4\pi^2} \int d\Omega_2 d\Omega_3 d\Omega_4 M_X \delta^3(\vec{p}_1 + \vec{p}_2 - \vec{p}_3 - \vec{p}_4). \tag{D.8}$$

These integrals will be solved explicitly in the following. The calculation of these integrals is strongly based on the approach in [137]. Yet, it develops this approach further by including medium effects, fully relativistic treatment, in some case more elaborate computation schemes.

Angular Integral I-A

I_A is given by

$$I_A \equiv \frac{\bar{p}_1 \bar{p}_2 \bar{p}_3 \bar{p}_4}{4\pi^2} \int d\Omega_2 d\Omega_3 d\Omega_4 \left(p_1 \cdot p_2^* \right) \left(p_3 \cdot p_4^* \right) \delta^3(\vec{p}_1 + \vec{p}_2 - \vec{p}_3 - \vec{p}_4). \tag{D.9}$$

Define the momentum $\vec{P}_1$ by

$$\vec{P}_1 \equiv \vec{p}_1 + \vec{p}_2 \qquad \text{and} \qquad P_1 = \sqrt{\bar{p}_1^2 + \bar{p}_2^2 + 2\bar{p}_1 \bar{p}_2 \cos\theta_2}. \tag{D.10}$$

The δ-function can then be expressed by

$$\delta^3(\vec{p}_1 + \vec{p}_2 - \vec{p}_3 - \vec{p}_4) = \frac{1}{\bar{p}_4^2} \delta\left(p_4 - \left| \vec{P}_1 - \vec{p}_3 \right| \right) \delta^2\left(\Omega_4 - \Omega_{|\vec{P}_1 - \vec{p}_3|} \right). \tag{D.11}$$

Integrating over $d\Omega_4$ results then into

$$I_A = \frac{\bar{p}_1 \bar{p}_2 \bar{p}_3}{4\pi^2 \bar{p}_4} \int d\Omega_2 d\Omega_3 \left(E_1 E_2^* - \vec{p}_1 \cdot \vec{p}_2 \right) \left(E_3 E_4^* - \vec{p}_3 \cdot \vec{p}_4 \right) \delta\left(p_4 - \left| \vec{P}_1 - \vec{p}_3 \right| \right). \tag{D.12}$$

The angular integral is given by $d\Omega_3 = d\phi_3 d\cos\theta_3 = d\phi_3 dx$. One has the freedom to define the angle x as the angle between $\vec{P}_1$ and $\vec{p}_3$. This allows for a variable substitution in the δ-function

$$\delta\left(p_4 - \left| \vec{P}_1 - \vec{p}_3 \right| \right) = \delta\left(p_4 - \sqrt{\vec{P}_2^2 + \vec{p}_3^2 - 2x\vec{P}_1\vec{p}_3} \right) = \frac{\bar{p}_4}{P_1 \bar{p}_3} \delta\left(x - \frac{P_1^2 + \bar{p}_3^2 - \bar{p}_4^2}{2 P_1 \bar{p}_3} \right). \tag{D.13}$$

Further the dot product $(\vec{p}_3 \cdot \vec{p}_4)$ can be rewritten by eliminating x according to the δ-function

$$\vec{p}_3 \cdot \vec{p}_4 = \vec{p}_3 \cdot \left(\vec{P}_1 - \vec{p}_3 \right) = \bar{p}_3 P_1 x - \bar{p}_3^2 = \frac{P_1^2 - \bar{p}_3^2 - \bar{p}_4^2}{2}. \tag{D.14}$$

Performing integrations over ϕ_3 and x, the integral I_A becomes

$$I_A = \frac{\bar{p}_1 \bar{p}_2}{2\pi} \int d\Omega_2 \frac{1}{P_1} \left(E_1 E_2^* - \vec{p}_1 \cdot \vec{p}_2 \right) \left(E_3 E_4^* + \frac{\bar{p}_3^2 + \bar{p}_4^2 - P_1^2}{2} \right) \Theta(\bar{p}_3 + \bar{p}_4 - P_1) \Theta(P_1 - |\bar{p}_3 - \bar{p}_4|). \tag{D.15}$$

The Heaviside functions arise from the limits of the angular range $-1 \leq x \leq 1$. Now one can substitute the angular integral $d\Omega_2$ by

$$d\Omega_2 = d\phi_2 d\cos\theta_2 = d\phi_2 dP_1 \frac{P_1}{\bar{p}_1 \bar{p}_2}. \tag{D.16}$$

Performing the integration over ϕ_2 the integral I_A takes the form

$$I_A = \int\limits_{P_{1,min}}^{P_{1,max}} dP_1 \left(E_1 E_2^* + \frac{\bar{p}_1^2 + \bar{p}_2^2 - P_1^2}{2} \right) \left(E_3 E_4^* + \frac{\bar{p}_3^2 + \bar{p}_4^2 - P_1^2}{2} \right), \tag{D.17}$$

where the limits $P_{1,min}$ and $P_{1,max}$ arise from the combined constraints on both angles $\cos\theta_2$ and $\cos\theta_3$. They are given by

$$P_{1,min} = \max\left\{ |\bar{p}_1 - \bar{p}_2|, |\bar{p}_3 - \bar{p}_4| \right\} \qquad \text{and} \qquad P_{1,max} = \min\left\{ \bar{p}_1 + \bar{p}_2, \bar{p}_3 + \bar{p}_4 \right\}. \tag{D.18}$$

After performing the integration over P_1 one finally obtains

$$I_A = \frac{1}{60} \left[3 \left(P_{1,max}^5 - P_{1,min}^5 \right) - 10 \left(a + b \right) \left(P_{1,max}^3 - P_{1,min}^3 \right) + 60ab \left(P_{1,max} - P_{1,min} \right) \right]. \tag{D.19}$$

The coefficients a and b are given by

$$a = E_1 E_2^* + \frac{\bar{p}_1^2 + \bar{p}_2^2}{2} \qquad \text{and} \qquad b = E_3 E_4^* + \frac{\bar{p}_3^2 + \bar{p}_4^2}{2}. \tag{D.20}$$

Angular Integral I-B

I_B is given by

$$I_B \equiv \frac{\bar{p}_1 \bar{p}_2 \bar{p}_3 \bar{p}_4}{4\pi^2} \int d\Omega_2 d\Omega_3 d\Omega_4 \, (p_1 \cdot p_4^*)(p_3 \cdot p_2^*) \, \delta^3(\vec{p}_1 + \vec{p}_2 - \vec{p}_3 - \vec{p}_4). \tag{D.21}$$

Define the momentum $\vec{P}_2$ by

$$\vec{P}_2 \equiv \vec{p}_4 - \vec{p}_1 \qquad \text{and} \qquad P_2 = \sqrt{\bar{p}_1^2 + \bar{p}_4^2 - 2\bar{p}_1 \bar{p}_4 \cos\theta_4}. \tag{D.22}$$

The δ-function can then be expressed by

$$\delta^3(\vec{p}_1 + \vec{p}_2 - \vec{p}_3 - \vec{p}_4) = \frac{1}{\bar{p}_2^2} \delta\left(p_2 - \left| \vec{P}_2 + \vec{p}_3 \right| \right) \delta^2\left(\Omega_2 - \Omega_{|\vec{P}_2 + \vec{p}_3|} \right). \tag{D.23}$$

Integrating over $d\Omega_2$ results then into

$$I_B = \frac{\bar{p}_1 \bar{p}_3 \bar{p}_4}{4\pi^2 \bar{p}_2} \int d\Omega_3 d\Omega_4 \, (E_1 E_4^* - \vec{p}_1 \cdot \vec{p}_4)(E_2^* E_3 - \vec{p}_2 \cdot \vec{p}_3) \, \delta\left(p_2 - \left| \vec{P}_2 + \vec{p}_3 \right| \right). \tag{D.24}$$

Substituting $d\Omega_3 = d\phi_3 d\cos\theta_3 = d\phi_3 dx$ with x as the angle between $\vec{P}_1$ and $\vec{p}_3$, the δ-function becomes

$$\delta\left(p_2 - \left| \vec{P}_2 + \vec{p}_3 \right| \right) = \delta\left(p_2 - \sqrt{\vec{P}_2^2 + \vec{p}_3^2 + 2x\vec{P}_2\vec{p}_3} \right) = \frac{\bar{p}_2}{P_2 \bar{p}_3} \delta\left(x - \frac{\bar{p}_2^2 - P_2^2 - \bar{p}_3^2}{2P_2 \bar{p}_3} \right). \tag{D.25}$$

Further the dot product $(\vec{p}_2 \cdot \vec{p}_3)$ can be rewritten by eliminating x

$$\vec{p}_2 \cdot \vec{p}_3 = \vec{p}_3 \cdot \left(\vec{P}_2 + \vec{p}_3 \right) = \bar{p}_3 P_2 x + \bar{p}_3^2 = \frac{\bar{p}_2^2 + \bar{p}_3^2 - P_2^2}{2}. \tag{D.26}$$

Performing integrations over ϕ_3 and x, the integral I_B becomes

$$I_B = \frac{\bar{p}_1 \bar{p}_4}{2\pi} \int d\Omega_4 \frac{1}{P_2} (E_1 E_4^* - \vec{p}_1 \cdot \vec{p}_4) \left(E_2^* E_3 + \frac{P_2^2 - \bar{p}_2^2 - \bar{p}_3^2}{2} \right) \Theta(\bar{p}_2 + \bar{p}_3 - P_2) \Theta(P_2 - |\bar{p}_2 - \bar{p}_3|). \tag{D.27}$$

Now one can substitute the angular integral $d\Omega_4$ by

$$d\Omega_4 = d\phi_4 d\cos\theta_4 = -d\phi_4 dP_2 \frac{P_2}{\bar{p}_1 \bar{p}_4}. \tag{D.28}$$

Performing the integration over ϕ_4, the integral I_B takes the form

$$I_B = \int\limits_{P_{2,min}}^{P_{2,max}} dP_2 \left(E_1 E_4^* + \frac{P_2^2 - \bar{p}_1^2 - \bar{p}_4^2}{2} \right) \left(E_2^* E_3 + \frac{P_2^2 - \bar{p}_2^2 - \bar{p}_3^2}{2} \right). \tag{D.29}$$

The limits $P_{2,min}$ and $P_{2,max}$ are given by

$$P_{2,min} = \max\left\{|\bar{p}_1 - \bar{p}_4|, |\bar{p}_2 - \bar{p}_3|\right\} \qquad \text{and} \qquad P_{2,max} = \min\left\{\bar{p}_1 + \bar{p}_4, \bar{p}_2 + \bar{p}_3\right\}. \tag{D.30}$$

After performing the integration over P_2 one finally obtains

$$I_B = \frac{1}{60} \left[3\left(P_{2,max}^5 - P_{2,min}^5\right) + 10\left(c + d\right)\left(P_{2,max}^3 - P_{2,min}^3\right) + 60cd\left(P_{2,max} - P_{2,min}\right) \right]. \tag{D.31}$$

The coefficients c and d are given by

$$c = E_1 E_4^* - \frac{\bar{p}_1^2 + \bar{p}_4^2}{2} \qquad \text{and} \qquad d = E_2^* E_3 - \frac{\bar{p}_2^2 + \bar{p}_3^2}{2}. \tag{D.32}$$

Angular Integral I-C

I_C is given by

$$I_C \equiv \frac{\bar{p}_1 \bar{p}_2 \bar{p}_3 \bar{p}_4}{4\pi^2} \int d\Omega_2 d\Omega_3 d\Omega_4 \left(p_1 \cdot p_2^*\right)^2 \left(p_1 \cdot p_3\right) \delta^3(\vec{p}_1 + \vec{p}_2 - \vec{p}_3 - \vec{p}_4). \tag{D.33}$$

First one defines the momentum $\vec{P}_1$ like in (D.10). The integration of I_C proceeds then completely analogous to I_A up to (D.15), except for the transformation of the dot product and the integral over ϕ_3. One arrives then at

$$I_C = \frac{\bar{p}_1 \bar{p}_2}{4\pi^2} \int d\Omega_2 d\phi_3 \frac{1}{P_1} \left(p_1 \cdot p_2^*\right)^2 \left(p_1 \cdot p_3\right) \Theta(\bar{p}_3 + \bar{p}_4 - P_1)\Theta(P_1 - |\bar{p}_3 - \bar{p}_4|). \tag{D.34}$$

Next the angular integral $d\Omega_2$ is substituted according to (D.16). Rewriting the four-momentum products yields then

$$I_C = \frac{1}{4\pi^2} \int d\phi_2 d\phi_3 \int\limits_{P_{1,min}}^{P_{1,max}} dP_1 \left(E_1 E_2^* + \frac{\bar{p}_1^2 + \bar{p}_2^2 - P_1^2}{2} \right)^2 \left(E_1 E_3 - \bar{p}_1 \bar{p}_3 \cos\theta_{1,3} \right). \tag{D.35}$$

Now one has to use a relation that connects the $\cos\theta_{a,b}$ between two vectors $\vec{v}_a$ and $\vec{v}_b$ to the cosines $\cos\theta_{a,c}$ and $\cos\theta_{b,c}$ of each vector to a third vector $\vec{v}_c$. Denoting $\cos\theta$ by x this relation is given by

$$x_{a,b} = x_{a,c} x_{b,c} - \sqrt{\left(1 - x_{a,c}^2\right)\left(1 - x_{b,c}^2\right)} \cos\left(\phi_{a,b}\right). \tag{D.36}$$

Inserting $\vec{v}_a = \vec{p}_1$, $\vec{v}_b = \vec{p}_3$, and $\vec{v}_c = \vec{P}_1$, this transforms into

$$x_{1,3} = x_{1,P} x_{3,P} - \sqrt{\left(1 - x_{1,P}^2\right)\left(1 - x_{3,P}^2\right)} \cos\phi_{1,3}. \tag{D.37}$$

Further one finds that the second term of $x_{1,3}$ does not contribute to an integral over $\phi_{1,3}$ because of the asymmetry of $\cos\phi_{1,3}$. Renaming $\phi_3 \to \phi_{1,3}$ it can be shown that

$$\int_0^{2\pi} d\phi_{1,3}\cos\phi_{1,3} = \int_0^{\pi} d\phi_{1,3}\cos\phi_{1,3} + \int_{\pi}^{2\pi} d\phi_{1,3}\cos\phi_{1,3} = \int_0^{\pi} d\phi_{1,3}\cos\phi_{1,3} - \int_0^{\pi} d\phi_{1,3}\cos\phi_{1,3} = 0. \tag{D.38}$$

Consequently the integral I_C can be rewritten into

$$I_C = \frac{1}{4\pi^2}\int d\phi_2 d\phi_3 \int_{P_{1,min}}^{P_{1,max}} dP_1 \left(E_1 E_2^* + \frac{\bar{p}_1^2 + \bar{p}_2^2 - P_1^2}{2}\right)^2 (E_1 E_3 - \bar{p}_1\bar{p}_3\bar{x}_{1,3}). \tag{D.39}$$

with $\bar{x}_{1,3} = x_{1,P}x_{3,P}$. The cosines $x_{3,P}$ is already fixed by momentum conservation, see (D.13)

$$x_{3,P} = \frac{P_1^2 + \bar{p}_3^2 - \bar{p}_4^2}{2P_1\bar{p}_3}. \tag{D.40}$$

For $x_{1,P}$ one finds

$$x_{1,P} = \frac{\vec{p}_1 \cdot \vec{P}_1}{\bar{p}_1 P_1} = \frac{\bar{p}_1^2 + \bar{p}_1\bar{p}_2\cos\theta_2}{\bar{p}_1 P_1} = \frac{P_1^2 + \bar{p}_1^2 - \bar{p}_2^2}{2\bar{p}_1 P_1} \qquad \text{with} \qquad \cos\theta_2 = \frac{P_1^2 - \bar{p}_1^2 - \bar{p}_2^2}{2\bar{p}_1\bar{p}_2}. \tag{D.41}$$

Plugging (D.40) and (D.41) into (D.39), the integral I_C takes the form

$$I_C = \frac{1}{4\pi^2}\int d\phi_2 d\phi_3 \int_{P_{1,min}}^{P_{1,max}} dP_1 \left(E_1 E_2^* + \frac{\bar{p}_1^2 + \bar{p}_2^2 - P_1^2}{2}\right)^2 \left[E_1 E_3 - \frac{1}{4P_1^2}\left(P_1^2 + \bar{p}_1^2 - \bar{p}_2^2\right)\left(P_1^2 + \bar{p}_3^2 - \bar{p}_4^2\right)\right]. \tag{D.42}$$

Performing the angular integrations one finds then

$$I_C = \int_{P_{1,min}}^{P_{1,max}} dP_1 \left(\alpha_0 + \alpha_1 P_1^2\right)^2 \left(\beta_0 P_1^{-2} + \beta_1 + \beta_2 P_1^2\right). \tag{D.43}$$

where the limits $P_{1,min}$ and $P_{1,max}$ are given in (D.18). The other coefficients are given by

$$\begin{aligned} \alpha_0 &= E_1 E_2^* + \frac{\bar{p}_1^2 + \bar{p}_2^2}{2}, & \beta_0 &= \frac{1}{4}\left(\bar{p}_1^2 - \bar{p}_2^2\right)\left(\bar{p}_4^2 - \bar{p}_3^2\right), \\ \alpha_1 &= -\frac{1}{2}, & \beta_1 &= E_1 E_3 - \frac{1}{4}\left(\bar{p}_1^2 - \bar{p}_2^2 + \bar{p}_3^2 - \bar{p}_4^2\right), \\ & & \beta_2 &= -\frac{1}{4}. \end{aligned} \tag{D.44}$$

Performing the integration over P_1 one finally obtains

$$\begin{aligned} I_C = \Bigg[&-\frac{\left(P_{1,max}^7 - P_{1,min}^7\right)}{56} + \frac{(\alpha_0 + \beta_1)}{20}\left(P_{1,max}^5 - P_{1,min}^5\right) - \frac{\left(\alpha_0^2 + 4\alpha_0\beta_1 - \beta_0\right)}{12}\left(P_{1,max}^3 - P_{1,min}^3\right) \\ &+ \left(\alpha_0^2\beta_1 - \alpha_0\beta_0\right)\left(P_{1,max} - P_{1,min}\right) - \alpha_0^2\beta_0\left(P_{1,max}^{-1} - P_{1,min}^{-1}\right)\Bigg]. \end{aligned} \tag{D.45}$$

Angular Integral I-D

I_D is given by

$$I_D \equiv \frac{\bar{p}_1\bar{p}_2\bar{p}_3\bar{p}_4}{4\pi^2} \int d\Omega_2 d\Omega_3 d\Omega_4 \, (p_1 \cdot p_3)^2 \, (p_1 \cdot p_2^*) \, \delta^3(\vec{p}_1 + \vec{p}_2 - \vec{p}_3 - \vec{p}_4). \tag{D.46}$$

Define the momentum $\vec{P}_3$ by

$$\vec{P}_3 \equiv \vec{p}_1 - \vec{p}_3 \qquad \text{and} \qquad P_3 = \sqrt{\bar{p}_1^2 + \bar{p}_3^2 - 2\bar{p}_1\bar{p}_3 \cos\theta_3}. \tag{D.47}$$

The δ-function can then be expressed by

$$\delta^3(\vec{p}_1 + \vec{p}_2 - \vec{p}_3 - \vec{p}_4) = \frac{1}{\bar{p}_4^2}\delta\Big(p_4 - \big|\vec{P}_3 + \vec{p}_2\big|\Big)\delta^2\Big(\Omega_4 - \Omega_{|\vec{P}_3+\vec{p}_2|}\Big). \tag{D.48}$$

Integrating over $d\Omega_4$ results then into

$$I_D = \frac{\bar{p}_1\bar{p}_2\bar{p}_3}{4\pi^2\bar{p}_4} \int d\Omega_2 d\Omega_3 \, (E_1 E_3 - \vec{p}_1 \cdot \vec{p}_3)^2 \, (E_1 E_2^* - \vec{p}_1 \cdot \vec{p}_2) \, \delta\Big(p_4 - \big|\vec{P}_3 + \vec{p}_2\big|\Big). \tag{D.49}$$

Substituting $d\Omega_2 = d\phi_2 d\cos\theta_2 = d\phi_2 dx_2$ with x_2 as the angle between $\vec{P}_3$ and $\vec{p}_2$, the δ-function becomes

$$\delta\Big(p_4 - \big|\vec{P}_3 + \vec{p}_2\big|\Big) = \delta\Big(p_4 - \sqrt{\vec{P}_3^2 + \vec{p}_2^2 + 2x_2\vec{P}_3\vec{p}_2}\Big) = \frac{\bar{p}_4}{P_3\bar{p}_2}\delta\Big(x_2 - \frac{\bar{p}_4^2 - P_3^2 - \bar{p}_2^2}{2P_3\bar{p}_2}\Big). \tag{D.50}$$

Performing the integration over x_2 and rewriting the momentum products one finds

$$I_D = \frac{\bar{p}_1\bar{p}_3}{4\pi^2}\int d\phi_2 d\Omega_3 \Big(E_1 E_3 + \frac{P_3^2 - \bar{p}_1^2 - \bar{p}_3^2}{2}\Big)^2 (E_1 E_2^* - \bar{p}_1\bar{p}_2 \cos\theta_{1,2}) \, \Theta(\bar{p}_2 + \bar{p}_4 - P_3)\Theta(P_3 - |\bar{p}_2 - \bar{p}_4|). \tag{D.51}$$

Now one can substitute the angular integral $d\Omega_3$ by

$$d\Omega_3 = d\phi_3 d\cos\theta_3 = -d\phi_3 dP_3 \frac{P_3}{\bar{p}_1\bar{p}_3}. \tag{D.52}$$

Using this relation the integral I_D becomes

$$I_D = \frac{1}{4\pi^2} \int d\phi_2 d\phi_3 \int\limits_{P_{3,min}}^{P_{3,max}} dP_3 \Big(E_1 E_3 + \frac{P_3^2 - \bar{p}_1^2 - \bar{p}_3^2}{2}\Big)^2 (E_1 E_2^* - \bar{p}_1\bar{p}_2 \cos\theta_{1,2}). \tag{D.53}$$

The limits $P_{3,min}$ and $P_{3,max}$ are given by

$$P_{3,min} = \max\{|\bar{p}_1 - \bar{p}_3|, |\bar{p}_2 - \bar{p}_4|\} \qquad \text{and} \qquad P_{3,max} = \min\{\bar{p}_1 + \bar{p}_3, \bar{p}_2 + \bar{p}_4\}. \tag{D.54}$$

Analogous to (D.37) one can derive a connection between the cosines $\cos\theta_{1,2} = x_{1,2}$, $x_{1,P}$, and $x_{2,P}$

$$x_{1,2} = x_{1,P}x_{2,P} - \sqrt{\Big(1 - x_{1,P}^2\Big)\Big(1 - x_{2,P}^2\Big)} \cos\phi_{1,2}. \tag{D.55}$$

The second part of $x_{1,2}$ does not contribute to the integral, analogous to the discussion for I_C in (D.38). Further, $x_{2,P} = x_2$ is already given in (D.50). The cosine $x_{1,P}$ equates to

$$x_{1,P} = \frac{\vec{p}_1 \cdot \vec{P}_3}{\bar{p}_1 P_3} = \frac{\bar{p}_1^2 - \bar{p}_1\bar{p}_3 \cos\theta_3}{\bar{p}_1 P_3} = \frac{P_3^2 + \bar{p}_1^2 - \bar{p}_3^2}{2\bar{p}_1 P_3} \qquad \text{with} \qquad \cos\theta_3 = \frac{\bar{p}_1^2 + \bar{p}_3^2 - P_3^2}{2\bar{p}_1\bar{p}_3}. \tag{D.56}$$

Plugging this into (D.53) the integral I_D takes the form

$$I_D = \frac{1}{4\pi^2} \int d\phi_2 d\phi_3 \int\limits_{P_{3,min}}^{P_{3,max}} dP_3 \left(E_1 E_3 + \frac{P_3^2 - \vec{p}_1^2 - \vec{p}_3^2}{2} \right)^2 \left[E_1 E_2^* + \frac{1}{4P_1^3} \left(P_3^2 + \vec{p}_1^2 - \vec{p}_3^2 \right) \left(P_3^2 + \vec{p}_2^2 - \vec{p}_4^2 \right) \right].$$

(D.57)

Performing the angular integrations one finds then

$$I_D = \int\limits_{P_{3,min}}^{P_{3,max}} dP_3 \left(\delta_0 + \delta_1 P_1^2 \right)^2 \left(\epsilon_0 P_1^{-2} + \epsilon_1 + \epsilon_2 P_1^2 \right).$$

(D.58)

The coefficients are defined by

$$\delta_0 = E_1 E_3 - \frac{\vec{p}_1^2 + \vec{p}_3^2}{2}, \qquad\qquad \epsilon_0 = \frac{1}{4} \left(\vec{p}_1^2 - \vec{p}_3^2 \right) \left(\vec{p}_2^2 - \vec{p}_4^2 \right),$$

$$\delta_1 = \frac{1}{2}, \qquad\qquad \epsilon_1 = E_1 E_2^* + \frac{1}{4} \left(\vec{p}_1^2 + \vec{p}_2^2 - \vec{p}_3^2 - \vec{p}_4^2 \right), \qquad \text{(D.59)}$$

$$\epsilon_2 = \frac{1}{4}.$$

Performing the integration over P_3 one finally obtains

$$I_D = \left[\frac{\left(P_{3,max}^7 - P_{3,min}^7 \right)}{56} + \frac{(\delta_0 + \epsilon_1)}{20} \left(P_{3,max}^5 - P_{3,min}^5 \right) + \frac{\left(\delta_0^2 + 4\delta_0\epsilon_1 + \epsilon_0 \right)}{12} \left(P_{3,max}^3 - P_{3,min}^3 \right) \right.$$

$$\left. + \left(\delta_0^2 \epsilon_1 + \delta_0 \epsilon_0 \right) \left(P_{3,max} - P_{3,min} \right) - \delta_0^2 \epsilon_0 \left(P_{3,max}^{-1} - P_{3,min}^{-1} \right) \right].$$

(D.60)

Angular Integral I-E

I_E is given by

$$I_E \equiv \frac{\bar{p}_1 \bar{p}_2 \bar{p}_3 \bar{p}_4}{4\pi^2} \int d\Omega_2 d\Omega_3 d\Omega_4 \, (p_1 \cdot p_2^*)^2 \, \delta^3(\vec{p}_1 + \vec{p}_2 - \vec{p}_3 - \vec{p}_4).$$

(D.61)

This integral can be solved completely analogous to I_A. Instead of (D.17) one obtains

$$I_E = \int\limits_{P_{1,min}}^{P_{1,max}} dP_1 \left(E_1 E_2^* + \frac{\vec{p}_1^2 + \vec{p}_2^2 - P_1^2}{2} \right)^2.$$

(D.62)

After performing the integration over P_1 the integral I_E results into

$$I_E = \frac{1}{60} \left[3 \left(P_{1,max}^5 - P_{1,min}^5 \right) - 20a \left(P_{1,max}^3 - P_{1,min}^3 \right) + 60a^2 \left(P_{1,max} - P_{1,min} \right) \right].$$

(D.63)

The expressions $P_{1,min}$ and $P_{1,max}$ are defined by (D.18) and a is given in (D.20).

Angular Integral I-G

I_G is given by

$$I_G \equiv \frac{\bar{p}_1 \bar{p}_2 \bar{p}_3 \bar{p}_4}{4\pi^2} \int d\Omega_2 d\Omega_3 d\Omega_4 \, (p_1 \cdot p_3)^2 \, \delta^3(\vec{p}_1 + \vec{p}_2 - \vec{p}_3 - \vec{p}_4).$$

(D.64)

First one defines the momentum $\vec{P}_3$ like in (D.47). The δ-function can then be expressed by

$$\delta^3(\vec{p}_1 + \vec{p}_2 - \vec{p}_3 - \vec{p}_4) = \frac{1}{\bar{p}_4^2}\delta\left(p_4 - \left|\vec{P}_3 + \vec{p}_2\right|\right)\delta^2\left(\Omega_4 - \Omega_{|\vec{P}_3 + \vec{p}_2|}\right). \tag{D.65}$$

Integrating over $d\Omega_4$ results then into

$$I_G = \frac{\bar{p}_1\bar{p}_2\bar{p}_3}{4\pi^2\bar{p}_4}\int d\Omega_2 d\Omega_3 \left(E_1 E_3 - \vec{p}_1 \cdot \vec{p}_3\right)^2 \delta\left(p_4 - \left|\vec{P}_3 + \vec{p}_2\right|\right). \tag{D.66}$$

Substituting $d\Omega_2 = d\phi_2 d\cos\theta_2 = d\phi_2 dx_2$ with x_2 as the angle between $\vec{P}_3$ and $\vec{p}_2$, the δ-function becomes

$$\delta\left(p_4 - \left|\vec{P}_3 + \vec{p}_2\right|\right) = \delta\left(p_4 - \sqrt{\vec{P}_3^{\,2} + \vec{p}_2^{\,2} + 2x_2\vec{P}_3\vec{p}_2}\right) = \frac{\bar{p}_4}{P_3\bar{p}_2}\delta\left(x_2 - \frac{\bar{p}_4^2 - P_3^2 - \bar{p}_2^2}{2P_3\bar{p}_2}\right). \tag{D.67}$$

Performing the integrations over ϕ_2 and x_2, the integral I_G becomes

$$I_G = \frac{\bar{p}_1\bar{p}_3}{2\pi}\int d\Omega_3 \left(E_1 E_3 + \frac{P_3^2 - \bar{p}_1^2 - \bar{p}_3^2}{2}\right)^2 \Theta(\bar{p}_2 + \bar{p}_4 - P_3)\Theta(P_3 - |\bar{p}_2 - \bar{p}_4|). \tag{D.68}$$

Now one can substitute the angular integral $d\Omega_3$ by

$$d\Omega_3 = d\phi_3 d\cos\theta_3 = -d\phi_3 dP_3\frac{P_3}{\bar{p}_1\bar{p}_3}. \tag{D.69}$$

Performing the integration over ϕ_3, the integral I_G takes the form

$$I_G = \int\limits_{P_{3,min}}^{P_{3,max}} dP_3 \left(E_1 E_3 + \frac{P_3^2 - \bar{p}_1^2 - \bar{p}_3^2}{2}\right)^2. \tag{D.70}$$

After performing the integration over P_3 one finally obtains

$$I_G = \frac{1}{60}\left[3\left(P_{3,max}^5 - P_{3,min}^5\right) + 20e\left(P_{3,max}^3 - P_{3,min}^3\right) + 60e^2\left(P_{3,max} - P_{3,min}\right)\right]. \tag{D.71}$$

The expressions $P_{3,min}$ and $P_{3,max}$ are defined by (D.54). The coefficient e is given by

$$e = E_1 E_3 - \frac{\bar{p}_1^2 + \bar{p}_3^2}{2}. \tag{D.72}$$

Angular Integral I-H

I_H is given by

$$I_H \equiv \frac{\bar{p}_1\bar{p}_2\bar{p}_3\bar{p}_4}{4\pi^2}\int d\Omega_2 d\Omega_3 d\Omega_4 \left(p_1 \cdot p_2^*\right)\left(p_1 \cdot p_3\right)\delta^3(\vec{p}_1 + \vec{p}_2 - \vec{p}_3 - \vec{p}_4). \tag{D.73}$$

This can be solved completely analogous to either I_C or I_D. Here I_D is chosen and so I_H is found to become

$$I_H = \int\limits_{P_{3,min}}^{P_{3,max}} dP_3 \left(\delta_0 + \delta_1 P_1^2\right)\left(\epsilon_0 P_1^{-2} + \epsilon_1 + \epsilon_2 P_1^2\right). \tag{D.74}$$

The coefficients $P_{3,min}$ and $P_{3,max}$ are defined in (D.54). The coefficients δ_i and ϵ_i are given in (D.59). Performing the integration over P_3 one finally obtains

$$I_H = \left[\frac{\left(P_{3,max}^5 - P_{3,min}^5\right)}{40} + \frac{(\delta_0 + 2\epsilon_1)}{12}\left(P_{3,max}^3 - P_{3,min}^3\right) + \frac{(2\delta_0\epsilon_1 + \epsilon_0)}{2}\left(P_{3,max} - P_{3,min}\right)\right. \tag{D.75}$$

$$\left. -\delta_0\epsilon_0\left(P_{3,max}^{-1} - P_{3,min}^{-1}\right)\right].$$

Angular Integral I-J

I_J is given by

$$I_J \equiv \frac{\bar{p}_1 \bar{p}_2 \bar{p}_3 \bar{p}_4}{4\pi^2} \int d\Omega_2 d\Omega_3 d\Omega_4 \, (p_1 \cdot p_2^*) \, \delta^3(\vec{p}_1 + \vec{p}_2 - \vec{p}_3 - \vec{p}_4). \tag{D.76}$$

This expression can be computed completely analogous to I_A. Following the integration there, I_J is found to become

$$I_J = \int_{P_{1,min}}^{P_{1,max}} dP_1 \left(E_1 E_2^* + \frac{\bar{p}_1^2 + \bar{p}_2^2 - P_1^2}{2} \right). \tag{D.77}$$

After performing the integration over P_1, the integral I_J results into

$$I_J = \frac{1}{60} \left[-10 \left(P_{1,max}^3 - P_{1,min}^3 \right) + 60a \left(P_{1,max} - P_{1,min} \right) \right]. \tag{D.78}$$

The expressions $P_{1,min}$ and $P_{1,max}$ are defined by (D.18) and a is given in (D.20).

Angular Integral I-K

I_K is given by

$$I_K \equiv \frac{\bar{p}_1 \bar{p}_2 \bar{p}_3 \bar{p}_4}{4\pi^2} \int d\Omega_2 d\Omega_3 d\Omega_4 \, (p_1 \cdot p_3) \, \delta^3(\vec{p}_1 + \vec{p}_2 - \vec{p}_3 - \vec{p}_4). \tag{D.79}$$

This expression can be computed completely analogous to I_G. Following the integration there, I_K is found to become

$$I_K = \int_{P_{3,min}}^{P_{3,max}} dP_3 \left(E_1 E_3 + \frac{P_3^2 - \bar{p}_1^2 - \bar{p}_3^2}{2} \right). \tag{D.80}$$

After performing the integration over P_3 one finally obtains

$$I_K = \frac{1}{60} \left[10 \left(P_{3,max}^3 - P_{3,min}^3 \right) + 60e \left(P_{3,max} - P_{3,min} \right) \right]. \tag{D.81}$$

The expressions $P_{3,min}$ and $P_{3,max}$ are defined by (D.54) and e is given in (D.72).

Angular Integral I-L

I_L is given by

$$I_L \equiv \frac{\bar{p}_1 \bar{p}_2 \bar{p}_3 \bar{p}_4}{4\pi^2} \int d\Omega_2 d\Omega_3 d\Omega_4 \delta^3(\vec{p}_1 + \vec{p}_2 - \vec{p}_3 - \vec{p}_4). \tag{D.82}$$

This expression can be computed completely analogous to either I_A or I_B or I_G. Hence I_L is found to become

$$I_L = \int_{P_{1,min}}^{P_{1,max}} dP_1 = \int_{P_{2,min}}^{P_{2,max}} dP_2 = \int_{P_{3,min}}^{P_{3,max}} dP_3. \tag{D.83}$$

After performing the integration one finally obtains

$$I_L = \left(P_{1,max} - P_{1,min} \right) = \left(P_{2,max} - P_{2,min} \right) = \left(P_{3,max} - P_{3,min} \right). \tag{D.84}$$

The limits for the momenta are given in (D.18), (D.30), and (D.54).

Limits for Energy Integration

For the two remaining energy integrals there are further constraints beyond the limits that are set in (D.4). They arise from the additional demand that the four-momentum configuration of all particles must not only comply with energy conservation but also momentum conservation. The corresponding constraint would be difficult to express in terms of explicit limits on the energy integrals. However, it can be simply expressed by the demand $P_{i,max} > P_{i,min}$. From (D.84) it is clear that this relation is fulfilled for all the P_i if it is fulfilled for one of them. Thus when numerically evaluating (D.4), the integrand must vanish if the condition is not met. In section (5.1) this is taken into account by multiplying the integrals I_X by $\Theta(P_{1,max} - P_{1,min})$.

D.2. Phasespace Integrals for Inverse Neutron Decay

The matrix element of inverse neutron decay (5.29) has a distinctly different kinematic structure to the neutrino capture reactions. For convenience and to compare with the capture reactions one denotes the incoming $\bar{\nu}_e$ by "1", the incoming proton by "2", the incoming electron by "3" and the outgoing neutron by "4". With this notation the cross section for inverse neutron decay can be written the following way

$$d\lambda^{-1}(E_1) = \int \frac{d^3p_p}{(2\pi)^3} \frac{d^3p_{e^-}}{(2\pi)^3} \frac{d^3p_n}{(2\pi)^3} 2G_F^2 V_{ud}^2 \frac{(A_3M_A + ... + L_3M_L)}{E_{\bar{\nu}_e} E_p^* E_{e^-} E_n^*} (2\pi)^4 \delta^4(p_{\bar{\nu}_e} + p_p + p_{e^-} - p_n)$$
$$\times f_p(E_p) f_{e^-}(E_{e^-})[1 - f_n(E_n)]. \tag{D.85}$$

Proceeding analogous to the capture reactions, this can be transformed into

$$d\lambda^{-1}(E_{\bar{\nu}_e}) = \frac{2G_F^2 V_{ud}^2}{(2\pi)^5} \int\limits_{m_p^*+U_p}^{\infty} dE_p \int\limits_{E_{min}}^{\infty} dE_{e^-} \frac{\bar{p}_p \bar{p}_{e^-} \bar{p}_n}{E_{\bar{\nu}_e}} f_p(E_p) f_{e^-}(E_{e^-})[1 - f_n(E_n)]$$
$$\int d\Omega_p d\Omega_{e^-} d\Omega_n (A_3M_A + ... + L_3M_L) \delta^3(\vec{p}_{\bar{\nu}_e} + \vec{p}_p + \vec{p}_{e^-} - \vec{p}_n). \tag{D.86}$$

The lower limit for E_{e^-} arises from the condition that for given $E_{\bar{\nu}_e}$ and E_p there must be enough total energy to create a final state neutron with minimal energy

$$E_{min} = \max\{m_n^* + U_n - E_{\bar{\nu}_e} - E_p, m_{e^-}\}. \tag{D.87}$$

The three angular integrals can again be solved analytically for all terms. For this purpose the integrals $(I_{A3}, ..., I_{L3})$ are defined by

$$I_{X3} \equiv \frac{\bar{p}_1 \bar{p}_2 \bar{p}_3 \bar{p}_4}{4\pi^2} \int d\Omega_p d\Omega_{e^-} d\Omega_n M_X \delta^3(\vec{p}_{\bar{\nu}_e} + \vec{p}_p + \vec{p}_{e^-} - \vec{p}_n). \tag{D.88}$$

The solution of these integrals can be obtained largely similar to the respective expressions of the capture reactions. For this purpose one replaces (only in the angular integrals I_X) the indices $\{1, 2, 3, 4\}$ by $\{\bar{\nu}_e, n, e^-, p\}$ respectively. Further one has to adjust for the different kinematics in the δ-function. Following this recipe the derivations do not change in the structure but only with respect to some signs. There are additional constraints on these integrals from momentum conservation. These are derived the same way as for the capture reactions.

Angular Integral I-A3

The angular integral I_{A3} has the form

$$I_{A3} = \frac{\bar{p}_1 \bar{p}_2 \bar{p}_3 \bar{p}_4}{4\pi^2} \int d\Omega_p d\Omega_{e^-} d\Omega_n \, (p_n^* \cdot p_{\bar{\nu}_e}) \, (p_p^* \cdot p_{e^-}) \, \delta^3(\vec{p}_{\bar{\nu}_e} + \vec{p}_p + \vec{p}_{e^-} - \vec{p}_n). \tag{D.89}$$

It can be computed similar to I_A. Eventually one obtains

$$I_{A3} = \frac{1}{60} \left[-3 \left(P_{1,max}^{*5} - P_{1,min}^{*5} \right) - 10 \left(a^* - b^* \right) \left(P_{1,max}^{*3} - P_{1,min}^{*3} \right) + 60 a^* b^* \left(P_{1,max}^* - P_{1,min}^* \right) \right], \tag{D.90}$$

with the limits for the momenta $P_{1,min}^*$ and $P_{1,max}^*$ and the coefficients a^* and b^* given by

$$P_{1,min}^* = \max \left\{ \left| \bar{p}_{\bar{\nu}_e} - \bar{p}_n \right|, \left| \bar{p}_p - \bar{p}_{e^-} \right| \right\} \qquad \text{and} \qquad P_{1,max}^* = \min \left\{ \bar{p}_{\bar{\nu}_e} + \bar{p}_n, \bar{p}_p + \bar{p}_{e^-} \right\}, \tag{D.91}$$

$$a^* = E_{\bar{\nu}_e} E_n^* - \frac{\bar{p}_{\bar{\nu}_e}^2 + \bar{p}_n^2}{2} \qquad \text{and} \qquad b^* = E_p^* E_{e^-} + \frac{\bar{p}_p^2 + \bar{p}_{e^-}^2}{2}. \tag{D.92}$$

Angular Integral I-B3

The angular integral I_{B3} has the form

$$I_{B3} = \frac{\bar{p}_1 \bar{p}_2 \bar{p}_3 \bar{p}_4}{4\pi^2} \int d\Omega_p d\Omega_{e^-} d\Omega_n \, (p_n^* \cdot p_{e^-}) \, (p_p^* \cdot p_{\bar{\nu}_e}) \, \delta^3(\vec{p}_{\bar{\nu}_e} + \vec{p}_p + \vec{p}_{e^-} - \vec{p}_n). \tag{D.93}$$

It can be computed similar to I_B. Eventually one obtains

$$I_{B3} = \frac{1}{60} \left[-3 \left(P_{2,max}^{*5} - P_{2,min}^{*5} \right) + 10 \left(c^* - d^* \right) \left(P_{2,max}^{*3} - P_{2,min}^{*3} \right) + 60 c^* c^* \left(P_{2,max}^* - P_{2,min}^* \right) \right], \tag{D.94}$$

with the limits for the momenta $P_{2,min}^*$ and $P_{2,max}^*$ and the coefficients c^* and d^* given by

$$P_{2,min}^* = \max \left\{ \left| \bar{p}_{\bar{\nu}_e} - \bar{p}_p \right|, \left| \bar{p}_n - \bar{p}_{e^-} \right| \right\} \qquad \text{and} \qquad P_{2,max}^* = \min \left\{ \bar{p}_{\bar{\nu}_e} + \bar{p}_p, \bar{p}_n + \bar{p}_{e^-} \right\}, \tag{D.95}$$

$$c^* = E_{\bar{\nu}_e} E_p^* + \frac{\bar{p}_{\bar{\nu}_e}^2 + \bar{p}_p^2}{2} \qquad \text{and} \qquad d^* = E_n^* E_{e^-} - \frac{\bar{p}_n^2 + \bar{p}_{e^-}^2}{2}. \tag{D.96}$$

Angular Integral I-C3

The angular integral I_{C3} has the form

$$I_{C3} = \frac{\bar{p}_1 \bar{p}_2 \bar{p}_3 \bar{p}_4}{4\pi^2} \int d\Omega_p d\Omega_{e^-} d\Omega_n \, (p_n^* \cdot p_{\bar{\nu}_e})^2 \, (p_{\bar{\nu}_e} \cdot p_{e^-}) \, \delta^3(\vec{p}_{\bar{\nu}_e} + \vec{p}_p + \vec{p}_{e^-} - \vec{p}_n). \tag{D.97}$$

It can be computed similar to I_C. Eventually one obtains

$$I_{C3} = \left[\frac{\left(P_{1,max}^{*7} - P_{1,min}^{*7} \right)}{56} + \frac{\left(\alpha_0^* + \beta_1^* \right)}{20} \left(P_{1,max}^{*5} - P_{1,min}^{*5} \right) + \frac{\left(\alpha_0^{*2} + 4\alpha_0^* \beta_1^* + \beta_0^* \right)}{12} \left(P_{1,max}^{*3} - P_{1,min}^{*3} \right) \right.$$

$$\left. + \left(\alpha_0^{*2} \beta_1^* + \alpha_0^* \beta_0^* \right) \left(P_{1,max}^* - P_{1,min}^* \right) - \alpha_0^{*2} \beta_0^* \left(P_{1,max}^{*-1} - P_{1,min}^{*-1} \right) \right], \tag{D.98}$$

with the coefficients α_0^*, β_0^*, and β_1^* given by

$$\alpha_0^* = E_{\bar{\nu}_e} E_n^* - \frac{\bar{p}_{\bar{\nu}_e}^2 + \bar{p}_n^2}{2}, \qquad\qquad \beta_0^* = \frac{1}{4} \left(\bar{p}_{\bar{\nu}_e}^2 - \bar{p}_n^2 \right) \left(\bar{p}_p^2 - \bar{p}_{e^-}^2 \right), \tag{D.99}$$

$$\beta_1^* = E_{\bar{\nu}_e} E_{e^-} + \frac{1}{4} \left(\bar{p}_{\bar{\nu}_e}^2 - \bar{p}_n^2 + \bar{p}_{e^-}^2 - \bar{p}_p^2 \right).$$

Angular Integral I-D3

The angular integral I_{D3} has the form

$$I_{D3} = \frac{\bar{p}_1 \bar{p}_2 \bar{p}_3 \bar{p}_4}{4\pi^2} \int d\Omega_p d\Omega_{e-} d\Omega_n \left(p_{\bar{\nu}_e} \cdot p_{e-}\right)^2 \left(p_n^* \cdot p_{\bar{\nu}_e}\right) \delta^3(\vec{p}_{\bar{\nu}_e} + \vec{p}_p + \vec{p}_{e-} - \vec{p}_n). \tag{D.100}$$

It can be computed similar to I_D. Eventually one obtains

$$I_{D3} = \left[\frac{-\left(P_{3,max}^{*7} - P_{3,min}^{*7}\right)}{56} + \frac{(\delta_0^* + \epsilon_1^*)}{20} \left(P_{3,max}^{*5} - P_{3,min}^{*5}\right) - \frac{(\delta_0^{*2} + 4\delta_0^* \epsilon_1^* - \epsilon_0^*)}{12} \left(P_{3,max}^{*3} - P_{3,min}^{*3}\right) \right.$$
$$\left. + \left(\delta_0^{*2} \epsilon_1^* - \delta_0^* \epsilon_0^*\right) \left(P_{3,max}^* - P_{3,min}^*\right) - \delta_0^{*2} \epsilon_0^* \left(P_{3,max}^{*-1} - P_{3,min}^{*-1}\right) \right], \tag{D.101}$$

with the limits for the momenta $P_{3,min}^*$ and $P_{3,max}^*$ and the coefficients δ_0^*, ϵ_0^*, and ϵ_1^* given by

$$P_{3,min}^* = \max\left\{ \left| \bar{p}_{\bar{\nu}_e} - \bar{p}_{e-} \right|, \left| \bar{p}_n - \bar{p}_p \right| \right\} \qquad \text{and} \qquad P_{3,max}^* = \min\left\{ \bar{p}_{\bar{\nu}_e} + \bar{p}_{e-}, \bar{p}_n + \bar{p}_p \right\}, \tag{D.102}$$

$$\delta_0^* = E_{\bar{\nu}_e} E_{e-}^* + \frac{\bar{p}_{\bar{\nu}_e}^2 + \bar{p}_{e-}^2}{2}, \qquad\qquad \epsilon_0^* = \frac{1}{4}\left(\bar{p}_{\bar{\nu}_e}^2 - \bar{p}_{e-}^2\right)\left(\bar{p}_p^2 - \bar{p}_n^2\right), \tag{D.103}$$

$$\epsilon_1^* = E_{\bar{\nu}_e} E_n - \frac{1}{4}\left(\bar{p}_{\bar{\nu}_e}^2 + \bar{p}_n^2 - \bar{p}_{e-}^2 - \bar{p}_p^2\right).$$

Angular Integral I-E3

The angular integral I_{E3} has the form

$$I_{E3} = \frac{\bar{p}_1 \bar{p}_2 \bar{p}_3 \bar{p}_4}{4\pi^2} \int d\Omega_p d\Omega_{e-} d\Omega_n \left(p_n^* \cdot p_{\bar{\nu}_e}\right)^2 \delta^3(\vec{p}_{\bar{\nu}_e} + \vec{p}_p + \vec{p}_{e-} - \vec{p}_n). \tag{D.104}$$

It can be computed similar to I_E. Eventually one obtains

$$I_{E3} = \frac{1}{60}\left[3\left(P_{1,max}^{*5} - P_{1,min}^{*5}\right) + 20a^*\left(P_{1,max}^{*3} - P_{1,min}^{*3}\right) + 60a^{*2}\left(P_{1,max}^* - P_{1,min}^*\right)\right]. \tag{D.105}$$

Angular Integral I-G3

The angular integral I_{G3} has the form

$$I_{G3} = \frac{\bar{p}_1 \bar{p}_2 \bar{p}_3 \bar{p}_4}{4\pi^2} \int d\Omega_p d\Omega_{e-} d\Omega_n \left(p_{\bar{\nu}_e} \cdot p_{e-}\right)^2 \delta^3(\vec{p}_{\bar{\nu}_e} + \vec{p}_p + \vec{p}_{e-} - \vec{p}_n). \tag{D.106}$$

It can be computed similar to I_G. Eventually one obtains

$$I_{G3} = \frac{1}{60}\left[3\left(P_{3,max}^{*5} - P_{3,min}^{*5}\right) - 20e^*\left(P_{3,max}^{*3} - P_{3,min}^{*3}\right) + 60e^{*2}\left(P_{3,max}^* - P_{3,min}^*\right)\right]. \tag{D.107}$$

The coefficient e^* is given by

$$e^* = E_{\bar{\nu}_e} E_{e-} + \frac{\bar{p}_{\bar{\nu}_e}^2 + \bar{p}_{e-}^2}{2}. \tag{D.108}$$

Angular Integral I-H3

The angular integral I_{H3} has the form

$$I_{H3} = \frac{\bar{p}_1 \bar{p}_2 \bar{p}_3 \bar{p}_4}{4\pi^2} \int d\Omega_p d\Omega_{e-} d\Omega_n \left(p_n^* \cdot p_{\bar{\nu}_e}\right)\left(p_{\bar{\nu}_e} \cdot p_{e-}\right) \delta^3(\vec{p}_{\bar{\nu}_e} + \vec{p}_p + \vec{p}_{e-} - \vec{p}_n). \tag{D.109}$$

It can be computed similar to I_H. Eventually one obtains

$$I_{H3} = \left[\frac{\left(P_{3,max}^{*5} - P_{3,min}^{*5}\right)}{40} - \frac{(\delta_0^* + 2\epsilon_1^*)}{12}\left(P_{3,max}^{*3} - P_{3,min}^{*3}\right) + \frac{(\delta_0^* \epsilon_1^* - \epsilon_0^*)}{2}\left(P_{3,max}^* - P_{3,min}^*\right) \right.$$
$$\left. - \delta_0^* \epsilon_0^* \left(P_{3,max}^{*-1} - P_{3,min}^{*-1}\right) \right]. \tag{D.110}$$

Angular Integral I-J3

The angular integral I_{J3} has the form

$$I_{J3} = \frac{\bar{p}_1 \bar{p}_2 \bar{p}_3 \bar{p}_4}{4\pi^2} \int d\Omega_p d\Omega_{e^-} d\Omega_n \left(p_n^* \cdot p_{\bar{\nu}_e}\right) \delta^3(\vec{p}_{\bar{\nu}_e} + \vec{p}_p + \vec{p}_{e^-} - \vec{p}_n). \tag{D.111}$$

It can be computed similar to I_J. Eventually one obtains

$$I_{J3} = \frac{1}{60} \left[10 \left(P_{1,max}^{*3} - P_{1,min}^{*3} \right) + 60 a^* \left(P_{1,max}^* - P_{1,min}^* \right) \right]. \tag{D.112}$$

Angular Integral I-K3

The angular integral I_{K3} has the form

$$I_{K3} = \frac{\bar{p}_1 \bar{p}_2 \bar{p}_3 \bar{p}_4}{4\pi^2} \int d\Omega_p d\Omega_{e^-} d\Omega_n \left(p_{\bar{\nu}_e} \cdot p_{e^-}\right) \delta^3(\vec{p}_{\bar{\nu}_e} + \vec{p}_p + \vec{p}_{e^-} - \vec{p}_n). \tag{D.113}$$

It can be computed similar to I_K. Eventually one obtains

$$I_{K3} = \frac{1}{60} \left[-10 \left(P_{3,max}^{*3} - P_{3,min}^{*3} \right) + 60 e^* \left(P_{3,max}^* - P_{3,min}^* \right) \right]. \tag{D.114}$$

Angular Integral I-L3

The angular integral I_{L3} has the form

$$I_{L3} = \frac{\bar{p}_1 \bar{p}_2 \bar{p}_3 \bar{p}_4}{4\pi^2} \int d\Omega_p d\Omega_{e^-} d\Omega_n \delta^3(\vec{p}_{\bar{\nu}_e} + \vec{p}_p + \vec{p}_{e^-} - \vec{p}_n). \tag{D.115}$$

It can be computed similar to I_L. Eventually one obtains

$$I_{L3} = \left(P_{1,max}^* - P_{1,min}^* \right). \tag{D.116}$$

E. Cross Sections for Nonrelativistic and Interacting Nucleons

E.1. Capture of Electron Neutrinos

Substitution of phase space integral

The integral over electron phase space can be described by

$$d^3 p_{e^-} = p_{e^-} E_{e^-} d\phi \, d\cos\theta \, dE_{e^-}.$$

The energy transfer q_0 is defined by $q_0 = E_{\nu_e} - E_{e^-}$. Hence, the energy integral can be substituted according to

$$\frac{dq_0}{dE_{e^-}} = -1 \qquad \Rightarrow \qquad \int\limits_{m_e}^{\infty} dE_{e^-} = \int\limits_{-\infty}^{E_{\nu_e} - m_e} dq_0.$$

Further, the momentum transfer q is related to $\cos\theta$ by

$$\bar{q} = \sqrt{(\vec{p}_{\nu_e} - \vec{p}_{e^-})^2} = \sqrt{E_{\nu_e}^2 + \vec{p}_{e^-}^2 - 2E_{\nu_e}\bar{p}_{e^-}\cos\theta}.$$

The angular integration over $\cos\theta$ can then be substitued by integration over $\bar{q}$

$$\frac{d\bar{q}}{d\cos\theta} = \frac{-E_{\nu_e}\bar{p}_{e^-}}{\bar{q}} \qquad \Rightarrow \qquad \int\limits_{-1}^{1} d\cos\theta = \frac{1}{E_{\nu_e}\bar{p}_{e^-}} \int\limits_{E_{\nu_e}-\bar{p}_{e^-}}^{E_{\nu_e}+\bar{p}_{e^-}} d\bar{q}\,\bar{q}.$$

Performing the integration over ϕ the whole phase space integral $d^3 p_{e^-}$ can eventually be substituted by

$$d^3 p_{e^-} = 2\pi \int\limits_{-\infty}^{E_{\nu_e}-m_e} dq_0 \frac{E_{e^-}}{E_{\nu_e}} \int\limits_{E_{\nu_e}-\bar{p}_{e^-}}^{E_{\nu_e}+\bar{p}_{e^-}} d\bar{q}\,\bar{q}.$$

Structure Function for different effective masses

Here it is assumed that the dispersion relations of neutrons and protons are given by

$$E_n = \frac{\bar{p}_n^2}{2m_n^*} + m_n^* + U_n \qquad \text{and} \qquad E_p = \frac{\bar{p}_p^2}{2m_p^*} + m_p^* + U_n.$$

The structure function $S(q_0, \vec{q})$ is given by

$$S(q_0, \vec{q}) \equiv 2 \int \frac{d^3 p_n}{(2\pi)^3} \frac{d^3 p_p}{(2\pi)^3} (2\pi)^4 \delta^4(p_{\nu_e} + p_n - p_{e^-} - p_p) f_n(E_n) \left[1 - f_p(E_p)\right].$$

By integrating over proton phase space the four-momentum conserving δ^4 is reduced to energy conserving δ. The structure function becomes then

$$S(q_0, \vec{q}) = \frac{1}{2\pi^2} \int d^3p_n \delta(q_0 + E_n - E_p) f_n(E_n) \left[1 - f_p(E_p)\right]. \tag{E.1}$$

Now the proton momentum $\vec{p}_p$ is given by $\vec{p}_p = \vec{p}_n + \vec{q}$. This allows to express the argument of the δ-function in terms of the angle $\cos\theta_n$ between the neutron and the momentum transfer.

$$0 = E_p - E_n - q_0 = \frac{(\vec{p}_n + \vec{q})^2}{2m_p^*} + m_p^* + U_p - \frac{\vec{p}_n^2}{2m_n^*} - m_n^* - U_n$$

$$= \frac{\bar{p}_n^2}{2m_p^*}\chi + \frac{\bar{p}_n\bar{q}}{m_p^*}\cos\theta_n + \frac{\bar{q}^2}{2m_p^*} - \Delta m^* - \Delta U - q_0 \quad \text{with} \quad \chi = 1 - \frac{m_p^*}{m_n^*}, \tag{E.2}$$

$$= f(\cos\theta_n).$$

Consequently the δ-function can be rewritten

$$\delta[f(\cos\theta_n)] = \delta(\cos\theta_n - \cos\theta_0)\left|\frac{df(\cos\theta_n)}{d\cos\theta_n}\right|^{-1}_{\cos\theta_0} = \delta(\cos\theta_n - \cos\theta_0)\frac{m_p^*}{\bar{p}_n\bar{q}}. \tag{E.3}$$

The angle $\cos\theta_0$ is given by

$$\cos\theta_0 = \frac{m_p^*}{\bar{p}_n\bar{q}}\left(c - \frac{\chi\bar{p}_n^2}{2m_p^*}\right) \quad \text{with} \quad c = q_0 + \Delta U + \Delta m^* - \frac{\bar{q}^2}{2m_p^*}.$$

Since $-1 < \cos\theta_n < 1$, the integration over $\cos\theta_n$ will result into constraints on $\bar{p}_n$. From (E.2) one can derive lower and upper limits

$$\bar{p}_{n\pm}^2 = \frac{2\bar{q}^2}{\chi^2}\left[\left(1 + \frac{\chi m_p^* c}{\bar{q}^2}\right) \pm \sqrt{1 + \frac{2\chi m_p^* c}{\bar{q}^2}}\right]. \tag{E.4}$$

This results in upper and lower limits for the neutron energy $E_{n\pm}$

$$E_{n\pm} = \frac{\bar{p}_{n\pm}^2}{2m_n^*} + m_n^* + U_n.$$

After rewriting the δ-function according to (E.3) and integrating over $\cos\theta_n$ and ϕ_n, the structure function becomes

$$S(q_0, \vec{q}) = \frac{m_p^*}{\pi\bar{q}} \int\limits_{\bar{p}_{n-}}^{\bar{p}_{n+}} d\bar{p}_n \, \bar{p}_n f_n(E_n)\left[1 - f_p(E_n + q_0)\right].$$

Next we define the variables x and z by

$$x \equiv \frac{E_n - \mu_n}{T} \quad \text{and} \quad z \equiv \frac{\mu_n - \mu_p + q_0}{T}.$$

The statistical factor can then be expressed in terms of these new expressions

$$f_n(E_n)\left[1 - f_p(E_n + q_0)\right] = \frac{1}{1 + \exp\left(\frac{E_n - \mu_n}{T}\right)}\frac{1}{1 + \exp\left(\frac{\mu_p - E_n - q_0}{T}\right)} = \frac{1}{1 + \exp(x)}\frac{1}{1 + \exp(-x - z)}.$$

Substituting the integration over $\bar{p}_n$ by x one gets

$$\frac{dx}{d\bar{p}_n} = \frac{\bar{p}_n}{m_n^* T} \quad \rightarrow \quad \int\limits_{\bar{p}_{n-}}^{\bar{p}_{n+}} d\bar{p}_n \, \bar{p}_n = m_n^* T \int\limits_{x_-}^{x_+} dx.$$

and the structure function becomes

$$S(q_0, \vec{q}) = \frac{m_n^* m_p^* T}{\pi \bar{q}} \int\limits_{x_-}^{x_+} dx \frac{1}{1 + \exp(x)} \frac{1}{1 + \exp(-x - z)}.$$

The integral over x can be solved analytically

$$\int dx \frac{1}{1 + \exp(x)} \frac{1}{1 + \exp(-x - z)} = \frac{1}{1 - \exp(-z)} \ln\left[\frac{1 + \exp(x)}{1 + \exp(x + z)}\right].$$

With the use of this expression the structure function finally results into

$$S(q_0, \vec{q}) = \frac{m_n^* m_p^* T}{\pi \bar{q}} \frac{\xi_- - \xi_+}{1 - \exp(-z)} \qquad \text{with} \qquad \xi_\pm = \ln\left[\frac{1 + \exp\left((E_{n\pm} - \mu_n)/T\right)}{1 + \exp\left((E_{n\pm} + q_0 - \mu_p)/T\right)}\right]. \qquad \text{(E.5)}$$

Structure Function for equal effective masses

Here it is assumed that the dispersion relations of neutrons and protons are given by

$$E_n = \frac{\bar{p}_n^2}{2m^*} + m^* + U_n \qquad \text{and} \qquad E_p = \frac{\bar{p}_p^2}{2m^*} + m^* + U_n.$$

This changes the relation between the neutron momentum $\bar{p}_n$ and the angle $\cos(\theta_n)$

$$0 = E_p - E_n - q_0 = \frac{\bar{p}_n \bar{q}}{m_p^*} \cos\theta_n + \frac{\bar{q}^2}{2m_p^*} - \Delta m^* - \Delta U - q_0.$$

the energy conserving δ-function can thus be transformed into

$$\delta(q_0 + E_2 - E_4) = \delta(\cos\theta_n - \cos\theta_0)\frac{m_p^*}{\bar{p}_n \bar{q}} \qquad \text{with} \qquad \cos\theta_0 = \frac{m_p^*}{\bar{p}_n \bar{q}}\left(q_0 + \Delta U + \Delta m^* - \frac{\bar{q}^2}{2m_p^*}\right).$$

From the limits of $\cos(\theta_n)$ there arises only a lower border for $\bar{p}_n$. By constructing the limiting value of (E.4) for equal effective nucleon masses, one finds that $\bar{p}_{n+}$ goes to infinity. For the lower limit one finds

$$\bar{p}_{n-}^2 = \frac{m^{*2}}{\bar{q}^2}\left(q_0 + \Delta U - \frac{\bar{q}^2}{2m_p^*}\right)^2.$$

Proceeding analogous to the general case of different effective masses the structure function can then be solved to become

$$S(q_0, \vec{q}) = \frac{m^{*2}T}{\pi \bar{q}} \frac{z + \xi_-}{1 - \exp(-z)}.$$

where z and ξ_- are defined in E.5.

Structure Function in Elastic Approximation

After integration over the proton phase space, the structure function has the form

$$S(q_0, \vec{q}) = 4\pi \int \frac{d^3 p_n}{(2\pi)^3} \delta(q_0 + E_n - E_p) f_n(E_n)\left[1 - f_p(E_p)\right].$$

In the elastic approximation the absolut momentum of the neutron and the proton is the same $\bar{p}_n = \bar{p}_p$. Consequently the argument of the energy conserving δ-function becomes

$$0 = E_p - E_n - q_0 = \frac{\bar{p}_n^2}{2m_p^*}\chi - \Delta m^* - \Delta U - q_0 \qquad \text{with} \qquad \chi = 1 - \frac{m_p^*}{m_n^*}, \qquad \text{(E.6)}$$

$$\simeq -\Delta m^* - \Delta U - q_0 \qquad \text{with} \qquad \chi \simeq 0. \qquad \text{(E.7)}$$

In the second step one neglects the difference in kinematic energy between neutrons and protons that arises from the different effective masses in the denominator. With this approximation the δ-function can be factored out of the phase space integral and the structure function becomes

$$S(q_0, \vec{q}) = 4\pi\delta(q_0 + \Delta m^* + \Delta U)\int \frac{d^3 p_n}{(2\pi)^3} f_n(E_n(\bar{p}_n))\left[1 - f_p(E_p(\bar{p}_n))\right]. \tag{E.8}$$

The integrand can be a transformed by the following usefull relation [139, 61]

$$f_n(E_n(\bar{p}_n))\left[1 - f_p(E_p(\bar{p}_n))\right] = \frac{f_n(E_n(\bar{p}_n)) - f_p(E_p(\bar{p}_n))}{1 - \exp\left((\Delta m^* + \Delta U - \mu_p + \mu_n)/T\right)}. \tag{E.9}$$

The denominator factors out of the integral. The integration over neutron phase space yields then

$$\int \frac{d^3 p_n}{(2\pi)^3} f_n(E_n(\bar{p}_n)) - f_p(E_p(\bar{p}_n)) = n_n - n_p, \tag{E.10}$$

where n_n and n_p are the neutron and proton number density, respectively. The structure function becomes eventually

$$S(q_0, \vec{q}) = 4\pi\delta(q_0 + \Delta m^* + \Delta U)\frac{n_n - n_p}{1 - \exp\left((\Delta m^* + \Delta U - \mu_p + \mu_n)/T\right)}. \tag{E.11}$$

E.2. Inverse Neutron Decay

Substitution of phase space integral

The integral over electron phase space can be described again by

$$d^3 p_{e^-} = p_{e^-}E_{e^-}\, d\phi\, d\cos\theta\, dE_{e^-}.$$

The energy transfer q_0 is defined by $q_0 = E_{\bar{\nu}_e} + E_{e^-}$. Hence, the energy integral can be substituted according to

$$\frac{dq_0}{dE_{e^-}} = 1 \qquad \Rightarrow \qquad \int\limits_{m_e}^{\infty} dE_{e^-} = \int\limits_{E_{\bar{\nu}_e}+m_e}^{\infty} dq_0.$$

Further, the momentum transfer q and $\cos\theta$ are related by

$$\bar{q} = \sqrt{(\vec{p}_{\bar{\nu}_e} + \vec{p}_{e^-})^2} = \sqrt{E_{\bar{\nu}_e}^2 + \bar{p}_{e^-}^2 + 2E_{\bar{\nu}_e}\bar{p}_{e^-}\cos\theta}.$$

The angular integration over $\cos\theta$ can then be substitued by integration over $\bar{q}$

$$\frac{dq}{d\cos\theta} = \frac{E_{\bar{\nu}_e}\bar{p}_{e^-}}{\bar{q}} \qquad \Rightarrow \qquad \int\limits_{-1}^{1} d\cos\theta = \frac{1}{E_{\bar{\nu}_e}\bar{p}_{e^-}}\int\limits_{E_{\bar{\nu}_e}-\bar{p}_{e^-}}^{E_{\bar{\nu}_e}+\bar{p}_{e^-}} d\bar{q}\,\bar{q}.$$

Performing the integration over ϕ the whole phase space integral $d^3 p_{e^-}$ can eventually be substituted by

$$d^3 p_{e^-} = 2\pi\int\limits_{E_{\bar{\nu}_e}+m_e}^{\infty} dq_0 \frac{E_{e^-}}{E_{\bar{\nu}_e}}\int\limits_{E_{\bar{\nu}_e}-\bar{p}_{e^-}}^{E_{\bar{\nu}_e}+\bar{p}_{e^-}} d\bar{q}\,\bar{q}.$$

Bibliography

[1] Stan Woosley and Thomas Janka. The physics of core-collapse supernovae. *Nature Phys.*, 1:147, 2005.

[2] W. Baade and F. Zwicky. Remarks on Super-Novae and Cosmic Rays. *Physical Review*, 46:76–77, July 1934.

[3] F. Hoyle and W. A. Fowler. Nucleosynthesis in Supernovae. *Astrophys. J.*, 132:565, November 1960.

[4] S. A. Colgate and M. H. Johnson. Hydrodynamic Origin of Cosmic Rays. *Physical Review Letters*, 5:235–238, September 1960.

[5] S. A. Colgate, W. H. Grasberger, and R. H. White. The Dynamics of Supernova Explosions. *Astron. J.*, 66:280, March 1961.

[6] S. A. Colgate and R. H. White. The Hydrodynamic Behavior of Supernovae Explosions. *Astrophys. J.*, 143:626, March 1966.

[7] Hans A. Bethe and James R. Wilson. Revival of a stalled supernova shock by neutrino heating. *Astrophys. J.*, 295:14–23, 1985.

[8] Daniel Z. Freedman. Coherent neutrino nucleus scattering as a probe of the weak neutral current. *Phys.Rev.*, D9:1389–1392, 1974.

[9] T. J. Mazurek. Chemical potential effects on neutrino diffusion in supernovae. *Astrophys.Sp.Sc.*, 35:117–135, June 1975.

[10] K. Sato. Supernova Explosion and Neutral Currents of Weak Interaction. *Prog.Theor.Phys.*, 54:1325–1338, 1975.

[11] J. Cooperstein. Neutrinos in Supernovae. *Phys.Rept.*, 163:95–126, 1988.

[12] Marc Herant, W. Benz, W. Raphael Hix, Chris L. Fryer, and Stirling A. Colgate. Inside the supernova: A Powerful convective engine. *Astrophys. J.*, 435:339, 1994.

[13] Adam Burrows, John Hayes, and Bruce A. Fryxell. On the nature of core collapse supernova explosions. *Astrophys. J.*, 450:830, 1995.

[14] H.T. Janka and E. Mueller. Neutrino heating, convection, and the mechanism of Type-II supernova explosions. *Astron.Astrophys.*, 306:167, 1996.

[15] C.L. Fryer and M.S. Warren. Modeling core-collapse supernovae in 3-dimensions. *Astrophys. J.*, 574:L65, 2002.

[16] John M. Blondin, Anthony Mezzacappa, and Christine DeMarino. Stability of standing accretion shocks, with an eye toward core collapse supernovae. *Astrophys. J.*, 584:971–980, 2003.

[17] T. Foglizzo. Entropic-acoustic instability of shocked bondi accretion I. what does perturbed bondi accretion sound like ? *Astron.Astrophys.*, 368:311, 2001.

[18] T. Foglizzo. Non-radial instabilities of isothermal Bondi accretion with a shock: Vortical-acoustic cycle versus post-shock acceleration. *Astron.Astrophys.*, 2002.

[19] R. Buras, Hans-Thomas Janka, M. Rampp, and K. Kifonidis. Two-dimensional hydrodynamic core-collapse supernova simulations with spectral neutrino transport. 2. models for different progenitor stars. *Astron.Astrophys.*, 457:281, 2006.

[20] A. Marek and H.-Th. Janka. Delayed neutrino-driven supernova explosions aided by the standing accretion-shock instability. *Astrophys. J.*, 694:664–696, 2009.

[21] Adam Burrows, Eli Livne, Luc Dessart, Christian Ott, and Jeremiah Murphy. A new mechanism for core-collapse supernova explosions. *Astrophys. J.*, 640:878–890, 2006.

[22] S. W. Bruenn, A. Mezzacappa, W. R. Hix, J. M. Blondin, P. Marronetti, O. E. B. Messer, C. J. Dirk, and S. Yoshida. 2D and 3D core-collapse supernovae simulation results obtained with the CHIMERA code. *Journal of Physics Conference Series*, 180(1):012018, July 2009.

[23] Yudai Suwa, Kei Kotake, Tomoya Takiwaki, Stuart C. Whitehouse, Matthias Liebendoerfer, et al. Explosion geometry of a rotating 13 $M_\odot$ star driven by the SASI-aided neutrino-heating supernova mechanism. *Publ. Astron. Soc. Jap.*, 62:L49–L53, 2010.

[24] Tomoya Takiwaki, Kei Kotake, and Yudai Suwa. Three-dimensional Hydrodynamic Core-Collapse Supernova Simulations for an $11.2 M_\odot$ Star with Spectral Neutrino Transport. *Astrophys. J.*, 749:98, 2012.

[25] Bernhard Muller, Hans-Thomas Janka, and Andreas Marek. A New Multi-Dimensional General Relativistic Neutrino Hydrodynamics Code for Core-Collapse Supernovae II. Relativistic Explosion Models of Core-Collapse Supernovae. *Astrophys. J.*, 756:84, 2012.

[26] Stephen W. Bruenn, Anthony Mezzacappa, W. Raphael Hix, Eric J. Lentz, O.E. Bronson Messer, et al. Axisymmetric Ab Initio Core-Collapse Supernova Simulations of 12-25 M_sol Stars. *Astrophys. J.*, 767:L6, 2013.

[27] Hans-Thomas Janka. Explosion Mechanisms of Core-Collapse Supernovae. *Ann. Rev. Nucl. Part. Sci.*, 62:407–451, 2012.

[28] K. Kotake, K. Sato, H. Sawai, and S. Yamada. Magnetorotational effects on anisotropic neutrino emission and convection in core-collapse supernovae. *Astrophys. J.*, 608:391–404, 2004.

[29] Adam Burrows, E. Livne, L. Dessart, C.D. Ott, and J. Murphy. Features of the Acoustic Mechanism of Core-Collapse Supernova Explosions. *Astrophys. J.*, 655:416–433, 2007.

[30] I. Sagert, T. Fischer, M. Hempel, G. Pagliara, J. Schaffner-Bielich, et al. Signals of the QCD phase transition in core-collapse supernovae. *Phys. Rev. Lett.*, 102:081101, 2009.

[31] T. Fischer, I. Sagert, G. Pagliara, M. Hempel, J. Schaffner-Bielich, et al. Core-collapse supernova explosions triggered by a quark-hadron phase transition during the early post-bounce phase. *Astrophys. J. Suppl.*, 194:39, 2011.

[32] K. Nomoto, F.K. Thielemann, and K. Yokoi. Accreting white dwarf models of Type I supernovae. 3. Carbon deflagration supernovae. *Astrophys. J.*, 286:644, 1984.

[33] K. Nomoto. Evolution of 8-10 solar mass stars toward electron capture supernovae. II - Collapse of an O + NE + MG core. *Astrophys. J.*, 322:206–214, November 1987.

[34] A.J.T. Poelarends, F. Herwig, N. Langer, and A. Heger. The Supernova Channel of Super-AGB Stars. *Astrophys. J.*, 675:614, 2008.

[35] F.S. Kitaura, Hans-Thomas Janka, and W. Hillebrandt. Explosions of O-Ne-Mg cores, the Crab supernova, and subluminous type II-P supernovae. *Astron. Astrophys.*, 450:345–350, 2006.

[36] H.-Th. Janka, B. Mueller, F.S. Kitaura, and R. Buras. Dynamics of shock propagation and nucleosynthesis conditions in O-Ne-Mg core supernovae. *Astron. Astrophys.*, 485:199, 2008.

[37] T. Fischer, S.C. Whitehouse, A. Mezzacappa, F.-K. Thielemann, and M. Liebendorfer. Protoneutron star evolution and the neutrino driven wind in general relativistic neutrino radiation hydrodynamics simulations. *Astron. Astrophys.*, 517:A80, 2010.

[38] K. Nomoto. Accreting white dwarf models for type I supernovae. I - Presupernova evolution and triggering mechanisms. *Astrophys. J.*, 253:798–810, 1982.

[39] Shinya Wanajo, Hans-Thomas Janka, and Bernhard Mueller. Electron-capture supernovae as the origin of elements beyond iron. *Astrophys. J.*, 726:L15, 2011.

[40] S. Wanajo, K. Nomoto, H.-Th. Janka, F.S. Kitaura, and B. Mueller. Nucleosynthesis in Electron Capture Supernovae of AGB Stars. *Astrophys. J.*, 695:208–220, 2009.

[41] C.J. Horowitz, D.K. Berry, C.M. Briggs, M.E. Caplan, A. Cumming, et al. Disordered nuclear pasta, magnetic field decay, and crust cooling in neutron stars. *Phys.Rev.Lett.*, 114:031102, 2015.

[42] James M. Lattimer and F. Douglas Swesty. A Generalized equation of state for hot, dense matter. *Nucl.Phys.*, A535:331–376, 1991.

[43] H. Shen, H. Toki, K. Oyamatsu, and K. Sumiyoshi. Relativistic equation of state of nuclear matter for supernova and neutron star. *Nucl.Phys.*, A637:435–450, 1998.

[44] Matthias Hempel and Jurgen Schaffner-Bielich. Statistical Model for a Complete Supernova Equation of State. *Nucl.Phys.*, A837:210–254, 2010.

[45] G. Shen, C.J. Horowitz, and S. Teige. A New Equation of State for Astrophysical Simulations. *Phys.Rev.*, C83:035802, 2011.

[46] G. Shen, C.J. Horowitz, and E. O'Connor. A Second Relativistic Mean Field and Virial Equation of State for Astrophysical Simulations. *Phys.Rev.*, C83:065808, 2011.

[47] H. Shen, H. Toki, K. Oyamatsu, and K. Sumiyoshi. Relativistic Equation of State for Core-Collapse Supernova Simulations. *Astrophys.J.Suppl.*, 197:20, 2011.

[48] Paul Demorest, Tim Pennucci, Scott Ransom, Mallory Roberts, and Jason Hessels. Shapiro Delay Measurement of A Two Solar Mass Neutron Star. *Nature*, 467:1081–1083, 2010.

[49] John Antoniadis, Paulo C.C. Freire, Norbert Wex, Thomas M. Tauris, Ryan S. Lynch, et al. A Massive Pulsar in a Compact Relativistic Binary. *Science*, 340:6131, 2013.

[50] Andrew W. Steiner, James M. Lattimer, and Edward F. Brown. The Equation of State from Observed Masses and Radii of Neutron Stars. *Astrophys.J.*, 722:33–54, 2010.

[51] K. Hebeler, J.M. Lattimer, C.J. Pethick, and A. Schwenk. Constraints on neutron star radii based on chiral effective field theory interactions. *Phys.Rev.Lett.*, 105:161102, 2010.

[52] S. Gandolfi, J. Carlson, S. Reddy, A.W. Steiner, and R.B. Wiringa. The equation of state of neutron matter, symmetry energy, and neutron star structure. *Eur.Phys.J.*, A50:10, 2014.

[53] Pawel Danielewicz and Jenny Lee. Symmetry Energy II: Isobaric Analog States. *Nucl.Phys.*, A922:1–70, 2014.

[54] James M. Lattimer and Yeunhwan Lim. Constraining the Symmetry Parameters of the Nuclear Interaction. *Astrophys.J.*, 771:51, 2013.

[55] Andrew W. Steiner. The High-density symmetry energy and direct Urca. *Phys.Rev.*, C74:045808, 2006.

[56] Hans-Thomas Janka, R. Buras, F.S. Kitaura Joyanes, A. Marek, M. Rampp, et al. Neutrino-driven supernovae: An Accretion instability in a nuclear physics controlled environment. *Nucl.Phys.*, A758:19–26, 2005.

[57] E. Lentz, W. R. Hix, M. L. Baird, O. E. B. Messer, and A. Mezzacappa. Evaluating nuclear physics inputs in core-collapse supernova models. In *Nuclei in the Cosmos*, page 152, 2010.

[58] Matthias Hempel, Tobias Fischer, Jurgen Schaffner-Bielich, and Matthias Liebendorfer. New Equations of State in Simulations of Core-Collapse Supernovae. *Astrophys.J.*, 748:70, 2012.

[59] James M. Lattimer and Madappa Prakash. Nuclear matter and its role in supernovae, neutron stars and compact object binary mergers. *Phys.Rept.*, 333:121–146, 2000.

[60] P. Haensel, A. Y. Potekhin, and D. G. Yakovlev, editors. *Neutron Stars 1 : Equation of State and Structure*, volume 326 of *Astrophysics and Space Science Library*, 2007.

[61] G. Martinez-Pinedo, T. Fischer, A. Lohs, and L. Huther. Charged-current weak interaction processes in hot and dense matter and its impact on the spectra of neutrinos emitted from proto-neutron star cooling. *Phys.Rev.Lett.*, 109:251104, 2012.

[62] L.F. Roberts. A New Code for Proto-Neutron Star Evolution. *Astrophys.J.*, 755:126, 2012.

[63] L.F. Roberts, Sanjay Reddy, and Gang Shen. Medium modification of the charged current neutrino opacity and its implications. *Phys.Rev.*, C86:065803, 2012.

[64] S. Typel, G. Ropke, T. Klahn, D. Blaschke, and H.H. Wolter. Composition and thermodynamics of nuclear matter with light clusters. *Phys.Rev.*, C81:015803, 2010.

[65] C.J. Horowitz and A. Schwenk. Cluster formation and the virial equation of state of low-density nuclear matter. *Nucl.Phys.*, A776:55–79, 2006.

[66] C.J. Horowitz and Gang Li. Charge conjugation violating neutrino interactions in supernovae. *Phys.Rev.*, D61:063002, 2000.

[67] A. Marek, H.-Th. Janka, and E. Mueller. Equation-of-State Dependent Features in Shock-Oscillation Modulated Neutrino and Gravitational-Wave Signals from Supernovae. *Astron.Astrophys.*, 496:475, 2009.

[68] L. Hudepohl, B. Muller, H.-T. Janka, A. Marek, and G.G. Raffelt. Neutrino Signal of Electron-Capture Supernovae from Core Collapse to Cooling. *Phys.Rev.Lett.*, 104:251101, 2010.

[69] T. Fischer, G. Martinez-Pinedo, M. Hempel, and M. Liebendorfer. Neutrino spectra evolution during proto-neutron star deleptonization. *Phys.Rev.*, D85:083003, 2012.

[70] Huaiyu Duan and James P Kneller. Neutrino flavour transformation in supernovae. *J.Phys.*, G36:113201, 2009.

[71] Huaiyu Duan, George M. Fuller, and Yong-Zhong Qian. Collective Neutrino Oscillations. *Ann.Rev.Nucl.Part.Sci.*, 60:569–594, 2010.

[72] Dany Page, Ulrich Geppert, and Fridolin Weber. The Cooling of compact stars. *Nucl.Phys.*, A777:497–530, 2006.

[73] J.M. Lattimer, M. Prakash, C.J. Pethick, and P. Haensel. Direct URCA process in neutron stars. *Phys.Rev.Lett.*, 66:2701–2704, 1991.

[74] Hong-Yee Chiu and E.E. Salpeter. Surface X-Ray Emission from Neutron Stars. *Phys.Rev.Lett.*, 12:413–415, 1964.

[75] B.L. Friman and O.V. Maxwell. Neutron Star Neutrino Emissivities. *Astrophys.J.*, 232:541–557, 1979.

[76] M. Prakash, M. Prakash, J. M. Lattimer, and C. J. Pethick. Rapid cooling of neutron stars by hyperons and Delta isobars. *Astrophys.J.*, 390:L77–L80, May 1992.

[77] O. Maxwell, G.E. Brown, D.K. Campbell, R.F. Dashen, and J.T. Manassah. Beta decay of pion condensates as a cooling mechanism for neutron stars. *Astrophys.J.*, 216:77–85, 1977.

[78] G.E. Brown, K. Kubodera, D. Page, and P. Pizzochero. Strangeness Condensation and Cooling of Neutron Stars. *Phys.Rev.*, D37:2042–2046, 1988.

[79] T. Tatsumi. K^-on Condensation and Cooling of Neutron Stars. *Prog.Theor.Phys.*, 80:22, 1988.

[80] Katharina Lodders. Solar System Abundances and Condensation Temperatures of the Elements. *Astrophys.J.*, 591:1220–1247, 2003.

[81] Margaret E. Burbidge, G.R. Burbidge, William A. Fowler, and F. Hoyle. Synthesis of the elements in stars. *Rev.Mod.Phys.*, 29:547–650, 1957.

[82] C. Freiburghaus, S. Rosswog, and F.-K. Thielemann. R-Process in Neutron Star Mergers. *Astrophys.J.*, 525:L121–L124, November 1999.

[83] Shin-Ya Wanajo and Hans-Thomas Janka. The r-process in the neutrino-driven wind from a black-hole torus. *Astrophys.J.*, 746:180, 2012.

[84] Doron Grossman, Oleg Korobkin, Stephan Rosswog, and Tsvi Piran. The long-term evolution of neutron star merger remnants - II. Radioactively powered transients. 2013.

[85] Satoshi Honda, W. Aoki, Y. Ishimaru, S. Wanajo, and S.G. Ryan. Neutron-capture elements in the very metal-poor star hd 122563. *Astrophys.J.*, 643:1180–1189, 2006.

[86] Yong-Zhong Qian. Astrophysical Models of r-Process Nucleosynthesis: An Update. *AIP Conf.Proc.*, 1484:201, 2012.

[87] A. Arcones and F. Montes. Production of Light Element Primary Process nuclei in neutrino-driven winds. *Astrophys.J.*, 731:5, 2011.

[88] S.E. Woosley, A. Heger, and T.A. Weaver. The evolution and explosion of massive stars. *Rev.Mod.Phys.*, 74:1015–1071, 2002.

[89] Hans-Thomas Janka, K. Langanke, A. Marek, G. Martinez-Pinedo, and B. Mueller. Theory of Core-Collapse Supernovae. *Phys.Rept.*, 442:38–74, 2007.

[90] R. C. Duncan, S. L. Shapiro, and I. Wasserman. Neutrino-driven winds from young, hot neutron stars. *Astrophys.J.*, 309:141–160, October 1986.

[91] Y.Z. Qian and S.E. Woosley. Nucleosynthesis in neutrino driven winds: 1. The Physical conditions. *Astrophys.J.*, 471:331–351, 1996.

[92] Todd A. Thompson, Adam Burrows, and Bradley S. Meyer. The Physics of protoneutron star winds: implications for r-process nucleosynthesis. *Astrophys.J.*, 562:887, 2001.

[93] Shinya Wanajo, Hans-Thomas Janka, and Shigeru Kubono. Uncertainties in the nu p-process: supernova dynamics versus nuclear physics. *Astrophys.J.*, 729:46, 2011.

[94] R.D. Hoffman, S.E. Woosley, and Y.Z. Qian. Nucleosynthesis in neutrino driven winds: 2. Implications for heavy element synthesis. *Astrophys.J.*, 482:951, 1997.

[95] A. Arcones and F.K. Thielemann. Neutrino-driven wind simulations and nucleosynthesis of heavy elements. *J.Phys.*, G40:013201, 2013.

[96] G. Martínez-Pinedo. Selected topics in nuclear astrophysics. *European Physical Journal Special Topics*, 156:123–149, April 2008.

[97] Takami Kuroda, Shinya Wanajo, and Ken'ichi Nomoto. The r-Process in Supersonic Neutrino-Driven Winds: The Roll of Wind Termination Shock. *AIP Conf.Proc.*, 1016:436–438, 2008.

[98] L.F. Roberts, S.E. Woosley, and R.D. Hoffman. Integrated Nucleosynthesis in Neutrino Driven Winds. *Astrophys.J.*, 722:954–967, 2010.

[99] Yong-Zhong Qian. The origin of the heavy elements: recent progress in the understanding of the r-process. *Prog.Part.Nucl.Phys.*, 50:153–199, 2003.

[100] C. Frohlich, P. Hauser, M. Liebendorfer, G. Martinez-Pinedo, F.-K. Thielemann, et al. Composition of the innermost supernova ejecta. *Astrophys.J.*, 637:415–426, 2006.

[101] K. Takahashi, J. Witti, and H.-T. Janka. Nucleosynthesis in neutrino-driven winds from protoneutron stars. 2. The R-process. *Astron.Astrophys.*, 286:857, 1994.

[102] A. Arcones, Hans-Thomas Janka, and L. Scheck. Nucleosynthesis-relevant conditions in neutrino-driven supernova outflows. 1. Spherically symmetric hydrodynamic simulations. *Astron.Astrophys.*, 467:1227, 2007.

[103] A. Arcones and H.-T. Janka. Nucleosynthesis-relevant conditions in neutrino-driven supernova outflows. II. The reverse shock in two-dimensional simulations. *Astron.Astrophys.*, 526:A160, 2011.

[104] G. Martínez-Pinedo, T. Fischer, and L. Huther. Supernova neutrinos and nucleosynthesis. *J.Phys.*, G41:044008, 2014.

[105] G.M. Fuller and B.S. Meyer. Neutrino capture and supernova nucleosynthesis. *Astrophys.J.*, 453:792–809, 1995.

[106] Shinya Wanajo. The r-process in proto-neutron-star wind revisited. *Astrophys.J.*, 770:L22, 2013.

[107] C. Frohlich, Gabriel Martinez-Pinedo, M. Liebendorfer, F.-K. Thielemann, E. Bravo, et al. Neutrino-induced nucleosynthesis of a>64 nuclei: the nu p-process. *Phys.Rev.Lett.*, 96:142502, 2006.

[108] K.N. Abazajian, M.A. Acero, S.K. Agarwalla, A.A. Aguilar-Arevalo, C.H. Albright, et al. Light Sterile Neutrinos: A White Paper. 2012.

[109] Meng-Ru Wu, Tobias Fischer, Lutz Huther, Gabriel Martínez-Pinedo, and Yong-Zhong Qian. Impact of active-sterile neutrino mixing on supernova explosion and nucleosynthesis. *Phys.Rev.*, D89(6):061303, 2014.

[110] S.E. Woosley, D.H. Hartmann, R.D. Hoffman, and W.C. Haxton. The Neutrino Process. *Astrophys.J.*, 356:272–301, 1990.

[111] K. Langanke and G. Martinez-Pinedo. Neutrino-nucleus reaction in supernovae. *Prog.Part.Nucl.Phys.*, 64:400–403, 2010.

[112] S.L. Glashow. Partial Symmetries of Weak Interactions. *Nucl.Phys.*, 22:579–588, 1961.

[113] Steven Weinberg. A Model of Leptons. *Phys.Rev.Lett.*, 19:1264–1266, 1967.

[114] A. Salam. *Proc. of the 8th Nobel Symposium on 'Elementary Particle Theory, Relativistic Groups and Analicity', 1968*, pages 367–377, 1969.

[115] Nicola Cabibbo. Unitary Symmetry and Leptonic Decays. *Phys.Rev.Lett.*, 10:531–533, 1963.

[116] Makoto Kobayashi and Toshihide Maskawa. CP Violation in the Renormalizable Theory of Weak Interaction. *Prog.Theor.Phys.*, 49:652–657, 1973.

[117] Carlo Giunti and Chung W. Kim. Fundamentals of Neutrino Physics and Astrophysics. 2007.

[118] M. E. Peskin and D. V. Schroeder. *An Introduction to Quantum Field Theory*. Westview Press, 1995.

[119] Adam Burrows, Sanjay Reddy, and Todd A. Thompson. Neutrino opacities in nuclear matter. *Nucl.Phys.*, A777:356–394, 2006.

[120] A. Bartl, C.J. Pethick, and A. Schwenk. Supernova matter at subnuclear densities as a resonant Fermi gas: Enhancement of neutrino rates. *Phys.Rev.Lett.*, 113:081101, 2014.

[121] K. Wehrberger. Electromagnetic response functions in quantum hadrodynamics. *Phys.Rept.*, 225:273–362, 1993.

[122] A. L. Fetter and J. D. Walecka. *Quantum theory of many-particle systems*. 1971.

[123] C.J. Horowitz and K. Wehrberger. Neutrino neutral current interactions in nuclear matter. *Nucl.Phys.*, A531:665–684, 1991.

[124] Sanjay Reddy, Madappa Prakash, and James M Lattimer. Neutrino interactions in hot and dense matter. *Phys.Rev.*, D58:013009, 1998.

[125] C.J. Horowitz and K. Wehrberger. Neutrino neutral current interactions in hot dense matter. *Phys.Lett.*, B266:236–242, 1991.

[126] Sanjay Reddy, Madappa Prakash, James M. Lattimer, and Jose A. Pons. Effects of strong and electromagnetic correlations on neutrino interactions in dense matter. *Phys.Rev.*, C59:2888–2918, 1999.

[127] Charles J. Horowitz and M.A. Perez-Garcia. Realistic neutrino opacities for supernova simulations with correlations and weak magnetism. *Phys.Rev.*, C68:025803, 2003.

[128] Eric J. Lentz, Anthony Mezzacappa, O.E. Bronson Messer, Matthias Liebendorfer, W. Raphael Hix, et al. On the Requirements for Realistic Modeling of Neutrino Transport in Simulations of Core-Collapse Supernovae. *Astrophys.J.*, 747:73, 2012.

[129] Robert Buras, Hans-Thomas Janka, Mathias T. Keil, Georg G. Raffelt, and Markus Rampp. Electron neutrino pair annihilation: A New source for muon and tau neutrinos in supernovae. *Astrophys.J.*, 587:320–326, 2003.

[130] C.J. Horowitz. Weak magnetism for anti-neutrinos in supernovae. *Phys.Rev.*, D65:043001, 2002.

[131] W. R. Yueh and J. R. Buchler. Scattering functions for neutrino transport. *Astrophys.Sp.Sc.*, 39:429–435, February 1976.

[132] W. R. Yueh and J. R. Buchler. Neutrino processes in dense matter. *Astrophys.Sp.Sc.*, 41:221–251, May 1976.

[133] David L. Tubbs. DIRECT SIMULATION NEUTRINO TRANSPORT: ASPECTS OF EQUILIBRA-TION. *Astrophys. J. Suppl.*, 1978.

[134] P. J. Schinder and S. L. Shapiro. Neutrino emission from a hot, dense, plane-parallel atmosphere in hydrostatic equilibrium. II - Numerical methods and interaction functions. *Astrophys.J.Suppl.*, 50:23–37, September 1982.

[135] A. Mezzacappa and S. W. Bruenn. Stellar core collapse - A Boltzmann treatment of neutrino-electron scattering. *Astrophys.J.*, 410:740–760, June 1993.

[136] K.S. Kölbig, J.A. Mignaco, and E. Remiddi. On Nielsen's generalized polylogarithms and their numerical calculation. *BIT Numerical Mathematics*, 10(1):38–73.

[137] Andrew W. Steiner, Madappa Prakash, and James M. Lattimer. Diffusion of neutrinos in protoneutron star matter with quarks. *Phys.Lett.*, B509:10–18, 2001.

[138] Adam Burrows and R.F. Sawyer. Many body corrections to charged current neutrino absorption rates in nuclear matter. *Phys.Rev.*, C59:510–514, 1999.

[139] Stephen W. Bruenn. Stellar core collapse: Numerical model and infall epoch. *Astrophys.J.Suppl.*, 58:771–841, 1985.

[140] Steen Hannestad and Georg Raffelt. Supernova neutrino opacity from nucleon-nucleon Bremsstrahlung and related processes. *Astrophys.J.*, 507:339–352, 1998.

[141] Todd A. Thompson and Adam Burrows. Neutrino processes in supernovae and the physics of protoneutron star winds. *Nucl.Phys.*, A688:377–381, 2001.

[142] Georg G. Raffelt. Muon-neutrino and tau-neutrino spectra formation in supernovae. *Astrophys.J.*, 561:890–914, 2001.

[143] C.J. Horowitz. Neutrino trapping in a supernova and ion screening. *Phys.Rev.*, D55:4577–4581, 1997.

[144] K. Langanke, G. Martinez-Pinedo, Berndt Muller, H.-Th. Janka, A. Marek, et al. Effects of Inelastic Neutrino-Nucleus Scattering on Supernova Dynamics and Radiated Neutrino Spectra. *Phys.Rev.Lett.*, 100:011101, 2008.

[145] K. Langanke, Gabriel Martinez-Pinedo, J.M. Sampaio, D.J. Dean, W.R. Hix, et al. Electron capture rates on nuclei and implications for stellar core collapse. *Phys.Rev.Lett.*, 90:241102, 2003.

[146] A. Arcones, G. Martinez-Pinedo, E. O'Connor, A. Schwenk, H.-Th. Janka, et al. Influence of light nuclei on neutrino-driven supernova outflows. *Phys.Rev.*, C78:015806, 2008.

[147] Kohsuke Sumiyoshi and Gerd Roepke. Appearance of light clusters in post-bounce evolution of core-collapse supernovae. *Phys.Rev.*, C77:055804, 2008.

[148] S. Nasu, S.X. Nakamura, K. Sumiyoshi, T. Sato, F. Myhrer, et al. Neutrino Emissivities from Deuteron-Breakup and Formation in Supernovae. 2014.

[149] A. Mezzacappa and S.W. Bruenn. Type II supernovae and Boltzmann neutrino transport: The Infall phase. *Astrophys.J.*, 405:637–668, 1993.

[150] S.L. Shapiro and S.A. Teukolsky. Black holes, white dwarfs, and neutron stars: The physics of compact objects. 1983.